# CARACTÉRISATION GÉOCHIMIQUE RÉGIONALE DES SÉDIMENTS MARINS DE SURFACE DE L'ARCTIQUE CANADIEN ET ÉVALUATION DE LA CONTAMINATION MÉTALLIQUE

Thèse présentée

dans le cadre du programme de doctorat en océanographie

en vue de l'obtention du grade de *philosophiae doctor* (Ph.D.)

PAR

**© CAMILLE BRICE**

**Décembre 2025**

**Composition du jury :**

**Stephanie Kusch, présidente du jury, Institut des sciences de la mer, Université du Québec à Rimouski**

**Jean-Carlos Montero-Serrano, directeur de recherche, Institut des sciences de la mer, Université du Québec À Rimouski**

**Richard St-Louis, codirecteur de recherche, Université du Québec à Rimouski**

**Christian Gagnon, examinateur externe, Environnement et Changement climatique Canada – Centre Saint-Laurent**

Dépôt initial le 10 juillet 2025 Dépôt final le 10 décembre 2025

« La beauté est une rivière d'arc-en-ciel où chaque murmure d'un papillon rappelle en chaque instant ce que devenir »

– *Gaby Gravel*

## REMERCIEMENTS

J’aimerais remercier mes directeurs, Jean-Carlos Montero-Serrano et Richard Saint-Louis qui m’ont permis de faire ce projet et de participer à de multiples séjours dans l’Arctique. Je tiens également à remercier Gwenaëlle Chaillou qui m’a toujours accueillie dans son bureau pour discuter de mes résultats et des difficultés rencontrées. Merci aussi chaudement pour l’opportunité de terrain à Cambridge Bay. Mes remerciements vont également à Maikel Rosabal pour son accueil dans son laboratoire et ses conseils, et Stephanie Kusch et Christian Gagnon pour la correction de cette thèse.

Merci à ArcTrain, Geotop et Québec Océan pour les rencontres et les activités qui ont toujours été motivantes. Merci à l’équipe scientifique et l’équipage de l’Amundsen pour l’aide lors de l’échantillonnage. Un merci tout particulier à Daniel et Amélie d’Amundsen Science pour votre merveilleuse compagnie à bord.

Merci à mes ami.e.s géologues avec qui la journée au bureau est toujours plus agréable, surtout avec un jeu de tarot : Arthur, Quentin D., Quentin B., Florian et Morgane. Je tiens également à remercier celles qui ont partagé ce parcours avec moi, Juliette et Kelsey pour tous les beaux moments entre la cafetière de la grotte et les carottiers sur le deck de l’Amundsen.

Merci à mes ami.e.s et partenaires d’aventures de Rimouski, Caro, Joëlle, Christian, Greg, Chris, Guillaume, Charlotte, Daniela et tant d’autres. J’ai aussi une pensée pour mes ami.e.s de Montréal et d’ailleurs : Jade, Dominique, Anthony, Damien, Marjo, François, Nina, Aristide, Frédérique, Estelle, Félicia.

Ce parcours jusqu’à la fin de la thèse n’aurait jamais été possible sans ma famille. J’aimerais remercier mes parents, ma sœur, mon frère, mon beau-frère et ma belle-sœur pour leur soutien et leur amour. Un petit merci spécial à mes nièces qui m’ont toujours offert du

bon divertissement et des sourires. J'aimerais surtout prendre le temps de remercier mon amoureuse Alice. Un merci infini de m'avoir aimée, soutenue, encouragée, divertie.

Finalement, j'aimerais terminer ces remerciements en ayant une pensée pour toi Dou. Merci pour les rires, les aventures *hardcores* et inopinées, les belles discussions. Merci d'avoir fait partie de ma vie.

## RÉSUMÉ

Ce projet de recherche a pour objectif principal de caractériser la distribution spatiale des éléments majeurs et traces dans les sédiments marins de l'Arctique canadien dans le but de faire une évaluation de la contamination métallique. Pour y parvenir, de multiples échantillons de sédiments marins de surface collectés à travers la zone d'étude ont été analysés pour leur composition chimique.

Le premier chapitre de ce projet cherche à définir la dynamique sédimentaire de l'Arctique canadien. La provenance, les mécanismes de transport et les conditions de déposition des sédiments ont été déterminés à partir de la concentration totale des éléments majeurs et traces, du contenu en carbone organique et de la granulométrie des échantillons. Puis, la zone d'étude, étant vaste et présentant des contextes océanographiques et géologiques hétérogènes, a été délimitée selon ces paramètres. Ainsi, les données obtenues combinées à des analyses multivariées ont révélé une grande variabilité dans la composition chimique du fond marin, qui a pu être décrit selon trois groupes chimiques. Cette caractérisation géochimique a permis d'identifier le fleuve Mackenzie comme étant la principale contributrice de métaux et le plateau de la mer de Beaufort comme la zone la plus sensible aux enrichissements. L'applicabilité des indices de pollution a été évaluée à partir de différents fonds géochimiques, dont un fond régional basé sur des sédiments marins préindustriels. Le facteur d'enrichissement et l'indice de géo-accumulation ont révélé des niveaux généralement faibles d'enrichissement et de contamination en métaux dans les sédiments de surface par rapport aux valeurs régionales naturelles.

Le deuxième chapitre établit une base de référence des concentrations en métaux trace dans les sédiments de surface de l'Arctique canadien. L'objectif est d'acquérir une meilleure compréhension de leurs sources et transports dans l'environnement marin arctique et d'évaluer leur risque écologique. Les métaux ont été mesurés dans la fraction extractible à l'acide des sédiments, ciblant la part la plus biodisponible. La variabilité régionale des métaux extractibles reflète bien celle des concentrations totales des éléments majeurs et traces, indiquant que la lithologie et les processus sédimentaires naturelles contrôlent leur répartition. Le fleuve Mackenzie constitue la principale source de métaux et les concentrations les plus élevées se trouvent dans la délimitation de son panache. Toutefois, les terres rares se concentrent surtout le long de la côte de l'île de Baffin, ceux-ci provenant des lithologies du Bouclier canadien. Les indices de pollution indiquent des niveaux d'enrichissement ou de contamination généralement faibles, mais des niveaux modérés d'As sont mesurés dans les sédiments de la mer de Beaufort et le détroit de Jones. D'après les Recommandations canadiennes pour la qualité des sédiments, la plupart des échantillons présentent des concentrations inférieures au seuil d'effets probables, bien que celui-ci soit

dépassé pour l'As et le Ni dans certains échantillons des golfes d'Amundsen et de Coronation, du détroit de Jones et de la baie de Baffin. Globalement, la composition en éléments traces des sédiments reflètent des niveaux naturels liés à la géologie et aux dynamiques sédimentaires régionales.

Finalement, le troisième chapitre évalue la contamination métallique à l'échelle locale dans les communautés nordiques de l'Arctique canadien. Les concentrations totales et extractibles à l'acide des métaux ont été mesurées dans les sédiments côtiers de six communautés inuites et de Milne Inlet, site du port de Mary River. Globalement, les résultats concordent avec la variabilité régionale. Les sites de Tuktoyaktuk, Resolute Bay, Grise Fiord, Qikiqtarjuaq et Milne Inlet présentent des niveaux naturels de métaux. Toutefois, des effets biologiques négatifs sur la faune aquatique sont possibles à Tuktoyaktuk en raison des apports naturels élevés du fleuve Mackenzie. À Pond Inlet, la composition chimique des sédiments reflète principalement la géologie locale. Toutefois, la variabilité lithologique le long de la côte entraîne parfois des concentrations élevées en ETM, et des apports anthropiques ponctuels sont également suspectés. À Kugluktuk, les résultats ont révélé des concentrations totales élevées en V et Cr possiblement résultant d'un mélange de sources naturelles et anthropiques locales. Les principales sources seraient l'érosion d'intrusions ultramafiques transportées par la rivière Coppermine et les décharges des eaux usées à proximité. Toutefois, les concentrations de métaux extractibles sont nettement plus faibles, ce qui suggère que les niveaux élevés de métaux sont probablement liés à des phases détritiques et que leur mobilité et leur biodisponibilité sont limitées.

Mots clés : Arctique canadien, sédiments marins, éléments traces métalliques, dynamique sédimentaire, indices de pollution, communautés nordiques

## ABSTRACT

The main objective of this research project is to characterize the spatial distribution of major and trace elements in marine sediments in the Canadian Arctic in order to assess metal contamination. To achieve this, multiple samples of surface marine sediments collected across the study area were analyzed for their chemical composition.

The first chapter of this project aims to define the sedimentary dynamics of the Canadian Arctic. The provenance, transport mechanisms and depositional conditions of the sediments were determined from the total concentration of major and trace elements, organic carbon content and grain size of the samples. Then, the study area, being vast and presenting heterogeneous oceanographic and geological contexts, was delimited according to these parameters. The data obtained, combined with multivariate analyses, revealed great variability in the chemical composition of the seabed, which could be described according to three chemical groups. This geochemical characterization identified the Mackenzie River as the main contributor of metals, and the Beaufort Sea shelf as the area most sensitive to enrichment. The applicability of pollution indices was assessed using different geochemical backgrounds, including a regional background based on pre-industrial marine sediments. The enrichment factor and geo-accumulation index revealed generally low levels of enrichment and metal contamination in surface sediments compared with natural regional values.

The second chapter establishes a baseline of trace metal concentrations in surface sediments in the Canadian Arctic. The aim is to gain a better understanding of their sources and transport in the Arctic marine environment, and to assess their ecological risk. Metals were measured in the acid-extractable fraction of sediments, targeting the most bioavailable part. The regional variability of acid-extractable metals closely mirrors that of total concentrations of major and trace elements, indicating that natural lithology and sedimentary processes control their distribution. The Mackenzie River is the main source of metals, with the highest concentrations in its plume boundary. However, rare earth elements are mostly concentrated along the Baffin Island coast, originating from the lithologies of the Canadian Shield. Pollution indices indicate generally low levels of enrichment or contamination, but moderate levels of As are measured in the sediments of the Beaufort Sea and Jones Sound. According to the Canadian Sediment Quality Guidelines, most samples show concentrations below the Probable Effects Level, although it is exceeded for As and Ni in some samples from Amundsen and Coronation gulfs, Jones Sound and Baffin Bay. Overall, the trace element composition of sediments reflects natural levels linked to geology and regional sedimentary dynamics.

Finally, the third chapter assesses local metal contamination in northern communities of the Canadian Arctic. Total and acid-extractable metal concentrations were measured in coastal sediments from six Inuit communities and from Milne Inlet, home to Mary River harbor. Overall, results were consistent with regional variability. The sites of Tuktoyaktuk, Resolute Bay, Grise Fiord, Qikiqtarjuaq and Milne Inlet show natural levels of metals. However, adverse biological effects on aquatic fauna are possible at Tuktoyaktuk due to high natural inputs from the Mackenzie River. At Pond Inlet, the chemical composition of sediments primarily reflects the local geology. However, lithological variability along the coast leads to occasionally elevated concentrations of trace metals, and localized anthropogenic inputs are also suspected. At Kugluktuk, results revealed high total V and Cr concentrations, possibly resulting from a mixture of natural and local anthropogenic sources. The main sources would be the erosion of ultramafic intrusions carried by the Coppermine River and nearby wastewater discharges. However, concentrations of acid-extractable metals are significantly lower, suggesting that elevated metal levels are probably related to detrital phases, and that their mobility and bioavailability are limited.

*Keywords*: Canadian Arctic, marine sediments, trace metals, sediment dynamics, pollution indices, northern communities

## TABLE DES MATIÈRES

## LISTE DES TABLEAUX

## LISTE DES FIGURES

## LISTE DES ABRÉVIATIONS, DES SIGLES ET DES ACRONYMES

| | |
|---|---|
| **AC / CA** | Arctique canadien / *Canadian Arctic* |
| **ACC** | Courant côtier de l'Alaska (pour *Alaska Coastal Current*) |
| **AMAP** | Programme de surveillance et d'évaluation de l'Arctique (pour *Arctic Monitoring and Assessment Programme*) |
| **ApW** | Eaux arctiques d'origine Pacifique (pour *Arctic waters of Pacific origin*) |
| **AS** | Schiste moyen (pour *Average shale*) |
| **AW** | Eaux atlantiques (pour *Atlantic water*) |
| **CC** | Groupe chimique (pour *Chemical cluster*) |
| **CCME** | Conseil canadien des ministres de l'environnement / *Canadian Council of Ministers of the Environment* |
| **CEP / PEL** | Concentration produisant un effet probable / *Probable effect level* |
| **clr** | Rapport log-ratio centré (pour *Centered log-ratio*) |
| **COT/TOC** | Carbone organique total / *Total organic carbon* |
| **CSE / TEL** | Concentration seuil produisant un effet / *Threshold effect level* |
| **CSQG** | Recommandations canadiennes pour la qualité des sédiments (pour *Canadian Sediment Quality Guidelines*) |
| **DL** | Limite de détection (pour *Detection limit*) |

| | |
|---|---|
| **ED-XRF** | Spectromètre de fluorescence X à dispersion d'énergie (pour *Energy Dispersive X-ray Fluorescence*) |
| **EF** | Facteur d'enrichissement (pour *Enrichment factor*) |
| **ER** | Facteur de risque écologique (*Ecological Risk Factor*) |
| **ETM** | Éléments traces métalliques |
| **ETR/REE** | Éléments des Terres Rares / *Rare Earth Elements* |
| **HREE** | Éléments des Terres Rares Lourds (pour *Heavy Rare Earth Elements*) |
| **ICP-QQQ** | Spectrométrie de masse par plasma à couplage inductif à triple quadrupôles (pour *Triple Quadrupole Inductively Coupled Plasma Mass Spectrometry*) |
| **Igeo** | Indice de géo-accumulation (pour *Geo-accumulation index*) |
| **LOI** | Perte au feu (pour *Loss on ignition*) |
| **LREE** | Éléments des Terres Rares Légers (pour *Light Rare Earth Elements*) |
| **NGCC/CCGS** | Navire de la Garde côtière canadienne / *Canadian Coast Guard Ship* |
| **NOW** | Polynie des eaux du Nord (pour *North Water Polynya*) |
| **PAAS** | Schiste précambrien australien (pour *Post-Archean Australian Shale*) |
| **PCA** | Analyses par composantes principales (pour *Principal Component Analysis*) |
| **PML** | Couche de mélange polaire **(**pour *Polar mixed layer*) |
| **UCC** | Croûte continentale supérieure (pour *Upper Continental Crust*) |

# INTRODUCTION GÉNÉRALE

## 1. CONTEXTE ET PROBLEMATIQUE

Les éléments traces métalliques (ETM) regroupent les métaux et les métalloïdes retrouvés en très faible concentration (<1000 mg/kg) dans la croûte terrestre ou tout autre milieu naturel donné (Alloway, 2012). Certains sont connus sous le nom de métaux lourds, un terme imprécis définissant les ETM ayant une densité supérieure à 3.5-7 g/cm$^3$ (Duffus, 2002), comme le cuivre (Cu), le zinc (Zn), le cadmium (Cd), le mercure (Hg) et le plomb (Pb). Parmi les ETM, on retrouve aussi l'important groupe des éléments des terres rares (ETR) qui est composé des lanthanides, de l'yttrium (Y), et parfois du scandium (Sc), bien que ce dernier ait un comportement géochimique différent (Barrat & Bayon, 2024).

Les ETM se retrouvent et circulent naturellement dans toutes les réservoirs terrestres via différents processus, tels que l'érosion du socle rocheux, les éruptions volcaniques ou encore les feux de forêt (Figure 1). La lithosphère, soit la croûte continentale et océanique, représente la source initiale des métaux et aussi le réservoir principal qui les stocke à des échelles géologiques (Alloway, 2012). Ainsi, la géologie exposée (roche mère et dépôts superficiels) influence indirectement la concentration d'ETM retrouvée dans les milieux environnants. Les sols et les sédiments sont également d'importants réservoirs d'ETM à long terme, suivis par l'hydrosphère et l'atmosphère (Simon, 2014). Les ETM sont retrouvés sous forme élémentaire, ionique et sous forme de différentes molécules organiques ou inorganiques. La forme dans laquelle se trouve un élément trace va influencer son mode de transport, son interaction avec les organismes vivants et sa déposition (Bini & Bech, 2014). Certains ETM comme le Cu et le Zn sont des nutriments essentiels en faible concentration,

mais à des concentrations élevées et sous certaine spéciation, tous les ETM peuvent être toxiques pour la flore et la faune, incluant les humains (Alloway, 2012).

Bien que les ETM puissent être introduits dans l'environnement par des processus naturels, les activités anthropiques sont devenues, au cours des dernières décennies, une source majeure de plusieurs de ces éléments (Alloway, 2012; Pacyna & Pacyna, 2001; Sen & Peucker-Ehrenbrink, 2012; Zhu et al., 2020). Les humains perturbent les cycles biogéochimiques naturels en augmentant la remobilisation et la redistribution des ETM, notamment par le biais d'activités minières et industrielles (Macdonald et al., 2000; Macdonald & Bewers, 1996). La combustion des énergies fossiles constitue aujourd'hui la principale source anthropique. Ainsi, la contamination en ETM, définie comme la présence de concentrations anormalement élevées, est un phénomène observé depuis plusieurs années dans différents milieux naturels (Nriagu & Pacyna, 1988).

Tout comme les autres ETM, les ETR sont considérés comme des contaminants préoccupants (González et al., 2015). Depuis les années 1980, la demande industrielle de ETR a augmenté de manière exponentielle (US EPA, 2012). Ces métaux sont désormais considérés comme hautement stratégiques et sont indispensables dans de nombreux domaines critiques, tels que la fabrication d'aimants et de catalyseurs (NRCAN, 2024). La constante augmentation de l'extraction et du traitement des ETR a pour conséquence l'émergence de nouvelles voies de pollution. En effet, les cas de contamination par les ETR sont récemment apparus dans la littérature (González et al., 2015). Au Canada, il y a d'importantes réserves d'ETR et plusieurs projets d'exploration sont déjà en cours, mais l'Arctique canadien (AC) reste largement intouché pour l'instant (NRCAN, 2024).

Bien que les régions arctiques soient éloignées des grands centres urbanisés et demeurent faiblement peuplées, elles sont également confrontées à des problèmes de contamination en métaux. À la fin des années 1990, le *Arctic Monitoring and Assessment Programme* (AMAP) a conclu que les ETM représentaient un risque pour les écosystèmes et les communautés biotiques de l'Arctique (AMAP, 1998, 2005). Au Canada, le Programme de lutte contre les contaminants dans le Nord a également identifié les métaux tels que le Cd,

Hg et Pb comme des contaminants préoccupants pour l'AC (Jensen et al., 1997). Plusieurs études ont depuis démontré la présence de contaminations en Cd, Pb, Hg et Zn dans les régions arctiques, en lien avec diverses activités anthropiques (AMAP, 1998, 2005, 2011, 2021; Bartley et al., 2024; Cai et al., 2011; Choudhary et al., 2023; Macdonald et al., 2005; Zheng et al., 2022).

Depuis plusieurs années, des programmes tels que l'AMAP et le Programme de lutte contre les contaminants dans le Nord assurent le suivi de la pollution par les ETM dans les écosystèmes arctiques. Leur objectif est d'approfondir les connaissances sur le comportement et les effets des ETM dans ces milieux sensibles (AMAP, 1998; 2005; 2021 ; Bidleman et al., 2003; Chételat and Braune, 2012; Jensen et al., 1997; Stow et al., 2017). Pour ce faire, il est essentiel de documenter les niveaux et tendances actuels, les voies d'entrée, ainsi que les processus qui contrôlent leur distribution et leurs impacts sur la faune, la flore et les populations humaines. Malgré les nombreuses études menées, d'importantes lacunes subsistent, notamment dans l'AC. Cette thèse s'inscrit dans le cadre de ces suivis en fournissant de nouvelles données sur les niveaux actuels d'ETM dans les sédiments marins d'une grande partie de l'AC. Ces données contribuent à une meilleure compréhension des sources et processus naturels, ainsi que des risques associés aux changements climatiques.

# 2. LES ETM DANS L'ENVIRONNEMENT

## 2.1 Origines et processus

### 2.1.1 Sources naturelles

La croûte terrestre est composée à ~99% de dix éléments majeurs (O, Si, Al, Fe, Ca, Na, K, Mg, P et Ti), alors que les 1% restant est composé des autres éléments du tableau périodique, les éléments traces, dont la majorité sont des ETM (Alloway, 2012). Les

concentrations en ETM dans la croûte varie significativement selon le type de roches retrouvées. Ainsi, les roches mafiques comme le gabbro et le basalte sont riches en Cu, Mn, V and Zn, alors que les roches ultramafiques (péridotites, serpentinites) sont riches en Co, Cr et Ni. Le tableau 1 présente la composition de différents types de lithologies. Les éléments traces sont incorporés dans la structure des minéraux primaires des roches lors de leur cristallisation, souvent par substitution d'ions (Alloway, 2012). Il y a également les minéraux lourds qui peuvent être composés à partir de métaux, comme la chromite ($FeCr_2O_4$) ou la galène (PbS). Les minéraux ferromagnésiens comme les pyroxènes sont associés à un nombre important d'ETM, alors que les roches felsiques sont plus pauvres en métaux (Turekian & Wedepohl, 1961). Les roches sédimentaires sont héritées de l'altération physique et chimique des roches ignées et métamorphiques. Ainsi, selon la roche initiale et le type d'altération, le contenu en ETM varie grandement d'une roche sédimentaire à l'autre. Par exemple, les grès, composés de minéraux primaires résistants comme le quartz, ont tendance à contenir peu de métaux alors que les schistes, composés de minéraux secondaires fins comme les argiles, peuvent avoir des concentrations élevées en As, Cd, Cu, Mo, Pb, U, V et Zn (Turekian & Wedepohl, 1961). Il y a également les gisements métalliques, une accumulation substantielle de métaux se trouvant dans différents contextes naturels, tels que les sulfures massifs volcanogènes (Yardley, 2005).

L'érosion et l'altération des roches sources transfèrent les métaux vers les sols. Comme les minéraux ferromagnésiens, riches en ETM, s'altèrent relativement rapidement, les sols dérivés des géologies mafiques sont généralement riches en ETM. Les roches felsiques, plus pauvres en métaux, s'altèrent plus difficilement, résultant en des sols plus pauvres en métaux. Le volcanisme joue également un rôle clé dans la circulation des ETM entre la lithosphère et les autres sphères terrestres. Les éruptions volcaniques émettent dans l'atmosphère et l'hydrosphère des gaz riches en métaux volatils, parfois en quantités comparables à celles présentes dans certains gisements minéraux (Edmonds et al., 2022). Par la suite, ces éléments sont redistribués entre les sols, les masses d'eau, l'atmosphère et la cryosphère par le biais de processus tels que l'évaporation, les précipitations, le gel-dégel et l'érosion (Figure 1).

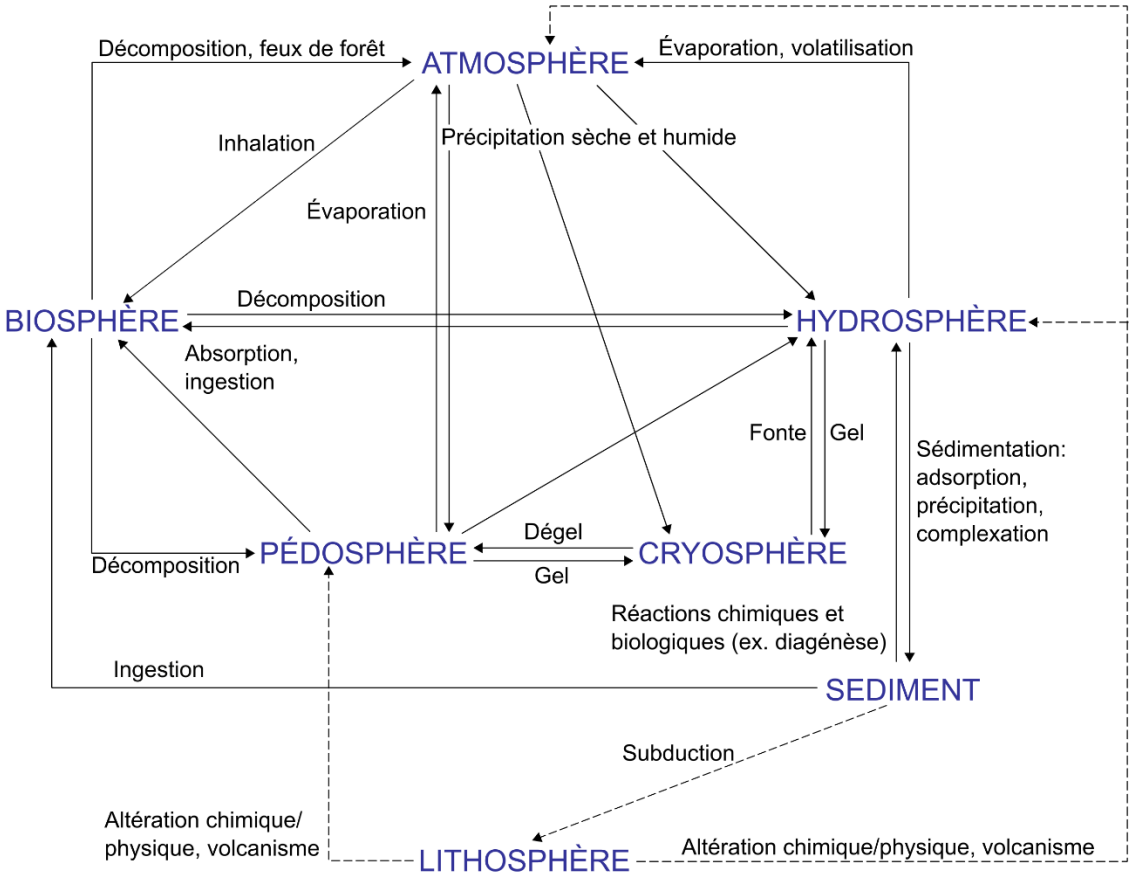


Figure 1. Principaux processus liés aux cycles biogéochimiques des ETM dans l'environnement. Figure adaptée de Paasivirta (1991) et Pelletier (2021). Les flèches en pointillé indiquent les processus se produisant à l'échelle géologique et les flèches pleines représentent des processus plus rapides (à l'échelle annuelle ou centennale).

L'absorption biologique des plantes et des microorganismes joue un rôle important dans les cycles biogéochimiques de plusieurs ETM. En effet, plusieurs ETM, tels que le Ni, Cu, Zn, V, et Co sont des micronutriments essentiels, tandis que d'autres, comme la As et le Se, bien que non essentiels, peuvent tout de même être utilisés par certains organismes (e.g. Duncan et al., 2015; Glabonjat et al., 2021). Les processus biotiques peuvent entraîner l'accumulation d'ETM dans la biomasse. La bioaccumulation, définie comme l'augmentation progressive de la concentration d'une substance chimique dans un organisme au fil du temps, est un phénomène bien documenté pour les ETM (Rainbow, 2007). Qu'ils

soient essentiels ou non, ces éléments ont tendance à s'accumuler plus rapidement qu'ils ne sont excrétés par les organismes. Ce phénomène peut aussi se transmettre le long de la chaîne alimentaire, et donc certains métaux s'accumulent dans les tissus des prédateurs. Les composés organométalliques sont particulièrement connus pour leur capacité à subir une bioamplification (Jenkins, 2004). Par ailleurs, bien que l'utilisation des ETR par les organismes ait été observée, les connaissances à ce sujet demeurent encore limitées (Barrat & Bayon, 2024).

La biosphère peut réémettre les ETM à l'environnement par la décomposition de la matière organique (MO) et par les feux de forêts (Isley & Taylor, 2020; Sutton et al., 2024). Toutefois, les métaux peuvent demeurer stockés dans la MO réfractaire. Ceci est observé à moyen terme (échelle centennale à millénaire) dans les milieux humides (Gambrell, 1994), le pergélisol (O'Donnell et al., 2024; Skierszkan et al., 2024) et les sédiments marins (Faust et al., 2021) et à long terme (échelle géologique) dans les schistes noirs (Alloway, 2012).

### 2.1.2 Sources anthropiques

Une évaluation globale des émissions anthropiques d'ETM a été publiée en 2001 (Pacyna & Pacyna, 2001). Elle a révélé les secteurs ayant le plus d'impact sur l'environnement dans les années 1980 et 1990. Zhu et al. (2020) ont ensuite dressé un inventaire des émissions mondiales de 12 ETM entre 1995-2012 (Figure 2). Dans leur inventaire, les auteurs ont conclu qu'il y a une diminution globale des émissions anthropiques d'ETM entre 1995 et 2012, avec un déclin annuel de 1%. Selon ces études, la combustion d'énergie fossile demeure le secteur émettant les plus grandes quantités d'ETM (notamment de Cr, Hg, Mn, Mo, Ni, Se, V). En effet, les métaux ont tendance à s'accumuler dans la MO et peuvent y être stockés à long terme. Les énergies fossiles sont issues de la combustion de cette MO préservée, sous forme de charbon, d'hydrocarbure ou de schistes bitumineux (Schobert, 2014). Ce processus libère des métaux qui étaient jusque-là séquestrés dans les roches sédimentaires. Après la combustion des énergies fossiles, l'étude de Zhu et al. (2012) révèle que la production de métaux non ferreux constitue le secteur industriel le plus polluant. Des

éléments tels que l'As, le Cd, le Cu, le Ni et le Zn proviennent principalement de ce secteur. En troisième position parmi les principales sources d'émissions, on retrouve la circulation automobile, notamment en ce qui concerne les particules fines. L'usure des freins contribuerait pour 42 à 75% des émissions de Sb et Cu en 2012. La production de métaux ferreux ainsi que la gestion des déchets solides et des eaux usées figurent également parmi les sources principales d'émissions métalliques.

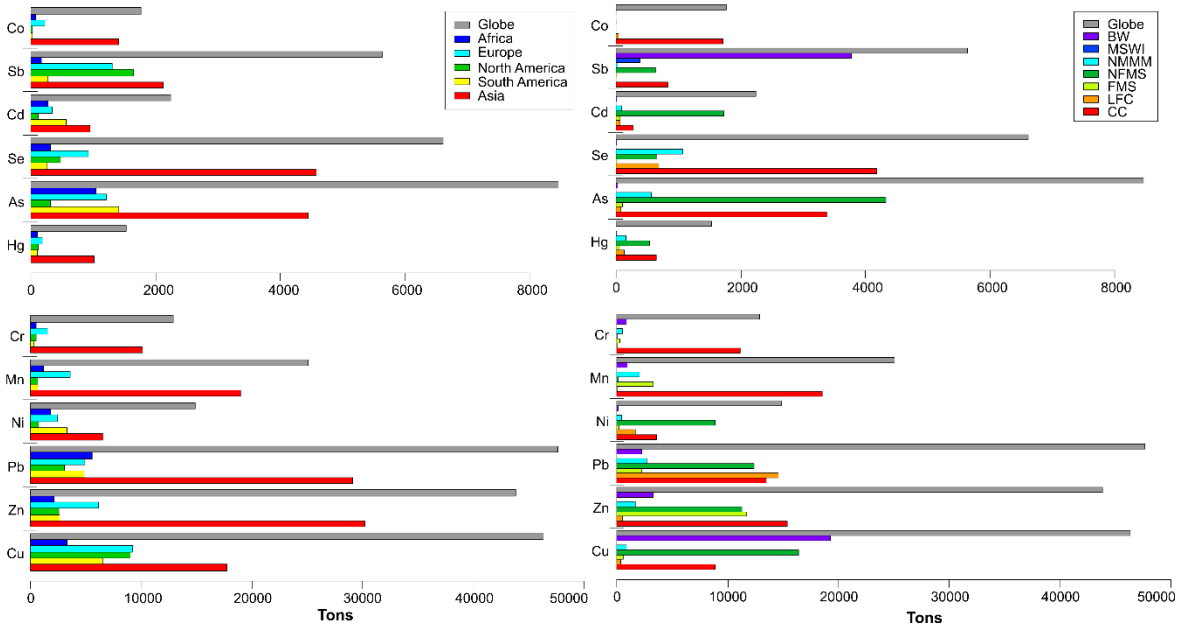


Figure 2. Émissions anthropiques d'ETM selon l'inventaire de 2012 par Zhu et al. (2020). Graphiques de gauche : Émissions selon les continents. Graphiques de droit : émissions selon les secteurs. BW : usure des freins; MSWI : incinération des déchets solides municipaux; NMMM : fabrication de minéraux non métalliques; NFMS : fusion de métaux non ferreux; FMS : fusion de métaux ferreux; LFC : combustion de combustibles liquides; CC : combustion de charbon.

Le transport des ETM issus de sources anthropiques vers les milieux naturels s'effectue à la fois par des rejets directs provenant de sources ponctuelles et par des rejets indirects, mobilisés par les processus de transport naturels. L'atmosphère, les océans et les rivières constituent les principaux vecteurs de dispersion des contaminants à grande échelle (Macdonald et al., 2000). Parmi ces mécanismes, le transport atmosphérique est le plus important, car les vents dominants peuvent entraîner les contaminants sur de très longues

distances en quelques jours. Les ETM peuvent être sous forme gazeuse ou particulaire (ex. aérosols), et leur transfert vers les sols ou les milieux aquatiques s'effectue par échange gazeux, déposition sèche ou déposition humide via les précipitations. Le transport océanique, notamment par les courants de surface, peut également disperser les contaminants sur de grandes distances. Par exemple, des polluants émis dans les zones industrialisées des basses latitudes peuvent atteindre l'Arctique en quelques années. Finalement, les rivières jouent un rôle crucial dans le transfert des contaminants provenant de sources terrestres vers les milieux marins. Les métaux y sont transportés soit sous forme dissoute, soit associés à des particules ou à des complexes organiques dissous.

## 2.2 Les sédiments marins

En milieu aquatique, les éléments traces peuvent se retrouver dans la colonne d'eau, dans le biote ou dans les sédiments (Figure 3). Les éléments traces dissous dans la colonne d'eau s'associent rapidement aux particules en suspension, puis sont transportés vers le fond, où ils s'accumulent dans les sédiments (Smrzka et al., 2019). À la mort des organismes, les éléments traces présents dans le biote, après plusieurs cycles de captation biologique, sont également transférés vers les sédiments (Tessier & Campbell, 1987). Par conséquent, les sédiments lacustres et marins constituent un puits important pour les éléments traces, jouant un rôle clé dans leur stockage à long terme (Calvert & Pedersen, 1993).

La répartition des ETM entre les phases liquide et solide dans la colonne d'eau et les sédiments dépend de plusieurs facteurs environnementaux, comme le potentiel redox, le pH et l'activité biologique (Tessier & Campbell, 1987). En effet, les ETM peuvent passer d'une forme dissoute, sous forme d'ions libres ou de complexes moléculaires, à une forme particulaire, en se fixant à d'autres particules. La spéciation d'un métal, soit sa forme chimique et structurale, influence ses interactions avec les particules, et par conséquent sa solubilité, sa mobilité et sa biodisponibilité. Les particules capables de transporter et retenir les métaux dans les sédiments, appelées les phases porteuses, incluent principalement les

(oxyhydr)oxydes de Fe et Mn, les sulfures de Fe, la MO et les argiles (Tessier & Campbell, 1987; Tribovillard et al., 2006). Les ETM peuvent être : adsorbés à la surface des oxydes, des argiles ou de la MO, coprécipités avec les carbonates, les sulfures ou les oxydes ou encore complexés avec des ligands organiques (ex. substances humiques) ou inorganiques (ex. ions carbonates), ce qui influence leur maintien en phase dissoute ou particulaire (Smrzka et al., 2019).

Les métaux dans les sédiments peuvent être inertes, non-labiles ou labiles, c'est-à-dire maintenus dans les sédiments sous une forme très résistante, stable et instable face aux changements des conditions environnementales, respectivement (Alloway, 2012). La fraction la plus labile représente les métaux adsorbés faiblement aux particules par l'intermédiaire de molécules d'eau (physisorption). Il s'agit de la fraction dite échangeable (Tessier et al., 1979). Les métaux associés aux carbonates sont également labiles, car une faible diminution du pH peut mener à la dissolution des carbonates et la libération des ETM dans l'eau. Les ETM adsorbés directement aux oxydes de Fe-Mn (chimiosorption) sont plus stables que ceux fixés par physiosorption, mais les oxydes sont sensibles aux conditions redox et peuvent se dissoudre en conditions réductrices. Les oxydes amorphes ou mal cristallisés (minéraux authigéniques) sont plus sensibles que les formes cristallines (ex. goethite). Inversement, la MO et les métaux adsorbés à sa surface ou absorbés par captage biologique sont sensibles à l'oxydation (Tessier, 1979). La fraction résiduelle représente la fraction non-labile des métaux. Elle correspond aux ETM intégrés dans le réseau cristallins des minéraux primaire ou secondaires, notamment dans les aluminosilicates. Dans ce cas, les métaux sont fixés par chimiosorption dans la structure interne des feuillets argileux. On considère que ces métaux ne peuvent pas être libérés dans des conditions environnementales normales (Tessier et al., 1979). Finalement, les métaux inertes sont ceux dans la structure interne de minéraux résistants, comme les minéraux lourds, ou de MO réfractaire.

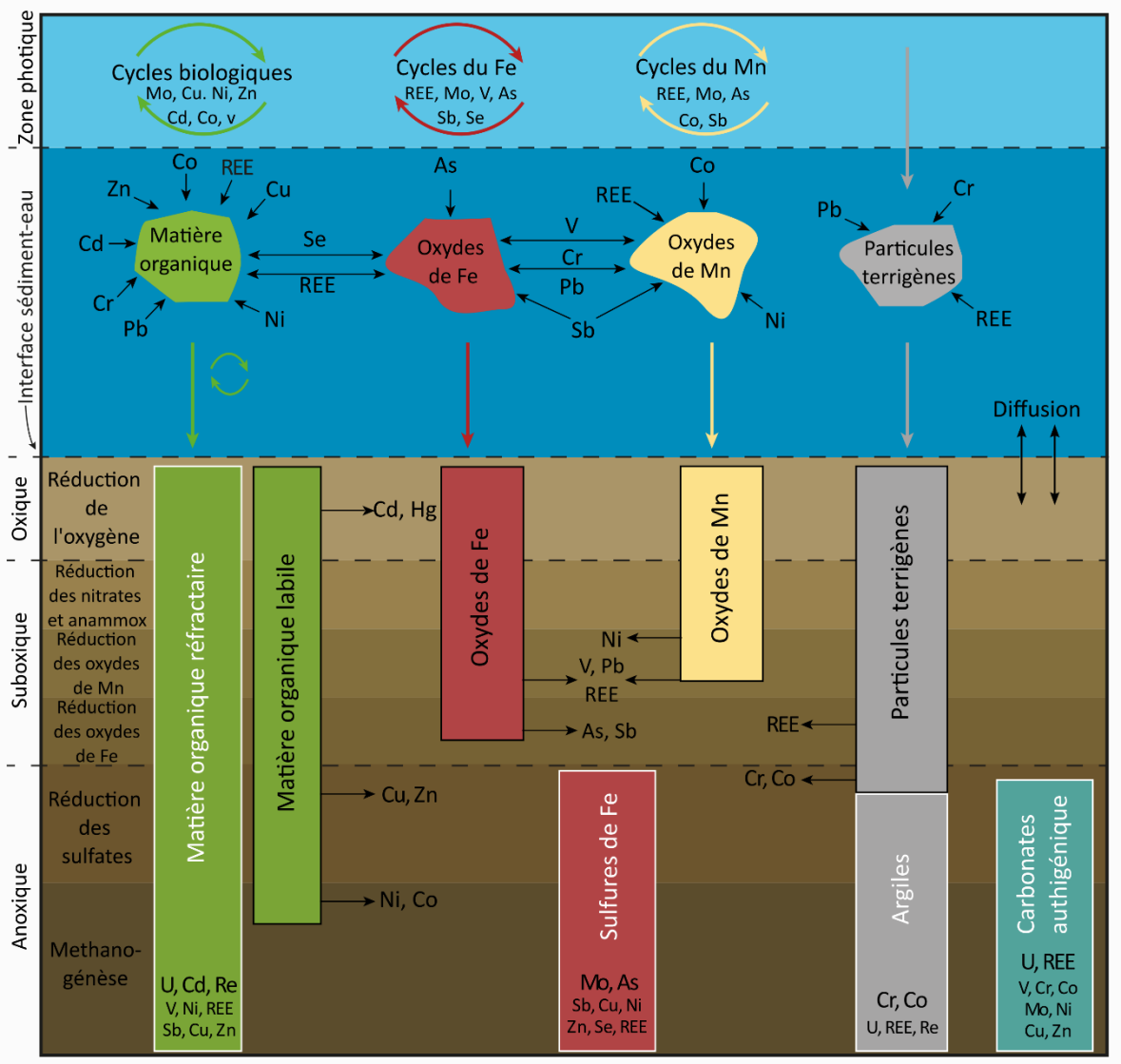


Figure 3. Schéma illustrant les principaux mécanismes contrôlant la distribution et la spéciation des éléments traces dans la colonne d'eau, les sédiments et les eaux interstitielles. Schéma modifié de Smrzka et al. (2019). Les flèches noires représentent les processus de sorption et les flèches de couleur représentent le trajet des éléments. Les sources relarguant les éléments traces dans les eaux interstitielles sont schématisé par un encadré noir, alors que les puits à long terme sont schématisés par un encadré blanc.

Les sédiments ne sont pas seulement une archive enregistrant les conditions géochimiques du milieu aquatique sus-jacent. Ils participent activement à ces conditions, notamment lors de la diagenèse précoce. À la surface des sédiments, la MO est reminéralisée

par les bactéries, d'abord en utilisant l'oxygène dissous, puis, une fois l'oxygène épuisé, en recourant à d'autres oxydants comme les nitrates, les oxydes de Fe-Mn, ainsi que les sulfates (Figure 3). La dégradation de la MO entraîne la libération d'éléments traces qui y étaient associés (ex. Cd, Cu, Zn) dans les eaux interstitielles. Ce processus s'accompagne également de la réduction des oxydes de Fe-Mn, ce qui libère d'autres éléments traces, comme l'As et le V (Tribovillard et al., 2006). Les éléments dissous dans les eaux interstitielles peuvent ensuite diffuser vers la colonne d'eau ou se fixer à des minéraux authigènes comme des sulfures, des carbonates et des argiles (Smrzka et al., 2019; Tribovillard et al., 2006). Les éléments traces piégés en profondeur dans les minéraux authigènes ou dans la MO réfractaire se trouvent alors dans une phase stable et peu mobile, ce qui permet leur séquestration à long terme. Par contre, des changements dans les taux de sédimentation, l'apport en MO, l'oxygénation ou le pH de la colonne d'eau, ainsi que des processus comme la bioturbation ou la remise en suspension des sédiments, peuvent modifier l'activité diagenétique et entraîner la libération d'éléments traces vers la colonne d'eau (Chapman et al., 1998; Tessier & Campbell, 1987).

Un enrichissement ou un appauvrissement en ETM dans les sédiments dépend non seulement de leur concentration dans le milieu aquatique, mais aussi de plusieurs facteurs biotiques et abiotiques. Les conditions d'oxydo-réduction, tant dans les sédiments que dans la colonne d'eau, influencent la solubilité des phases porteuses ainsi que celle des ETM eux-mêmes (Yuan et al., 2021). Plusieurs ETM sont sensibles aux conditions redox (p. ex. As, Cr, V), car ils tendent à être plus solubles en milieu oxydant et moins solubles en milieu réducteur, ce qui entraîne leur enrichissement dans les environnements anoxiques (Tribovillard et al., 2006). La minéralogie et la granulométrie des sédiments influencent l'affinité des ETM pour les particules. D'une part, la présence de phases porteuses favorise leur élimination de la colonne d'eau par sédimentation. D'autre part, il est bien reconnu que les sédiments fins contiennent généralement davantage d'ETM, en raison de leur surface spécifique plus élevée qui favorise l'adsorption (Chen et al., 2016). Enfin, la productivité primaire dans les eaux de surface joue un rôle important, car elle capte plusieurs ETM

dissous, qui sont ensuite transférés vers les sédiments à la mort des organismes (Smrzka et al., 2016).

Cette dynamique des ETM entre les phases dissoutes et les phases solides labiles et non-labiles est importante pour étudier leur mobilité et biodisponibilité. La biodisponibilité d'un métal est la capacité de ce dernier à être absorbé par un organisme. Par exemple, la forme la plus biodisponible est les ions libres ($Cd^{2+}$, $Cu^{2+}$, $Zn^{2+}$, etc.), qu'on peut retrouver dans les eaux interstitielles ou encore à l'interface eau-sédiment (Alloway, 2012). Les composés organiques comme le méthyl-mercure sont également facilement assimilables pour les organismes (Pickhardt & Fisher, 2007). Les risques écotoxicologiques liés aux ETM dans l'environnement marin peuvent donc être estimés par la mesure des concentrations dans les sédiments de surface et par l'évaluation de la toxicité via la spéciation, la mobilité et la biodisponibilité (Chapman et al., 1998).

## 2.3 Les ETM à l'étude

La grande majorité des éléments traces ont été évalués dans le cadre de cette étude. Toutefois, certains ETM ont fait l'objet d'une évaluation plus approfondie, en raison de leur potentiel écotoxicologique élevé et/ou de leur présence à des concentrations anormalement élevées dans l'AC. Toutes les concentrations discutées ci-dessous sont présentés sous forme de microgramme (µg) par gramme (g) de poids sec.

### 2.3.1 Arsenic (As)

L'As est un métalloïde jugé non essentiel aux organismes vivants (CCME, 1999), mais il est tout de même utilisé comme micronutriment par le phytoplancton dans l'océan (Andreae, 1979; Azizur Rahman et al., 2012). On retrouve l'As dans quatre états d'oxydation (5+, 3+, 0 et 3-) et sous formes inorganique et organométallique. L'arséniate $AsO_4^{3-}$ et l'arsénite $AsO_3^{3-}$ sont les deux espèces dissoutes les plus courantes dans les eaux oxiques et

anoxiques, respectivement (Andreae, 1979; Kalia & Khambholja, 2023). En milieu oxique, l'As a tendance à s'associer avec les (oxyhydr)oxydes métalliques et tout particulièrement avec les oxydes de Fe (Chaillou et al., 2003). La spéciation de l'As, dépendante du pH et du potentiel d'oxydoréduction (Belzile, 1988; Belzile & Tessier, 1990; Edenborn et al., 1986) contrôle sa mobilité et sa toxicité (De Vitre et al., 1991; Kalia & Khambholja, 2023). Une fois dans les sédiments, l'As est mobilisé dans la zone de réduction du Fe (Chaillou et al., 2003). L'As dissout diffusant vers le haut peut se fixer par adsorption ou coprécipitation dans la zone oxique ou être libéré dans la colonne d'eau. L'As qui diffuse vers le bas est incorporé dans les sulfures de Fe, qui deviennent des puits à long terme (Acquavita et al., 2021; Belzile & Lebel, 1986; Chaillou et al., 2003). Les micro-organismes présents dans les sédiments peuvent aussi transformer l'As inorganique en une forme organique, telle que des acides, pouvant s'accumuler dans les organismes aquatiques (Azizur Rahman et al., 2012; Francesconi & Edmonds, 1996).

La concentration d'As dans les différentes lithologies varie entre 1 et 10 µg/g (Tableau 1) et entre 5 et 10 µg/g dans les sédiments marins (CCME, 1999). Des concentrations variant entre 1 et 140 µg/g ont été mesurées dans les sédiments marins de l'Arctique (Budko et al., 2017; Budko et al., 2022; Holemann et al., 1999; Loring et al., 1998; Naidu et al., 2005; Trefry et al., 2013; Trefry & Neff, 2019; Wang et al., 2022; Zheng et al., 2022). Au Canada, des concentrations élevées d'As dans les sédiments ont été rapportées dans plusieurs zones affectées par des activités industrielles ou minières : de 6 à 3500 µg/g dans des lacs près de Yellowknife (Wagemann et al., 1978), de 3 à 74 µg/g dans la baie des Chaleurs à proximité de fonderies (Parsons & Cranston, 2006) et de 4 à 568 µg/g dans le port de Wine en Nouvelle-Écosse, près d'une ancienne mine d'or (Little et al., 2015).

### 2.3.2 Cadmium (Cd)

Le Cd est un élément non essentiel et hautement toxique pour les organismes vivants (Bernhoft, 2013; CCME, 1999, 2014). Dans l'eau et les sédiments, il présente un unique état d'oxydation, soit $Cd^{2+}$. En milieu marin, il se trouve principalement sous forme dissoute,

associé à des complexes de chlorure (Bini & Bech, 2014). Une fraction subsiste toutefois sous forme d'ion libre $Cd^{2+}$, peu soluble, mais représentant la forme la plus biodisponible et toxique (CCME, 2014). Bien qu'il ne soit pas un nutriment, le Cd présente un comportement similaire à celui de certains éléments nutritifs, avec un appauvrissement dans la zone photique (Tribovillard et al., 2006). Il est principalement apporté aux sédiments marins en association avec la MO, puis libéré dans les eaux interstitielles lors de la dégradation de celle-ci (Piper & Perkins, 2004). Le Cd tend à s'enrichir dans les sédiments sous conditions faiblement ou fortement réductrices (Rosenthal et al., 1995), probablement sous forme de sulfure (CdS; Bryan et al., 2021; Gobeil et al., 1987). Sa remobilisation à partir des sédiments est influencée par plusieurs facteurs, notamment le pH, les conditions d'oxydoréduction et la présence d'agents complexant dans l'eau (Gobeil et al., 1987).

La concentration moyenne du Cd dans la lithosphère est de ~0,1 µg/g (Tableau 1) et il est fortement chalcophile (Callender, 2005). Dans les sédiments marins canadiens, les concentrations moyennes varient entre 0.16 et 4.24 µg/g (CCME, 1999), alors que dans les sédiments marins arctiques, les concentrations se trouvent entre 0.01 et 0.9 µg/g (Budko et al., 2017; Budko et al., 2022; Cai et al., 2011; Choudhary et al., 2020; Holemann et al., 1999; Loring et al., 1998; Lu et al., 2013; Lu & Kang, 2018; Naidu et al., 2005; Trefry et al., 2013; Trefry & Neff, 2019; Wang et al., 2022). Les concentrations de Cd dans les sédiments marins contaminés sont de 0.2-64 µg/g dans les ports de Colombie-Britannique (Garrett, 1985) et de 0.02-69 µg/g à proximité de fonderies dans la baie des Chaleurs (Parsons & Cranston, 2006).

### 2.3.3 Cobalt (Co)

Le Co est un micronutriment essentiel pour le phytoplancton. Dans les environnements oxiques, le Co est présent sous les formes dissoutes de $Co^{2+}$ et de complexes avec la MO (Bini & Bech, 2014; Ellwood & van den Berg, 2001). Il est rapidement éliminé de la colonne d'eau par les oxydes de Mn. Dans les eaux anoxiques, le Co forme le sulfure insoluble CoS (Huerta-Diaz & Morse, 1992). Dans les sédiments, le Co est préférentiellement libéré dans la zone de réduction du Mn (Stockdale et al., 2010), puis se fixe au matériel clastique, qui

constitue un puits à long terme (Tribovillard et al., 2006). Par contre, le Co demeure très mobile dans les sédiments anoxiques, notamment lors de la dissolution des particules détritiques (Tribovillard et al., 2006).

La croûte terrestre supérieure contient une concentration moyenne de 10 µg/g, mais les concentrations peuvent dépasser 40 µg/g dans les roches mafiques et 100 µg/g dans les roches ultramafiques (Tableau 1). Le Co varie entre 0.1 et 42 µg/g dans les sédiments marins arctiques (Budko et al., 2017; Budko et al., 2022; Campbell & Loring, 1980; Choudhary et al., 2020; Holemann et al., 1999; Loring et al., 1998; Lu et al., 2013). Des concentrations autour de 89 µg/g ont été mesurées dans les sédiments marins de Little Bay Arm, à Terre-Neuve, dix ans après un déversement de résidus miniers (Veinott et al., 2003).

Tableau 1.

Composition chimique moyenne de différentes lithologies et de sédiments marins en µg/g, sauf pour Fe en %. UCC : croûte continentale supérieure. 1- données tirées Taylor and McLennan (1985); 2- données tirées de Turekian and Wedepohl (1961); 3- tableau modifié de Alloway (2012); 4- données tirées de Wedepohl (1971). ND : non-disponible.

| | | **Roches ignées** | | | **Roches sédimentaires** | | | | | **Sédiments profonds** | |
|---|---|---|---|---|---|---|---|---|---|---|---|
| | UCC[1] | Ultra-mafique[2] | Mafique[2] | Granodiorite, granite[3] | Schiste[2,4] | Carbonate[2] | Grès[3] | Schiste noir[3] | Charbon[3] | Carbonate[2] | Argile[2] |
| As | 1.5 | 1 | 2 | 3 | 10 | 1 | 0.5 | <500 | 10 | 1 | 13 |
| Ba | 550 | 0.4 | 330 | 600 | 580 | 10 | 300 | 67 | 250 | 190 | 2300 |
| Cd | 0.098 | ND | 0.22 | 0.1 | 0.8 | 0.035 | <0.04 | <240 | 1 | ND | 0.42 |
| Co | 10 | 150 | 48 | 4 | 19 | 0.1 | 0.3 | 67 | 10 | 7 | 74 |
| Cr | 35 | 1600 | 170 | 10 | 90 | 11 | 35 | <700 | 20 | 11 | 90 |
| Cu | 25 | 10 | 87 | 12 | 45 | 4 | 2 | <300 | 20 | 30 | 250 |
| Mn | 600 | 1650 | 1500 | 400 | 850 | 1100 | 100 | ND | 40 | 1000 | 6700 |
| Fe* | 3.5 | 9.43 | 8.65 | ND | 4.72 | 0.38 | ND | ND | ND | 0.9 | 6.5 |
| Mo | 1.5 | 0.3 | 1.5 | 1.5 | 2.6 | 0.04 | 0.3 | <570 | 3 | 3 | 27 |
| Ni | 20 | 2000 | 130 | 5 | 68 | 20 | 2 | <300 | 20 | 30 | 225 |
| Pb | 20 | 1 | 6 | 20 | 20 | 9 | 10 | <100 | 20 | 9 | 80 |
| Se | ND | 0.05 | 0.05 | ND | 0.6 | 0.08 | ND | ND | ND | 0.17 | 0.17 |
| Sb | 0.2 | 0.1 | 0.2 | 0.3 | 1.5 | 0.2 | 0.05 | <10 | 2 | 0.15 | 1 |
| V | 60 | 40 | 250 | 70 | 130 | 20 | 20 | <2422 | 40 | 20 | 120 |
| Zn | 71 | 50 | 105 | 50 | 95 | 20 | 20 | <2314 | 50 | 35 | 165 |

### 2.3.4 Chrome (Cr)

Le Cr est considéré comme un micronutriment essentiel par certains (CCME, 1999; US EPA, 2000) et non essentiel par d'autres organismes (Smrzka et al., 2019). En milieu marin oxique, le Cr est présent principalement sous la forme soluble de $Cr^{6+}$ ($CrO_4^{2-}$). Dans des conditions anoxiques, le $Cr^{6+}$ est réduit en $Cr^{3+}$, et peut se complexer avec la MO ou s'adsorber sur des oxyhydroxydes de Fe-Mn, puis est exporté vers les sédiments (Bruggmann et al., 2023; Calvert & Pedersen, 1993; Gorny et al., 2016). Dans les sédiments anoxiques, le $Cr^{3+}$ libéré de la MO reminéralisée n'est pas facilement piégé dans les sédiments sous forme de sulfure et peut être perdu dans la colonne d'eau sus-jacente (Bruggmann et al., 2023). Le Cr est modérément toxique pour les organismes aquatiques et le $Cr^{6+}$ est beaucoup plus toxique que le $Cr^{3+}$ (CCME, 1999).

Le Cr, un élément trace abondant dans la croûte terrestre, ses concentrations varient entre 35 µg/g dans la croûte continentale supérieure, 90 µg/g dans les shales et <1000 µg/g dans les roches ultramafiques (Tableau 1). Dans les sédiments marins du Canada, les concentrations varient entre 20 et 85 µg/g à travers le Canada (CCME, 1999) alors que dans l'Arctique, elles varient entre 9 et 149 µg/g (Budko et al., 2017; Budko et al., 2022; Cai et al., 2011; Campbell & Loring, 1980; Choudhary et al., 2020; Holemann et al., 1999; Loring et al., 1998; Lu et al., 2013; Lu & Kang, 2018; Naidu et al., 2005; Trefry et al., 2013; Trefry & Neff, 2019; Wang et al., 2022; Zheng et al., 2022). Près des sites industriels, des concentrations entre 89 et 31 000 µg/g ont été mesurées dans la région des Grands-Lacs (Nriagu & Kabir, 1995).

### 2.3.5 Cuivre (Cu)

Le Cu est un micronutriment essentiel, mais il devient toxique à des concentrations aussi faibles que 10 µg/g (Callender, 2005). En milieu marin oxique, le Cu est principalement présent sous forme de complexes organiques, mais aussi sous forme de complexes inorganiques et d'ions libres. Les ions libres $Cu^{+}$ et $Cu^{2+}$ figurent parmi les formes les plus

toxiques pour les organismes marins (Buck et al., 2007). Le Cu présente une distribution verticale typique des micronutriments, mais il est également transporté vers les sédiments par adsorption sur la MO et les oxyhydroxides de Fe-Mn (Calvert & Pedersen, 1993; Fernex et al., 1992). Dans les sédiments, la décomposition de la MO et/ou la réduction des oxyhydroxydes de Fe-Mn peuvent entraîner la libération du Cu dans les eaux interstitielles. En conditions réductrices, le $Cu^{2+}$ est réduit en $Cu^{+}$, qui peut alors être incorporé dans la pyrite ou former des sulfures CuS (Huerta-Diaz & Morse, 1992).

Le Cu est un métal modérément abondant dont la concentration moyenne dans la lithosphère supérieure est de 25 µg/g (Tableau 1). Des concentrations entre 4 et 123 µg/g ont été mesurées dans les sédiments marins du Canada (CCME, 1999), et entre 2 et 96 µg/g dans l'Arctique (Budko et al., 2017; Budko et al., 2022; Cai et al., 2011; Campbell & Loring, 1980; Choudhary et al., 2020; Holemann et al., 1999; Loring et al., 1998; Lu et al., 2013; Lu & Kang, 2018; Naidu et al., 2005; Trefry et al., 2013; Trefry & Neff, 2019; Wang et al., 2022; Zheng et al., 2022). Des sédiments pollués ont enregistré des teneurs de 3 – 200 µg/g dans la baie des Chaleurs (Parsons & Cranston, 2006) et en moyenne 373 µg/g à Little Bay Arm (Veinott et al., 2003).

### 2.3.6 Plomb (Pb)

Le Pb est un micronutriment non essentiel. Il se retrouve majoritairement sous forme d'ion libre $Pb^{2+}$, mais peut également exister sous les formes $Pb^{+}$ et $Pb^{4+}$. Le Pb peut former des composés organométalliques, qui sont biodisponibles, toxiques et bioaccumulants (Denton et al., 1997). Le Pb tétraéthyle, un composé organométallique, constituait la principale source de Pb atmosphérique avant 1990, lorsqu'il était encore utilisé comme agent antidétonant dans l'essence (Lavallée & Fedoruk, 1989). Selon le pH, le Pb peut fortement s'adsorber sur les oxydes de Fe-Mn, les argiles et la MO (Fernex et al., 1992; Nelson et al., 1999). Dans les sédiments, il est mobilisé près de la surface des sédiments lors de la dégradation aérobique de la MO, ainsi qu'à des profondeurs intermédiaires, lors de la

réduction des oxydes (Loring, 1978). Il peut être recapté par les sulfures (Huerta-Diaz & Morse, 1992).

La concentration moyenne de Pb de la croûte continentale supérieure, des schistes et des granites est de 20 µg/g (Tableau 1), et est comprise entre 15 et 50 µg/g des sédiments côtiers et estuariens dans le monde entier (Denton et al., 1997). Dans les sédiments marins canadiens, les concentrations moyennes varient entre 7 et 23 µg/g (CCME, 1999). Dans l'Arctique, les concentrations se situent entre 1 et 37 µg/g (Budko et al., 2017; Budko et al., 2022; Cai et al., 2011; Campbell & Loring, 1980; Choudhary et al., 2020; Holemann et al., 1999; Loring et al., 1998; Lu et al., 2013; Lu & Kang, 2018; Naidu et al., 2005; Trefry et al., 2013; Trefry & Neff, 2019; Wang et al., 2022; Zheng et al., 2022). Des concentrations atteignant 341 µg/g ont été mesurées dans des sédiments lacustres à proximité d'une mine d'or des Territoire du Nord-Ouest (Pelletier et al., 2020) et 2000 µg/g dans la baie des Chaleurs, à proximité de fonderies (Parsons & Cranston, 2006).

### 2.3.7 Nickel (Ni)

Le Ni est un micronutriment essentiel recyclé dans la colonne d'eau (Dupont et al., 2010). Les invertébrés constituent le groupe taxonomique le plus sensible à la toxicité du Ni et les connaissances sont limitées pour les espèces arctiques (Gauthier et al., 2021). Dans les milieux marins oxiques, le Ni se comporte comme un micronutriment et peut être présent sous forme de cations $Ni^{2+}$ solubles, mais il est surtout présent sous forme de carbonate de Ni soluble ($NiCO_3$) ou adsorbé/complexé avec la MO et les oxydes de Mn (Calvert & Pedersen, 1993). Lors de la décomposition de la MO, le Ni peut être libéré des complexes organiques dans les eaux interstitielles. Dans les sédiments modérément réducteurs, le Ni est libéré des eaux sus-jacentes en raison de l'absence de sulfures et d'oxydes de Mn. Dans les sédiments anoxiques, le Ni peut être incorporé dans la pyrite et co-enrichi avec le Cd, Co, Zn et Cu (Bruggmann et al., 2024; Huerta-Diaz & Morse, 1992). Dans des conditions oxiques, le Ni est capté par les oxydes de Mn (Bruggmann et al., 2024).

La concentration moyenne de Ni dans la croûte continentale supérieure est de 20 µg/g, mais elle peut atteindre 2000 µg/g dans les roches ultramafiques (Tableau 1). Dans les sédiments marins de l'Arctique, les concentrations varient entre 6 et 164 µg/g (Budko et al., 2017; Budko et al., 2022; Campbell & Loring, 1980; Choudhary et al., 2020; Holemann et al., 1999; Loring et al., 1998; Lu et al., 2013; Lu & Kang, 2018; Naidu et al., 2005; Trefry et al., 2013; Trefry & Neff, 2019; Wang et al., 2022; Zheng et al., 2022). Les sédiments pollués de Little Bay Arm présentent une teneur moyenne de 77 µg/g (Veinott et al., 2003).

### 2.3.8 Vanadium (V)

Le V est un nutriment essentiel pour le phytoplancton (Osterholz et al., 2014). Ces dernières années, le V a été classé comme un élément potentiellement toxique dans la même catégorie que le Pb, l'As et le Hg, selon l'Agence américaine de protection de l'environnement (USEPA; Naeem et al., 2007). Il possède différents états d'oxydation, mais il est principalement sous les formes oxydées $V^{5+}$ et $V^{4+}$. Le $V^{5+}$ est plus mobile, soluble et toxique que le $V^{4+}$ (Pinto et al., 2013). Dans les eaux oxiques et les océans de surface, le $V^{5+}$ est sous forme de vanadate et est facilement adsorbé sur les oxyhydroxydes de Fe-Mn (Tribovillard et al., 2006). Dans l'océan Arctique, le V dissout est majoritairement éliminé de la colonne d'eau et transporté vers les sédiments par les oxyhydroxydes de Fe (Whitmore et al., 2019). Dans les environnements fortement réducteurs, le $V^{5+}$ est réduit en $V^{4+}$, puis transféré vers les sédiments par adsorption ou complexation avec la MO. Lors de la réduction des oxydes dans les sédiments, le V est libéré sous forme de $V^{4+}$, qui peut ensuite s'associer à la MO. Le V est fortement enrichi dans les sédiments réducteurs, car il peut être réduit par le $H_2S$ en $V^{3+}$. Sous cette forme, il précipite en phases insolubles ou s'incorpore dans les argiles authigéniques (Breit & Wanty, 1991; Wanty & Goldhaber, 1992).

Les concentrations naturelles du V est de 60 µg/g dans la croûte continentale supérieure, 130 µg/g dans les schistes et 250 µg/g dans les basaltes (Tableau 1). Les concentrations en V dans les sédiments de surface varient entre 22 et 210 µg/g dans les sédiments marins arctiques (Budko et al., 2017; Budko et al., 2022; Campbell & Loring,

1980; Holemann et al., 1999; Loring et al., 1998; Naidu et al., 2005; Trefry & Neff, 2019). À Little Bay, les sédiments contaminés présentaient une concentration moyenne de 246 µg/g en V (Veinott et al., 2003).

### 2.3.9 Zinc (Zn)

Le Zn est un micronutriment essentiel, présentant un profil vertical typique dans la colonne d'eau, soit un appauvrissement dans les eaux de surface. En milieu marin oxique, le Zn est principalement présent sous forme de complexes avec la MO, mais il peut également exister sous forme d'ions solubles tels que $ZnCl^{+}$ et $Zn^{2+}$, cette dernière étant la forme la plus biodisponible (Calvert & Pedersen, 1993). Le Zn peut aussi être adsorbé sur des hydroxydes de Fe-Mn (Fernex et al., 1992). Lors de la décomposition de la MO et de la réduction des oxydes, il peut être libéré dans les eaux interstitielles. En conditions réductrices, le Zn peut être incorporé dans des phases sulfurées (Huerta-Diaz et Morse, 1992 ; Morse et Luther, 1999).

La teneur moyenne en Zn de la lithosphère est d'environ 80 µg/g (Callender 2003), variant de 50 µg/g pour les roches granitiques à ~100 µg/g pour les schistes et les roches basaltiques (Tableau 1). Les sédiments non contaminés contiennent généralement une concentration de Zn de l'ordre de 5-50 µg/g. Les concentrations varient de 8 à 391 µg/g dans l'Arctique (Budko et al., 2017; Budko et al., 2022; Cai et al., 2011; Campbell & Loring, 1980; Choudhary et al., 2020; Holemann et al., 1999; Loring et al., 1998; Lu et al., 2013; Lu & Kang, 2018; Naidu et al., 2005; Trefry et al., 2013; Trefry & Neff, 2019; Wang et al., 2022; Zheng et al., 2022), mais peuvent aller jusqu'à 1170 µg/g dans certaines régions du Canada (CCME, 1999). À proximité de sources polluantes, les valeurs sont de 11-1343 µg/g dans le lac Ontario, où sont présents des effluents industriels (Forsythe et al., 2010) et de 22-3200 µg/g dans la baie des Chaleurs, à proximité de fonderies (Parsons & Cranston, 2006).

### 2.3.10 Fer (Fe) et manganèse (Mn)

Le Fe n'est pas un élément trace, mais il interagit fortement avec ces derniers. Il est un macronutriment essentiel, limitant dans certains environnements marins (Sunda, 2012), mais ne l'est pas dans les eaux arctiques canadiennes, qui sont naturellement enrichis en Fe (Colombo et al., 2020; Jensen & Colombo, 2024). Dans l'eau de mer, Le Fe existe sous deux états d'oxydation : $Fe^{2+}$ et $Fe^{3+}$. En conditions oxiques, la forme dominante est $Fe^{3+}$, mais celle-ci devient rapidement insoluble en formant des oxyhydroxydes, qui sont éliminés de la colonne d'eau. Le $Fe^{2+}$, plus soluble, s'oxyde rapidement pour former également des oxyhydroxydes (Bruland & Rue, 2001). La majorité du $Fe^{3+}$ dissous est complexée par des ligands organiques produits par le phytoplancton en situation de carence en Fe (Gledhill & Buck, 2012). Dans les sédiments oxiques, les oxydes de Fe jouent un rôle important en tant que pièges pour les ETM. En conditions anoxiques, ces oxydes se dissolvent et le $Fe^{3+}$ est réduit en $Fe^{2+}$, qui peut soit diffuser vers la surface et se réoxyder, soit précipiter sous forme de sulfures de Fe, tels que la pyrite, un important piège à ETM à long terme (Huerta-Diaz & Morse, 1992). Les concentrations varient entre 0.7 et 6.9 % en poids sec dans les sédiments marins de l'océan Arctique (Budko et al., 2017; Budko et al., 2022; Holemann et al., 1999; Loring et al., 1998; Naidu et al., 2005; Trefry et al., 2013; Trefry & Neff, 2019; Wang et al., 2022).

Le Mn est un élément mineur essentiel aux organismes marins. Le Mn existe sous les états d'oxydations $Mn^{2+}$, $Mn^{3+}$ et $Mn^{4+}$. Le $Mn^{2+}$ est la forme la plus soluble et biodisponible, tandis que $Mn^{3+}$ et $Mn^{4+}$ forment des oxydes insolubles. Dans les sédiments marins de surface, soit la couche oxique, les oxydes de $Mn^{4+}$ dominent, alors que les oxydes de $Mn^{3+}$ se retrouvent principalement à la base de cette couche (Madison et al., 2013). Les oxydes de Mn possèdent une forte capacité d'adsorption des métaux, ce qui en fait une importante phase porteuse, tant dans la colonne d'eau que dans les sédiments. En milieu anoxique, ces oxydes sont dissous et le Mn est réduit en $Mn^{2+}$, qui peut être diffusé vers la colonne d'eau et s'y reprécipiter sous forme d'oxydes (Calvert & Pedersen, 1993). Dans les sédiments anoxiques, le $Mn^{2+}$ peut également être enfoui sous forme de carbonates (Mucci, 1988). Dans l'océan

Arctique, les concentration en Mn varient entre 62 et 27 100 µg/g l'Arctique (Budko et al., 2017; Budko et al., 2022; Campbell & Loring, 1980; Holemann et al., 1999; Loring et al., 1998; Lu et al., 2013; Naidu et al., 2005; Trefry et al., 2013; Trefry & Neff, 2019; Wang et al., 2022).

### 2.3.11 Les éléments des terres rares

Les ETR sont un groupe d'éléments ayant des comportements géochimiques similaires. Ils sont constitués des lanthanides (La-Lu), de l'Y et parfois du Sc, bien que ce dernier ait un comportement différent (Barrat & Bayon, 2024). Les ETR ont une configuration électronique comparable, mais leur rayon ionique diminue avec le numéro atomique : il s'agit de la contraction des lanthanides (Shannon, 1976). Les ETR sont tous trivalents (3+), toutefois le Ce et l'Eu ont un deuxième état d'oxydation : $Ce^{4+}$ et $Eu^{2+}$. Ces caractéristiques font en sorte que la composition en ETR d'une source mère est modifiée par des processus géochimiques et physicochimiques au cours de l'altération, du transport et du dépôt des sédiments (Bossé-Demers et al., 2025; Su et al., 2017).

Afin de faciliter les interprétations et d'éliminer l'effet Oddo-Harkins, les concentrations en ETR sont normalisées (Barrat & Bayon, 2024). Plusieurs valeurs de référence sont utilisées dans la littérature pour la normalisation, soit la chondrite CI (Barrat et al., 2012), le schiste australien post-archéen (PAAS; Pourmand et al., 2012) ou encore le schiste nord-américain (NASC; Gromet et al., 1984). Les ETR sont également subdivisés en trois sous-groupes pour les interprétations : les ETR légers (LREE; La-Nd), ETR moyens (MREE; Sm-Dy) et ETR lourds (HREE; Ho-Lu).

Dans l'eau de mer, les complexes ETR-carbonates sont la forme dissoute dominante, avec une augmentation de la complexation avec le numéro atomique (Sholkovitz et al., 1994). Cette complexation préférentielle des HREE occasionne l'adsorption préférentielle des LREE et MREE sur des oxides de Fe-Mn et la MO (Bayon et al., 2004). L'oxydation du $Ce^{3+}$ en $Ce^{4+}$ favorise également son adsorption sur des oxides de Mn (Sholkovitz et al., 1994). La signature dans l'eau de mer, lorsque normalisée, est donc un enrichissement en HREE and

une anomalie négative en Ce (Smrzka et al., 2019). Dans les sédiments, on retrouve les LREE associés à la MO et aux oxides, les MREE associés oxides et les HREE associés aux zircons (Sholkovith, 1990).

La concentration totale des lanthanides du PAAS est de 224.6 µg/g. Dans les sédiments marins des mers arctiques russes, les concentrations varient entre 115 et 239 µg/g (Astakhov et al.,2018; Ruban et al., 2024).

# 3. CONTEXTE GEOGRAPHIQUE

## 3.1 Arctique canadien

L'AC est une vaste région englobant le plateau polaire canadien, qui relie le bassin du Canada à la baie de Baffin, ainsi que les îles de l'archipel Arctique canadien (Figure 4). Dans le cadre de cette étude, la région se situe entre 60 et 83 °N et 55 et 140 °O. Elle s'étend de la mer de Beaufort et du plateau du Mackenzie à l'ouest, en passant par les chenaux étroits et peu profonds de l'archipel, jusqu'à la baie de Baffin et le détroit de Nares à l'est.

L'AC est l'une des régions les plus arides du monde (Brown, 1972). Il est entièrement recouvert d'un pergélisol continu, occupant entre 90 et 100% du sol (Heginbottom, 1995). Par conséquent, l'hydrologie y est fortement influencée par le gel hivernal et la fonte estivale, et reste largement contrainte par la présence du pergélisol. On y trouve un ensemble de petites rivières saisonnières (ex. Freshwater Creek), ainsi que quelques grandes rivières s'écoulant à longueur d'année (ex. rivière Coppermine; Figure 4). Le débit total de ces rivières est d'environ 257 $km^3$/a (Alkire et al., 2017). On retrouve aussi le fleuve Mackenzie, le plus long et grand système fluvial du Canada, avec un débit annuel d'environ 290 $km^3$/a (Rood et al., 2017). La contribution des rivières est ainsi significative dans le bilan en eau douce de l'AC.

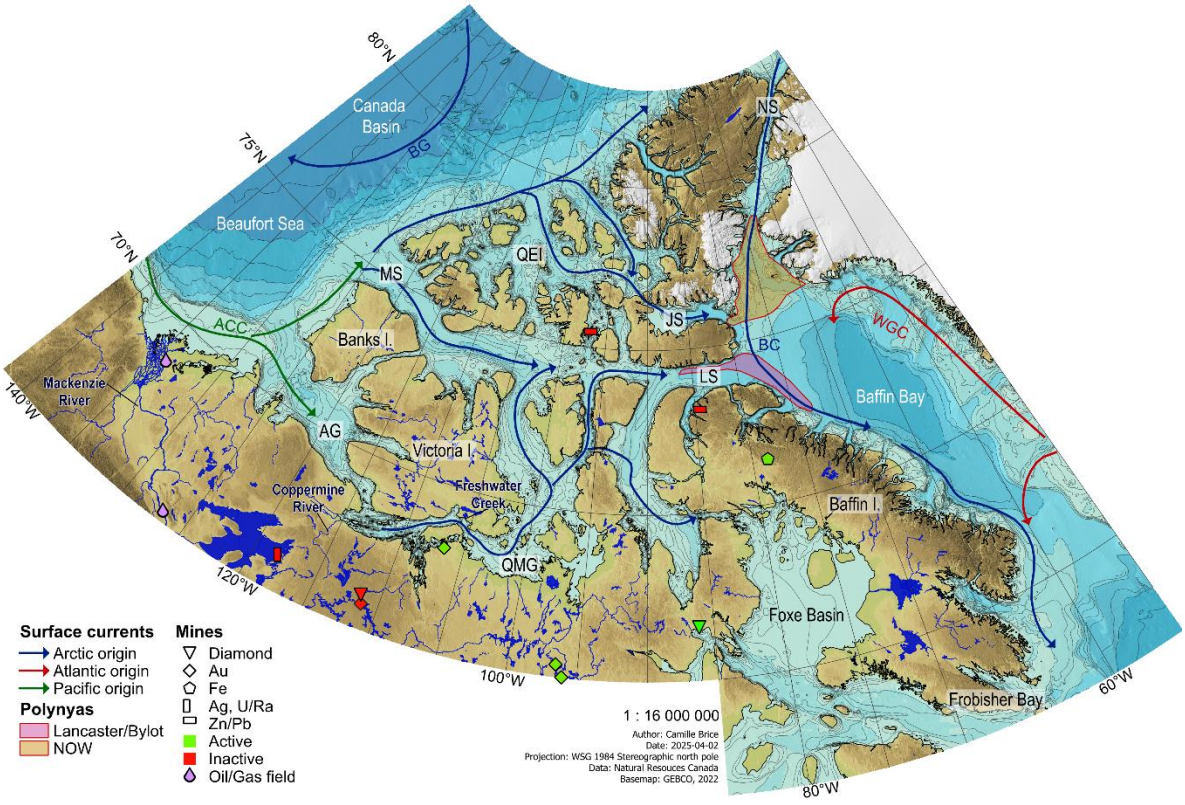


Figure 4. Carte de la région d'étude.AG : golfe d'Amundsen; JS : détroit de Jones; LS : détroit de Lancaster; MS : détroit de M'Clure; NS: détroit de Nares; QEI : îles de la Reine-Élizabeth; QMG : golfe de la reine Maud. ACC : courant côtier d'Alaska; BC : courant de Baffin; WGC : courant ouest groenlandais.

La région d'étude est approximativement composée des régions Inuvialuit et Nunavut (Figure 5). Un peu plus de 40 000 personnes habitent dans ces régions (Statistics Canada, 2023). L'île de Baffin est la plus populeuse de l'archipel, avec plusieurs villes et villages dont Iqaluit (capitale du Nunavut) et Mittimatalik (Pond Inlet). Des communautés inuites sont aussi présentes sur plusieurs îles et sur la partie continentale (Figure 5). Quelques mines d'or, de diamant et de fer sont présentes dans l'AC. Un gisement de gaz est situé au niveau du delta du Mackenzie et un gisement pétrolier est situé plus au sud le long de la rivière. Selon l'Inventaire des sites contaminés fédéraux (Government of Canada, 2022), plusieurs localisations dans l'AC ont été répertoriées pour la présence de contaminations en métaux, métalloïdes et organométalliques dues à d'anciens sites d'exploration minières, à des réservoirs de stockage ou encore à des sites d'enfouissement.

### 3.1.1 Océanographie et glace de mer

Dans l'AC, et l'océan Arctique en général, la colonne d'eau est composée de trois masses d'eau (Niemi et al., 2024): l'eau Arctique (ou couche polaire de mélange), l'eau pacifique (PW) et l'eau atlantique (AW). L'eau Arctique occupe les 50 à 100 premiers mètres de la colonne d'eau et est formée dans l'océan Arctique d'un mélange d'eaux Pacifique et Atlantique et d'eau douce issue de la fonte de la glace de mer et des rivières. Elle est donc de faible salinité et température (<31; < 0°C). Elle est isolée de l'AW par une halocline froide occupant les profondeurs de 100 à 300 mètres et correspondant à la PW (31 à 33; -1.5 à 3°C) qui est légèrement saline. La PW est une masse d'eau provenant de l'océan Pacifique introduite par le détroit de Béring qui a incorporé de l'eau douce des rivières Yukon et Mackenzie en longeant la côte via le courant côtier d'Alaska (ACC, Figure 4). L'AW (34,5 à 34,95; 0 à 3°C), qui est très saline comparativement à la PW, occupe la couche la plus profonde de l'océan Arctique. Cette masse d'eau provient de la dérive nord-atlantique qui est entrée par le détroit de Fram et la mer de Barents.

Les eaux situées dans le bassin du Canada transitent vers l'océan Atlantique en traversant les chenaux de l'archipel Arctique canadien. Les trois masses d'eau se retrouvent dans les chenaux ouest, dont les profondeurs d'environ 500 mètres le permettent. Toutefois, seules les eaux Arctique et Pacifique peuvent traverser les passages peu profonds de l'archipel pour rejoindre la baie de Baffin, c'est-à-dire le détroit de Barrow (125 m de profond), le détroit de Jones (190 m) et le détroit de Nares (250 m) (Niemi et al., 2024). Ces eaux, s'étant mélangée pendant le trajet, forment la couche de surface de la baie de Baffin. Sous cette couche, du côté est de la baie, on retrouve les eaux amenées par le courant ouest groenlandais (WGC) qui remonte la côte ouest du Groenland. Il s'agit d'un courant amenant des eaux chaudes (~4°C) et salines (~34.8) de l'Atlantique. Le long de côte, les eaux du WGC se mélangent aux eaux côtières, puis traverse la baie de Baffin et se mélangent aux eaux de l'archipel et du détroit de Nares pour former le courant de Baffin (BC).

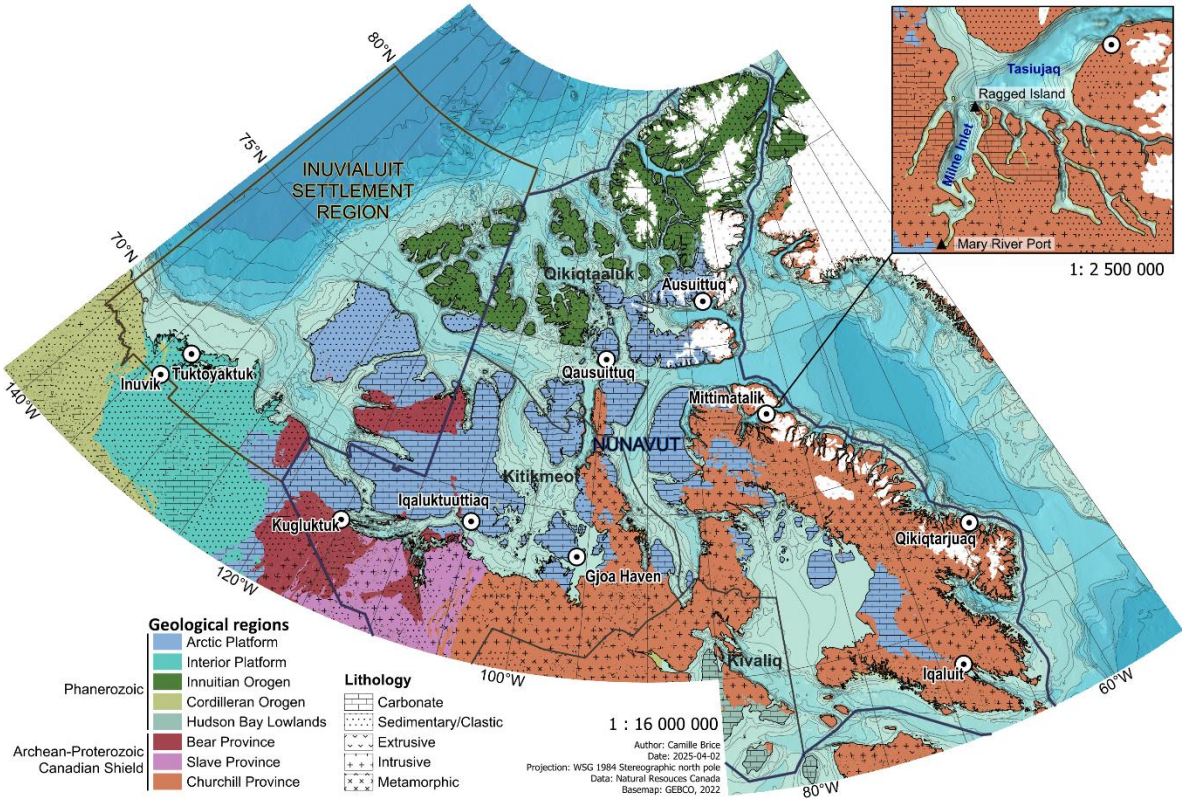


Figure 5. Carte géologique de la région d'étude avec la délimitation de la région d'Inuvialuit et du Nunavut.

Chaque hiver, la totalité des chenaux est couvert par la glace de mer saisonnière et de la glace de mer pluriannuelle est présente dans le nord-ouest de l'AC (Canadian Ice Services, 2023; Michel et al., 2015). Dans le restant de l'archipel, la glace se forme généralement vers la mi-septembre et font à la fin du mois de mai. Le couvert de glace de mer minimum est observé à la fin août (Canadian Ice Services, 2023). La circulation de la glace de mer dans l'AC est principalement gouvernée par les vents dominants, les courants de surface et la configuration géographique de l'archipel. De façon générale, la glace de mer circule de façon anticyclonique dans la mer de Beaufort, puis entre dans l'AC principalement par le détroit de McClure, mais aussi via le golfe d'Amundsen et les îles de la Reine-Élizabeth. Les voies de sortie de l'archipel vers la baie de Baffin sont les détroits de Lancaster et de Jones. La glace circule également de l'Océan Arctique vers la baie de Baffin via le détroit de Nares (Terwisscha van Scheltinga et al., 2010; Wang et al., 2012). Plusieurs polynies récurrentes

sont présentes dans les eaux de l'AC, dont la polynie des eaux du Nord (NOW; Pikialasorsuaq) et les polynies du détroit de Lancaster et de l'île Bylot (Figure 4; Hannah et al., 2009; Stirling & Cleator, 1981). Celles-ci sont maintenues par la chaleur latente et les arcs de glace formés dans le détroit de Nares et le détroit de Lancaster (Vincent, 2023). Ces polynies, en particulier la Pikialasorsuaq, sont des zones très productives (Ribeiro et al., 2021) avec des flux élevés de carbone organique vers les sédiments (1.1 – 1.5 mg $C_{org}$ $cm^{-2}$ $yr^{-1}$; Hamel et al., 2002).

### 3.1.2 Géologie

Quatre grandes régions géologiques caractérisent l'AC, soit le Bouclier canadien, les plateformes intérieure et arctique, l'orogène Innuitien et l'orogène des Cordillères (Figure 5; de Kemp et al., 2006). Trois provinces du Bouclier canadien occupent le centre et l'est de l'AC. La province de Churchill couvre la majeure partie de l'île de Baffin ainsi que l'est du continent. Les provinces de Slave et Bear s'étendent sur le centre continental et une partie de l'île de Victoria. Le Bouclier est principalement composé de roches ignées précambriennes, telles que les granites et les granodiorites, ainsi que de roches métamorphiques comme les gneiss (Harrison et al., 2011). Les plateformes intérieure et arctique couvrent les îles de l'ouest et du centre de l'archipel, ainsi que la partie continentale située entre les Cordillères et le Bouclier. Elles sont composées de roches sédimentaires, avec une dominance de carbonates détritiques d'âge Cambrien à Silurien sur la plateforme arctique, et des roches clastiques d'âge Dévonien-Crétacé sur la plateforme intérieure. La partie occidentale du continent est caractérisée par la Cordillère nord-américaine, qui comprend les chaînes de montagnes des Rocheuses et du Mackenzie. Cette région est constituée d'un assemblage de roches sédimentaires et volcaniques (Harrison et al., 2011). Le fleuve Mackenzie (Figure 4), qui se jette dans la mer de Beaufort, draine une grande superficie de l'ouest de l'Amérique du Nord, incluant des portions du Bouclier canadien, de la plateforme intérieure et de la Cordillère (Millot et al., 2003). Enfin, la région montagneuse Innuitienne, située dans la partie nord de l'archipel, est formée de roches sédimentaires, volcaniques et métamorphiques intensément déformées, d'âge variant du Protérozoïque au Tertiaire (de Kemp et al., 2006).

Cette région comprend également le bassin de Sverdrup, une séquence sédimentaire composée de schistes riches en pétrole et gaz naturel du Paléozoïque supérieur au Cénozoïque inférieur (Embry & Beauchamp, 2019).

### 3.1.3 Dynamique sédimentaire

Letaïef et al. (2021) ont divisé l'AC en trois provinces distinctes selon les processus sédimentaires dominants. Les sédiments marins de l'ouest de l'Arctique canadien sont principalement influencés par les apports du fleuve Mackenzie. La gyre de Beaufort joue également un rôle important dans la composition des sédiments du fond marin. Le centre sud de l'AC, incluant les golfes de la Reine-Maud et de Coronation, est dominé par les apports des petites rivières qui traversent le Bouclier canadien du sud vers le nord. Quant à l'est de l'AC, il est caractérisé par l'érosion côtière et les apports sédimentaires par la glace de mer. La glace de mer joue un rôle prédominant dans le transport des sédiments, tant dans l'AC que dans l'océan Arctique en général (Darby et al., 2011; Eicken et al., 2005). Lors de la formation de frasil en milieux peu profonds, les sédiments en suspension, provenant de rivières ou de l'érosion côtière, s'incorporent à la glace. Ces sédiments peuvent ensuite être transportés sur de longues distances par les courants de surface, puis déposés lors de la fonte estivale. Par exemple, la glace de mer amène des sédiments provenant de la mer de Laptev jusqu'à la gyre de Beaufort via la dérive transpolaire (Darby, 2003). Enfin, le transport éolien dans l'AC est limité, localisé et saisonnier (Lewkowicz & Young, 1991).

## 3.2 Les éléments traces métalliques de sources anthropiques dans l'Arctique

La contamination des régions arctiques provient de sources locales à globales. Elle peut provenir de sources locales comme les villes nordiques, ou encore l'exploration et exploitation minière et pétrolière (Macdonald et al., 2000). Les communautés établies dans les régions arctiques contribuent à la pollution en ETM par leur gestion des eaux usées et des déchets, par la présence d'industries sur place (ex. activités minières, entreposage de pétrole, tourisme) et par le transport. Par exemple, les mines et les fonderies dans l'Arctique russe

représentent une source locale majeure en ETM et la pollution en découlant peut être sévère (Poland et al., 2003). Le développement minier intensif de la péninsule de Kola (Russie) est un bon exemple (Yakovlev et al., 2022). Ces activités anthropiques perturbent l'environnement adjacent, comme les sols, le milieu côtier, les rivières et les eaux souterraines. L'AC n'est pas aussi développé que l'Arctique eurasien, mais les émissions de ces activités anthropiques très polluantes peuvent aussi atteindre l'AC par les courants océaniques et la glace de mer (AMAP, 2011). Les métaux peuvent se fixer à la MO ou aux sédiments en suspension, et être transportés sur de longues distances par les eaux Atlantiques dans les courants de bord de l'océan Arctique (Aarkrog, 2003; Macdonald et al., 2005). Les émissions en milieu marin, comme le transport maritime et l'exploration pétrolière en mer via la combustion de carburant, les déversements, la peinture antifouling, causent la contamination des régions arctiques à l'échelle régionale (AMAP, 1998). Plusieurs grandes rivières drainent les régions nordiques de l'Asie, l'Europe et l'Amérique du Nord, et se déchargent dans l'océan Arctique. Ces rivières peuvent constituer d'importants vecteurs de contaminants provenant de sources situées en amont (Macdonald et al., 2005). En Russie, les apports en ETM dans les mers arctiques via les rivières sont particulièrement élevés et dépassent les flux atmosphériques (Vinogradova & Kotova, 2019).

Le transport atmosphérique de longue distance est un mécanisme majeur de dispersion des éléments traces, entraînant la pollution de régions très éloignées des sources d'émission (Macdonald et al., 2005). Les régions arctiques sont particulièrement vulnérables aux émissions anthropiques de Hg, Cd, As et Pb provenant de régions très éloignées (AMAP, 2005). Par exemple, il a été établi que l'Asie représente la principale source de Hg se déposant dans l'océan Arctique, si l'on considère seulement les émissions d'origine anthropique (AMAP, 2021; Chen & and Taylor, 2018). Le phénomène de la « brume arctique » (*Arctic haze*) favorise leur déposition de ces polluants au printemps, période où les conditions atmosphériques facilitent leur transport et leur accumulation dans l'Arctique (Quinn et al., 2007).

Indirectement, les activités humaines perturbent également les cycles biogéochimiques des éléments traces par le biais des changements climatiques. En région arctique, le réchauffement climatique entraîne le dégel du pergélisol, ce qui provoque la libération de MO, de nutriments et de contaminants, parmi lesquels on retrouve les ETM accumulés au fil du temps (Hugelius et al., 2014). La dégradation de la MO stockée dans le pergélisol libérera les éléments traces accumulés au cours du temps. Le pergélisol contient des quantités importantes de plusieurs ETM (Antcibor et al., 2014; O'Donnell et al., 2024; Skierszkan et al., 2024), et constitue un réservoir majeur de mercure à l'échelle mondiale (Schuster et al., 2018). Cet enrichissement est particulièrement marqué dans l'ouest de l'AC et en Alaska.

## 4. OBJECTIFS DE LA THESE

L'objectif principal de cette thèse est d'évaluer l'état actuel de la contamination métallique dans les sédiments de l'Arctique canadien. Pour ce faire, un portrait spatial exhaustif de la composition géochimique des sédiments de surface a été établi, afin d'approfondir nos connaissances sur le comportement des ETM et d'évaluer leur risque écotoxicologique dans l'environnement marin arctique. La réalisation de cet objectif principal repose sur trois objectifs spécifiques, chacun apportant un éclairage complémentaire sur la composition géochimique des sédiments, tant pour la fraction totale que pour la fraction extractible à l'acide, à différentes échelles spatiales, allant du niveau régional jusqu'à celui des communautés inuites locales.

*Objectif 1 : Documenter la dynamique sédimentaire régionale et évaluer l'applicabilité d'indices de pollution*

L'AC est une vaste région aux lithologies et aux conditions océaniques très variées, ce qui mène à une composition chimique du fond marin hétérogène. Afin d'évaluer l'état des lieux en termes de contamination en ETM dans les sédiments de la région, il est important de préalablement caractériser la dynamique sédimentaire et comprendre comment celle-ci

régit la distribution des éléments majeurs et traces. Dans ce contexte, le premier objectif de cette thèse est d'**établir un portrait général spatial de la dynamique sédimentaire moderne de l'Arctique canadien** en analysant une centaine d'échantillons de sédiments marins de surface collectés à travers la région.

Les sédiments marins dans l'AC sont principalement issus d'apports continentaux présentant des signatures géochimiques et sédimentologiques distinctes (Deschamps et al., 2018; Gamboa et al., 2017; Letaïef et al., 2021). Ainsi, la provenance des sédiments peut être déterminée à partir de leur composition chimique, de leur granulométrie et de leur contenu en matière organique, puisque ces propriétés reflètent la géologie des régions sources, les mécanismes de transport et les cycles biogéochimiques impliqués. La concentration en éléments majeurs et en certains éléments traces (V, Zn, Sr, Zr) est mesurée par spectrométrie de fluorescence X à énergie dispersive (ED-XRF). Les propriétés chimiques et physiques des sédiments marins de surface permettent de caractériser la variabilité régionale de la composition chimique du fond marin et d'approfondir notre compréhension des processus sédimentaires et géochimiques modernes qui contrôlent la distribution des éléments majeurs et traces dans l'AC. Combinées à des analyses multivariées, ces données serviront également à caractériser et délimiter spatialement les différentes provinces géochimiques de l'AC. Les analyses de regroupement (clustering) permettent de subdiviser la région selon les compositions chimiques dominantes, tandis que l'analyse en composantes principales regroupera les variables présentant des comportements similaires. Pour évaluer la contamination et l'enrichissement en ETM, les concentrations en Zn, V, Fe et Mn dans les sédiments de surface seront comparées à des valeurs de référence telles que celles de la croûte continentale supérieure (Taylor & McLennan, 1985), du schiste moyen (Turekian & Wedepohl, 1961) ainsi qu'à des teneurs régionales préindustrielles, à l'aide d'indices de pollution. L'applicabilité de deux indices de pollution sera évaluée dans le cadre de cette étude à grande échelle.

*Objectif 2 : Établir une base géochimique de référence*

Le deuxième objectif de cette thèse est de **d'établir une base de référence des concentrations des ETM dans la fraction extractible à l'acide des sédiments de l'Arctique canadien**. Cette base de référence permettra de compléter la couverture spatiale de la composition géochimique des fonds marins avec de nouvelles données, d'évaluer l'état actuel de la contamination par les ETM et d'identifier les facteurs naturels et/ou anthropiques qui influencent leur distribution. À plus long terme, ces données serviront à suivre l'évolution temporelle des concentrations en ETM et à évaluer les impacts des perturbations anthropogéniques croissantes. Une meilleure compréhension de la distribution des ETM, de leur comportement et des processus qui les contrôlent contribuera à une évaluation plus précise des risques écotoxicologiques associés aux changements environnementaux actuels et futurs dans les milieux marins arctiques.

Ce portrait plus détaillé sera établi à partir d'une digestion partielle des sédiments marins de surface (les mêmes que ceux utilisés pour l'Objectif 1), à l'aide d'un mélange d'acides nitrique et chlorhydrique concentrés, suivie d'analyses par spectrométrie de masse à triple quadrupôle (ICP-QQQ). Cette méthode complète les analyses par ED-XRF permettant la quantification des concentrations en éléments traces extractibles à l'acide, incluant ceux potentiellement accessibles aux organismes. Les ETM extraits proviennent principalement des phases réactives telles que la phase échangeable, les (oxyhydr)oxides de Fe-Mn, la MO, les sulfures, les carbonates et les aluminosilicates hydratés. En revanche, les ETM associés à la MO réfractaire, aux silicates ou aux minéraux lourds ne sont pas extradés et quantifiés par cette méthode (Xu et al., 2012). Les concentrations ainsi obtenues reflètent principalement les contributions anthropiques et les échanges biogéochimiques actifs dans le milieu marin. L'influence lithogénique y est donc moins marquée, mais celle-ci ayant déjà bien caractérisée dans l'Objectif 1, elle est intégrée à l'interprétation globale du comportement des ETM.

*Objectif 3 : Réaliser une étude à l'échelle locale des communautés inuites*

Les populations de l'Arctique figurent parmi les plus exposées aux contaminants métalliques, l'alimentation représentant la principale voie d'exposition (Basu et al., 2022). Or, dans l'Arctique canadien, la grande majorité des apports anthropiques en métaux et autres contaminants provient de sources situées aux basses latitudes, transportés par voie atmosphérique, océanique et fluviale (Macdonald et al., 2000). De plus, les changements environnementaux rapides en cours dans l'Arctique, tels que le dégel du pergélisol et la fonte de glaciers, contribuent à la libération de ces contaminants métalliques jusque-là stockés à long terme dans les sols et les glaces. En réponse à ces enjeux, plusieurs études et programmes de recherche ont été mis en place depuis plusieurs années afin de surveiller les polluants environnementaux dans l'Arctique, en évaluant les voies d'entrée, leurs concentrations, les tendances temporelles ainsi que leurs effets sur la santé humaine (AMAP, 2005, 2011, 2021; Dudarev & Odland, 2022; Palaniswamy et al., 2024).

Cependant, la contribution de contaminants métalliques provenant d'activités humaines locales dans les communautés nordiques a suscité moins d'attention et demeure largement sous-étudiée. Ces communautés, peu nombreuses et faiblement peuplées par rapport aux centres urbains du sud, sont souvent perçues comme représentant un enjeu environnemental moindre. Pourtant, au-delà des sources régionales et à longue distance, les sources locales, telles que les eaux usées, les sites d'enfouissement, les activités minières et les rejets liés aux infrastructures aéroportuaires peuvent avoir des impacts substantiels sur les milieux naturels avoisinants. Afin d'évaluer la contribution des activités anthropiques locales, l'Objectif 3 de cette thèse vise à **déterminer les teneurs en éléments majeurs et traces dans les sédiments côtiers situés à proximité de six communautés inuites de l'Arctique canadien**. Ces sédiments ont accumulé, au fil du temps, des apports métalliques d'origine locale et régionale, qu'ils soient naturels ou anthropiques. L'analyse de ces sédiments par ED-XRF (fraction totale) et par ICP-QQQ (fraction extractible à l'acide) permettra de dresser un portrait de l'état actuel de la contamination métallique locale.

# 5. METHODOLOGIE

## 5.1 Échantillonnage

Des échantillons de sédiments ont été collectés à 141 sites entre la baie de Baffin et la mer de Beaufort, et ont été analysés dans le cadre de ce projet (Figure 6; voir Annexe I). Un total de 128 carottes boîtes a été prélevé en milieu marin, ainsi que 17 échantillons terrestres ont été collectés à proximité de glaciers et de rivières. Tous ces échantillons ont été recueillis dans le cadre des expéditions estivales d'ArcticNet, à bord du navire de la Garde côtière canadienne et brise-glace Amundsen, entre 2016 et 2022. Les échantillons terrestres ont été collectés à l'aide de l'hélicoptère du navire. Les carottes boîtes ont été sous-échantillonnées dans le premier centimètre afin d'avoir les sédiments de surface, considérés comme « modernes ». Letaïef et al. (2021) ont utilisé les taux de sédimentation disponibles dans l'AC, étant très variables d'une région à l'autre, ainsi que la susceptibilité magnétique pour conclure que les sédiments de surface se sont accumulés après 1900. Par ailleurs, des carottes *push cores* ont été prélevées à partir de certaines carottes à boîtes (Figure 6), et la base de ces *push cores* a été sous-échantillonnée pour permettre l'établissement d'un fond géochimique régional.

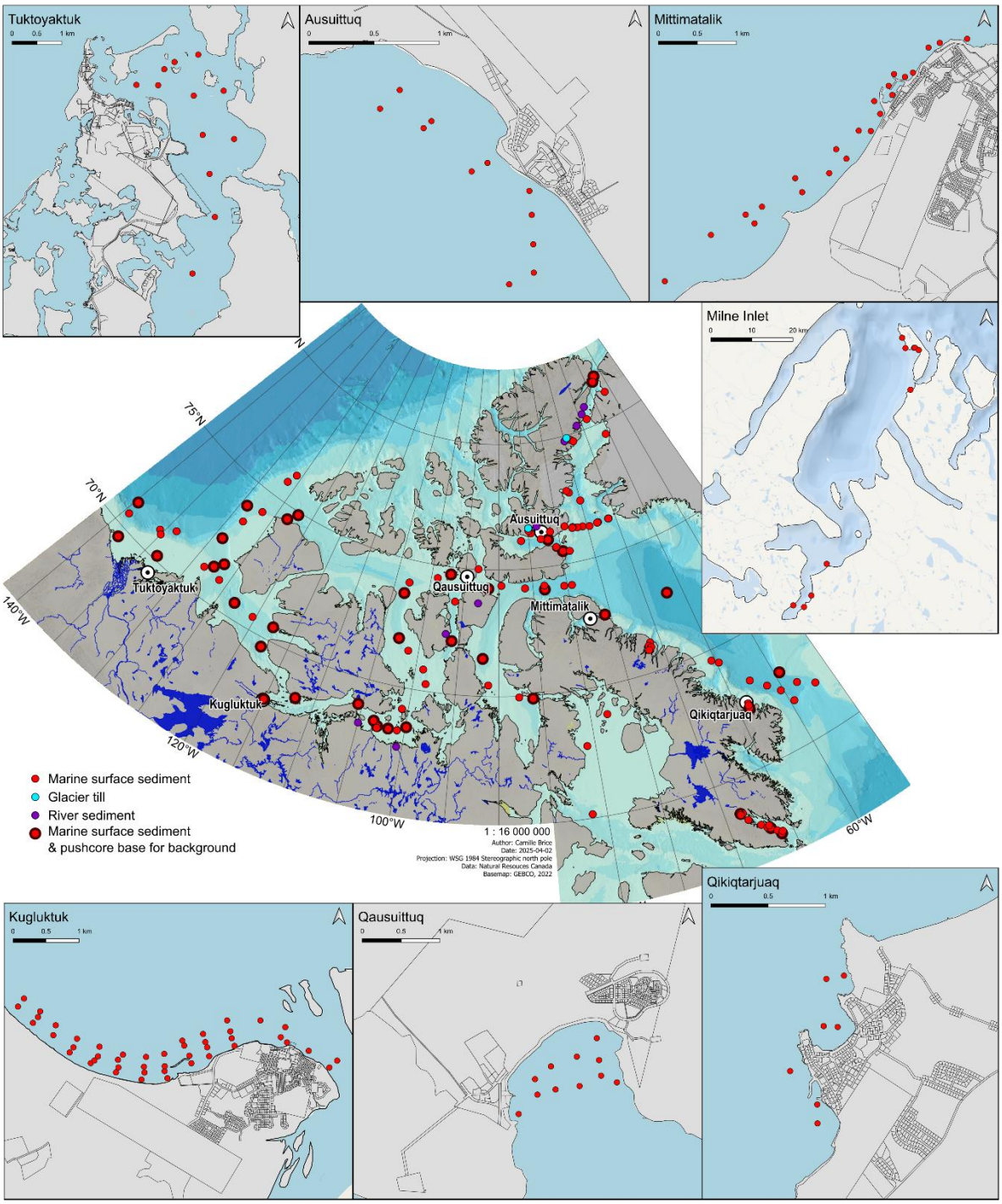


Figure 6. Cartes présentant la localisation des échantillons de sédiments.

Des échantillons de sédiments côtières ont également été prélevés le long des côtes de Tuktoyaktuk (n=12), Kugluktuk (n=49), Qausuittuq (Resolute, n=11), Ausuittuq (Grise Fiord, n=11), Mittimatalik (Pond Inlet, n=30) et Qikiqtarjuaq (n=7). D'autres échantillons ont été prélevés à Milne Inlet, près de Ragged Island (n=6), ainsi qu'à proximité du port de Mary River (n=4; Figure 6; voir Annexe I). Les sédiments de surface ont été échantillonnés à l'aide d'une benne Petite Ponar déployée manuellement. À Kugluktuk et Pond Inlet, l'échantillonnage a été réalisé respectivement en août 2022 et 2023, avec le soutien de guides locaux. L'échantillonnage près de Qikiqtarjuaq a été réalisé lors du leg 2 de l'expédition Amundsen 2022, tandis que ceux de Grise Fiord et Resolute l'ont été durant le leg 3 de l'expédition Amundsen 2023. Enfin, les échantillons de sédiments de surface du port de Tuktoyaktuk et de Milne Inlet ont été prélevés dans le cadre d'autres projets de recherche menés par l'Alfred Wegener Institue et l'UQAR, et l'ISMER-UQAR, respectivement.

## 5.2 Analyses en laboratoire

La totalité des échantillons de sédiments marins de surface et terrestres utilisés dans les Chapitres 1 et 2 (n=141) a été analysés pour la granulométrie, la teneur en carbone organique total (COT) et la géochimie élémentaire au ED-XRF et à l'ICP-QQQ. Une partie des données sur le COT utilisées dans cette thèse provient de Corminboeuf et al. (2021). Les analyses du COT effectuées dans le cadre de cette thèse ont été réalisés selon la même méthodologie et en utilisant le même instrument. Pour l'analyse du COT et la géochimie élémentaire, tous les échantillons ont d'abord été tamisés avec un tamis Nitex® de 150 µm en utilisant de l'eau distillée, puis séchés au four (<60 °C) pendant 72 heures, broyés et homogénéisés à l'aide d'un mortier en agate. Les sédiments côtiers de surface utilisés dans le Chapitre 3 ont été analysés de la même manière. Toutefois, certains échantillons de Kugluktuk (n=4) et de Pond Inlet (n=8) n'ont pas été analysés, car la fraction < 150 µm était insuffisante. Ainsi, 118 échantillons côtiers ont été analysés pour la granulométrie et la géochimie au ED-XRF. Pour les analyses à l'ICP-QQQ, une sélection d'échantillons (n=68) a été effectuée à partir des résultats obtenus au ED-XRF.

### 5.2.1 Granulométrie

Les analyses granulométriques ont été réalisées sur la fraction détritique. Les échantillons ont d'abord été traités avec 5-10 mL de peroxyde d'hydrogène (30% $H_2O_2$) pour éliminer la MO. Puis, la fraction détritique obtenue a été diluée avec ~30 mL d'hexamétaphosphate de sodium (20% v/v), agissant comme agent défloculant, et tamisée à <2 mm. Avant les mesures granulométriques, les échantillons ont été mélangés pendant 12 heures pour désagréger les particules à l'aide d'un rotateur. Les mesures ont été prises à l'aide d'un analyseur granulométrique à diffraction laser Malvern PANalytical Mastersizer 3000 équipé d'un module Hydro LV en suivant les conditions instrumentales décrites dans Belzile and Montero-Serrano (2022). Les résultats ont été traités à l'aide du logiciel GRADISTAT v.9.1 (Blott et Pye, 2001).

### 5.2.2 Contenu en carbone organique total

La teneur en carbone total et COT de la fraction <150 μm a été mesurée au laboratoire de géochimie des isotopes stables légers du Geotop (Montréal, Québec) avec un analyseur élémentaire Carlo-Erba NC 2500 et en suivant la méthode d'acidification en solution décrite dans Hélie (2009). Chaque échantillon de sédiment est divisé en deux aliquotes. La première aliquote de sédiment est utilisée pour déterminer la teneur en carbone total. La seconde aliquote est acidifiée avec 1 M HCl pour éliminer les carbonates, puis séchée et broyée. Celle-ci est utilisée pour déterminer la teneur en COT. Pour tenir compte de la perte de masse de carbone inorganique, une correction a été appliquée aux résultats en suivant la méthodologie décrite dans Hélie (2009).

### 5.2.3 Analyses géochimiques

La composition en éléments majeurs (Mg, Al, Si, K, Ca, Ti, Mn, Fe) et éléments traces (Cr, V, Zn, Sr, Zr) a été analysée sur la fraction < 150 μm des sédiments par ED-XRF en utilisant un PANalytical Epsilon 3-XL (Croffie et al., 2020). Avant l'analyse, 2 g

d'échantillon de sédiment ont été pesés avant et après incinération dans un four à moufle à 950 °C pendant 4 heures afin de déterminer la perte au feu (Loss on Ignition, LOI). Ensuite, environ 1,1 g d'échantillon incinéré a été mélangé avec 5,5 g de fondant au tétraborate de lithium (CLAISSE, pur, 99 % $Li_2B_4O_7$, 1 % LiBr), puis fondu à l'aide d'un four de fusion automatisé CLAISSE M4 dans des creusets en platine-or pour former des pastilles vitrifiées. Ces pastilles ont ensuite été analysées pour leur composition géochimique élémentaire à l'aide du spectromètre Epsilon 3-XL. L'analyse par ED-XRF permet d'obtenir la concentration totale de ces éléments dans les échantillons et ainsi fournir des informations essentielles sur la dynamique sédimentaire de la région. Cependant, les limites de détection élevées de cet instrument ne permettent pas de mesurer la majorité des éléments en trace.

La teneur en éléments majeurs (Mg, Al, K, Ca, Ti, Mn, Fe) et éléments traces (Cr, Co, Ni, Sc, Cu, Zn, V, As, Sr, Cd, Pb, lanthanides, Y) dans les sédiments a également été déterminée par digestion acide partielle en suivant une version légèrement modifiée de la méthode 3051A de l'US EPA (US EPA, 2007). La digestion acide partielle, ou digestion à l'eau régale inverse, consiste à dissoudre les sédiments avec un mélange de trois volumes d'acide nitrique concentré ($HNO_3$) et d'un volume d'acide chlorhydrique concentré (HCl). La solution obtenue est ensuite analysée avec un ICP-QQQ dont la sensibilité permet la mesure de la majorité des éléments traces. Cette technique permet de dissoudre les sulfures, les carbonates, certains sulfates, certains oxydes de Fe-Mn et la MO, et donc de mesurer les ETM y étant associés. Les oxydes métalliques bien cristallisés et les silicates ne sont pas affectés par cette digestion (Krasnodębska-Ostręga et al., 2001; Xu et al., 2012). Les données acquises, soit les concentrations extractibles des éléments traces et majeurs, nous renseignent sur la fraction des ETM accessible aux organismes.

Les concentrations en ETR ont été normalisées sur le schiste précambrien australien (PAAS; Pourmand et al., 2012). Les ETR ont été subdivisés en ETR légers (La-Nd), moyens (Sm-Dy) et lourds (Ho-Lu +Y) pour les interprétations. Les anomalies en Ce et en Eu ont été calculées avec les formules suivantes (Barrat & Bayon, 2024; Barrat et al., 2023) :

(1) $Ce/Ce^* = Ce_{PAAS}/ / (La_{PAAS} \times Pr_{PAAS})^{1/2}$

(2) $Eu/Eu^* = Eu_{PAAS} / (Sm_{PAAS} \times Gd_{PAAS})^{1/2}$

## 5.3 Traitement de données

### 5.3.1 Analyses statistiques

Le traitement des données et les analyses statistiques ont été effectués avec le logiciel R (R Core Team, 2024). Une imputation lognormale multiplicative (Palarea-Albaladejo & Martín-Fernández, 2013, 2015) a été appliquée aux données ED-XRF pour imputer les valeurs inférieures à la limite de détection. Puisqu'il s'agit de données compositionnelles, soit des données quantitatives relatives à un tout, une transformation centrée-log ratio (clr) a été appliquée aux données ED-XRF et ICP-QQQ pour supprimer les contraintes statistiques reliées à cette relativité (Aitchison, 1982). Des analyses multivariées ont ensuite été utilisées afin de structurer les informations obtenues.

Étant donné sa grande superficie, la zone d'étude présente différentes provinces sédimentaires, chacune définie par leurs propres processus sédimentaires dominants (Letaïef et al., 2021). Pour identifier et délimiter ces provinces, des analyses de partitionnement de données ont été appliquées aux données géochimiques, permettant de regrouper et hiérarchiser les échantillons en fonction des concentrations en éléments majeurs et en traces caractérisant la composition des sédiments. Les analyses de *K-means clustering*, ou partitionnement de données par K-moyennes, ont été réalisées à partir des données géochimiques, de la perte au feu et du COT. Par la suite, des analyses en composantes principales ont été effectuées sur l'ensemble des données afin d'extraire les tendances communes entre les éléments majeurs, les éléments traces et les paramètres sédimentologiques (granulométrie, COT). Le but est d'associer les éléments ayant une variabilité spatiale similaire, dans le but d'identifier les paramètres environnementaux influençant le comportement des ETM en milieu marin. Enfin, des matrices de corrélation de

Spearman ont été utilisées pour comparer les variables entre elles et ainsi mettre en évidence les affinités entre les ETM et les différentes phases porteuses.

Finalement, les cartes de distribution géochimique ont été générées à l'aide du logiciel QGIS version 3.40.6. Une interpolation spatiale *Empirical Bayesian Kriging* a été réalisée sur les données de Kugluktuk à l'aide de ArcGIS Pro.

### 5.3.2 Qualité des sédiments

Trois indices de pollution ont été utilisés pour évaluer la contamination, l'enrichissement et le risque écologique potentiel associé aux ETM dans les sédiments marins (Tableau 2). De manière générale, ces indices visent à déterminer l'éventuelle contribution anthropique dans un milieu en comparant les valeurs mesurées à un fond géochimique représentant les concentrations naturelles.

Le facteur d'enrichissement (EF) permet d'identifier s'il y a eu une augmentation des niveaux d'un métal par une contribution anthropique en utilisant la formule suivante (Sutherland, 2000) :

(3) $$EF = \frac{X_{éch}/Y_{éch}}{X_{fond}/Y_{fond}}$$

où $X_{éch}$ est la concentration de l'élément trace dans l'échantillon et $Y_{éch}$ est la concentration d'un élément de normalisation dans le même échantillon. $X_{fond}$ et $Y_{fond}$ sont les concentrations de l'élément trace et de l'élément normalisateur, respectivement, dans le fond géochimique. L'élément normalisateur est un élément utilisé pour compenser les effets liés à la granulométrie et à la provenance sur la variabilité naturelle des métaux. Les éléments normalisateurs les plus couramment utilisés dans la littérature sont l'Al et le Fe (Birch, 2020). Cependant, l'utilisation d'un élément unique comme normalisateur a été critiquée, car sa variabilité naturelle peut parfois dépasser celle du métal étudié (Desaules, 2012; Poh & Tahir, 2017; Reimann & de Caritat, 2000, 2005). Par exemple, le Fe est sensible aux conditions d'oxydo-réduction et est impliqué dans des processus diagénétiques pouvant entraîner son enrichissement dans les sédiments de surface (Birch, 2020). De plus, les interactions entre

l'océan Arctique et les marges continentales peuvent générer des zones fortement enrichies en Fe (Colombo et al., 2021; Jensen & Colombo, 2024). L'Al a été utilisé comme élément normalisateur dans le Chapitre 1, car il n'est généralement pas affecté par les perturbations anthropiques directes ni par les conditions redox. Il constitue un composant majeur des sédiments détritiques et a été couramment utilisé dans des études géochimiques antérieures portant sur l'Arctique canadien (Trefry & Neff, 2019). Toutefois, la distribution de l'Al peut varier considérablement en raison des hétérogénéités lithologiques dans l'AC. C'est pourquoi le Ti, un autre élément normalisateur fiable et fréquemment utilisé (Boës et al., 2011), a également été testé afin d'évaluer les divergences par rapport à l'Al. Dans le Chapitre 2, le Sc a été utilisé comme élément normalisateur (Bergamaschi et al., 2002; Shotyk et al., 2002), car l'Al n'a pas été mesuré par ICP-QQQ et certaines concentrations en Ti dépassent la plage de calibration.

L'indice de géo-accumulation (Igeo) classe le niveau de contamination d'un ETM en sept classes (Müller, 1969). Les valeurs de l'indice sont calculées à partir de la formule suivante :

(4) $Igeo = \log_2(Cn/1{,}5Bn)$

où Cn est la concentration en µg/g en poids sec de l'élément trace dans l'échantillon et Bn est la concentration (µg/g) en poids sec de cet élément dans le fond géochimique. La constante 1,5 est le facteur qui prend en compte les variations possibles des valeurs du fond géochimique générées par les changements lithologiques.

Le facteur de risque écologique (ER) combine le facteur de contamination (CF) avec un facteur de réponse toxique (Tr). Le CF est la comparaison entre la concentration mesurée dans l'échantillon ($C_{metal}$)et le fond géochimique ($C_{fond}$), alors qu'un Tr est une valeur attribuée à chaque ETM selon leur toxicité. Ainsi, le Tr est de 1 pour Mn et Zn; 2 pour V; 5 pour Cu, Pb et Ni; 10 pour As; et 30 pour Cd (Hakanson, 1980). Le ER est calculé ainsi :

(5) $ER = (C_{metal}/C_{fond}) * Tr$

Les résultats ont été interprétés avec les *Recommandations canadiennes pour la qualité des sédiments : protection de la vie aquatique* établies par le Conseil de Ministres de l'Environnement du Canada (CCME, 1999). Ces recommandations fournissent des critères de qualité sous forme des valeurs de références, exprimées en grammes par kilogramme de sédiment sec, pour certains ETM. Ces repères permettent d'évaluer le risque d'occurrence d'effets biologiques nuisibles dans les milieux aquatiques. À partir de base de données sur l'occurrence et les concentrations, deux critères principaux ont été définis pour les milieux lacustres et marins : la concentration seuil produisant un effet (CSE) et la concentration produisant un effet probable (CEP). En dessous de la CSE, la probabilité d'observer des effets biologiques nuisibles est faible, tandis qu'au-dessus de la CEP, cette probabilité est considérée comme élevée. Les valeurs des recommandations représentent les concentrations totales dans les sédiments des 5 premiers cm.

## 6. ORGANISATION DE LA THESE

Cette thèse est structurée en trois chapitres présentés sous forme d'article scientifique, chacun correspondant à l'un des trois objectifs spécifiques de la thèse. Les références bibliographiques de l'introduction et de la conclusion générales sont regroupées à la fin de la thèse, tandis que celles propres à chaque article figurent à la fin des chapitres concernés.

Le premier chapitre présente une étude géochimique spatiale des sédiments de surface de l'Arctique canadien qui permet d'établir la dynamique sédimentaire régionale. L'utilisation d'indices de pollution, souvent critiquée dans les études écotoxicologiques, a été évaluée en utilisant différents fonds géochimiques et éléments normalisateurs. Les résultats de ce chapitre ont été publiés dans la revue *Applied Geochemistry* en mai 2025.

Brice, C., Montero-Serrano, J.-C., & Saint-Louis, R. (2025). Regional geochemical survey of Canadian Arctic sediments: insights into provenance, sediment dynamics and trace metal enrichment. *Applied Geochemistry, 189*, 106432. https://doi.org/https://doi.org/10.1016/j.apgeochem.2025.106432

Le deuxième chapitre vise à fournir les concentrations de références des métaux dans l'Arctique canadien. À l'aide de l'étude géochimique régionale préalablement réalisée, les teneurs, la répartition et le comportement des métaux traces dans la fraction extractible à l'acide des sédiments de surface sont analysés et définis. La contamination métallique et le risque écologique associé sont également étudiés avec les indices de pollution et les directives sur la qualité des sédiments. Cet article a été publié dans la revue internationale *Marine Pollution Bulletin* en novembre 2025.

Brice, C., Montero-Serrano, J.-C., St-Louis, R., & Rosabal, M. (2026). Establishing baseline levels of extractable trace metals in marine surface sediment of the Canadian Arctic. *Marine Pollution Bulletin*, 223, 119043. https://doi.org/https://doi.org/10.1016/j.marpolbul.2025.119043

Le troisième chapitre porte sur l'évaluation de la contamination métallique le long des côtes de communautés inuites de l'Arctique canadien. La distribution des éléments majeurs et traces a été étudiée à la fois dans la fraction totale, par ED-XRF, et dans la fraction extractible à l'acide, par ICP-QQQ. Cet article a été soumis à la revue *Environmental Pollution* en décembre 2025.

Brice, C., Montero-Serrano, J.-C., St-Louis, R., & Rosabal, M. (soumis). Spatial distribution of trace metal and pollution assessment in surface coastal sediments of Canadian Arctic communities. Soumis à *Environmental Pollution*.

La conclusion générale synthétise les principaux enseignements tirés des trois chapitres de cette thèse. Elle prend la forme d'une discussion résumant l'ensemble des thématiques abordées dans le cadre de cette thèse. Cette section met en lumière les résultats majeurs, les limites de l'étude, ainsi que les pistes de recherche envisagées pour la suite.

## 7. COMMUNICATIONS ET AUTRES REALISATIONS

Au cours de ce projet de thèse, j'ai pu participer à un congrès national (ArcticNet 2023), deux congrès internationaux (SETAC et Arctic Frontiers), ainsi qu'à 11 conférences institutionnelles (ArcTrain, Geotop et Québec Océan), où j'ai présenté les résultats de mon doctorat (liste détaillée ci-dessous). Dans le cadre de mon doctorat, j'ai eu la chance de participer à deux missions en mer à bord du NGCC Amundsen dans l'Arctique canadien. J'ai également organisé deux campagnes d'échantillonnage à Kugluktuk (2022) et Mittimatalik (2023), et participé à une campagne de terrain à Cambridge Bay (2024). J'ai participé à l'école d'été de l'Institut France-Québec Maritime 2022 à Bordeaux (France).

**Brice, C.**, Montero-Serrano, J.-C., St-Louis, R., & Rosabal, M. (14-16 mars 2025). *Distribution of labile rare earth elements in surface sediments in the Canadian Arctic* [présentation orale, conférence institutionnelle]. Congrès des étudiants du Geotop 2025. Montréal (QC), Canada.

**Brice, C.**, Rosabal, M., St-Louis, R., & Montero-Serrano, J.-C. (25-26 février 2025). *Spatial distribution and pollution assessment of metals in surface sediment along the coasts of Canadian Arctic communities* [présentation par affiche, conférence institutionnelle]. Rencontre Scientifique Annuelle 2025 de Québec Océan. Rivière-du-Loup (QC), Canada.

**Brice, C.**, Rosabal, M., St-Louis, R., & Montero-Serrano, J.-C. (2-5 février 2025). *Spatial distribution and pollution assessment of metals in surface sediment along the coasts of Canadian Arctic communities* [présentation par affiche virtuelle, conférence internationale]. Arctic Frontiers 2025 Beyond Borders, Tromsø, Norway (conférence hybride).

**Brice, C.**, Rosabal, M., St-Louis, R., & Montero-Serrano, J.-C. (20-24 octobre 2024). *Distribution of trace metals and rare earth elements in surface sediments in the Canadian Arctic: establishment of a geochemical baseline* [présentation par affiche, conférence internationale]. SETAC North America 2024. Fort Worth (TX), USA.

**Brice, C**., Montero-Serrano, J.-C., & St-Louis, R. (22-24 mars 2024). *Trace metal assessment in coastal sediment near Inuit communities of the Canadian Arctic* [présentation orale, conférence institutionnelle]. Congrès des étudiants du Geotop 2024. Lac Delage (QC), Canada.

**Brice, C.**, Montero-Serrano, J.-C., St-Louis, R. et Rosabal-Rodriguez, M. (6-7 février 2024). *Répartition des métaux traces dans les sédiments de surface dans l'Arctique canadien: évaluation des contributions naturelles et anthropiques* [présentation par affiche, conférence institutionnelle]. Rencontre Scientifique Annuelle 2024 de Québec Océan. Rivière-du-Loup (QC), Canada.

**Brice, C.**, Montero-Serrano, J.-C. et St-Louis, R. (4-7 décembre 2023). *Trace metal assessment in coastal sediment near Inuit communities of the Canadian Arctic Archipelago* [présentation par affiche, conférence nationale]. ArcticNet Annual Scientific Meeting 2023. Iqaluit (NU), Canada.

Limoges, A., Montero-Serrano, J.-C., Normandeau, A., Ribeiro, S., Belko, A., **Brice, C.**, Girard, J., Harker, B., Koerner, K., Stancu, C. (2023). *Sediment and phytoplankton sampling for the programs ArcticNet Seafloor Mapping and Data Processing and Dissemination & ArcticNet Rapidly changing ecosystem dynamics in the Arctic Ocean' Last Ice Area (RED-AO)*. ArcticNet Leg 3 Cruise Report - CCGS Amundsen (7 September to 5 October 2023), chapter 12.

**Brice, C.**, Montero-Serrano, J.-C. et St-Louis, R. (27-31 mars 2023). *Geochemical baseline and trace metals distribution in marine surface sediments of the Canadian Arctic Archipelago* [présentation par affiche, conférence institutionnelle]. ArcTrain Annual Meeting. Etelsen, Allemange.

**Brice, C.**, Montero-Serrano, J.-C. et St-Louis, R. (10-12 mars 2023). *Geochemical baseline and trace metals distribution in marine surface sediments of the Canadian Arctic Archipelago* [présentation par affiche, conférence institutionnelle]. Congrès des étudiants du Geotop 2023. Orford (QC), Canada.

**Brice, C.**, Montero-Serrano, J.-C. et St-Louis, R. (6-7 février 2023). *Geochemistry of marine surface sediments in the Canadian Arctic Archipelago: assessment of sedimentary sources and trace metals enrichments* [présentation orale, conférence institutionnelle]. Rencontre Scientifique Annuelle 2023 de Québec Océan. Rivière-du-Loup (QC), Canada. (Prix de la meilleure présentation orale)

**Brice, C.** (décembre 2022). Les sédiments : un puit à contaminants. *Infolettre du Geotop, décembre 2022*. https://mailchi.mp/4d3583ca6029/infolettre-du-geotop-decembre-2022-geotop-newsletter-december?e=04adb7e751

**Brice, C.** (15 novembre 2022). *La collecte de sédiments dans l'arctique canadien* [présentation orale]. 4 à 7 Nordicité du Comité nordique de l'UQAR. Rimouski, QC.

Montero-Serrano, J.-C., Bracquart, E., **Brice, C.**, Koerner, K. (2022). *ArcticNet seafloor mapping and marine geology projet*. ArcticNet Leg 2 Cruise Report - CCGS Amundsen (22 September to 19 October 2022) 30 p.

**Brice, C.**, Montero-Serrano, J.-C. et St-Louis, R. (13-17 mai 2022). *Geochemical baseline of major and trace elements in sediments from the Canadian Arctic Archipelago* [présentation par affiche, conférence institutionnelle]. ArcTrain Annual Meeting 2022. Jouvence (QC), Canada. (Prix de la 2$^{e}$ meilleure affiche)

**Brice, C.**, Montero-Serrano, J.-C. et St-Louis, R. (29-31 mars 2022). *Spatial and temporal variations of major and trace elements in marine sediments of the Canadian Arctic Archipelago* [présentation par affiche, conférence institutionnelle]. Congrès des étudiants du Geotop 2022. En ligne.

**Brice, C.**, Montero-Serrano, J.-C. et St-Louis, R. (31 janvier-3 février 2022). *Variations spatio-temporelles des éléments majeurs et traces dans les sédiments de surface de l'archipel arctique canadien* [présentation par affiche, conférence institutionnelle]. Rencontre Scientifique Annuelle 2022 de Québec Océan. En ligne.

**Brice, C.**, Montero-Serrano, J.-C. et St-Louis, R. (12-16 octobre 2021). *Spatio-temporal variations of heavy metals in sediments of the Canadian Arctic Archipelago* [présentation orale et par affiche, conférence institutionnelle]. ArcTrain Annual Meeting 2021. Isle-aux-Coudres (QC), Canada.

# CHAPITRE 1
# ÉTUDE GEOCHIMIQUE REGIONALE DES SEDIMENTS DE L'ARCTIQUE CANADIEN : APERÇU DE LA PROVENANCE, DE LA DYNAMIQUE SEDIMENTAIRE ET DE L'ENRICHISSEMENT EN METAUX TRACES

## 1.1 RESUME EN FRANÇAIS DU PREMIER ARTICLE

Les teneurs en éléments majeurs et traces, la granulométrie et les teneurs en carbone organique total ont été mesurées dans 141 échantillons de sédiments marins de surface et terrestres afin d'étudier la dynamique moderne des sédiments dans l'Arctique canadien (AC) et de fournir une évaluation de l'enrichissement en métaux pour V, Zn, Mn et Fe. Les échantillons ont été prélevés dans différentes zones entre la baie de Baffin et la mer de Beaufort au cours des expéditions ArcticNet 2016-2022 à bord du brise-glace Amundsen de la Garde côtière canadienne. Les données géochimiques combinées à des analyses statistiques multivariées ont permis de diviser l'AC en trois groupes chimiques (CC) et quatre provinces régionales. L'AC central (CC#1) et l'AC du sud-est (CC#2) sont principalement composées de sédiments relativement grossiers riches en carbonates détritiques (Ca, Mg) et en éléments silicoclastiques (Si, K, Zr), respectivement, reflétant l'érosion côtière des terres environnantes (par exemple, l'île Victoria, l'île de Baffin) et le transport de la glace de mer chargée de sédiments. Les sédiments du CC#3, qui comprennent l'AC de l'ouest et de l'est, sont caractérisés par du carbone organique et des oxyhydroxydes de Fe-Mn. L'ouest de l'AC, qui est également caractérisée par des aluminosilicates à grains fins, est influencé par le débit du fleuve Mackenzie, tandis que l'est de l'AC est définie par les polynies et l'érosion glaciaire. Les concentrations les plus élevées de V et de Zn sont enregistrées dans l'AC de l'ouest. Dans l'ensemble de la région, des corrélations positives significatives entre Al et Zn, V et Fe suggèrent que les apports lithogéniques influencent la distribution de ces métaux dans les sédiments de l'AC et que les oxydes de Fe représentent la principale phase porteuse. Dans

l'ouest de l'AC, le Mn présente des relations positives mais plus faibles avec Al et Fe, ce qui suggère une source mixte d'oxyhydroxydes de Mn liée à la fois à des fractions détritiques et à des processus authigéniques près de l'interface eau-sédiment. Les apports élevés d'oxyhydroxydes de Mn terrestres provenant de la rivière Mackenzie sont remobilisés et transportés vers des zones où la consommation d'oxygène dans les sédiments est plus faible, c'est-à-dire les côtes du golfe d'Amundsen et de l'île Banks, ce qui entraîne un enrichissement des sédiments de surface en Mn. Le facteur d'enrichissement et l'indice de géo-accumulation, deux indices de pollution couramment utilisés pour identifier les apports anthropiques de métaux, ont également été étudiés afin d'évaluer leur pertinence dans le cadre de cette étude. Les divergences résultant de la normalisation des métaux avec un fond géochimique et un élément de normalisation ont révélé que les indices de pollution doivent être utilisés avec prudence. Dans l'ensemble, selon les indices de pollution et l'étude régionale, les sédiments de surface de l'AC montrent un enrichissement mineur en métaux traces et présentent donc des concentrations naturelles par rapport aux valeurs de fond régionales.

## 1.2 REGIONAL GEOCHEMICAL SURVEY OF CANADIAN ARCTIC SEDIMENTS: INSIGHTS INTO PROVENANCE, SEDIMENT DYNAMICS AND TRACE METAL ENRICHMENT

Major and trace element contents, grain size distribution and total organic carbon contents were measured in 141 marine surface and terrestrial sediment samples to study modern sediment dynamics in the Canadian Arctic (CA) and to provide an assessment of metal enrichment for V, Zn, Mn and Fe. Samples were collected from different areas between Baffin Bay and the Beaufort Sea during the ArcticNet 2016–2022 expeditions onboard the Canadian Coast Guard icebreaker Amundsen. Geochemical data combined with multivariate statistical analyses allowed the division of the CA into three chemical clusters (CC) and four regional provinces. Central CA (CC#1) and southeastern CA (CC#2) are mainly composed of relatively coarse sediments rich in detrital carbonates (Ca, Mg) and siliciclastic elements (Si, K, Zr), respectively, reflecting coastal erosion of surrounding land (e.g., Victoria Island, Baffin Island) and transport of sediment-laden sea ice. The sediments of CC#3, comprising western and eastern CA, are characterized by organic carbon and Fe–Mn oxyhydroxides. Western CA, which is also characterized by fine-grained aluminosilicates, is influenced by the Mackenzie River discharge, while eastern CA is shaped by polynyas and glacial erosion. The highest concentrations of V and Zn are recorded in the western CA. Over the whole region, significant positive correlations of Al with Zn, V and Fe suggest that lithogenic-derived inputs influence the distribution of these metals in sediments from the CA and that Fe oxides represent the main carrier phase. In western CA, Mn displays positive but weaker relationships with Al and Fe, suggesting a mixed source of Mn oxyhydroxides linked to both detrital fractions and authigenic processes near the sediment-water interface. High terrestrial Mn oxyhydroxide inputs from the Mackenzie River are remobilized and transported to areas with lower oxygen consumption in sediment, i.e., the Amundsen Gulf and Banks Island coasts, which leads to surface sediment enrichment in Mn. The enrichment factor and the geo-accumulation index, two pollution indices commonly used for identifying anthropogenic metal inputs, were also studied to evaluate their suitability in the context of this study. Discrepancies from the normalization of metals with a geochemical background and a normalizing element revealed that pollution indices should be used with caution. Overall,

according to the pollution indices and the regional survey, the surface sediments of the CA show minor enrichment in trace metals and thus present natural concentrations relative to regional background values.

## 1.3 INTRODUCTION

Trace metals naturally occur in the environment, and some are essential elements for biological systems. However, some of them, also known as heavy metals, have become contaminants of concern affecting all systems (AMAP, 1998, 2005), including aquatic environments, because human activities disrupt their natural cycles (Macdonald & Bewers, 1996). Arctic coastal environments and shelves are particularly important areas for biogeochemical cycles and are recognized as regions that are naturally rich in trace elements (Stein & Macdonald, 2004). High inputs of land-derived dissolved and particulate trace elements make these areas sensitive to metal enrichment (Brown et al., 2020; Colombo et al., 2019; Jensen & Colombo, 2024). Indeed, scavenging of dissolved trace metals from the water column to sediments by adsorption, precipitation or complexation with mineral phases (such as clays), Fe-organic colloids, particulate organic carbon and Fe–Mn oxyhydroxide coatings can be very high in the Arctic Ocean (Jensen & Colombo, 2024), making sediments a major sink for those metals. Despite limited human settlements in the Arctic, and thus limited localized direct anthropogenic trace metal emissions, Arctic environments are nonetheless affected by important inputs of inorganic (e.g., Hg, Pb, and Cd) and organic (e.g., polycyclic aromatic hydrocarbons and persistent synthetic organic compounds) contaminants via long-range atmospheric transport (AMAP, 2005, 2021a, 2021b), making anthropogenic emissions a substantial source of trace metals in the region.

Properly assessing trace metal contamination in Arctic marine sediments requires a clear understanding of the natural geochemical variability across the region. Therefore, analyses of sediment provenance, transport pathways, and depositional conditions are essential, as they establish the geochemical and sedimentological framework needed to

distinguish natural background levels from potential anthropogenic inputs (Domingo et al., 2023; Loring, 1991). Studies on the trace metal concentrations and sediment dynamics in Arctic Ocean have been performed in Chukchi and Beaufort seas and Siberian Shelf (e.g., (Budko et al., 2022; Crecelius et al., 1991; Kondo et al., 2016; Myers & Darby, 2022; Naidu et al., 2012; Trefry & Neff, 2019; Viscosi-Shirley et al., 2003; Zhang et al., 2021) and in Canadian Arctic rivers (Brown et al., 2020; Colombo et al., 2019; Grenier et al., 2022). However, the vast network of channels, continental shelves, and slopes within the CA remains comparatively understudied (e.g., (Deschamps et al., 2018; Gamboa et al., 2017; Kutos et al., 2021; Kuzyk et al., 2017; Letaïef et al., 2021). The spatial distribution of major and trace metals in surface sediments within the CA is influenced by a complex interplay of factors, including the diversity of surrounding geological provinces, the nature of terrigenous source material, the grain size variability, and the presence of geochemical carriers such as metallic oxides and organic matter (Letaïef et al., 2021). These factors, governed by sediment provenance and transport dynamics, ultimately control the natural variability of trace metal concentrations and must be accounted for when evaluating potential contamination (e.g., (Domingo et al., 2023).

Chemical pollution indices are a widespread technique for assessing the level and impact of sediment contamination by metals, and discerning the human impacts (e.g., (Reimann & de Caritat, 2000). These indices attribute a value that reflects the level of contamination or pollution in the sample by normalizing the elements to a natural geochemical background and a conservative element. Even though the pollution indices have been used in multiple environmental studies, the concept of normalization has been questioned because of the natural variability of chemical composition of the natural background and geochemical processes (e.g., redox conditions and bottom scavenging) modify elemental concentrations (Anderson & Kravitz, 2010; Desaules, 2012; Poh & Tahir, 2017; Reimann & de Caritat, 2000, 2005; Tribovillard et al., 2006; Van der Weijden, 2002).

In this context, major and trace elements content, grain size and total organic carbon (TOC) content were measured in this study on marine surface and terrestrial sediment

samples from the CA to (1) establish a portrait of the spatial regional variability of the chemical composition of the seafloor, (2) acquire a better understanding of the sediment provenance and the sedimentary and geochemical processes that govern the distributions of major and trace elements, and (3) evaluate the applicability of commonly used pollution indices for assessing trace metal enrichment in surface sediments. Additionally, this study provides a geochemical baseline and contribute to a comprehensive understanding of sediment transport processes that operate across the Canadian Arctic.

## 1.4 STUDY AREA

The study area comprises the Canadian mainland north of 65°N and the Archipelago, a network of islands, and narrow and shallow channels connecting the Arctic Ocean to the Labrador Sea (Fig. 7). It is entirely covered by a continued permafrost (Heginbottom, 1995), which stores large amounts of soil organic carbon, especially in the western part of the CA (Hugelius et al., 2014). Hydrology is restricted and controlled by seasonal freezing and thawing of the permafrost. Located on the western coast of the mainland (Fig. 7), the Mackenzie River is the most important river of the CA. It drains an area of approximately $1.78 \times 10^6$ km$^2$ and has a mean discharge of ~300 km$^3$/yr (Millot et al., 2003). It is also the largest Arctic river in terms of suspended sediment flux and the second largest in terms of dissolved material to the Arctic Ocean (Millot et al., 2003). Smaller rivers also contribute significantly to the global discharge in central CA (Fig. 7), with an annual discharge estimated to be ~260 km$^3$/yr (Alkire et al., 2017). This includes the Coppermine River, whose outlet is situated in the community of Kugluktuk (~8.77 km$^3$/yr), the Ellice River (~2.82 km$^3$/yr), the Back River (~15.52 km$^3$/yr) and the Anderson River (~4.72 km$^3$/yr; (Déry et al., 2016).

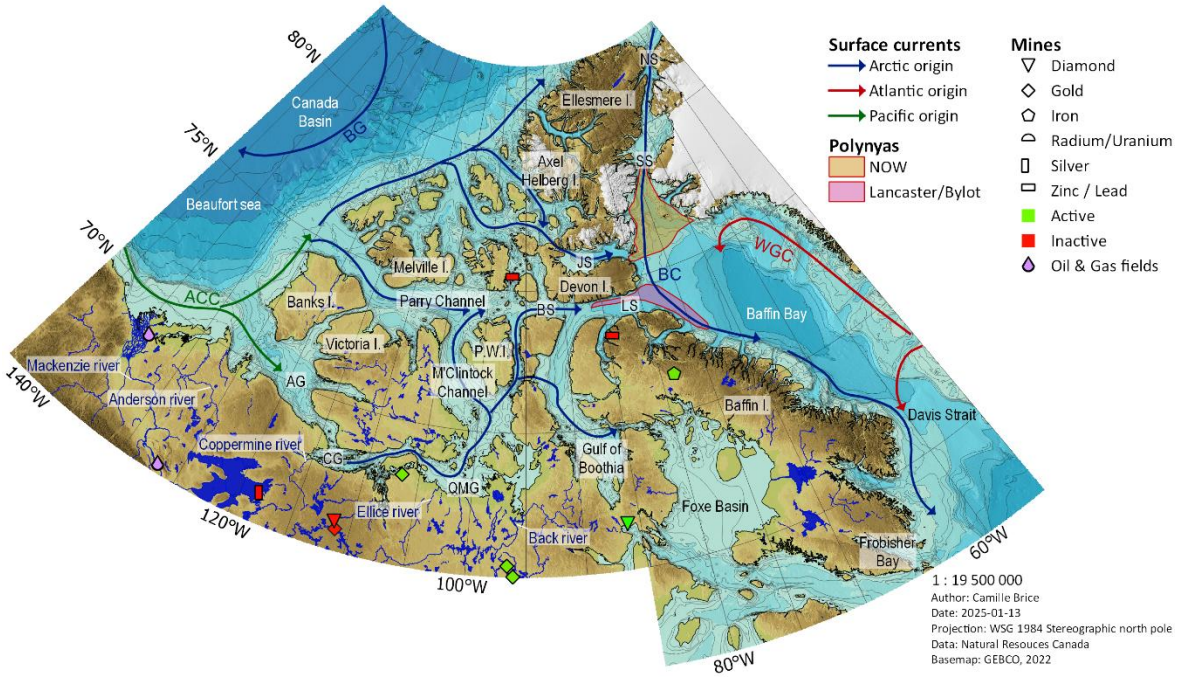


Figure 7. Map of the Canadian Arctic showing the main geographical setting, i.e., surface currents, polynyas and active and abandoned mines and gas/oil fields. AG: Amundsen Gulf, BS: Barrow Strait, CG: Coronation Gulf, JS: Jones Sound, LS: Lancaster Sound, NS: Nares Strait, QMG: Queen Maud Gulf and SS: Smith Sound. ACC: Alaska Coastal Current, BC: Baffin Current, BG: Beaufort Gyre and WGC: West Greenland Current. P.W.I.: Prince of Wales Island.

Within the CA, three water masses are found (McLaughlin et al., 2005; Steele et al., 2004): the Polar Mixed Layer (PML), the Arctic waters of Pacific origin (ApW) and the Atlantic waters (AW). The PML is found in the upper 50–100 m of the water column and consists of summer meltwater and river discharge. The ApW occupy the 100–300 m water depth layer. It is a fresh and nutrient-rich water mass dominating the western CA that flows eastward along the coast via the Alaska Coastal Current (ACC; Fig. 7). The saline and warmer AW are found beneath the ApW in the Canada Basin and in the Baffin Bay. The shallow channels in central CA are composed of only the first two water masses. A prevailing west-east current flows through the islands of the Canadian Arctic, transporting Arctic and Pacific waters eastward toward the Atlantic, propelled by the elevated sea level in the Pacific. Sea ice completely covers the CA waters seasonally, with freeze-up starting in September

and break-up starting in June (Canadian Ice Services, 2023). First-year sea ice is predominant in the CA and covers most of the area, except in areas such as the northern Beaufort Sea and channels north of the Parry Channel, where old ice predominates (Canadian Ice Services, 2023). Freshet from the Mackenzie River combined with wind and summer temperatures lead to ice-free waters on the Beaufort Shelf and slope in July/August (O'Brien et al., 2006). Multiple polynyas are present in Canadian Arctic waters, namely the well-known North Water Polynya (NOW; Pikialasorsuaq), and the Lancaster Sound and Bylot Island Polynyas (Fig. 7; Hannah et al., 2009; Stirling & Cleator, 1981). They are maintained by latent heat and ice arches formed in the Nares Strait and Lancaster Sound (Vincent, 2023). These polynyas, especially the Pikialasorsuaq, are highly productive areas (Ribeiro et al., 2021) with high resulting fluxes of organic carbon (Hamel et al., 2002).

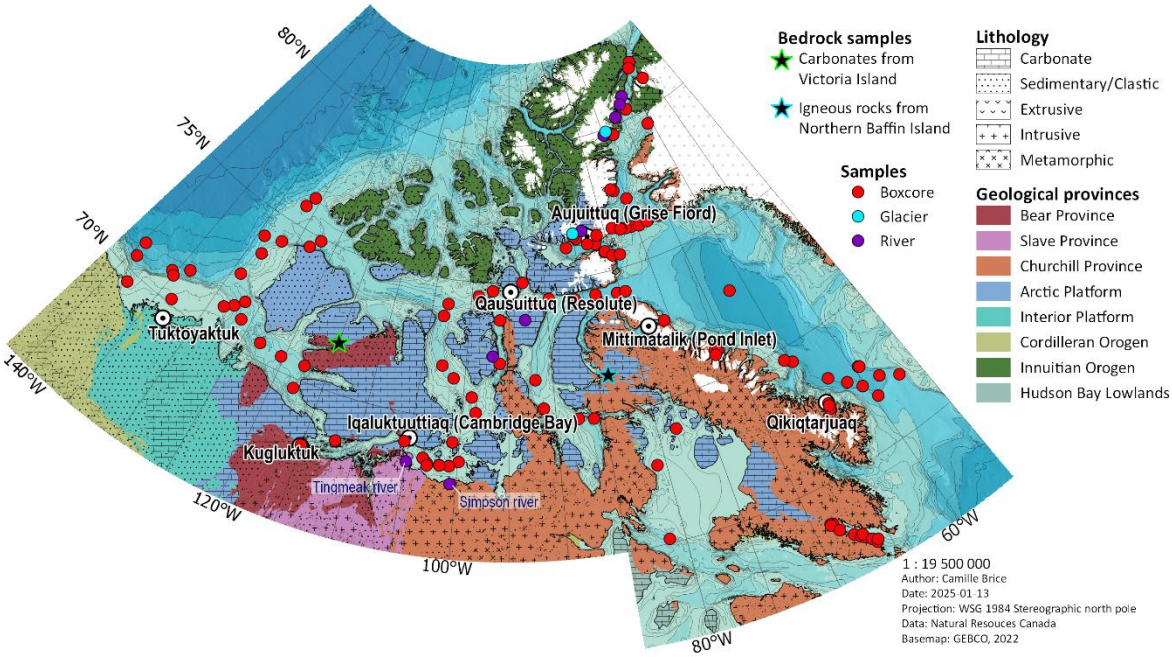


Figure 8. Geological map of the Canadian Arctic (data from Harrison et al., 2011) with the location of the samples. Comparative bedrock samples include carbonates from Victoria Island (Bédard et al., 2016) and igneous rocks from the Jungersen River in the Churchill Province (Lebeau, 2022).

Three main regional geological units characterize the CA: the Canadian Shield, the Interior Plains and the Innuitian Orogen (Fig. 8; Brown, 1972; Harrison et al., 2011). The

Canadian Shield, which occupies the eastern part of the study area, is divided into the provinces of Churchill, Bear and Slave, and is mainly composed of Archean and Proterozoic gneiss, granites and gabbros (Harrison et al., 2011). Younger interior and Arctic platforms form the Interior Plains, which are made up of carbonate rocks, mostly dolostones, in central CA and sedimentary rocks, such as siltstone and sandstone, in western CA. The Silurian-Devonian Innuitian Orogen consists of mildly to strongly folded and deformed sedimentary units (Harrison et al., 2011; Trettin et al., 1989). It occupies the islands of northern CA, i.e., the Queen Elizabeth Islands.

Modern sedimentary processes across the CA are dominated by river discharge, entrainment by sea ice, and coastal and glacial erosion (Letaïef et al., 2021). The Mackenzie River, along with the small rivers of the CA, are exporting significant amounts of land-derived inorganic and organic material to the ocean originating from the surrounding geology, i.e., Precambrian igneous and metamorphic rocks to central and eastern CA and younger sedimentary rock to western CA (Millot et al., 2003). The erosion of Arctic coasts and the resulting sediment inputs are substantial, mainly because of permafrost thaw. On average, Arctic coastal erosion rate is 0.5 $m.yr^{-1}$, though rates can exceed 3 $m.yr^{-1}$ along the Beaufort Sea coast. This process contributes to significant fluxes of material, including contaminants, to the marine environment (Lantuit et al., 2012). Although data on coastal erosion within the Canadian Arctic Archipelago remain limited, the existing studies suggest that most coastlines are relatively stable (Lantuit et al., 2012; St-Hilaire-Gravel et al., 2012). Letaïef et al. (2021) however identified coastal erosion as a key driver for sediments transport for the Banks Island area, the M'Clure Strait and the Barrow Strait/Lancaster Sound. Suspended fine-grained sediments coming from rivers and coastal erosion can also be entrained by frazil and anchor ice (Darby et al., 2011; Reimnitz et al., 1993). The incorporation of sediments into sea ice during its formation is an important sedimentary transport process, mainly in the Beaufort Sea. As sea ice is transported by surface currents and subsequently melts, the entrained particles are redistributed, with their presence observed further east, as interpreted by Letaïef et al. (2021). Finally, several glaciers are present along

the eastern coasts of Ellesmere, Devon and Baffin Islands, which highly contribute to the sediment supply, mainly in fjords (Normandeau et al., 2019; Syvitski & Normandeau, 2023).

## 1.5 METHODOLOGY

### 1.5.1 Sampling

A total of 128 surface sediment samples and 13 terrestrial samples (including glacial till and sediments from riverbanks) were collected from different areas between Baffin Bay and the Beaufort Sea as well as in the Nares Strait during the ArcticNet summer expeditions (2016–2019 and 2022) onboard the Canadian Coast Guard Ship (CCGS) icebreaker Amundsen (Fig. 8; Table 3). The terrestrial sampling sites were accessed with the ship helicopter as the CCGS Amundsen traveled through the CA. The marine sediments were sampled with a box corer (50 cm × 50 cm x 60 cm) and the surface uppermost 1 cm of each box core was sampled onboard using a plastic spatula and stored in plastic bags at 4 °C. Push cores (10 cm diameter) were taken from each box core collected during the expeditions; they were subsequently subsampled in the laboratory. The bases (lowermost 1–1.5 cm) of 37 of these push cores were used in this study to establish a regional geochemical background (Table S2). Based on a compilation of sedimentation rates from various studies within the CA (modified from Letaïef et al., 2021), we estimate that the basal sediments of the push cores correspond to pre-industrial times (pre-1900 Common Era or CE; Table 4), and therefore to natural values.

### 1.5.2 Laboratory analyses

All samples were analyzed for major and trace element contents and grain size. While most of the TOC data used in this study are from Corminboeuf et al. (2021), additional TOC analyses were performed on new sediment samples to enhance regional coverage, following the same methodology and using the same instrument. For TOC analysis and elemental

geochemistry, all samples were first wet-sieved through a 150-µm Nitex® mesh using distilled water and then oven-dried (<60 °C) for 12 h, crushed and homogenized with an agate mortar. The <150 µm fraction includes fine-grained sediments, such as clay, silt and fine sand, which allow not only to avoid spatial biases in elemental concentrations linked to coarse-grained size variations, but also to capture the regional geochemical signature of the environment and the different sediment transport processes operating across the CA.

The total carbon (TC) and TOC contents in the <150 µm sediment fraction were measured at the Geotop Light Stable Isotope Geochemistry Laboratory (Montreal, Quebec) with a Carlo-Erba NC 2500 elemental analyzer following the acidification in solution method described in Hélie (2009). Briefly, each sample was divided into two aliquots. The first one (bulk sediment) was used to determine the TC content. The second aliquot was acidified with 1 M HCl to remove carbonates, dried and milled. This carbonate-free aliquot was used to determine the TOC content. To account for inorganic carbon mass loss, a correction was applied to the results (Hélie, 2009). Analytical precision and accuracy were determined by duplicate analyses of samples and replicate analyses of in-house and international standards (low organic content soil, cyclohexanone-2,4-dinitrophenylhydrazone, atropine and acetanilide) and were better than ±0.02 % (1σ).

Grain size analysis was performed with a Malvern PANalytical Mastersizer 3000 laser diffraction grain size analyzer equipped with a Hydro LV module following the instrumental conditions outlined in Belzile and Montero-Serrano (2022). Before measurement, an aliquot of the bulk fraction of each sediment sample was treated with 5–10 mL 30 % $H_2O_2$ to remove organic matter. The dry residues were then diluted with ~30 mL of sodium hexametaphosphate (20 % v/v), sieved at <2 mm, and disaggregated using an in-house rotator for 12 h prior to particle size measurements. The grain size data obtained was processed using the GRADISTAT software version 9.1 (Blott & Pye, 2001).

A total of eight major elements (Mg, Al, Si, K, Ca, Ti, Mn, and Fe) and five trace elements (V, Cr, Zn, Sr, and Zr) were measured in the <150 µm sediment fraction using a Malvern PANalytical Epsilon 3-XL energy dispersive X-ray fluorescence spectrometer (ED-

XRF). Prior to ED-XRF measurements, the loss on ignition (LOI) was determined gravimetrically by weighing an aliquot of 2 g before and after heating it for 4 h at 950 °C. Following the LOI, ~1.1 g of the ignited samples were mixed with 5.5 g of lithium tetraborate (CLAISSE, pure, 99,00 % $Li_2B_4O_7$, and 1,00 % LiBr) and fused with a CLAISSE M4 Fluxer automated fusion furnace to form glass disks. The glass disks were analyzed for elemental geochemistry with the ED-XRF. The acquired ED-XRF spectra were treated with the Malvern PANalytical Omnian standardless software package calibration, and the acquired data are expressed as percent mass (wt.%) for major elements and micrograms per gram (µg/g) for trace elements. Procedural blanks were prepared with synthesized silicon oxide powder (99.999 % $SiO_2$; American Elements; SI-OX-05M-P.325 M). The $SiO_2$ blank concentrations are less than the detection limit (DL; Fig. 16; Table 5) for most major and trace elements, except for $Al_2O_3$ (~0.83 %; Table 6). This Al contamination is probably derived from the ceramic crucibles used for LOI determination. Thus, the Al concentrations in the sediment samples are corrected by subtracting the mean Al values of the procedural blanks. The accuracy of the overall method, including the digestion and glass disks preparation, was assessed by analyzing the USGS certified material SDC-1 and BCR-2. The results obtained for these reference materials are in good agreement with reference values from the GeoREM database (http://georem.mpch-mainz.gwdg.de/; Fig. 16). Except for MgO in the analysis of SDC-1, the recovery values (accuracy) for all the measured elements were between 91 and 118 % (Table 7), which corresponds to the usual acceptable deviation limits (Thompson et al., 2002). The reproducibility of ED-XRF analysis, based on replicate analysis of USGS standards SDC-1 and BCR-2 every 9 samples, was <8 % relative standard deviation (RSD, 1σ) for major elements, <11 % for V and <5 % for the other elements (Table 7). Cr was excluded from the statistical analysis because the majority of the results were below the DL, and the accuracy with certified material was not acceptable; however, few results were kept as qualitative values in the interpretation.

### 1.5.3 Pollution indices

Two pollution indices were used to determine metal contamination/enrichment in the sediment and to assess anthropogenic influence. Different geochemical backgrounds were employed for the calculation of the indices to consider the warnings mentioned by several studies (Anderson & Kravitz, 2010; Desaules, 2012; Poh & Tahir, 2017; Reimann & de Caritat, 2000, 2005; Tribovillard et al., 2006; Van der Weijden, 2002). Three geochemical backgrounds were used in the calculations of the pollution indices for comparison: 1) Average Shale (AS; (Turekian & Wedepohl, 1961), 2) Upper Continental Crust (UCC; (Taylor & McLennan, 1985), and 3) a regional geochemical background obtained from basal sediment samples from 37 push cores collected in the CA representing pre-industrial times. This pre-industrial background was subdivided into local backgrounds according to the clusters determined with the surface samples. The pollution indices used in the study are as follows, and the sediment quality classification levels are shown in Table 2:

Tableau 2.

Classes of pollution indices used in this study. EF: enrichment factor, Igeo: Geo-accumulation index.

| Indice | Classes | Values | Sediment quality | References |
|---|---|---|---|---|
| EF | | EF < 1 | No enrichment | Hakanson (1980) |
| | | EF = 1–3 | Minor enrichment | |
| | | EF = 3–5 | Moderate enrichment | |
| | | EF = 5–25 | Moderately severe enrichment | |
| | | EF = 25–50 | Very severe enrichment | |
| | | EF > 50 | Extremely severe enrichment | |
| Igeo | 0 | Igeo < 0 | Uncontaminated | Müller (1969) |
| | 1 | 0 < Igeo < 1 | Uncontaminated to moderately contaminated | |
| | 2 | 1 < Igeo < 2 | Moderately contaminated | |
| | 3 | 2 < Igeo < 3 | Moderately to heavily contaminated | |
| | 4 | 3 < Igeo < 4 | Heavily contaminated | |
| | 5 | 4 < Igeo < 5 | Heavily to extremely contaminated | |
| | 6 | 5 > Igeo | Extremely contaminated | |

*Enrichment factor* - The enrichment factor (EF) is used to determine if there has been an increase in the levels of that element by an anthropogenic contribution using the following equation:

$$EF=\frac{X_{sample}/Y_{sample}}{X_{background}/Y_{background}}$$

where $X_{sample}$ is the concentration of the trace element in the sample and $Y_{sample}$ is the concentration of a normalizing element in the same sample. $X_{background}$ and $Y_{background}$ are the concentrations of the trace element and the normalizing element, respectively, in the geochemical background. Iron and aluminum are both proposed in the literature as normalizing elements (Birch, 2020), but iron is involved in diagenetic processes that can lead to its enrichment in the first layers of marine sediment. Also, large land-ocean interactions are rapidly evolving in the Arctic, which impact the iron inputs to coastal marine sediments (Colombo et al., 2021; Jensen & Colombo, 2024; O'Donnell et al., 2024). Thus, to study the biogeochemical processes that influence the metal composition of surface sediment, including iron, another element should be used as the normalizer. Aluminum is the normalizing element used here because it is not affected by direct anthropogenic disturbance and redox conditions, it is a major component of detrital sediments and Al has been used as a normalizing element in previous geochemical studies on the Canadian Arctic Archipelago (Trefry & Neff, 2019). Ti, a frequently used and reliable normalizing element (Boës et al., 2011), was also tested to assess discrepancies with Al (Fig. 19).

Geo-accumulation index - The geo-accumulation index (Igeo) classifies the contamination level of a trace element into seven classes (Müller, 1969), as reported in Table 1. The index is calculated with the following equation:

$$Igeo = \log_2 (Cn/1.5Bn)$$

where Cn is the concentration in μg/g of the trace element in the sample and Bn is the concentration (μg/g) of that element in the geochemical background. The constant 1.5 is a

factor that considers the possible variations in the geochemical background values generated by lithological changes.

### 1.5.4 Statistical and spatial approach

Statistical analyses were performed on the ED-XRF data using R software (R Core Team, 2024). A multiplicative lognormal imputation (Palarea-Albaladejo & Martín-Fernández, 2013, 2015) was implemented to impute values below the DL of the data. Prior to multivariate analysis, a centered-log ratio (clr) transformation was applied to remove the statistical constraints on the compositional data (Aitchison, 1982) using the R package "compositions" (van den Boogaart & Tolosana-Delgado, 2008). A K-means clustering analysis was performed with ED-XRF, LOI and TOC data to group samples with similar chemical compositions within the CA. The cluster analysis was conducted with the R package "stats" (R Core Team, 2024). The quality of the analysis was evaluate using a silhouette plot ("factoextra" R package; Kassambara & Mundt, 2020), where negative values indicate an incorrect and/or questionable assignment (Borcard et al., 2011). Principal component analysis (PCA) was performed with the package "FactoMineR" (Lê et al., 2008) to identify elemental associations with similar relative variation patterns and to extract common trends between all variables and clusters. A Spearman correlation matrix was also applied to data, using the package 'corrplot' (Wei et al., 2017) to compare major and trace elements with $D_{90}$ particle size, LOI and TOC data. Nonsignificant correlation coefficients (p-value >0.05) are not shown in the matrix. Geochemical distribution maps were generated using QGIS version 3.22.10.

## 1.6 RESULTS AND INTERPRETATIONS

The elemental concentration revealed significant spatial variation within the CA. Values for major elements ranged from 0.2 to 11 wt % for Mg, 0.6 to 9 wt % for Al, 3 to 38 wt % for Si, 0.1 to 21 wt % for Ca, 0.3 to 6 wt % for Fe, and 0.01 to 2 wt % for Mn (Fig. 9).

The LOI also presents important variability, with values ranging from 2 to 43 %. Central CA and Foxe Basin are marked by the highest values for Mg and Ca and the lowest values for Fe, Al and Si, while the Beaufort Sea and Baffin Bay areas roughly show opposite results. High Mn contents in sediment are observed in Amundsen Gulf and in northern Davis Strait. For trace elements, V shows high variability, with concentrations ranging from <50 (DL) to 306 µg/g, with the highest concentrations found in samples located from the Beaufort Sea and the Amundsen Gulf. Most samples had Cr concentrations <100 µg/g (DL), but some samples from the Beaufort Sea, Amundsen Gulf and Baffin Bay recorded concentrations between 100 and 135 µg/g.

The texture of the sediments (<150 µm fraction) found in the CA range from silt, sandy silt and silty sand (Fig. 17), which is consistent with previous regional studies performed from the Beaufort Shelf to Baffin Bay (e.g., (Corminboeuf et al., 2021; Crecelius et al., 1991; Gamboa et al., 2017; Letaïef et al., 2021; Loring, 1984). The $D_{90}$ for the <150 µm fraction ranges from 12 to 212 µm, with a west-east increasing trend (Fig. 10a). The Beaufort Sea, and the Amundsen and Coronation Gulfs are mostly composed of fine silt. A mix of fine to coarse silt characterizes the Queen Maud Gulf and central channels. The grain size in Baffin Bay and Nares Strait varies from fine silt to fine sand, depending on the proximity to the coast and water depth. The coarsest material, i.e., very coarse silt to fine sand, is found in Frobisher Bay and Baffin Island fjords.

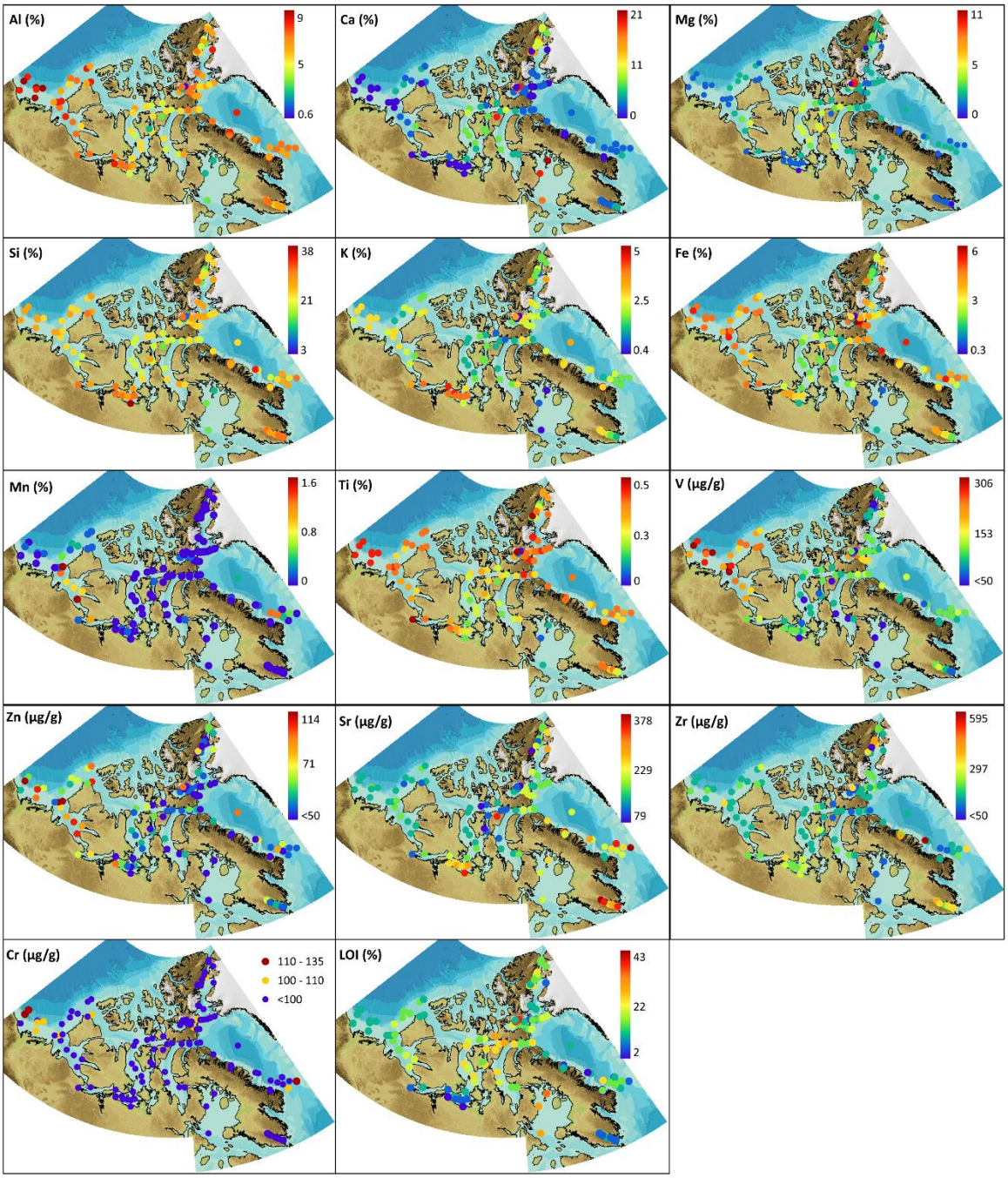


Figure 9. Distribution map of major elements (in wt %) and trace elements (in µg/g) in surface marine and terrestrial sediments of the CA. Fig. 7 presents the geographical information.

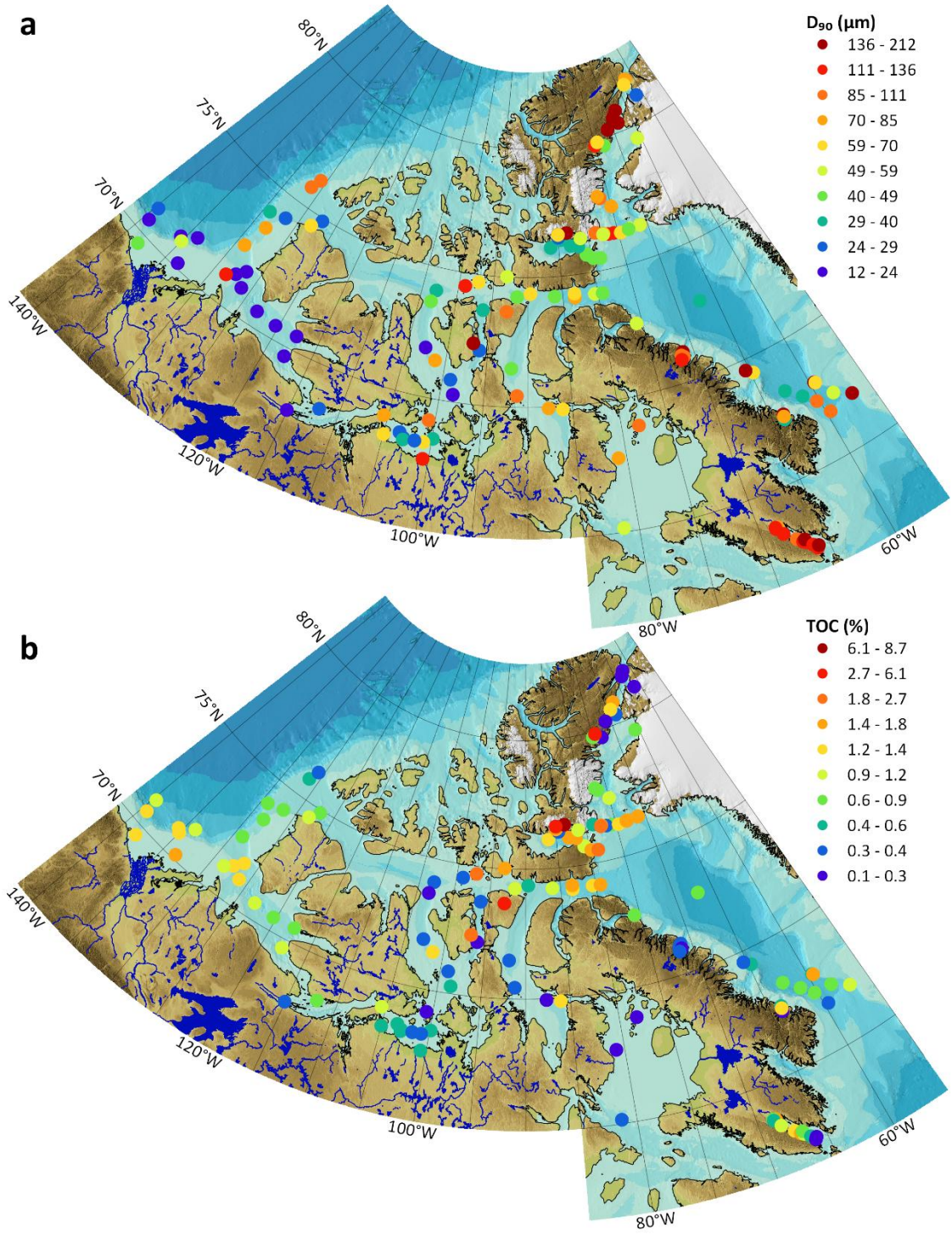


Figure 10. (a) Distribution map of sediment grain size in µm. (b) Distribution map of the total organic carbon content in %. Fig. 7 presents the geographical information.

The TOC content ranges from 0.1 to 2 % throughout the CA, with higher concentrations observed in the fine-grained sediment samples (silt; Fig. 10b & 17). The highest TOC content is found in Jones Sound, Lancaster Sound and Smith Sound, with concentrations around 1–2 %. A gradient is observed in the TOC content in Western CA, with values reaching 2 % close to the Mackenzie River mouth and decreasing when moving away from it, i.e., to 0.4 % north of Banks Island and 0.7 % in Amundsen Gulf. Frobisher Bay samples have values varying from 0.2 to 2 % and show an unclear decreasing trend from the inner to the outer bay. The TOC content in Baffin Bay is within the same values range. The samples from Baffin Bay fjords have low values and those from Davis Strait have values around 0.7–1 %. The lowest concentrations are measured in the Foxe Basin and northern Nares Strait. In terrestrial samples, the TOC content varies between 0.1 and 9 %, with the highest content found in proglacial rivers and glaciers of southern Ellesmere Island.

K-means cluster analysis revealed that the marine surface sediment samples in the CA can be divided into three chemical clusters (CC). A geographical component is clearly observable in the distribution of the clusters within the CA (Fig. 11a). Except for two samples, the clustering analysis correctly classified all the samples according to the silhouette plot (Fig. 11b). The first CC regrouped samples in central CA, i.e., Barrow Strait, M'Clintock Channel, Gulf of Boothia, Foxe Basin, and northern Nares Strait. CC #2 consists of samples located in eastern Baffin Island fjords and Frobisher Bay, and Coronation and Queen Maud Gulfs. The third and largest CC can be subdivided into two parts: western and eastern CA. Western CA is represented by samples originating from the Beaufort Sea, western Banks Island Coast and Amundsen Gulf, whereas eastern CA is mostly represented by samples located around Lancaster and Jones Sounds, and Baffin Bay (south of Smith Sound and north of the Davis Strait). PCA based on ED-XRF, LOI and TOC data indicates that the first two principal components (PC) explain 79 % of the total variance (Fig. 12a). PC1 scores (52 % of the total variance) are positively associated with Ca–Mg-LOI, whereas PC2 scores (27 % of the total variance) are positively associated with Zr–Sr–Si–K–Al and negatively associated with TOC-V-Fe and Mg-LOI (Fig. 12b). The samples are presented in the biplot as points with size varying according to their grain size, which reveals that PC2 scores are mostly

associated with coarse-grained sediments. Mn was not included in the PCA because of its strong influence on elemental geochemical variability. The three clusters determined were clearly distinct in the biplot. Samples in CC#1 are all located on the positive side of PC1 with Ca, the samples in CC#2 are grouped in positive PC2, where coarse-grained sediments are predominant, and the samples in CC#3 are roughly situated in the negative PC1/negative PC2 quadrant.

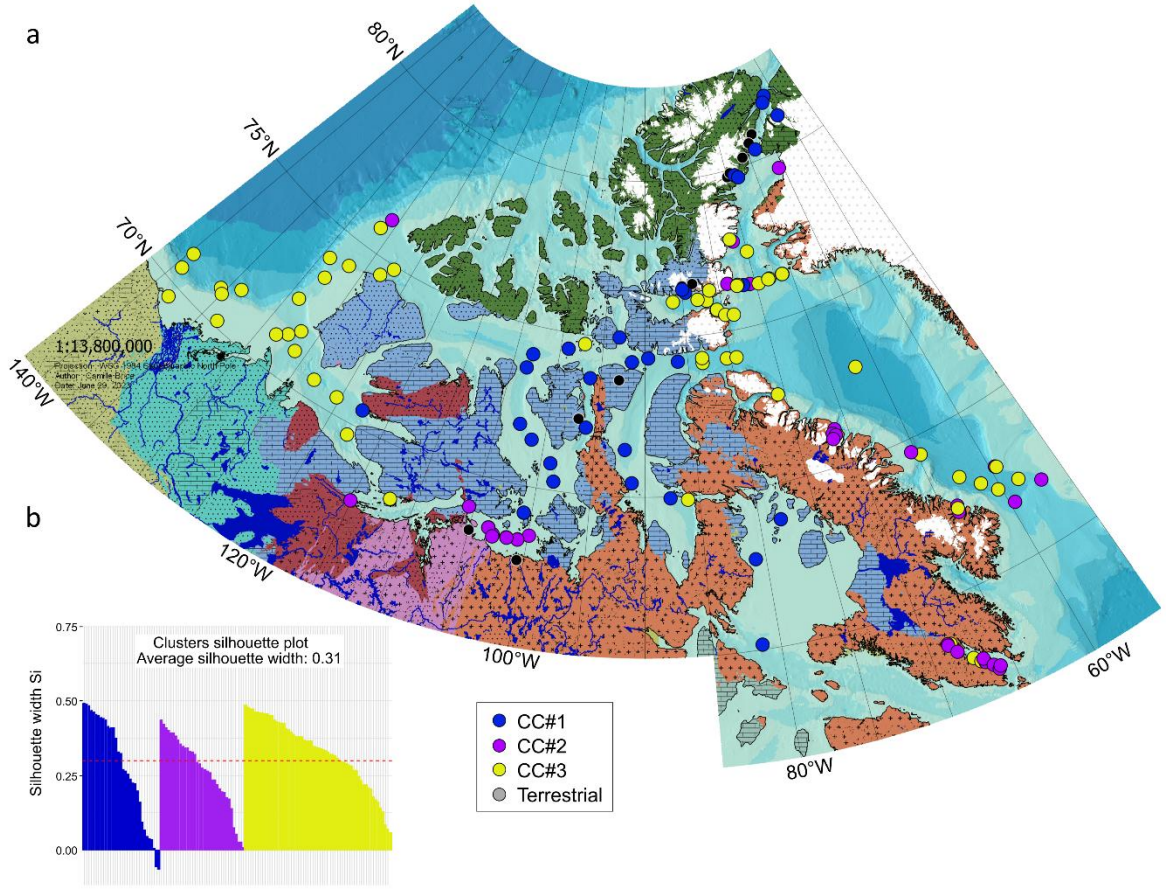


Figure 11. (a) Map showing the repartition of the three chemical clusters. (b) Silhouette plot resulting from the K-means clustering analysis of the marine surface sediments. Fig. 7 shows the geographical information.

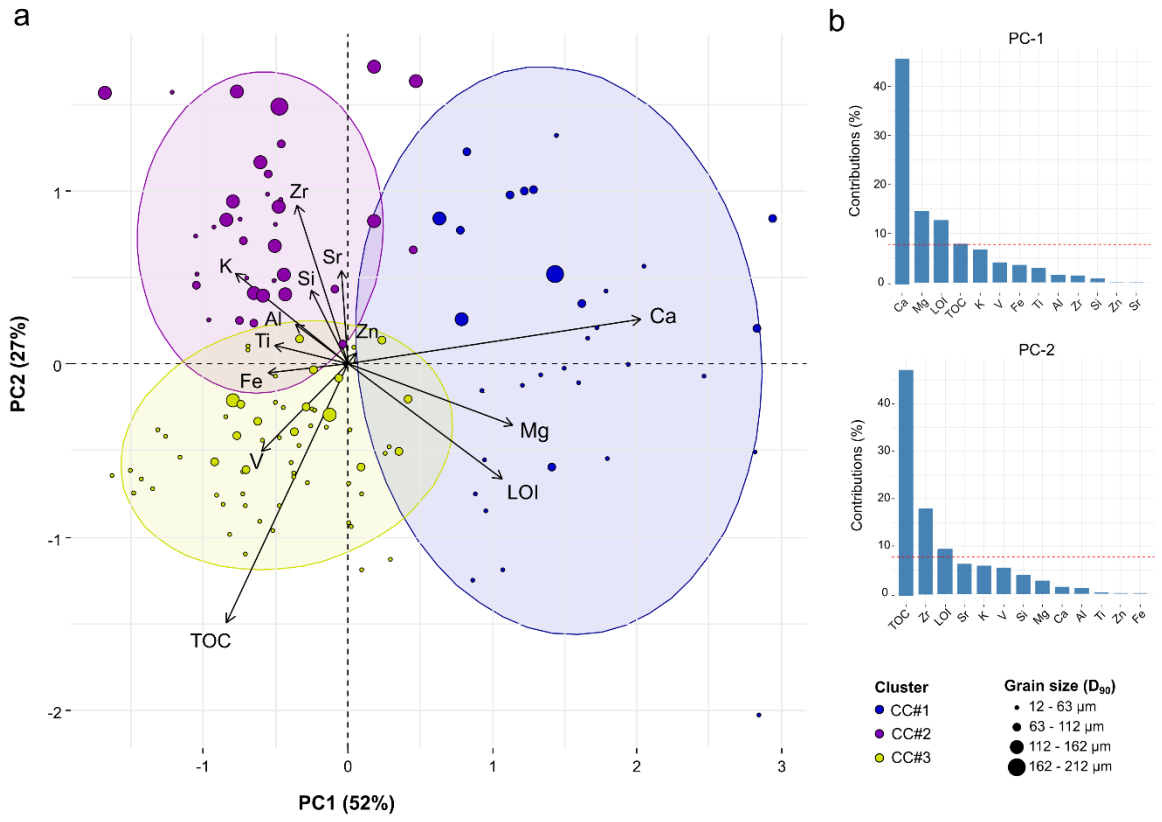


Figure 12. (a) Biplot of the first and second principal components of the principal component analysis obtained from the ED-XRF, LOI and TOC data. The color of the individuals represents the associated cluster and size of the individuals represents their grain size ($D_{90}$). Colored ellipses were generated assuming a multivariate t-distribution. (b) Contribution of all variables to the first and second principal components. The red dashed line on the graph above indicates the expected average contribution.

For all clusters, the Spearman rank correlation matrix (Fig. 13a) shows a negative correlation of all elements except Sr, Si and Zr, with $D_{90}$, suggesting that they are more concentrated in the fine-grained fraction (silt). In contrast, Si and Zr are indicators of coarse-grained sediments (sandy silt and silty sand; (Rothwell & Croudace, 2015). Al and Ti are closely correlated with each other (0.71), and with K (0.77 and 0.55), Fe (0.79 and 0.77) and V (0.62 and 0.68), which suggests that lithogenic-derived inputs influence the distribution of these elements (Askari Dehno et al., 2022; Choudhary et al., 2023; Rothwell & Croudace, 2015). However, the moderate positive correlations of Mn with Al (0.55), Fe (0.55) and the absence of correlation with Ti may indicate that Mn likely derives from both continental and

authigenic sources (Macdonald & Gobeil, 2012). As shown in Fig. 13b, the correlation between Mn and Fe can be divided into two main types reflecting the two sources. The light gray circle highlights a linear Fe–Mn relationship, indicating lithogenic provenance, which is observable in all the clusters, except for some CC#3 samples. These samples, mainly from the Amundsen Gulf and Baffin Bay (dark gray circles), exhibit authigenic Mn enrichment. The observed positive correlations of V and Zn with Fe (0.85 and 0.49) and with Al (0.62 and 0.47) suggest that their distributions are partly associated with aluminosilicates but are mainly controlled by adsorption onto Fe oxides (Choudhary et al., 2023). Organic matter accumulation seems also to be an important process influencing V sedimentation, as shown by the positive correlation between V and TOC. Ca, Mg and LOI present good positive correlations, highlighting their association with detrital carbonates.

The Si–Ca–Al ternary plot (Fig. 14) shows that the CC#2 and CC#3 samples consist of detrital material similar to UCC and AS, whereas CC#1 samples plot along a mixing trend between UCC/AS values, Nares Strait sediment composition (Caron et al., 2020) and the carbonate endmember (Bédard et al., 2016). Compared with CC#3, CC#2 is slightly enriched in Si, which is consistent with the composition of the UCC and the igneous rocks from the Jungersen River (Lebeau, 2022), as well as the sediments from Baffin Bay (Loring, 1991). In contrast, CC#3 exhibits a higher Al content than CC#2 and shows a chemical composition similar to suspended sediment samples from the Mackenzie River Basin (Dellinger et al., 2017), Mackenzie Shelf sediments (Gamboa et al., 2017) and AS.

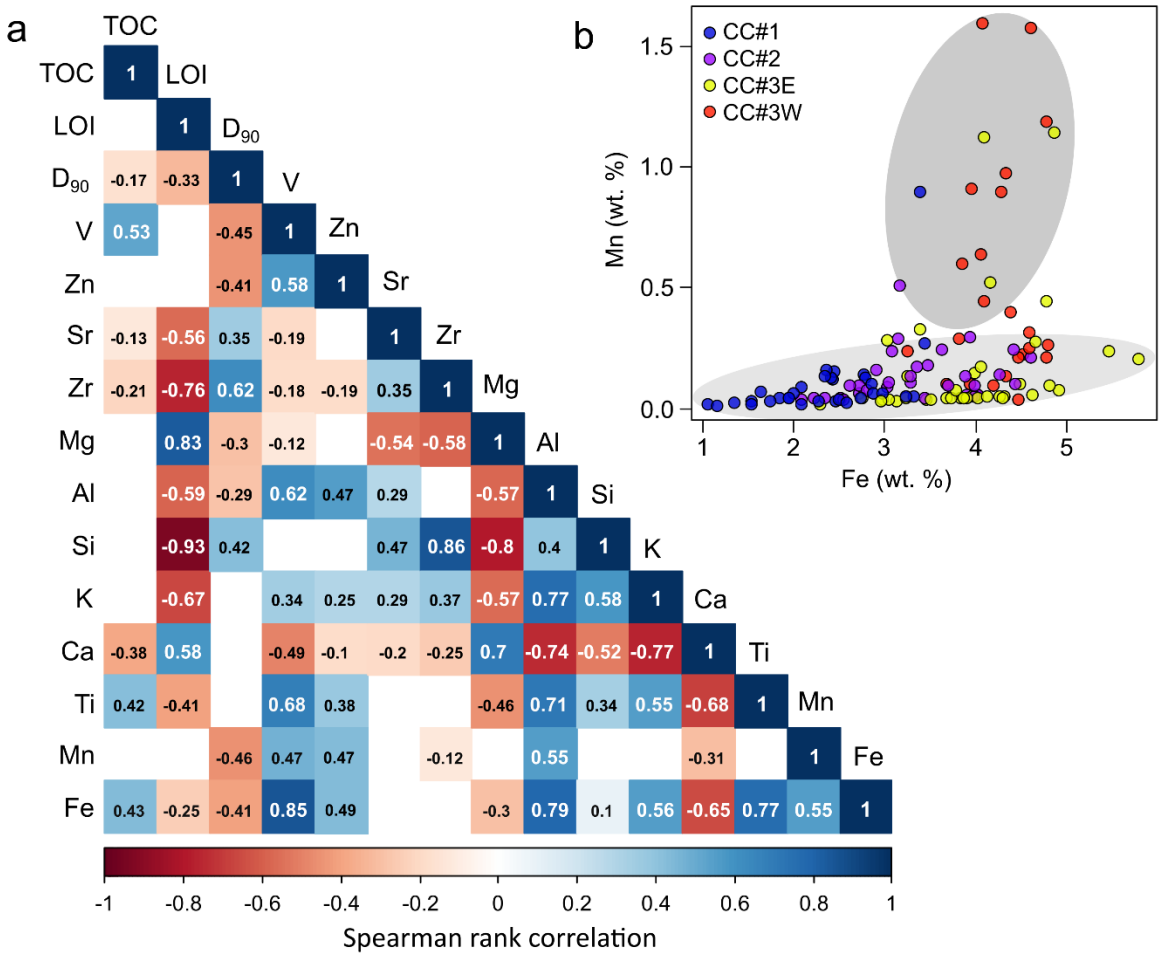


Figure 13. (a) Spearman rank correlation matrix of all variables measured in the study. The red squares represent significant negative correlations, the blue squares represent significant positive correlations, and the blank squares represent nonsignificant correlations. (b) Correlation between Fe and Mn in the CA according to the provinces. Samples within the dark gray circle are mainly from the Amundsen Gulf and close to it, or from Baffin Bay.

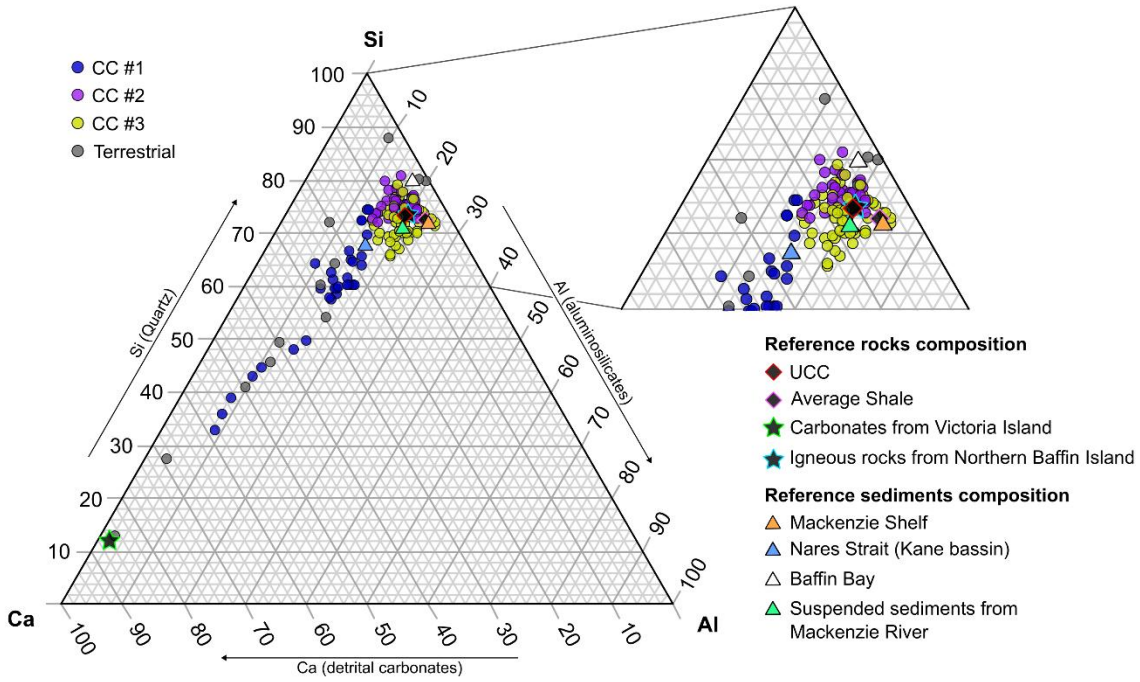


Figure 14. Si–Ca–Al ternary plot of the marine and terrestrial samples. See Fig. 8 for comparative bedrock information and locations. The reference sediments are from Gamboa et al. (2017) for the Mackenzie Shelf, Caron et al. (2020) for Nares Strait, Loring (1984) for Baffin Bay and Dellinger et al. (2017) for suspended sediment samples from the Mackenzie River.

Compared with all three background levels, the EF and Igeo indices indicated that there was no significant enrichment or contamination in Zn or Fe. However, there are some indications of enrichment in V and Mn (Fig. 15). With the UCC values as background, moderately severe enrichment in V is observed in four samples: two river samples from southern Ellesmere Island (EF = 18 and 8; Fig. 19a) and two marine surface samples from the Amundsen Gulf and southern Banks Island (EF = 5.4 and 5.2, respectively). The reason for such high EF results in terrestrial samples is the very low Al content rather than the high V content. All the samples from the Beaufort Sea and Amundsen Gulf, and most of the samples from Jones Sound present moderate enrichment. When the AS values were used as the background, the EF values decreased significantly compared with those of the UCC, with only the river samples showing enrichment in V. The EF values, when the chemical

composition of the base of push cores were used as the background, revealed no to minor enrichment of V–Zn–Mn–Fe.

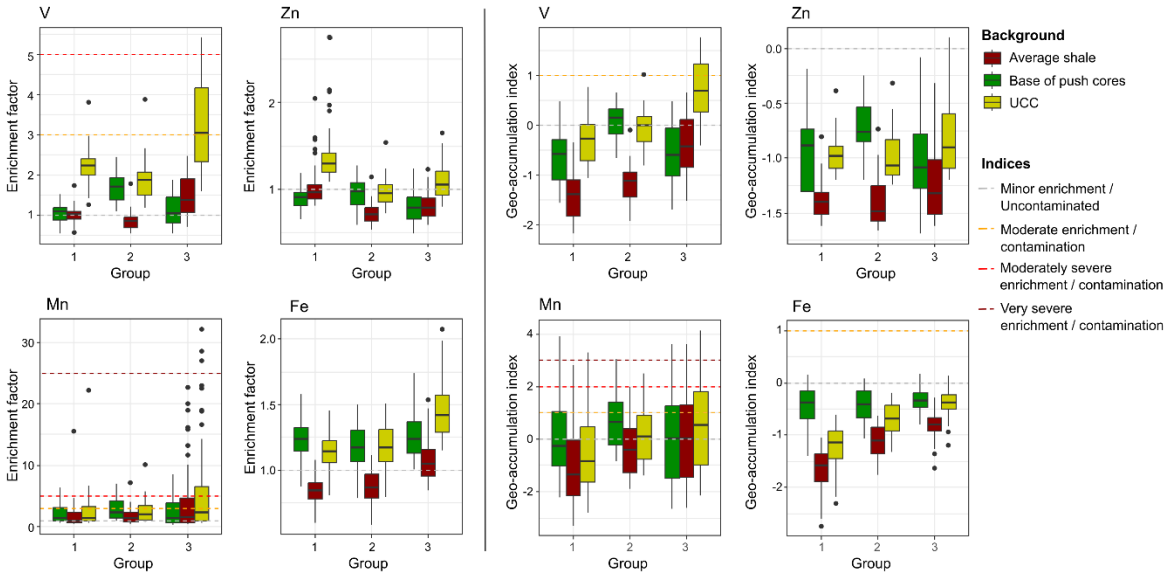


Figure 15. Boxplots presenting the enrichment factor results and the geo-accumulation index of V, Zn, Mn and Fe. The boxplots are divided into three clusters and three boxes are shown per group, representing the three geochemical backgrounds used.

According to the Igeo with UCC as background, sediment samples from the Beaufort Sea and Amundsen Gulf are moderately polluted in V, along with two samples from central Jones Sound. The two river samples from southern Ellesmere Island show unpolluted levels (Fig. 19a). When the AS values were used as the background, Igeo values differ, with values significantly lower (Fig. 15). Without indicating any polluted samples, the Igeo values with the basal samples from the push cores as background are generally higher for Zn and Fe than for the AS and UCC values.

Regardless of the geochemical background used to calculate the EF, dozens of samples present moderate to moderately severe enrichment in Mn throughout the CA, mainly south of the Parry Channel (Fig. 15 & 18). Amundsen Gulf and Davis Strait contain the largest number of moderately severely enriched samples in Mn. Similar results are observed with Igeo, with samples classified as moderately to strongly polluted.

## 1.7 DISCUSSION

### 1.7.1 Spatial variability and sediment provenance

A large regional variability is observed in the chemical composition of surface sediments across the CA. The three chemical clusters identified four spatial zones in the study area: CC#1 occupying central CA, CC#2 in southeastern CA, and CC#3 subdivided into western CA and eastern CA.

The samples from CC#1 in central CA present sediment rich in calcite and dolomite (Belt et al., 2010; Lakeman et al., 2018; Myers & Darby, 2022). The 32 samples found in this cluster are associated with detrital carbonates derived from the erosion of the dolostone of the Arctic platform and the limestone from the Innuitian Orogen in northern CA. These rocks are predominant in multiples islands in central CA, such as Victoria, Prince of Wales, Devon Islands (Fig. 7 & 8). It is therefore reasonable to conclude that the surrounding geology is the main source for Ca and Mg in the central CA cluster. However, the notable variability observed in grain size and Al–Si content in CC#1 (Fig. 10 & 14) indicates that different transport processes are affecting the distribution of sediment. The sediments with the coarsest grain size combined with the lowest Al content and highest Ca–Mg content are observed in Nares Strait, Gulf of Boothia, Foxe Basin, where coastal erosion of nearby carbonate bedrock predominates. The presence of finer sediments enriched in Al in Lancaster Sound and M'Clintock Channel suggests a more distant source. The sediments are slightly better sorted but, though still classified as poorly sorted (Fig. 20), indicating that they are likely transported by surface currents flowing northward from the Amundsen Gulf and eastward through Barrow Strait (Fig. 7), as well as by drifting sea ice. Indeed, sediment-laden sea ice is an important process in the Arctic Ocean that transports fine particles over long distances (Reimnitz et al., 1993), which was also observed by Letaïef et al. (2021) in Lancaster Sound and M'Clure Strait. The negative correlation between Ca–Mg-LOI and Al, along with all the other variables (Fig. 13a), demonstrates that detrital carbonate sediments and

aluminosilicates originate from distinct regions. These findings also reveal that these sediments are poor trace metal carriers.

CC#2, in the southeastern CA region, includes Coronation and Queen Maud Gulfs, eastern Baffin Island fjords and Frobisher Bay. This cluster is characterized by elements (Al, Si, K, Sr and Zr; Fig. 12 & 14) that can be associated with K-feldspar, illite, quartz and zircon (Gamboa et al., 2017). Zr contributes greatly to the total variance in this cluster, as shown in the biplot (Fig. 12). This element, which is a ubiquitous mineral in the crust and occurs in zircon grains in igneous and sedimentary rocks, is a coarse grain size indicator (Rothwell & Croudace, 2015). In addition to terrestrial sediments, this cluster is indeed composed of the coarsest sediment of the dataset (sandy silt to silty sand; Fig. 17), with finer sediments found in the Queen Maud Gulf and coarser sediment found in eastern Baffin Island fjords and Frobisher Bay. Proximity of the samples to the coast and to the Canadian Shield rocks explains the composition of this cluster. For example, Queen Maud Gulf sediments are particularly rich in Si (25–30 %, Fig. 14) and K (3.5–4.0 %), which is similar to the Tingmeak and Simpson Rivers (Si: 29 % and K: 3.7 %, and Si: 38 % and K: 2.4 %, respectively), draining granitoid rocks form the Slave and Churchill Provinces (McMartin et al., 2013). Letaïef et al. (2021) reported similar results in Coronation and Queen Maud Gulfs, with dominant content of Si–Al–Zr–Sr–K. As suggested by these authors, the local seafloor of these gulfs is primarily fed by sediments from surrounding rivers (such as Coppermine in Coronation Gulf and Back, Hayes, Perry, Armark, Simpson, Hayes and Ellice rivers in Queen Maud Gulf; Alkire et al., 2017) draining the Canadian Shield and flowing northward to the gulfs, but also by sea ice transport that contributes finer sediments (Belt et al., 2010). The sediments from Baffin Island fjords mostly originated from glacial erosion of Precambrian granites and gneiss from tidewater glaciers. Sandy gravity flows resulting from summer chute failures at the fjord head explain the sediment transport of coarse-grained sediment into Baffin Island fjords (Fig. 10; Syvitski and Normandeau, 2023). In Frobisher Bay, the Si–Sr–Zr–Fe–Ti sediment-rich seafloor is supplied by erosion of proglacial material (such as monzogranite-derived till) and remobilization of postglacial mud (Deering et al., 2018; Forbes et al., 2018). In addition, even though anthropogenic activities from Iqaluit have an

impact on contaminant inputs in Frobisher Bay (Bartley et al., 2024; Corminboeuf et al., 2021), our results indicate no enrichment in V, Zn or Fe. The absence or the negative correlation between trace metals and $D_{90}$, Si and Zr (Fig. 13a) reveals that the relatively coarse sediments characterizing Frobisher Bay do not serve as effective carriers for trace metals and, therefore, do not favor their transport through the bay (Chen et al., 2016).

CC#3 is subdivided into two geographical zones: western and eastern CA. Even though substantially different sources and processes affect the zones, both are characterized by high TOC, trace metals and Fe contents and generally fine-grained sediments (Fig. 12). Most of the western CA subcluster is located within the Mackenzie River plume, and the latter represents the dominant source of sediment supply to the Canadian Beaufort Shelf (Fig. 14; Deschamps et al., 2018; Gamboa et al., 2017; Hill et al., 1991; Kutos et al., 2021). The sedimentary region is characterized by fine-grained sediments containing relatively high concentrations of Al–Fe–Mn–Ti and V–Zn–Cr, which can be related to clay minerals, such as kaolinite and illite (Deschamps et al., 2018; Myers & Darby, 2022), and Fe–Mn continental oxides derived from the Paleozoic to Mesozoic sedimentary rocks of the Mackenzie Valley (Gamboa et al., 2017; Harrison et al., 2011; Kutos et al., 2021). These interpretations are consistent with the chemical end-member calculations derived from suspended sediment samples in the Mackenzie River Basin (Dellinger et al., 2017; Millot et al., 2003), suggesting that the primary source of the Mackenzie River sediments is the shales of the Interior Platform. Carbonates and calcareous shales (Fraser & Hutchison, 2017) and igneous rocks from the Bear Province (Fig. 8) also contribute significantly to the composition of the sediment. Likewise, significant abundances of magnetite (a Fe oxide mineral) are also found on the Mackenzie Shelf (Gamboa et al., 2017) and may result from the intrusive dikes on Banks Island (Myers & Darby, 2022). The high TOC content recorded in the sediments in western CA is mainly terrigenous, i.e., of petrogenic origin and from soils and wetlands, whereas the TOC from marine production accounts for a minor contribution (Drenzek et al., 2007). The organic material is mainly delivered by the Mackenzie River discharge (Goñi et al., 2013) which carry organic rich Devonian shale and coal material (Harrison et al., 2011; Yunker et al., 2011), and by coastal erosion of organic rich permafrost (Couture et al., 2018).

A decreasing gradient in Al–Fe–Ti–V and TOC contents is observed in an overall W-E direction toward the Amundsen Gulf and toward Banks Island, confirming that the influence of the Mackenzie River plume is likely diluted eastward by other sedimentary processes, such as input from erosion of the coastal cliffs west of Banks Island (Gamboa et al., 2017). Mn concentrations are however showing an opposite trend, with the highest concentrations occurring in the Amundsen Gulf (Fig. 9 & 11b), indicating that other processes are influencing its distribution, such as different redox conditions near the sediment-water interface. Most Mn in the Arctic Ocean originates from rivers and coastal erosion, making the Mackenzie Shelf an area with very high inputs (Macdonald & Gobeil, 2012). However, high organic fluxes from the Mackenzie River maintain a shallow oxygen penetration depth (<2 cm; Magen, 2008), which leads to the reduction of Mn oxides close to the sediment-water interface and allows the dissolved $Mn^{2+}$ to escape into the overlying waters (Macdonald & Gobeil, 2012). Particulate and dissolved Mn transported eastward by the Alaskan Coastal Current to the Amundsen Gulf and along the Banks Island coast are enriched in surface sediment because (1) the thicker oxygen penetration depth in the Amundsen Gulf (6 cm; Magen, 2008) allows the stability of the oxides at the surface and (2) below the oxic zone, reduced Mn diffuses upward and reprecipitates in the uppermost cm of sediment, causing surface enrichment. Surprisingly, there is stronger stratification and lower oxygenation of bottom waters in Amundsen Gulf and along Banks Island coast than the Beaufort Shelf (Magen, 2008; Reagan, 2024). The Mn enrichment observed in our dataset is thus attributed to the low oxygen consumption rates in the sediments resulting from low organic matter inputs (Macdonald & Gobeil, 2012; Magen, 2008; Magen et al., 2010).

The highest trace metal (V, Zn and Cr; Fig. 9 & 15) contents are found in the western CA subcluster, first because of important inputs from the Mackenzie River (Vonk et al., 2015) and second because of the presence of phase carriers (such clays, organic matter, Fe–Mn oxyhydroxides) that remove the dissolved trace metals from the water and scavenge them to the sediments. The Mackenzie River discharges high contents of fine-grained clay minerals, organic matter and Fe–Mn oxides. It is known that trace elements are preferentially retained in the fine fraction of sediment, as a relatively high specific surface area favors their

sorption (Chen et al., 2016). However, the moderate negative correlation between $D_{90}$, and V and Zn highlights the association with clay minerals and reveals that other variables are influencing the distribution of metals, such as the sediment composition. Indeed, the adsorption of V and Zn onto Fe–Mn oxides, as well as their sorption/complexation with organic matter, are important processes in the region (Jensen & Colombo, 2024). As shown by their positive correlation with Al (Fig. 13a), it is likely that these metals have a lithogenic provenance. However, because Mn is also strongly controlled by redox processes, its influence on trace metal distribution is limited. This observation aligns with findings from the Canadian Arctic waters, where particulate Fe and V, which correlate with particulate Al, are primarily controlled by lithogenic sources, whereas the distribution of particulate Mn is governed by oxidation conditions (Colombo et al., 2021; Jensen & Colombo, 2024).

High TOC concentrations primarily define the sediments from the eastern CA subcluster. This sedimentary region is distinct from the western CA region by a higher contribution of marine organic carbon than terrestrial organic carbon (Goñi et al., 2013). The locations of the samples in northeast Baffin Bay correspond to the North Water Polynya and the Bylot Island–Lancaster Sound Polynyas (Hannah et al., 2009; Stirling & Cleator, 1981), a highly biologically productive region (Tremblay et al., 2012). The samples located close to Davis Strait exhibit lower but still higher-than-average TOC contents, indicating less biologically productive conditions. In addition to the relatively high concentrations of Si and Al, the sediments from this region are particularly characterized by high Fe and Ti content. Because Ti is not involved in any biological or redox processes, it principally indicates a terrigenous continental source, specifically when associated with Fe (Calvert & Pedersen, 2007). Several glaciers and icefields are present on Devon Island, Sirmilik National Park, SE Ellesmere Island (e.g., Manson and Prince of Wales Icefields) and west Greenland margin, and thus impact the sedimentation in these areas by generating sediment-laden meltwater plumes and iceberg rafting. These glaciers erode a mix of the Precambrian Canadian Shield composed of igneous rocks and gneiss, and the Arctic platform composed of sedimentary carbonate rocks, resulting in heterogeneous inputs composed of heavy minerals, quartz, K-feldspar, plagioclase and detrital carbonates (Marlowe, 1966).

Overall, low concentrations of Zn and V are observed in the eastern CA subcluster, despite high concentrations of Fe, Ti, and TOC (Fig. 9, 10 & 15). However, Jones Sound exhibits elevated V concentrations (150–228 μg/g), coinciding with the highest Fe and Mn content. The low V and Zn content measured in river and glacier samples from the north coast of Jones Sound (Fig. 9) suggest the absence of significant natural metal sources in the area. These concentrations are likely explained by increased scavenging enhanced by metal oxides.

Although Cr concentrations are mostly <DL, some samples display values between 100 and 135 μg/g in both the Canadian Beaufort Shelf and eastern CA regions (Fig. 9). These concentrations are twice as high as those reported in the Chukchi Sea region for the <160 μm sediment fraction (Cai et al., 2011) and higher than those reported in coastal and sound areas of northern Baffin Bay. However, these concentrations are comparable to those observed in deep-water mud from Baffin Bay (<50 μm; (Campbell & Loring, 1980; Loring, 1984). In western CA, the highest concentrations are found close to the Mackenzie River mouth. Vonk et al. (2015) measured lower concentrations in channel and bank sediments of the Mackenzie Delta system (67–94 μg/g), but similar concentrations in shelf and lake sediments (96–141 μg/g) and suggest a depositional sorting pattern. This implies that there is an enrichment along the transect of fine particles (clay minerals, organic matter and metallic oxides) carrying metals such as Cr, leading to their deposition on the shelf and slope. In eastern CA, concentrations > DL are observed in central Nares Strait, outer Jones Sound, and northern Davis Strait. Terrestrial samples from the southern Ellesmere region consistently show low Cr concentrations. Thus, we infer that higher Cr scavenging by Fe–Mn oxides and organic matter drives its distribution in these areas.

### 1.7.2 Pollution indices

Pollution indices revealed no general enrichment or contamination of V or Zn in the CA sediments. However, EF and Igeo present divergent results depending on the geochemical background used. The difference is clearly visible for V enrichment (Fig. 15),

for which the EF presents moderately severe enrichment in western CA, with UCC as background, while no enrichment is observed with local geochemical background. This highlights that the regional concentration in V is naturally high, most probably related to the discharge of the Mackenzie River, whose tributaries drain V-rich shales (Yukon Geological Survey, 2023; Yunker et al., 2011). Thus, the choice of background is an important variable that can significantly change the conclusions of a pollution study, and this is especially true in large spatial studies, such as those where bedrock geology varies greatly. The use of a local, onsite background is therefore more representative of the geological variability and natural concentration of the areas. The local background used in this study was associated with the chemical clusters identified with surface sediment data, and the difference between the background values of each cluster is significant. The V background concentration in CC#3 is indeed twice the values of the two other clusters. This highlights that the values from UCC or AS, which are usually suggested for normalization, are therefore far from the local background values in the CA.

Normalization is a method to consider the natural regional variability of trace metal content in sediment, like granulometric and mineralogical variations, to enable the identification and quantification of anthropogenic metal contributions (Loring, 1991). In the calculation of EFs, a normalizing element is used to compensate for these variations (Loring, 1991). Aluminum is commonly used for chemical normalization because it is a major element in marine sediments (generally composed of aluminosilicates). Additionally, it remains unaffected by biological, diagenetic, and anthropogenic processes (Boës et al., 2011). However, the use of a normalizing element has been criticized because its variability can be greater than that of the evaluated metal (Desaules, 2012; Poh & Tahir, 2017; Reimann & de Caritat, 2000, 2005). To evaluate this, EFs were also calculated with Ti as the normalizer, and the results were overall similar but noteworthy differences were identified for all the elements (Fig. 19b). Also, terrestrial sediment samples collected at southern Ellesmere Island have high EF values because of their low Al contents. The pollution classification of those sediments was very different from that of Igeo, which does not use a normalizing element (Fig. 19a). Thus, our results suggest that the use of EFs can lead to misinterpretation of

contamination in the sediments if the reference metal/element ratio is not consistent with the natural background (e.g., (Anderson & Kravitz, 2010; Poh & Tahir, 2017; Reimann & de Caritat, 2000, 2005; Van der Weijden, 2002).

Another factor to consider when the pollution indices values are interpreted, especially when deeper sediment values are used as a background, is the influence of early diagenesis and other geochemical processes (e.g., bottom scavenging within the nepheloid layer; Casse et al., 2019) within the sediment. Sediments at certain depths are naturally enriched or depleted in trace elements due to the dissolution and precipitation of redox host phases, such as Mn and Fe oxyhydroxides and sulfides (Kuzyk et al., 2017; Tribovillard et al., 2006). This phenomenon was observed in this study with respect to the Mn distribution, which presented severe enrichment in Amundsen Gulf sediments due to Mn remobilization and reprecipitation during early diagenesis. In this context, and to avoid misinterpretations stemming from early diagenesis, depth profiles of elemental concentrations in sediments and pore water should be used to provide essential information on the natural enrichment and depletion of trace elements required to assess anthropogenic influence (e.g., Trefry & Neff, 2019).

## 1.8 CONCLUSIONS

This study presents a vast geochemical survey of the Canadian Arctic, providing valuable new data on the chemical composition of surface sediment and new insights into the sedimentary dynamics of the region. The application of pollution indices in the assessment of sediment contamination was also studied to review the benefits and drawbacks of the method.

Geochemical data revealed a large regional variability in the seafloor composition of the CA, shaped by the regional bedrock geology. Three chemical clusters define the CA:

1) CC#1 (central CA) is dominated by high detrital carbonate content originating from the Arctic Platform though coastal erosion and sea ice transport.

2) CC#2 (southeastern CA: Queen Maud Gulf and the Baffin Island fjords and bays) is characterized by relatively coarse siliciclastic sediments influenced by small CA rivers and glaciers from Baffin Island eroding Canadian Shield rocks.

3) CC#3 (western and eastern CA) is characterized by sediments rich in TOC and Fe–Mn oxyhydroxides. The Western CA is highly influenced by the Mackenzie River discharge, containing high terrestrial organic carbon as well as lithogenic aluminosilicates and metallic oxides. The highest content of trace metals (V, Zn and Cr) are observed in this region and are associated with Fe–Mn oxides and clay minerals derived from the weathering of shales and siltstones that constitute the Mackenzie River Basin. In contrast, eastern CA is influenced by the high primary production of polynyas and glacial discharge from the surrounding glaciers of Devon and Ellesmere Islands.

Throughout the CA, the pollution indices suggest that trace metals originate from natural sources and pose a low ecological risk for benthic or other organisms living near the water-sediment interface. However, discrepancies were observed in the EF and Igeo results depending on the background used. Thus, those indices should be interpreted carefully. In addition, normalization of the metal data with a conservative element in the EF calculation also revealed several flaws. To avoid potential misinterpretations, it is recommended that EFs be validated with different conservative normalizing elements.

Finally, while pollution indices are useful for identifying elevated concentrations of trace elements, they should not be solely relied upon to assess metallic contamination or characterize human contributions in sediments. A regional geochemical survey, such as the one conducted in this study, combined with spatial variations in EFs and Igeo, provides a more comprehensive approach for understanding metal distribution, natural enrichment/depletion processes, and the impact of human activities on trace metal contamination.

## 1.9 ACKNOWLEDGEMENTS

We acknowledge the captains, officers, crews, and scientific participants of the 2016, 2017, 2018, 2019, and 2022 ArcticNet expeditions onboard CCGS Amundsen for the recovery of the sediment samples used in this study. We thank Claude Belzile (ISMER-UQAR), Dominique Lavallée (ISMER-UQAR), Agnieszka Adamowicz (UQAM-Geotop), and Jean-François Hélie (UQAM-Geotop) for providing technical support in the laboratory. This study was supported by ArcticNet (ArcticSeafloor project), Québec-Océan, Geotop, the Northern Scientific Training Program (NSTP), the Fonds de recherche du Québec - Nature et technologies (FRQNT) and the Natural Sciences and Engineering Research Council of Canada (NSERC) PhD scholarships provided to C. Brice, and NSERC Discovery Grants provided to J.-C. Montero-Serrano (RGPIN-2020-06600 and RGPNS-2020-06600). Finally, the authors thank one anonymous reviewer and John S. Armstrong-Altrin (National Autonomous University of Mexico) for their constructive reviews, which improved the quality of the manuscript, as well as Daniel S. Alessi and Zimeng Wang for their editorial work.

## 1.10 REFERENCES

Aitchison, J. (1982). The Statistical Analysis of Compositional Data. *Journal of the Royal Statistical Society: Series B (Methodological)*, *44*(2), 139-160. https://doi.org/https://doi.org/10.1111/j.2517-6161.1982.tb01195.x

Alkire, M. B., Jacobson, A. D., Lehn, G. O., Macdonald, R. W., & Rossi, M. W. (2017). On the geochemical heterogeneity of rivers draining into the straits and channels of the Canadian Arctic Archipelago. *Journal of Geophysical Research: Biogeosciences*, *122*(10), 2527-2547. https://doi.org/https://doi.org/10.1002/2016JG003723

AMAP. (1998). *AMAP Assessment Report: Arctic Pollution Issues.* Arctic Monitoring and Assessment Programme (AMAP), Oslo, Norway. xii + 859 pp.

AMAP. (2005). *AMAP Assessment 2002: Heavy Metals in the Arctic.* Arctic Monitoring and Assessment Programme (AMAP), Oslo, Norway. xvi + 265 pp.

AMAP. (2021a). *AMAP Assessment 2020: POPs and Chemicals of Emerging Arctic Concern: Influence of Climate Change.* Arctic Monitoring and Assessment Programme (AMAP), Tromsø, Norway. viii + 134pp.

AMAP. (2021b). *AMAP Assessment 2021: Mercury in the Arctic.* Arctic Monitoring and Assessment Programme (AMAP), Tromsø, Norway. 324 pp.

Anderson, R. H., & Kravitz, M. J. (2010). Evaluation of geochemical associations as a screening tool for identifying anthropogenic trace metal contamination. *Environmental Monitoring and Assessment*, *167*(1), 631-641. https://doi.org/10.1007/s10661-009-1079-2

Askari Dehno, M., Mousavi Harami, S. R., & Noora, M. R. (2022). Environmental geochemistry of heavy metals in coral reefs and sediments of Chabahar Bay. *Results in Engineering*, *13*, 100346. https://doi.org/https://doi.org/10.1016/j.rineng.2022.100346

Bartley, M. C., Tremblay, T., De Silva, A. O., Michelle Kamula, C., Ciastek, S., & Kuzyk, Z. Z. A. (2024). Sedimentary records of contaminant inputs in Frobisher Bay, Nunavut. *Environmental Science and Ecotechnology*, *18*, 100313. https://doi.org/https://doi.org/10.1016/j.ese.2023.100313

Bédard, J., Hayes, B., Hryciuk, M., Beard, C., Williamson, N., Dell'Oro, T., Rainbird, R., Prince, J., Baragar, W., Nabelek, P., Weis, D., Wing, B., Scoates, J., Naslund, H. R., Cousens, B., Williamson, M.-C., Hulbert, L.J., , Montjoie, R., Girard, É., Ernst, R., & Lissenberg, C. J. (2016). Geochemical database of Franklin sills, Natkusiak Basalts and Shaler Supergroup rocks, Victoria Island, Northwest Territories, and correlatives from Nunavut and the mainland. *Geological Survey of Canada*, *Open File 8009*(1). https://doi.org/doi:10.4095/297842

Belt, S. T., Vare, L. L., Massé, G., Manners, H. R., Price, J. C., MacLachlan, S. E., Andrews, J. T., & Schmidt, S. (2010). Striking similarities in temporal changes to spring sea ice occurrence across the central Canadian Arctic Archipelago over the last 7000 years. *Quaternary Science Reviews*, *29*(25), 3489-3504. https://doi.org/https://doi.org/10.1016/j.quascirev.2010.06.041

Belzile, C., & Montero-Serrano, J.-C. (2022). Quantifying simulated fine sand fraction in muddy sediment using laser diffraction. *Canadian Journal of Earth Sciences*, *59*(7), 455-461. https://doi.org/10.1139/cjes-2022-0011

Birch, G. F. (2020). An assessment of aluminum and iron in normalisation and enrichment procedures for environmental assessment of marine sediment. *Science of The Total Environment*, *727*, 138123. https://doi.org/https://doi.org/10.1016/j.scitotenv.2020.138123

Blott, S. J., & Pye, K. (2001). GRADISTAT: a grain size distribution and statistics package for the analysis of unconsolidated sediments. *Earth surface processes and Landforms*, *26*(11), 1237-1248.

Boës, X., Rydberg, J., Martinez-Cortizas, A., Bindler, R., & Renberg, I. (2011). Evaluation of conservative lithogenic elements (Ti, Zr, Al, and Rb) to study anthropogenic element enrichments in lake sediments. *Journal of Paleolimnology*, *46*(1), 75-87. https://doi.org/10.1007/s10933-011-9515-z

Borcard, D., Gillet, F., & Legendre, P. (2011). Spatial analysis of ecological data. In *Numerical ecology with R* (pp. 227-292). Springer.

Brown, K. A., Williams, W. J., Carmack, E. C., Fiske, G., François, R., McLennan, D., & Peucker-Ehrenbrink, B. (2020). Geochemistry of Small Canadian Arctic Rivers with Diverse Geological and Hydrological Settings. *Journal of Geophysical Research: Biogeosciences*, *125*(1), e2019JG005414. https://doi.org/https://doi.org/10.1029/2019JG005414

Brown, R. J. E. (1972). Permafrost in the Canadian Arctic Archipelago. *Zeitschrift fur Geomorphologie*, *13*, 102-130. https://cir.nii.ac.jp/crid/1570572699166533888

Budko, D. F., Demina, L. L., Travkina, A. V., Starodymova, D. P., & Alekseeva, T. N. (2022). The Features of Distribution of Chemical Elements, including Heavy Metals and Cs-137, in Surface Sediments of the Barents, Kara, Laptev and East Siberian Seas. *Minerals*, *12*(3), 328. https://www.mdpi.com/2075-163X/12/3/328

Cai, M., Lin, J., Hong, Q., Wang, Y., & Cai, M. (2011). Content and distribution of trace metals in surface sediments from the northern Bering Sea, Chukchi Sea and adjacent Arctic areas. *Marine Pollution Bulletin*, *63*(5-12), 523-527.

Calvert, S. E., & Pedersen, T. F. (2007). Chapter Fourteen Elemental Proxies for Palaeoclimatic and Palaeoceanographic Variability in Marine Sediments: Interpretation and Application. In C. Hillaire–Marcel & A. De Vernal (Eds.), *Developments in Marine Geology* (Vol. 1, pp. 567-644). Elsevier. https://doi.org/https://doi.org/10.1016/S1572-5480(07)01019-6

Campbell, J. A., & Loring, D. H. (1980). Baseline levels of heavy metals in the waters and sediments of Baffin Bay. *Marine Pollution Bulletin*, *11*(9), 257-261. https://doi.org/https://doi.org/10.1016/0025-326X(80)90314-8

Canadian Ice Services. (2023). *Annual Arctic Ice Atlas, Winter 2022-2023*. Ottawa: Government of Canada

Caron, M., Montero-Serrano, J.-C., St-Onge, G., & Rochon, A. (2020). Quantifying Provenance and Transport Pathways of Holocene Sediments From the Northwestern Greenland Margin. *Paleoceanography and Paleoclimatology*, *35*(5), e2019PA003809. https://doi.org/https://doi.org/10.1029/2019PA003809

Casse, M., Montero-Serrano, J.-C., St-Onge, G., & Poirier, A. (2019). REE distribution and Nd isotope composition of estuarine waters and bulk sediment leachates tracing lithogenic inputs in eastern Canada. *Marine Chemistry*, *211*, 117-130. https://doi.org/https://doi.org/10.1016/j.marchem.2019.03.012

Chen, Y.-M., Gao, J.-b., Yuan, Y.-Q., Ma, J., & Yu, S. (2016). Relationship between heavy metal contents and clay mineral properties in surface sediments: Implications for metal pollution assessment. *Continental Shelf Research*, *124*, 125-133. https://doi.org/https://doi.org/10.1016/j.csr.2016.06.002

Choudhary, S., Nayak, G. N., & Khare, N. (2023). Sedimentary processes, metal enrichment and potential ecological risk of metals in lacustrine sediments of Svalbard, Arctic. *Environmental Science and Pollution Research*, *30*(49), 106967-106981. https://doi.org/10.1007/s11356-022-23600-w

Colombo, M., Brown, K. A., De Vera, J., Bergquist, B. A., & Orians, K. J. (2019). Trace metal geochemistry of remote rivers in the Canadian Arctic Archipelago. *Chemical Geology*, *525*, 479-491. https://doi.org/https://doi.org/10.1016/j.chemgeo.2019.08.006

Colombo, M., Rogalla, B., Li, J., Allen, S. E., Orians, K. J., & Maldonado, M. T. (2021). Canadian Arctic Archipelago Shelf-Ocean Interactions: A Major Iron Source to Pacific Derived Waters Transiting to the Atlantic. *Global Biogeochemical Cycles*, *35*(10), e2021GB007058. https://doi.org/https://doi.org/10.1029/2021GB007058

Corminboeuf, A., Montero-Serrano, J.-C., & St-Louis, R. (2021). Spatial and temporal distributions of polycyclic aromatic hydrocarbons in sediments from the Canadian Arctic Archipelago. *Marine Pollution Bulletin*, *171*, 112729. https://doi.org/https://doi.org/10.1016/j.marpolbul.2021.112729

Couture, N. J., Irrgang, A., Pollard, W., Lantuit, H., & Fritz, M. (2018). Coastal Erosion of Permafrost Soils Along the Yukon Coastal Plain and Fluxes of Organic Carbon to the Canadian Beaufort Sea. *Journal of Geophysical Research: Biogeosciences*, *123*(2), 406-422. https://doi.org/https://doi.org/10.1002/2017JG004166

Crecelius, E. A., Trefry, J. H., Steinhauer, M. S., & Boehm, P. D. (1991). Trace metals in sediments from the inner continental shelf of the western Beaufort Sea. *Environmental Geology and Water Sciences*, *18*(1), 71-79. https://doi.org/10.1007/BF01704579

Darby, D. A., Myers, W. B., Jakobsson, M., & Rigor, I. (2011). Modern dirty sea ice characteristics and sources: The role of anchor ice. *Journal of Geophysical Research: Oceans*, *116*(C9). https://doi.org/https://doi.org/10.1029/2010JC006675

Deering, R., Misiuk, B., Bell, T., Forbes, D., Edinger, E., Tremblay, T., Telka, A., Aitken, A., & Campbell, C. (2018). Characterization of the seabed and postglacial sediments of inner Frobisher Bay, Baffin Island, Nunavut. *Summary of Activities 2018, Canada-Nunavut Geoscience Office*, 139-152.

Dellinger, M., Bouchez, J., Gaillardet, J., Faure, L., & Moureau, J. (2017). Tracing weathering regimes using the lithium isotope composition of detrital sediments. *Geology*, *45*(5), 411-414. https://doi.org/10.1130/g38671.1

Déry, S. J., Stadnyk, T. A., MacDonald, M. K., & Gauli-Sharma, B. (2016). Recent trends and variability in river discharge across northern Canada. *Hydrol. Earth Syst. Sci.*, *20*(12), 4801-4818. https://doi.org/10.5194/hess-20-4801-2016

Desaules, A. (2012). Critical evaluation of soil contamination assessment methods for trace metals. *Science of The Total Environment*, *426*, 120-131. https://doi.org/https://doi.org/10.1016/j.scitotenv.2012.03.035

Deschamps, C.-E., Montero-Serrano, J.-C., & St-Onge, G. (2018). Sediment Provenance Changes in the Western Arctic Ocean in Response to Ice Rafting, Sea Level, and Oceanic Circulation Variations Since the Last Deglaciation. *Geochemistry, Geophysics, Geosystems*, *19*(7), 2147-2165. https://doi.org/https://doi.org/10.1029/2017GC007411

Domingo, J. P. T., Ngwenya, B. T., Attal, M., David, C. P. C., & Mudd, S. M. (2023). Geochemical fingerprinting to determine sediment source contribution and improve contamination assessment in mining-impacted floodplains in the Philippines. *Applied Geochemistry*, *159*, 105808. https://doi.org/https://doi.org/10.1016/j.apgeochem.2023.105808

Drenzek, N. J., Montluçon, D. B., Yunker, M. B., Macdonald, R. W., & Eglinton, T. I. (2007). Constraints on the origin of sedimentary organic carbon in the Beaufort Sea from coupled molecular 13C and 14C measurements. *Marine Chemistry*, *103*(1), 146-162. https://doi.org/https://doi.org/10.1016/j.marchem.2006.06.017

Forbes, D. L., Bell, T., Manson, G. K., Couture, N. J., Cowan, B., Deering, R. L., Hatcher, S. V., Misiuk, B., & St-Hilaire-Gravel, D. (2018). Chapter 8: Coastal environments and drivers. *From Science to Policy in the Eastern Canadian Arctic: An Integrated Regional Impact Study (IRIS) of Climate Change and Moderization. ArcticNet, Quebec City, 560 pp*, 211.

Fraser, T., & Hutchison, M. P. (2017). Lithogeochemical characterization of the Middle–Upper Devonian Road River Group and Canol and Imperial formations on Trail River, east Richardson Mountains, Yukon: age constraints and a depositional model for fine-grained strata in the Lower Paleozoic Richardson trough. *Canadian Journal of Earth Sciences*, *54*(7), 731-765. https://doi.org/10.1139/cjes-2016-0216

Gamboa, A., Montero-Serrano, J.-C., St-Onge, G., Rochon, A., & Desiage, P.-A. (2017). Mineralogical, geochemical, and magnetic signatures of surface sediments from the Canadian Beaufort Shelf and Amundsen Gulf (Canadian Arctic). *Geochemistry, Geophysics, Geosystems*, *18*(2), 488-512. https://doi.org/https://doi.org/10.1002/2016GC006477

Goñi, M. A., O'Connor, A. E., Kuzyk, Z. Z., Yunker, M. B., Gobeil, C., & Macdonald, R. W. (2013). Distribution and sources of organic matter in surface marine sediments across the North American Arctic margin. *Journal of Geophysical Research: Oceans*, *118*(9), 4017-4035. https://doi.org/https://doi.org/10.1002/jgrc.20286

Grenier, M., Brown, K. A., Colombo, M., Belhadj, M., Baconnais, I., Pham, V., Soon, M., Myers, P. G., Jeandel, C., & François, R. (2022). Controlling factors and impacts of river-borne neodymium isotope signatures and rare earth element concentrations supplied to the Canadian Arctic Archipelago. *Earth and Planetary Science Letters*, *578*, 117341. https://doi.org/https://doi.org/10.1016/j.epsl.2021.117341

Hakanson, L. (1980). An ecological risk index for aquatic pollution control. A sedimentological approach. *Water Research*, *14*(8), 975-1001. https://doi.org/https://doi.org/10.1016/0043-1354(80)90143-8

Hamel, D., Vernal, A. d., Gosselin, M., & Hillaire-Marcel, C. (2002). Organic-walled microfossils and geochemical tracers: sedimentary indicators of productivity changes in the North Water and northern Baffin Bay during the last centuries. *Deep Sea Research Part II: Topical Studies in Oceanography*, *49*(22), 5277-5295. https://doi.org/https://doi.org/10.1016/S0967-0645(02)00190-X

Hannah, C. G., Dupont, F., & Dunphy, M. (2009). Polynyas and Tidal Currents in the Canadian Arctic Archipelago. *Arctic*, *62*(1), 83-95. http://www.jstor.org/stable/40513267

Harrison, J. C., St-Onge, M., Petrov, O., Strelnikov, S., Lopatin, B., Wilson, F., Tella, S., Paul, D., Lynds, T., Shokalsky, S., Hults, C. K., Bergman, S., Jepsen, H., & Solli, A. (2011). *Geological map of the Arctic / Carte géologique de l'Arctique* [ "A" Series Map 2159A, 2011, 2159 sheets, 2151:2155,2000,2000]. Natural Resources Canada.

Heginbottom, J. A. D., M A; Harker, P T. (1995). *Canada, permafrost* [The National Atlas of Canada; Natural Resources Canada, Geomatics Canada, MCR Series no. 4177, 1995, 4171 sheet]. Natural Resources Canada.

Hélie, J. F. (2009). Elemental and stable isotopic approaches for studying the organic and inorganic carbon components in natural samples. *IOP Conference Series: Earth and Environmental Science*, *5*(1), 012005. https://doi.org/10.1088/1755-1307/5/1/012005

Hill, P. R., Blasco, S. M., Harper, J. R., & Fissel, D. B. (1991). Sedimentation on the Canadian Beaufort Shelf. *Continental Shelf Research*, *11*(8), 821-842. https://doi.org/https://doi.org/10.1016/0278-4343(91)90081-G

Hugelius, G., Strauss, J., Zubrzycki, S., Harden, J. W., Schuur, E. A. G., Ping, C. L., Schirrmeister, L., Grosse, G., Michaelson, G. J., Koven, C. D., O'Donnell, J. A., Elberling, B., Mishra, U., Camill, P., Yu, Z., Palmtag, J., & Kuhry, P. (2014). Estimated stocks of circumpolar permafrost carbon with quantified uncertainty ranges and identified data gaps. *Biogeosciences*, *11*(23), 6573-6593. https://doi.org/10.5194/bg-11-6573-2014

Jensen, L., & Colombo, M. (2024). Shelf-basin connectivity drives dissolved Fe and Mn distributions in the western arctic ocean: A synoptic view into polar trace metal cycling. *Oceanography*, *37*(2), 60-71. https://www.jstor.org/stable/27309822

Kassambara, A., & Mundt, F. (2020). Factoextra: Extract and Visualize the Results of Multivariate Data Analyses. R Package Version 1.0.7. https://CRAN.R-project.org/package=factoextra

Kondo, Y., Obata, H., Hioki, N., Ooki, A., Nishino, S., Kikuchi, T., & Kuma, K. (2016). Transport of trace metals (Mn, Fe, Ni, Zn and Cd) in the western Arctic Ocean (Chukchi Sea and Canada Basin) in late summer 2012. *Deep Sea Research Part I: Oceanographic Research Papers*, *116*, 236-252. https://doi.org/https://doi.org/10.1016/j.dsr.2016.08.010

Kutos, O., Rochon, A., & Montero-Serrano, J.-C. (2021). Evolution of palaeo-sea-surface conditions and sediment dynamics over the last 2700 years on the Mackenzie Slope, Beaufort Sea (Canadian Arctic). *Boreas*, *50*(3), 893-914. https://doi.org/https://doi.org/10.1111/bor.12513

Kuzyk, Z. Z. A., Gobeil, C., Goñi, M. A., & Macdonald, R. W. (2017). Early diagenesis and trace element accumulation in North American Arctic margin sediments. *Geochimica et Cosmochimica Acta*, *203*, 175-200. https://doi.org/https://doi.org/10.1016/j.gca.2016.12.015

Lakeman, T. R., Pieńkowski, A. J., Nixon, F. C., Furze, M. F., Blasco, S., Andrews, J. T., & King, E. L. (2018). Collapse of a marine-based ice stream during the early Younger Dryas chronozone, western Canadian Arctic. *Geology*, *46*(3), 211-214.

Lantuit, H., Overduin, P. P., Couture, N., Wetterich, S., Aré, F., Atkinson, D., Brown, J., Cherkashov, G., Drozdov, D., Forbes, D. L., Graves-Gaylord, A., Grigoriev, M., Hubberten, H.-W., Jordan, J., Jorgenson, T., Ødegård, R. S., Ogorodov, S., Pollard, W. H., Rachold, V., . . . Vasiliev, A. (2012). The Arctic Coastal Dynamics Database: A New Classification Scheme and Statistics on Arctic Permafrost Coastlines. *Estuaries and Coasts*, *35*(2), 383-400. https://doi.org/10.1007/s12237-010-9362-6

Lê, S., Josse, J., & Husson, F. (2008). FactoMineR: An R Package for Multivariate Analysis. *Journal of Statistical Software*, *25*(1), 1 - 18. https://doi.org/10.18637/jss.v025.i01

Lebeau, L. E. (2022). The Fury and Hecla Geoscience Project: whole rock and assay analysis from the Jungersen River area, northwestern Baffin Island, Nunavut. Geoscience Data Series GDS2022-002. Canada-Nunavut Geoscience Office

Letaïef, S., Montero-Serrano, J. C., & St-Onge, G. (2021). Sedimentary processes within the Canadian Arctic Archipelago: Relationships among sedimentological, geochemical, and magnetic sediment properties. *Geochemistry, Geophysics, Geosystems*, *22*(7), e2021GC009719.

Loring, D. H. (1984). Trace-metal geochemistry of sediments from Baffin Bay. *Canadian Journal of Earth Sciences*, *21*(12), 1368-1378. https://doi.org/10.1139/e84-142

Loring, D. H. (1991). Normalization of heavy-metal data from estuarine and coastal sediments. *ICES Journal of Marine Science*, *48*(1), 101-115. https://doi.org/10.1093/icesjms/48.1.101

Macdonald, R. W., & Bewers, J. M. (1996). Contaminants in the arctic marine environment: priorities for protection. *ICES Journal of Marine Science*, *53*(3), 537-563. https://doi.org/10.1006/jmsc.1996.0077

Macdonald, R. W., & Gobeil, C. (2012). Manganese Sources and Sinks in the Arctic Ocean with Reference to Periodic Enrichments in Basin Sediments. *Aquatic Geochemistry*, *18*(6), 565-591. https://doi.org/10.1007/s10498-011-9149-9

Magen, C. (2008). Origin, sedimentation and diagenesis of organic matter in coastal sediments of the southern Beaufort Sea region, Canadian Arctic McGill University]. Montreal.

Magen, C., Chaillou, G., Crowe, S. A., Mucci, A., Sundby, B., Gao, A., Makabe, R., & Sasaki, H. (2010). Origin and fate of particulate organic matter in the southern Beaufort Sea – Amundsen Gulf region, Canadian Arctic. *Estuarine, Coastal and Shelf Science*, *86*(1), 31-41. https://doi.org/https://doi.org/10.1016/j.ecss.2009.09.009

Marlowe, J. I. (1966). Mineralogy as an indicator of long-term current fluctuations in Baffin Bay. *Canadian Journal of Earth Sciences*, *3*(2), 191-201. https://doi.org/10.1139/e66-015

McLaughlin, F., Shimada, K., Carmack, E., Itoh, M., & Nishino, S. (2005). The hydrography of the southern Canada Basin, 2002. *Polar Biology*, *28*(3), 182-189. https://doi.org/10.1007/s00300-004-0701-6

McMartin, I., Berman, R., Normandeau, P., & Percival, J. (2013). Till composition of a transect across the Thelon tectonic zone, Queen Maud block, and adjacent Rae craton: Results from the Geo-Mapping Frontiers' Chantrey Project. *Geological Survey of Canada, Open File*, *7418*, 22.

Millot, R., Gaillardet, J. é., Dupré, B., & Allègre, C. J. (2003). Northern latitude chemical weathering rates: clues from the Mackenzie River Basin, Canada. *Geochimica et Cosmochimica Acta*, *67*(7), 1305-1329. https://doi.org/https://doi.org/10.1016/S0016-7037(02)01207-3

Müller, G. (1969). Index of geoaccumulation in sediments of the Rhine River. *Geojournal*, *2*, 108-118.

Myers, W. B., & Darby, D. A. (2022). A compilation of the silt and clay mineralogy from coastal and shelf regions of the Arctic Ocean. *Marine Geology*, *454*, 106948. https://doi.org/https://doi.org/10.1016/j.margeo.2022.106948

Naidu, A. S., Blanchard, A. L., Misra, D., Trefry, J. H., Dasher, D. H., Kelley, J. J., & Venkatesan, M. I. (2012). Historical changes in trace metals and hydrocarbons in nearshore sediments, Alaskan Beaufort Sea, prior and subsequent to petroleum-related industrial development: Part I. Trace metals. *Marine Pollution Bulletin*, *64*(10), 2177-2189. https://doi.org/https://doi.org/10.1016/j.marpolbul.2012.07.037

Normandeau, A., Dietrich, P., Hughes Clarke, J., Van Wychen, W., Lajeunesse, P., Burgess, D., & Ghienne, J.-F. (2019). Retreat Pattern of Glaciers Controls the Occurrence of Turbidity Currents on High-Latitude Fjord Deltas (Eastern Baffin Island). *Journal of Geophysical Research: Earth Surface*, *124*(6), 1559-1571. https://doi.org/https://doi.org/10.1029/2018JF004970

O'Brien, M. C., Macdonald, R. W., Melling, H., & Iseki, K. (2006). Particle fluxes and geochemistry on the Canadian Beaufort Shelf: Implications for sediment transport and deposition. *Continental Shelf Research*, *26*(1), 41-81. https://doi.org/https://doi.org/10.1016/j.csr.2005.09.007

O'Donnell, J. A., Carey, M. P., Koch, J. C., Baughman, C., Hill, K., Zimmerman, C. E., Sullivan, P. F., Dial, R., Lyons, T., Cooper, D. J., & Poulin, B. A. (2024). Metal mobilization from thawing permafrost to aquatic ecosystems is driving rusting of Arctic streams. *Communications Earth & Environment*, *5*(1), 268. https://doi.org/10.1038/s43247-024-01446-z

Palarea-Albaladejo, J., & Martín-Fernández, J. A. (2013). Values below detection limit in compositional chemical data. *Analytica Chimica Acta*, *764*, 32-43. https://doi.org/https://doi.org/10.1016/j.aca.2012.12.029

Palarea-Albaladejo, J., & Martín-Fernández, J. A. (2015). zCompositions — R package for multivariate imputation of left-censored data under a compositional approach. *Chemometrics and Intelligent Laboratory Systems*, *143*, 85-96. https://doi.org/https://doi.org/10.1016/j.chemolab.2015.02.019

Poh, S.-C., & Tahir, N. M. (2017). The common pitfall of using enrichment factor in assessing soil heavy metal pollution. *Malays. J. Anal. Sci*, *21*, 52-59.

R Core Team. (2024). *R: A language and environment for statistical computing*. In R Foundation for Statistical Computing. https://www.R-project.org/

Reagan, J. R. B., Tim P.; García, Hernán E.; Locarnini, Ricardo A.; Baranova, Olga K.; Bouchard, Courtney; Cross, Scott L.; Mishonov, Alexey V.; Paver, Christopher R.; Seidov, Dan; Wang, Zhankun; Dukhovskoy, Dmitry. (2024). *World Ocean Atlas 2023*.

Reimann, C., & de Caritat, P. (2000). Intrinsic Flaws of Element Enrichment Factors (EFs) in Environmental Geochemistry. *Environmental Science & Technology*, *34*(24), 5084-5091. https://doi.org/10.1021/es001339o

Reimann, C., & de Caritat, P. (2005). Distinguishing between natural and anthropogenic sources for elements in the environment: regional geochemical surveys versus enrichment factors. *Science of The Total Environment*, *337*(1), 91-107. https://doi.org/https://doi.org/10.1016/j.scitotenv.2004.06.011

Reimnitz, E., Clayton, J. R., Kempema, E. W., Payne, J. R., & Weber, W. S. (1993). Interaction of rising frazil with suspended particles: tank experiments with applications to nature. *Cold Regions Science and Technology*, *21*(2), 117-135. https://doi.org/https://doi.org/10.1016/0165-232X(93)90002-P

Ribeiro, S., Limoges, A., Massé, G., Johansen, K. L., Colgan, W., Weckström, K., Jackson, R., Georgiadis, E., Mikkelsen, N., Kuijpers, A., Olsen, J., Olsen, S. M., Nissen, M., Andersen, T. J., Strunk, A., Wetterich, S., Syväranta, J., Henderson, A. C. G., Mackay, H., . . . Davidson, T. A. (2021). Vulnerability of the North Water ecosystem to climate change. *Nature Communications*, *12*(1), 4475. https://doi.org/10.1038/s41467-021-24742-0

Rothwell, R., & Croudace, I. (2015). Twenty Years of XRF Core Scanning Marine Sediments: What Do Geochemical Proxies Tell Us? In I. Croudace & R. Rothwell (Eds.), *Micro-XRF Studies of Sediment Cores: Applications of a non-destructive tool for the environmental sciences* (pp. 25-102). Springer Netherlands. https://doi.org/10.1007/978-94-017-9849-5_2

St-Hilaire-Gravel, D., Forbes, D. L., & Bell, T. (2012). Multitemporal Analysis of a Gravel-Dominated Coastline in the Central Canadian Arctic Archipelago. *Journal of Coastal Research*, *28*(2), 421-441. https://doi.org/10.2112/jcoastres-d-11-00020.1

Steele, M., Morison, J., Ermold, W., Rigor, I., Ortmeyer, M., & Shimada, K. (2004). Circulation of summer Pacific halocline water in the Arctic Ocean. *Journal of Geophysical Research: Oceans*, *109*(C2). https://doi.org/https://doi.org/10.1029/2003JC002009

Stein, R., & Macdonald, R. W. (2004). The organic carbon cycle in the Arctic Ocean.

Stirling, I., & Cleator, H. (1981). *Polynyas in the Canadian Arctic*. (Occasional Paper Number 45). Ottawa: Canadian Wildlife Service

Syvitski, J., & Normandeau, A. (2023). Sediment redistribution processes in Baffin Island fjords. *Marine Geology*, *458*, 107024. https://doi.org/https://doi.org/10.1016/j.margeo.2023.107024

Taylor, S. R., & McLennan, S. M. (1985). *The continental crust: Its composition and evolution*. Blackwell Scientific Pub.,Palo Alto, CA. https://www.osti.gov/biblio/6582885

Thompson, M., Ellison, S. L. R., & Wood, R. (2002). Harmonized guidelines for single-laboratory validation of methods of analysis (IUPAC Technical Report). *Pure and Applied Chemistry*, *74*(5), 835-855. https://doi.org/doi:10.1351/pac200274050835

Trefry, J. H., & Neff, J. M. (2019). Effects of offshore oil exploration and development in the Alaskan Beaufort Sea: A three-decade record for sediment metals. *Integrated Environmental Assessment and Management*, *15*(2), 209-223. https://doi.org/https://doi.org/10.1002/ieam.4069

Tremblay, J.-É., Robert, D., Varela, D. E., Lovejoy, C., Darnis, G., Nelson, R. J., & Sastri, A. R. (2012). Current state and trends in Canadian Arctic marine ecosystems: I. Primary production. *Climatic Change*, *115*(1), 161-178. https://doi.org/10.1007/s10584-012-0496-3

Trettin, H., Bally, A., & Palmer, A. (1989). *The arctic islands*. Geological Society of America.

Tribovillard, N., Algeo, T. J., Lyons, T., & Riboulleau, A. (2006). Trace metals as paleoredox and paleoproductivity proxies: An update. *Chemical Geology*, *232*(1), 12-32. https://doi.org/https://doi.org/10.1016/j.chemgeo.2006.02.012

Turekian, K. K., & Wedepohl, K. H. (1961). Distribution of the Elements in Some Major Units of the Earth's Crust. *GSA Bulletin*, *72*(2), 175-192. https://doi.org/10.1130/0016-7606(1961)72[175:Doteis]2.0.Co;2

van den Boogaart, K. G., & Tolosana-Delgado, R. (2008). "compositions": A unified R package to analyze compositional data. *Computers & Geosciences*, *34*(4), 320-338. https://doi.org/https://doi.org/10.1016/j.cageo.2006.11.017

Van der Weijden, C. H. (2002). Pitfalls of normalization of marine geochemical data using a common divisor. *Marine Geology*, *184*(3), 167-187. https://doi.org/https://doi.org/10.1016/S0025-3227(01)00297-3

Vincent, R. F. (2023). An Assessment of the Lancaster Sound Polynya Using Satellite Data 1979 to 2022. *Remote Sensing*, *15*(4), 954. https://www.mdpi.com/2072-4292/15/4/954

Viscosi-Shirley, C., Mammone, K., Pisias, N., & Dymond, J. (2003). Clay mineralogy and multi-element chemistry of surface sediments on the Siberian-Arctic shelf: implications for sediment provenance and grain size sorting. *Continental Shelf Research*, *23*(11), 1175-1200. https://doi.org/https://doi.org/10.1016/S0278-4343(03)00091-8

Vonk, J. E., Giosan, L., Blusztajn, J., Montlucon, D., Graf Pannatier, E., McIntyre, C., Wacker, L., Macdonald, R. W., Yunker, M. B., & Eglinton, T. I. (2015). Spatial variations in geochemical characteristics of the modern Mackenzie Delta sedimentary system. *Geochimica et Cosmochimica Acta*, *171*, 100-120. https://doi.org/https://doi.org/10.1016/j.gca.2015.08.005

Wei, T., Simko, V., Levy, M., Xie, Y., Jin, Y., & Zemla, J. (2017). Package 'corrplot'. *Statistician*, *56*(316), e24.

Yukon Geological Survey. (2023). *Yukon Lithogeochemistry data set* https://data.geology.gov.yk.ca/Compilation/35

Yunker, M. B., Macdonald, R. W., Snowdon, L. R., & Fowler, B. R. (2011). Alkane and PAH biomarkers as tracers of terrigenous organic carbon in Arctic Ocean sediments. *Organic Geochemistry*, *42*(9), 1109-1146. https://doi.org/https://doi.org/10.1016/j.orggeochem.2011.06.007

Zhang, T., Wang, R., Xiao, W., Polyak, L., Astakhov, A., Dong, L., Wang, C., Liu, Y., & Shi, X. (2021). Characteristics of terrigenous components of Amerasian Arctic Ocean surface sediments: Implications for reconstructing provenance and transport modes. *Marine Geology*, *437*, 106497. https://doi.org/https://doi.org/10.1016/j.margeo.2021.106497

## 1.11 SUPPLEMENTARY MATERIAL (FIGURES AND TABLES)

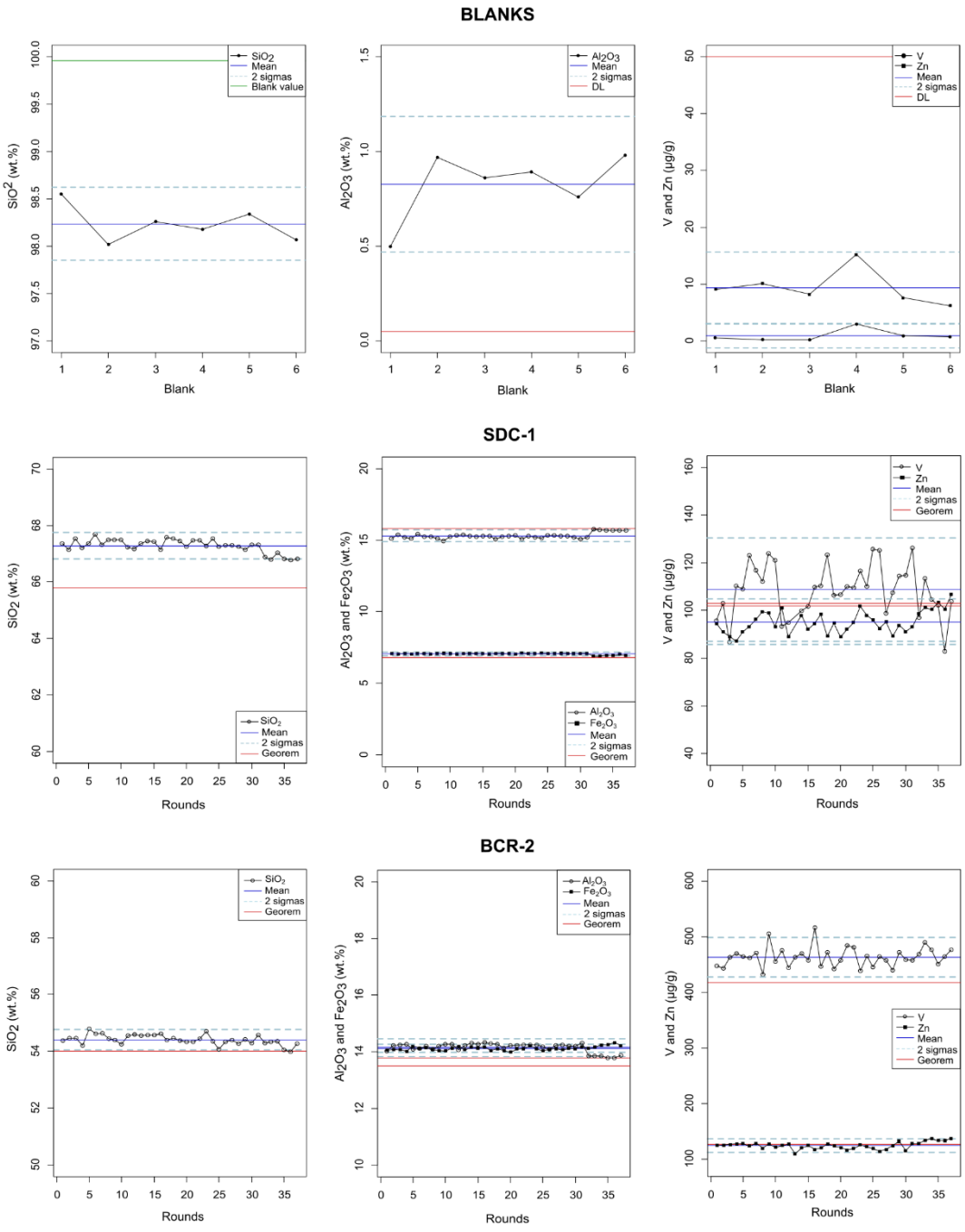


Figure 16. Plots of energy dispersive X-ray fluorescence (ED-XRF) results for some major and trace elements of the blanks and the USGS certified materials (SDC-1 and BCR-2).

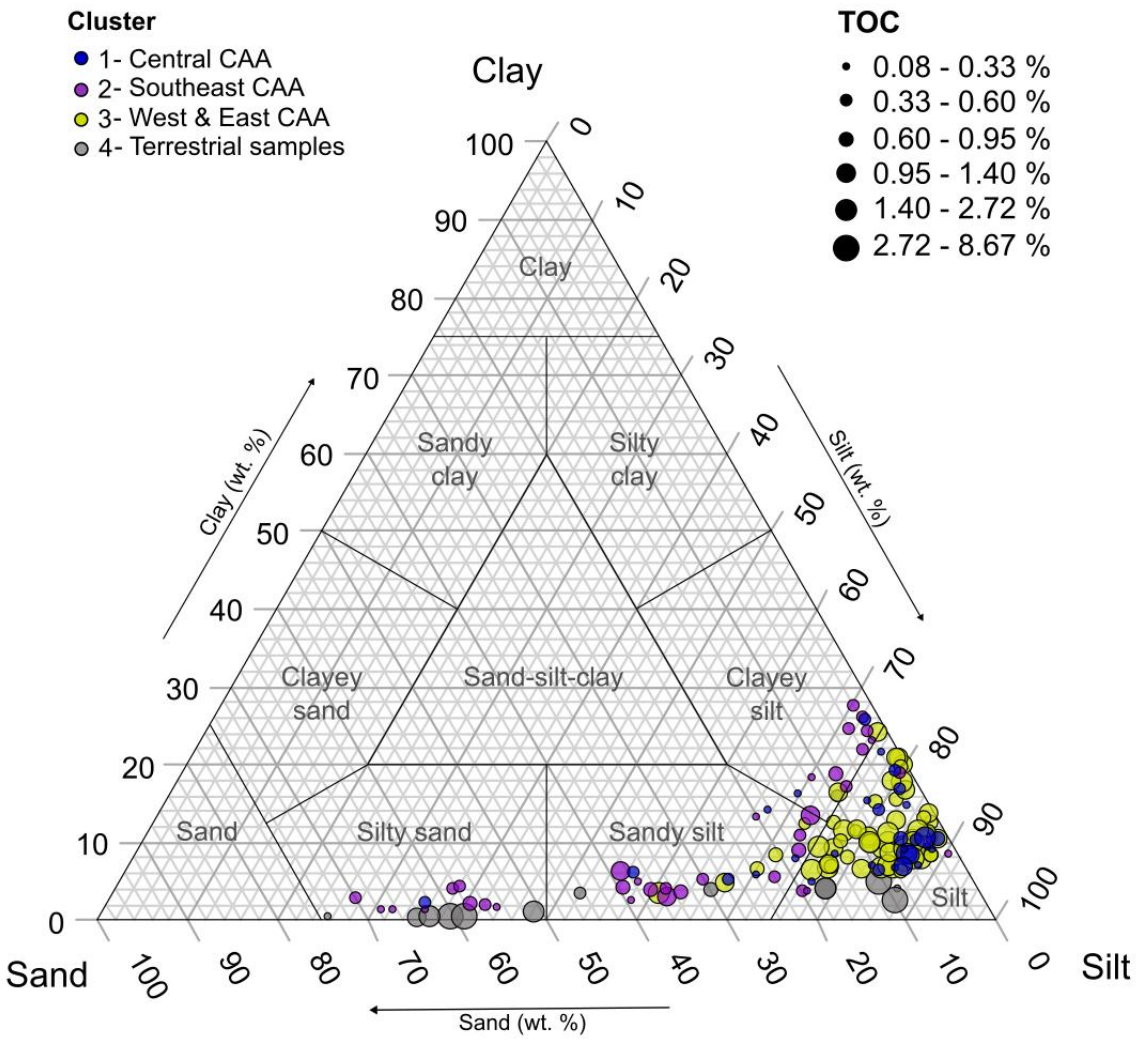


Figure 17. Ternary diagram sand-silt-clay showing Shepard's sediment classification (Shepard, 1954) of the <150 µm fraction of the sediments. The color of the dots represents the associated cluster and the size represents their TOC content (%).

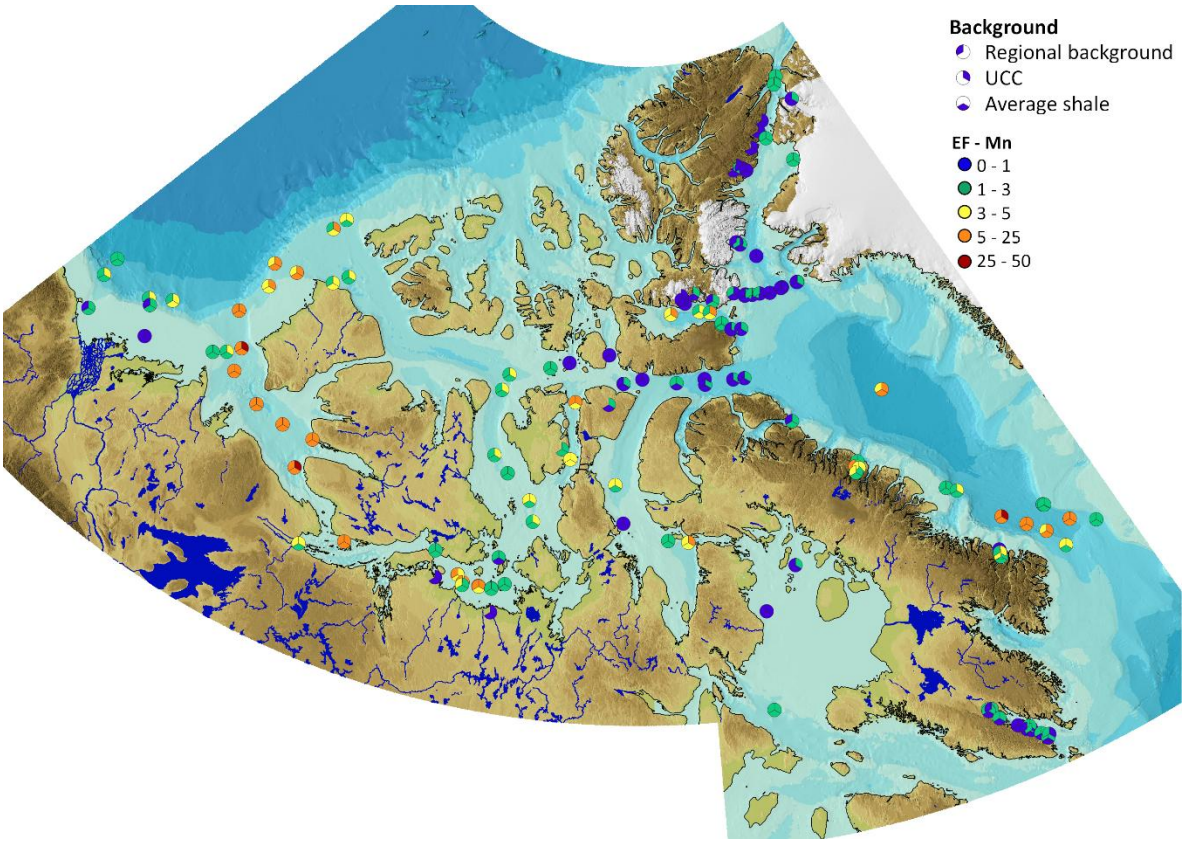


Figure 18. Map of the distribution of the enrichment factor values of Mn. Dots are divided into three thirds representing results of the three geochemical backgrounds used in this study.

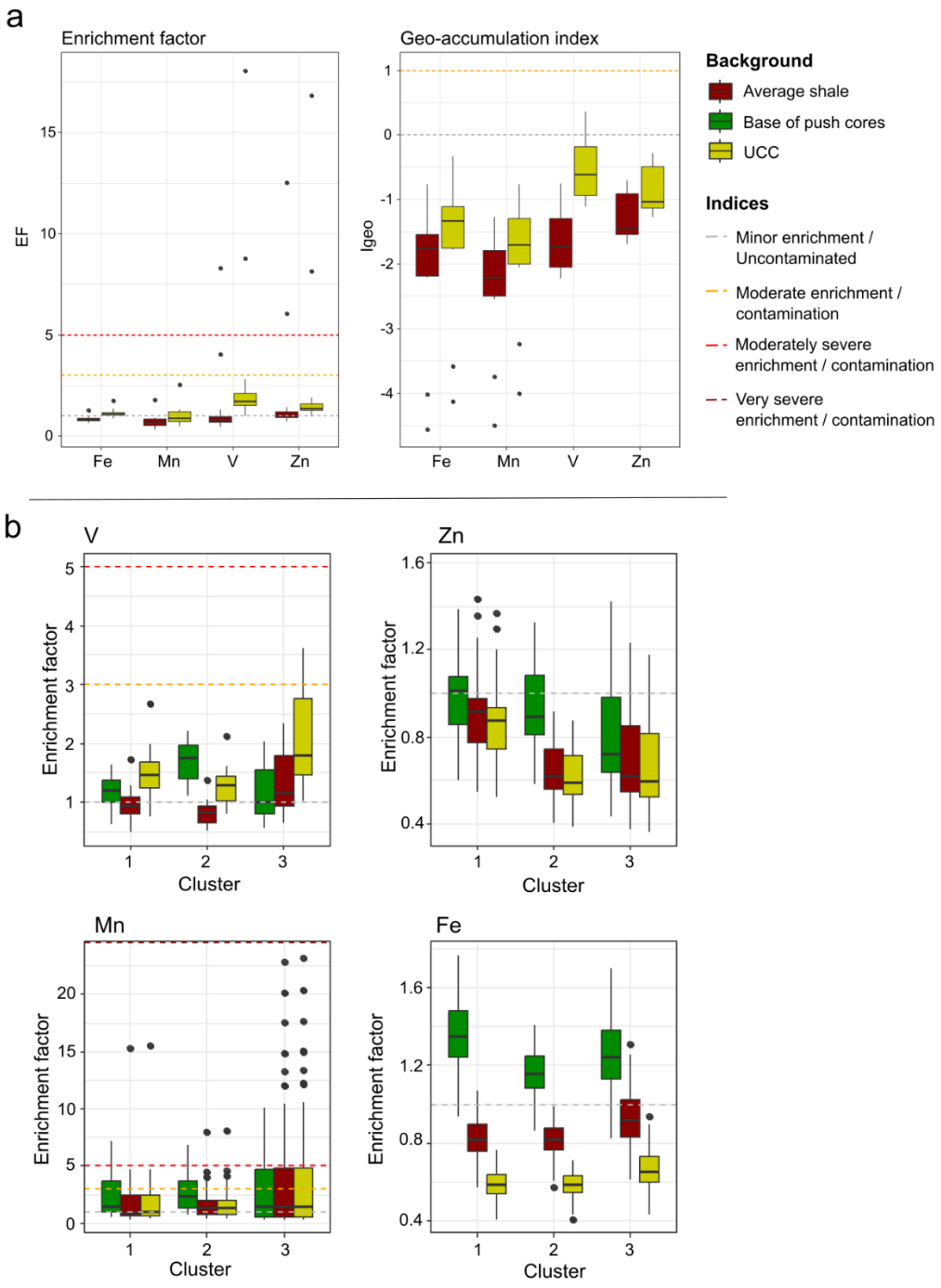


Figure 19. (a) Boxplots of the pollution indices values of terrestrial samples. Only the Upper Continental Crust and the Average Shale were used as background. Note that EFs using the base of push cores as background were not calculated for terrestrial samples because background values come from marine sediments. (b) Boxplots the enrichment factor values of marine surface samples using Ti as normalizing element.

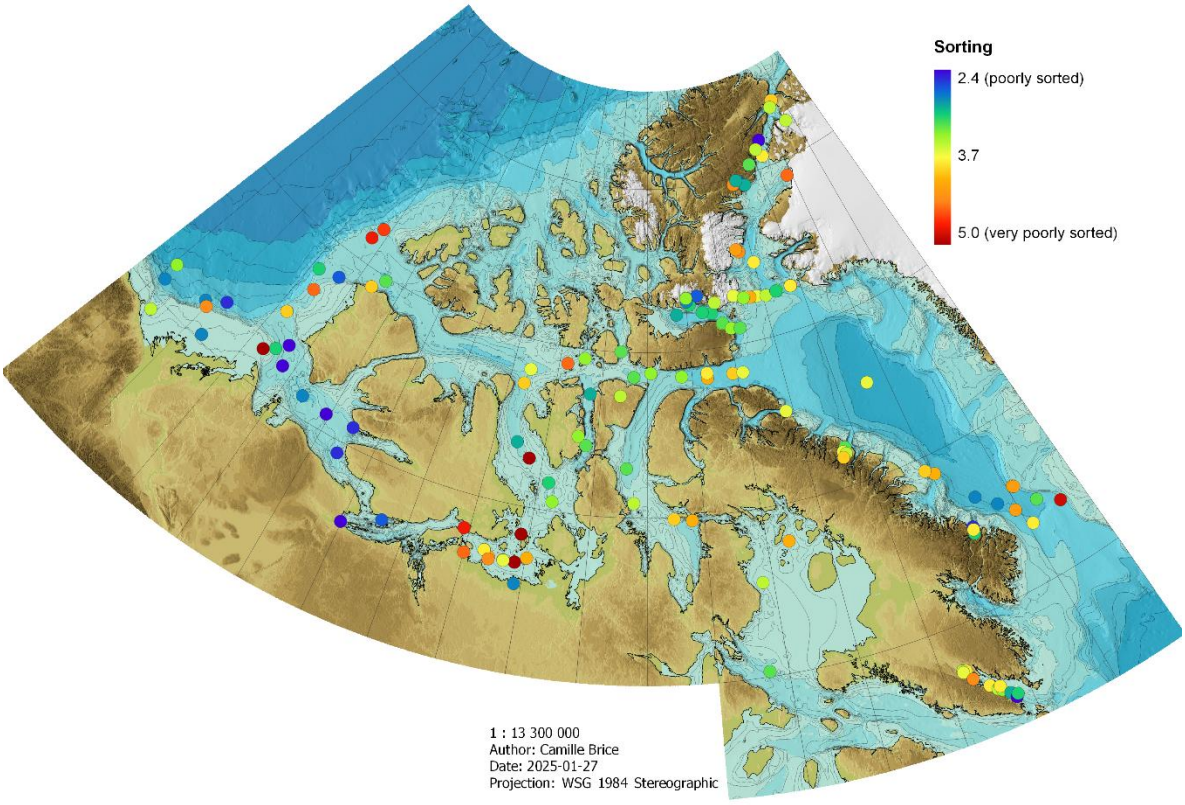


Figure 20. Map presenting spatial distribution of sediment sorting.

Tableau 3.

Coordinates and depths for the studied sediment samples.

| Expedition | Year / leg | Station | Core name | Type | Longitude | Latitude | Depth (m) |
|---|---|---|---|---|---|---|---|
| AMD1603 | 2016 / leg 3a | 165 | AMD1603-165-BC | Boxcore | -75.761 | 72.709 | 645 |
| AMD1603 | 2016 / leg 3a | 177 | AMD1603-177-BC | Boxcore | -63.801 | 67.475 | 385 |
| AMD1603 | 2016 / leg 3a | 301 | AMD1603-301-BC | Boxcore | -83.319 | 74.121 | 740 |
| AMD1603 | 2016 / leg 3a | 304 | AMD1603-304-BC | Boxcore | -91.521 | 74.246 | 314 |
| AMD1603 | 2016 / leg 3a | 307 | AMD1603-307-BC | Boxcore | -103.014 | 74.102 | 350 |
| AMD1603 | 2016 / leg 3a | 311 | AMD1603-311-BC | Boxcore | -98.534 | 70.280 | 170 |
| AMD1603 | 2016 / leg 3a | 312 | AMD1603-312-BC | Boxcore | -100.697 | 69.166 | 66 |
| AMD1603 | 2016 / leg 3a | 314 | AMD1603-314-BC | Boxcore | -105.475 | 68.971 | 89 |
| AMD1603 | 2016 / leg 3a | 316 | AMD1603-316-BC | Boxcore | -112.100 | 68.400 | 182 |
| AMD1603 | 2016 / leg 3a | 407 | AMD1603-407-BC | Boxcore | -126.090 | 71.009 | 390 |
| AMD1603 | 2016 / leg 3a | 408 | AMD1603-408-BC | Boxcore | -127.574 | 71.303 | 205 |
| AMD1603 | 2016 / leg 3a | 411 | AMD1603-411-BC | Boxcore | -126.731 | 71.623 | 435 |
| AMD1603 | 2016 / leg 3a | 420 | AMD1603-420-BC | Boxcore | -128.491 | 71.066 | 43 |
| AMD1603 | 2016 / leg 3a | 421 | AMD1603-421-BC | Boxcore | -133.891 | 71.399 | 1135 |
| AMD1603 | 2016 / leg 3a | 434 | AMD1603-434-BC | Boxcore | -133.544 | 70.174 | 46 |
| AMD1603 | 2016 / leg 3a | 435 | AMD1603-435-BC | Boxcore | -139.657 | 71.076 | 290 |
| AMD1603 | 2016 / leg 3a | 472 | AMD1603-472-BC | Boxcore | -138.227 | 69.611 | 124 |
| AMD1603 | 2016 / leg 3a | 482 | AMD1603-482-BC | Boxcore | -139.384 | 70.524 | 821 |
| AMD1603 | 2016 / leg 3a | 525 | AMD1603-525-BC | Boxcore | -128.952 | 72.392 | 347 |
| AMD1603 | 2016 / leg 3a | 535 | AMD1603-535-BC | Boxcore | -128.192 | 73.416 | 289 |
| AMD1603 | 2016 / leg 3a | 545 | AMD1603-545-BC | Boxcore | -126.823 | 74.178 | 315 |
| AMD1603 | 2016 / leg 3a | 575 | AMD1603-575-BC | Boxcore | -125.874 | 76.156 | 318 |
| AMD1603 | 2016 / leg 3a | 585 | AMD1603-585-BC | Boxcore | -123.222 | 74.513 | 382 |
| AMD1603 | 2016 / leg 3a | 1402 | AMD1603-1402-BC | Boxcore | -117.632 | 70.546 | 400 |
| AMD1603 | 2016 / leg 3b | 0416-01 | AMD1603-0416-01-BC | Boxcore | -122.170 | 74.885 | 505 |
| AMD1603 | 2016 / leg 3b | 0416-02 | AMD1603-0416-02-BC | Boxcore | -123.028 | 70.608 | 628 |
| AMD1603 | 2016 / leg 3b | 0416-03 | AMD1603-0416-03-BC | Boxcore | -120.348 | 70.513 | 330 |
| AMD1603 | 2016 / leg 3b | 0416-04 | AMD1603-0416-04-BC | Boxcore | -117.856 | 69.653 | 415 |
| AMD1603 | 2016 / leg 3b | 0416-05 | AMD1603-0416-05-BC | Boxcore | -115.071 | 67.864 | 60 |
| AMD1603 | 2016 / leg 3b | 0416-07 | AMD1603-0416-07-BC | Boxcore | -102.725 | 71.869 | 245 |
| AMD1603 | 2016 / leg 3a | 2016-805-18 | AMD1603-2016-805-18-BC | Boxcore | -129.127 | 74.007 | 420 |
| AMD1603 | 2016 / leg 3a | 2016-805-20 | AMD1603-2016-805-20-BC | Boxcore | -126.476 | 75.741 | 373 |
| AMD1603 | 2016 / leg 3a | 310E | AMD1603-310E-BC | Boxcore | -99.076 | 70.832 | 216 |
| AMD1603 | 2016 / leg 3a | 310W | AMD1603-310W-BC | Boxcore | -101.272 | 71.459 | 163 |
| AMD1603 | 2016 / leg 3a | BRG | AMD1603-BRG-BC | Boxcore | -135.462 | 70.992 | 664 |
| AMD1603 | 2016 / leg 3a | FURZE04 | AMD1603-Furze04-BC | Boxcore | -103.389 | 73.648 | 245 |
| AMD1603 | 2016 / leg 3a | FURZE07 | AMD1603-Furze07-BC | Boxcore | -97.195 | 74.706 | 318 |
| AMD1603 | 2016 / leg 3a | GSCLander2 | AMD1603-GSCLander2-BC | Boxcore | -135.000 | 70.875 | 200 |

| | | | | | | | |
|---|---|---|---|---|---|---|---|
| AMD1603 | 2016 / leg 3a | QMG2 | AMD1603-QMG2-BC | Boxcore | -100.803 | 68.316 | 53 |
| AMD1603 | 2016 / leg 3a | QMG3 | AMD1603-QMG3-BC | Boxcore | -102.944 | 68.314 | 56 |
| AMD1603 | 2016 / leg 3a | QMG4 | AMD1603-QMG4-BC | Boxcore | -103.418 | 68.490 | 82 |
| AMD1603 | 2016 / leg 3a | QMGM | AMD1603-QMGM-BC | Boxcore | -101.765 | 68.310 | 107 |
| AMD1702 | 2017 / leg 2 | OF-B2 | AMD1702-01BC | Boxcore | -67.333 | 62.999 | 442 |
| AMD1702 | 2017 / leg 2 | OF-S23 | AMD1702-03BC | Boxcore | -66.939 | 62.818 | 507 |
| AMD1702 | 2017 / leg 2 | OF-B6 | AMD1702-04BC | Boxcore | -66.705 | 62.745 | 493 |
| AMD1702 | 2017 / leg 2 | FB2-2-5d | AMD1702-05BC | Boxcore | -68.420 | 63.663 | 82 |
| AMD1702 | 2017 / leg 2 | BELL12 | AMD1702-07BC | Boxcore | -68.624 | 63.687 | 141 |
| AMD1702 | 2017 / leg 2 | A16 | AMD1702-08BC | Boxcore | -68.626 | 63.639 | 140 |
| AMD1702 | 2017 / leg 2 | BELL11 | AMD1702-09BC | Boxcore | -68.182 | 63.359 | 118 |
| AMD1702 | 2017 / leg 2 | OF-S22 | AMD1702-10BC | Boxcore | -66.746 | 62.866 | 289 |
| AMD1702 | 2017 / leg 2 | OF-B9 | AMD1702-11BC | Boxcore | -66.282 | 62.566 | 375 |
| AMD1702 | 2017 / leg 2 | OF-B14 | AMD1702-12BC | Boxcore | -66.021 | 62.386 | 411 |
| AMD1702 | 2017 / leg 2 | OF-B5 | AMD1702-13BC | Boxcore | -65.882 | 62.463 | 278 |
| AMD1702 | 2017 / leg 2 | DISKO FAN 1 | AMD1702-14BC | Boxcore | -59.565 | 67.992 | 947 |
| AMD1702 | 2017 / leg 2 | DISKO FAN 3 | AMD1702-15BC | Boxcore | -59.564 | 67.992 | 1012 |
| AMD1702 | 2017 / leg 2 | DISKO FAN 5 | AMD1702-16BC | Boxcore | -59.485 | 67.964 | 873 |
| AMD1702 | 2017 / leg 2 | 8.1 | AMD1702-17BC | Boxcore | -64.732 | 69.407 | 1054 |
| AMD1702 | 2017 / leg 2 | 176 | AMD1702-18BC | Boxcore | -65.403 | 69.597 | 267 |
| AMD1702 | 2017 / leg 2 | BB2 | AMD1702-19BC | Boxcore | -67.015 | 72.751 | 2373 |
| AMD1702 | 2017 / leg 2 | 101 | AMD1702-20BC | Boxcore | -77.516 | 76.357 | 378 |
| AMD1702 | 2017 / leg 2 | 105 | AMD1702-21BC | Boxcore | -75.758 | 76.317 | 331 |
| AMD1702 | 2017 / leg 2 | 115 | AMD1702-22BC | Boxcore | -71.254 | 76.331 | 668 |
| AMD1702 | 2017 / leg 2 | 129 | AMD1702-23BC | Boxcore | -76.647 | 76.331 | 521 |
| AMD1702 | 2017 / leg 2 | TS-233 | AMD1702-24BC | Boxcore | -76.686 | 77.755 | 396 |
| AMD1702 | 2017 / leg 2 | 111 | AMD1702-25BC | Boxcore | -73.207 | 76.308 | 593 |
| AMD1702 | 2017 / leg 2 | 108 | AMD1702-26BC | Boxcore | -74.606 | 76.264 | 448 |
| AMD1702 | 2017 / leg 2 | Belcher Glacier | AMD1702-27BC | Boxcore | -80.752 | 75.702 | 623 |
| AMD1702 | 2017 / leg 2 | 323 | AMD1702-28BC | Boxcore | -80.467 | 74.156 | 792 |
| AMD1702 | 2017 / leg 2 | 301-1 | AMD1702-29BC | Boxcore | -83.318 | 74.277 | 715 |
| AMD1702 | 2017 / leg 2 | 304 | AMD1702-30BC | Boxcore | -91.515 | 74.246 | 315 |
| AMD1702 | 2017 / leg 2 | 5.1 | AMD1702-31BC | Boxcore | -99.076 | 74.489 | 223 |
| AMD1702 | 2017 / leg 2 | 3.9 | AMD1702-32BC | Boxcore | -96.161 | 73.654 | 262 |
| AMD1702 | 2017 / leg 2 | QMGM | AMD1702-33BC | Boxcore | -101.741 | 68.302 | 114 |
| AMD1702 | 2017 / leg 2 | QMG4 | AMD1702-34BC | Boxcore | -103.430 | 68.484 | 71 |
| AMD1702 | 2017 / leg 2 | QMG3 | AMD1702-35BC | Boxcore | -102.941 | 68.244 | 46 |
| AMD1702 | 2017 / leg 2 | QMG1 | AMD1702-36BC | Boxcore | -99.898 | 68.492 | 40 |
| AMD1702 | 2017 / leg 2 | QMG2 | AMD1702-37BC | Boxcore | -100.807 | 68.306 | 95 |
| AMD1702 | 2017 / leg 2 | 312 | AMD1702-38BC | Boxcore | -100.695 | 69.170 | 65 |
| AMD1702 | 2017 / leg 2 | 3.7 | AMD1702-39BC | Boxcore | -96.065 | 72.089 | 474 |
| AMD1702 | 2017 / leg 2 | 3.4 | AMD1702-40BC | Boxcore | -91.993 | 71.475 | 270 |
| AMD1702 | 2017 / leg 2 | 3.5 | AMD1702-41BC | Boxcore | -91.236 | 70.436 | 224 |

| | | | | | | | |
|---|---|---|---|---|---|---|---|
| AMD1702 | 2017 / leg 2 | 5.11W | AMD1702-42BC | Boxcore | -87.666 | 69.954 | 184 |
| AMD1702 | 2017 / leg 2 | 5.11 | AMD1702-43BC | Boxcore | -86.084 | 69.882 | 298 |
| AMD1702 | 2017 / leg 2 | 3.10-2 | AMD1702-45BC | Boxcore | -78.162 | 68.878 | 52 |
| AMD1702 | 2017 / leg 2 | 3.10 | AMD1702-46BC | Boxcore | -80.847 | 67.797 | 96 |
| AMD1702 | 2017 / leg 2 | 1.1 | AMD1702-47BC | Boxcore | -81.353 | 65.155 | 418 |
| AMD1803 | 2018 / leg 3 | QMGM | AMD1803-01BC | Boxcore | -101.741 | 68.299 | 112 |
| AMD1803 | 2018 / leg 3 | 1.4 | AMD1803-02BC | Boxcore | -78.740 | 76.480 | 124 |
| AMD1803 | 2018 / leg 3 | 101 | AMD1803-03BC | Boxcore | -77.409 | 76.382 | 373 |
| AMD1803 | 2018 / leg 3 | 115 | AMD1803-04BC | Boxcore | -71.176 | 76.331 | 662 |
| AMD1803 | 2018 / leg 3 | 1.5 | AMD1803-05BC | Boxcore | -63.910 | 67.284 | 609 |
| AMD1902 | 2019 / leg 2 | 2.6 | AMD1902-01BC | Boxcore | -73.065 | 76.318 | 575 |
| AMD1902 | 2019 / leg 2 | 122 | AMD1902-02BC | Boxcore | -75.014 | 77.341 | 647 |
| AMD1902 | 2019 / leg 2 | 6.2 | AMD1902-03BC | Boxcore | -65.764 | 79.514 | 378 |
| AMD1902 | 2019 / leg 2 | 134 | AMD1902-04BC | Boxcore | -68.453 | 80.356 | 377 |
| AMD1902 | 2019 / leg 2 | Rob1 | AMD1902-05BC | Boxcore | -62.247 | 81.802 | 716 |
| AMD1902 | 2019 / leg 2 | 6.4 | AMD1902-06BC | Boxcore | -63.217 | 81.626 | 796 |
| AMD1902 | 2019 / leg 2 | 251b | AMD1902-08BC | Boxcore | -61.557 | 81.042 | 1135 |
| AMD1902 | 2019 / leg 2 | 6.1 | AMD1902-09BC | Boxcore | -73.659 | 79.786 | 205 |
| AMD1902 | 2019 / leg 2 | 6.1 | AMD1902-10BC | Boxcore | -73.095 | 79.692 | 245 |
| AMD1902 | 2019 / leg 2 | Talbot Inlet | AMD1902-11BC | Boxcore | -77.075 | 77.843 | 515 |
| AMD1902 | 2019 / leg 2 | 2.5 | AMD1902-12BC | Boxcore | -77.505 | 76.356 | 379 |
| AMD1902 | 2019 / leg 2 | 293 | AMD1902-13BC | Boxcore | -80.689 | 75.728 | 627 |
| AMD1902 | 2019 / leg 2 | 2.2 | AMD1902-14BC | Boxcore | -81.849 | 76.064 | 770 |
| AMD1902 | 2019 / leg 2 | 2.3 | AMD1902-15BC | Boxcore | -83.023 | 76.129 | 827 |
| AMD1902 | 2019 / leg 2 | 2.4 | AMD1902-16BC | Boxcore | -86.300 | 76.126 | 674 |
| AMD1902 | 2019 / leg 2 | 1.4 | AMD1902-17BC | Boxcore | -84.571 | 76.395 | 139 |
| AMD1902 | 2019 / leg 2 | 1.4 | AMD1902-18BC | Boxcore | -84.931 | 76.500 | 125 |
| AMD1902 | 2019 / leg 2 | 297 | AMD1902-19BC | Boxcore | -81.314 | 76.370 | 451 |
| AMD1902 | 2019 / leg 2 | 296 | AMD1902-20BC | Boxcore | -79.753 | 75.523 | 556 |
| AMD1902 | 2019 / leg 2 | 2.7 | AMD1902-21BC | Boxcore | -78.675 | 75.482 | 521 |
| AMD1902 | 2019 / leg 2 | 302 | AMD1902-22BC | Boxcore | -86.170 | 74.234 | 553 |
| AMD1902 | 2019 / leg 2 | 303 | AMD1902-23BC | Boxcore | -89.616 | 74.368 | 294 |
| AMD1902 | 2019 / leg 2 | Wel02 | AMD1902-25BC | Boxcore | -93.112 | 75.013 | 247 |
| AMD2202 | 2022 / leg 2 | KEBABB A3 | AMD2202-01BC | Boxcore | -59.604 | 66.733 | 872 |
| AMD2202 | 2022 / leg 2 | 195 | AMD2202-04BC | Boxcore | -56.929 | 66.891 | 655 |
| AMD2202 | 2022 / leg 2 | KEBABB B6 | AMD2202-06BC | Boxcore | -58.447 | 67.288 | 1134 |
| AMD2202 | 2022 / leg 2 | KEBABB B3 | AMD2202-07BC | Boxcore | -60.272 | 67.326 | 1074 |
| AMD2202 | 2022 / leg 2 | KEBABB C3 | AMD2202-09BC | Boxcore | -61.262 | 67.750 | 1558 |
| AMD2202 | 2022 / leg 2 | KEBABB D1 | AMD2202-10BC | Boxcore | -63.853 | 67.395 | 464 |
| AMD2202 | 2022 / leg 2 | KEBABB D3 | AMD2202-11BC | Boxcore | -62.594 | 68.241 | 1540 |
| AMD2202 | 2022 / leg 2 | Scott Inlet sill | AMD2202-12BC | Boxcore | -71.259 | 71.152 | 459 |
| AMD2202 | 2022 / leg 2 | SI_coring1 | AMD2202-13BC | Boxcore | -71.557 | 71.041 | 672 |
| AMD2202 | 2022 / leg 2 | SI_coring2 | AMD2202-14BC | Boxcore | -71.323 | 70.966 | 661 |

| | | | | | | | |
|---|---|---|---|---|---|---|---|
| AMD2202 | 2022 / leg 2 | SI_coring 3 | AMD2202-15BC | Boxcore | -71.661 | 70.875 | 682 |
| AMD2202 | 2022 / leg 2 | 323_east | AMD2202-16BC | Boxcore | -79.339 | 74.137 | 788 |
| AMD2202 | 2022 / leg 2 | 115 | AMD2202-17BC | Boxcore | -71.222 | 76.329 | 652 |
| AMD2202 | 2022 / leg 2 | 111 | AMD2202-18BC | Boxcore | -73.215 | 76.307 | 589 |
| AMD1803 | 2018 / leg 3 | Garnier River | AMD1803-Garnier river | River | -92.912 | 73.658 | 0 |
| AMD1803 | 2018 / leg 3 | Prince of Wales River | AMD1803-Prince of Wales river | River | -96.917 | 72.341 | 0 |
| AMD1803 | 2018 / leg 3 | Simpson River | AMD1803-Simpson river | River | -100.568 | 67.676 | 0 |
| AMD1803 | 2018 / leg 3 | Tingmeak River | AMD1803-Tingmeak river | River | -104.986 | 68.268 | 0 |
| AMD1902 | 2019 / leg 2 | Ellesmere South Central River | AMD1902-Ellesmere south central river | River | -83.504 | 76.646 | 0 |
| AMD1902 | 2019 / leg 2 | Eugenie Glacier | AMD1902-Eugenie Glacier | Glacier | -74.859 | 79.810 | 0 |
| AMD1902 | 2019 / leg 2 | Eugenie River | AMD1902-Eugenie River | River | -74.996 | 79.792 | 0 |
| AMD1902 | 2019 / leg 2 | RISG River (Near 1.4) | AMD1902-RISGRiver | River | -84.931 | 76.610 | 0 |
| AMD1902 | 2019 / leg 2 | Near Eugenie Glacier | AMD1902-Near Eugenie glacier | Glacier | -74.356 | 79.893 | 0 |
| AMD1902 | 2019 / leg 2 | Near Hans Island River | AMD1902-Near Hans Island River | River | -68.001 | 80.846 | 0 |
| AMD1902 | 2019 / leg 2 | River Ellesmere East | AMD1902-River Ellesmere East | River | -69.191 | 80.611 | 0 |
| AMD1902 | 2019 / leg 2 | River near 135 | AMD1902-River near 135 | River | -71.263 | 80.246 | 0 |
| AMD1902 | 2019 / leg 2 | Sydkap Glacier | AMD1902-Sydkap Glacier | River | -84.939 | 76.605 | 0 |

Tableau 4

List of the push cores basal samples used in this study for the regional geochemical background with estimated age of the sediment based on sedimentation rates calculated close to our sites. ** Sedimentation rates calculated for the push cores used in this study.

| Core | Depth of basal sample (cm) | Longitude | Latitude | Cluster | Sedimentation rate (cm/kyr) | Approximate basal age (CE) | References for sedimentation rate |
|---|---|---|---|---|---|---|---|
| AMD1603-0416-01-BC | 39-40 | -122.167 | 74.885 | 3 | 88 | 1561 | Letaief et al. 2021 |
| AMD1603-0416-02-BC | 39-39.5 | -123.028 | 70.608 | 3 | 23 | 299 | Gibb et al. 2009 |
| AMD1603-0416-04-BC | 42-42.5 | -117.856 | 69.653 | 3 | 160 | 1750 | Schell etal. 2008 |
| AMD1603-0416-05-BC | 37-37.5 | -115.071 | 67.864 | 2 | 276-178** | 1823 | Letaief et al. 2021 |
| AMD1603-0416-07-BC | 39-39.5 | -102.725 | 71.869 | 1 | 50 | 1226 | Kuzyck et al. 2013 |
| AMD1603-1402-BC | 39-40 | -117.632 | 70.546 | 1 | 160 | 1766 | Schell etal. 2008 |
| AMD1603-165-BC | 42-43 | -75.761 | 72.709 | 3 | 370-82** | 1556 | Letaief et al. 2021 |
| AMD1603-2016-805-018-BC | 44-44.5 | -129.127 | 74.007 | 3 | 88 | 1510 | Letaief et al. 2021 |
| AMD1603-301-BC | 37-38 | -83.319 | 74.121 | 3 | 60 | 1383 | Ledu et al. 2010b |
| AMD1603-304-BC | 44-45 | -91.521 | 74.246 | 1 | 184** | 1791 | Letaief et al. 2021 |
| AMD1603-314-BC | 35-36 | -105.475 | 68.971 | 2 | 70 | 1502 | Belt et al. 2010; Ledu et al. 2010 |
| AMD1603-316-BC | 40-41 | -112.100 | 68.400 | 3 | 271-111** | 1682 | Letaief et al. 2021 |
| AMD1603-408-BC | 40-41 | -127.574 | 71.303 | 3 | 87** | 1547 | Letaief et al. 2021 |
| AMD1603-411-BC | 42-42.5 | -126.731 | 71.623 | 3 | 87 | 1527 | Letaief et al. 2021 |
| AMD1603-434-BC | 48-49 | -133.544 | 70.174 | 3 | 139 | 1663 | Bringué & Rochon, 2012 |
| AMD1603-435-BC | 38-38.5 | -139.657 | 71.076 | 3 | 27 | 590 | Wu et al. 2020 |
| AMD1603-472-BC | 39-40 | -138.227 | 69.611 | 3 | 320 | 1891 | Durantou et al. 2012 |
| AMD1603-525-BC | 39-40 | -128.952 | 72.392 | 3 | 88 | 1561 | Letaief et al. 2021 |
| AMD1603-585-BC | 37-37.5 | -123.222 | 74.513 | 3 | 88 | 1590 | Letaief et al. 2021 |
| AMD1603-FURZE04-BC | 31-31.5 | -103.389 | 73.648 | 1 | 50 | 1386 | Kuzyck et al. 2013; Piénkowski et al. 2017 |
| AMD1603-FURZE07-BC | 43-44 | -97.195 | 74.706 | 3 | 50 | 1136 | Pienkowski et al. 2017 |
| AMD1603-QMG3-BC | 39-40 | -102.944 | 68.314 | 2 | 164 | 1772 | Letaief et al. 2021 |
| AMD1603-QMG4-BC | 37-38 | -103.418 | 68.490 | 2 | 164** | 1744 | Letaief et al. 2021* |
| AMD1702-04BC | 34-35 | -66.706 | 62.746 | 2 | 71 | 1524 | Osterman & Andrews |
| AMD1702-07BC | 28-29 | -68.624 | 63.687 | 2 | 190 | 1864 | Tremblay et al. 2020 |
| AMD1702-12BC | 25-26 | -66.021 | 62.386 | 2 | 71 | 1651 | Osterman & Andrews |
| AMD1702-16BC | 34-35 | -59.485 | 67.965 | 3 | 14.3 | 2450 BP | Cofaigh et al. 2015 |

| | | | | | | | |
|---|---|---|---|---|---|---|---|
| AMD1702-19BC | 34-35 | -67.015 | 72.751 | 3 | 2 | 17500 BP | Simon et al. 2016 |
| AMD1702-36BC | 38-38.5 | -99.898 | 68.492 | 2 | 180 | 1803 | Kuzyck et al. 2013 |
| AMD1702-39BC | 45-45.5 | -96.065 | 72.089 | 1 | 90 | 1511 | Kuzyck et al. 2013 |
| AMD1702-40BC | 46-46.5 | -91.993 | 71.475 | 1 | 90 | 1500 | Kuzyck et al. 2013 |
| AMD1702-43BC | 38-39 | -86.084 | 69.882 | 3 | 90 | 1584 | Kuzyck et al. 2013 |
| AMD1803-05BC | 42-43 | -63.910 | 67.284 | 2 | 90 | 1540 | Syviski etal. 2022 |
| AMD1902-05BC | 29-30 | -62.247 | 81.802 | 1 | 14.5 | 2070 BP | Jennings et al. 2019 |
| AMD1902-06BC | 28-29 | -63.217 | 81.626 | 1 | 14.5 | 19 | Jennings et al. 2019 |
| AMD1902-14BC | 43-44 | -81.849 | 76.064 | 3 | 160 | 1744 | Mudie et al. 2006 |
| AMD1902-20BC | 50-51 | -79.753 | 75.523 | 3 | 160 | 1700 | Mudie et al. 2006 |

Tableau 5

Detection limit for the Malvern PANalytical Epsilon 3-XL energy dispersive X-ray fluorescence spectrometer (ED-XRF).

| | **Detection limit** | **Units** |
|---|---|---|
| $Na_2O$ | 4 | % |
| MgO | 0.1 | % |
| $Al_2O_3$ | 0.05 | % |
| SiO2 | 0.05 | % |
| $P_2O_5$ | 1 | % |
| $K_2O$ | 0.05 | % |
| CaO | 0.05 | % |
| $TiO_2$ | 0.05 | % |
| V | 50 | µg/g |
| Cr | 100 | µg/g |
| MnO | 0.05 | % |
| $Fe_2O_3$ | 0.05 | % |
| Co | 400 | µg/g |
| Ni | 50 | µg/g |
| Cu | 100 | µg/g |
| Zn | 50 | µg/g |
| Sr | 50 | µg/g |
| Y | 50 | µg/g |
| Zr | 30 | µg/g |
| As | 50 | µg/g |

Tableau 6

ED-XRF results from the blanks (synthesized silicon oxide powder, 99.999% $SiO_2$).

| **Blanks** | **L.O.I. (wt.%)** | **$Al_2O_3$ (wt.%)** | **$SiO_2$ (wt.%)** | **$TiO_2$ (wt.%)** | **V (µg/g)** | **Cr (µg/g)** | **Zn (µg/g)** | **Sr (µg/g)** | **Y (µg/g)** | **Zr (µg/g)** |
|---|---|---|---|---|---|---|---|---|---|---|
| 1 | 0.95 | 0.50 | 98.55 | 0.001 | 0.5 | 19.6 | 9.1 | 2.5 | 5.5 | 6 |
| 2 | 1 | 0.97 | 98.02 | 0.001 | 0.2 | 3.4 | 10.1 | 4 | 8.2 | 5.9 |
| 3 | 0.88 | 0.86 | 98.26 | 0.001 | 0.2 | 6.8 | 8.2 | 2.1 | 7.8 | 7.1 |
| 4 | 0.93 | 0.89 | 98.18 | 0.001 | 3 | 1.9 | 15.2 | 4.5 | 3.8 | 10.6 |
| 5 | 0.89 | 0.76 | 98.34 | 0.001 | 0.9 | 7.4 | 7.6 | 2.4 | 4.3 | 5 |
| 6 | 0.95 | 0.98 | 98.07 | 0.002 | 0.7 | 5.1 | 6.2 | 2.7 | 4.3 | 4.7 |
| Average | | 0.83 | 98.22 | 0.00 | 0.92 | 7.37 | 8.24 | 2.74 | 6.02 | 5.74 |
| SD | | 0.16 | 0.18 | 0.00 | 0.97 | 5.78 | 2.86 | 0.89 | 1.74 | 1.97 |
| DL | | 0.05 | 0.05 | 0.05 | 50 | 100 | 50 | 50 | 50 | 30 |
| Below DL ? | | No | NA | Yes | Yes | Yes | Yes | Yes | Yes | Yes |
| Samples minimum value | | 1.94 | | | | | | | | |
| Samples mean | | 11.82 | | | | | | | | |
| Blank/mean | | 7% | | | | | | | | |
| Blank/minimum | | 43% | | | | | | | | |

Tableau 7

ED-XRF results for the USGS certified materials SDC-1 and BCR-2. NA: Not available.

| | **Certified value** | **Uncertainty** | **Average** | **±2σ** | **Unit** | **RSD (1σ; %)** | **Accuracy (2σ; %)** |
|---|---|---|---|---|---|---|---|
| *SDC-1* | | | | | | | |
| MgO | 1.69 | 0.1 | 1.32 | 0.2 | % | 7.9 | 78 ± 12 |
| $Al_2O_3$ | 15.8 | 0.3 | 15.3 | 1.3 | % | 1.3 | 97 ± 3 |
| $SiO_2$ | 65.8 | 0.4 | 67.1 | 0.8 | % | 0.3 | 102 ± 1 |
| CaO | 1.4 | 0.1 | 1.4 | 0.1 | % | 1.3 | 102 ± 3 |
| $TiO_2$ | 1.0 | 0.0 | 1.1 | 0.0 | % | 3.3 | 108 ± 7 |
| MnO | 0.1 | NA | 0.1 | 0.0 | % | 4.4 | 109 ± 10 |
| $Fe_2O_3$ | 6.8 | NA | 7.0 | 0.5 | % | 0.8 | 104 ± 2 |
| V | 102.0 | 12.0 | 108.6 | 24.0 | µg/g | 10.4 | 107 ± 22 |
| Cr* | 64.0 | 7.0 | 72.2 | 24.0 | µg/g | 13.7 | 118 ± 32 |
| Zn | 103.0 | 8.0 | 93.7 | 9.9 | µg/g | 4.9 | 92 ± 9 |
| Sr | 180.0 | 9.0 | 191.0 | 7.9 | µg/g | 4.8 | 107 ± 10 |
| Zr | 290.0 | 30.0 | 343.3 | 13.7 | µg/g | 4.6 | 120 ± 11 |
| *BCR-2* | | | | | | | |
| MgO | 3.6 | 0.0 | 3.2 | 0.2 | % | 3.9 | 89 ± 7 |
| $Al_2O_3$ | 13.5 | 0.1 | 14.2 | 0.3 | % | 1.1 | 105 ± 2 |
| $SiO_2$ | 54.0 | 0.2 | 54.4 | 0.3 | % | 0.3 | 101 ± 1 |
| CaO | 7.1 | 0.1 | 7.2 | 0.2 | % | 1.3 | 101 ± 3 |
| $TiO_2$ | 2.3 | 0.0 | 2.4 | 0.1 | % | 2.7 | 106 ± 6 |
| MnO | 0.2 | 0.0 | 0.2 | 0.0 | % | 4.6 | 111 ± 10 |
| $Fe_2O_3$ | 13.8 | 0.2 | 14.1 | 0.1 | % | 0.5 | 103 ± 1 |
| V | 417.6 | 4.5 | 463.4 | 35.1 | µg/g | 3.8 | 111 ± 8 |
| Cr* | 15.9 | 0.4 | 35.7 | 24.8 | µg/g | 35.2 | 225 ± 156 |
| Zn | 129.5 | 1.8 | 124.7 | 12.5 | µg/g | 5.1 | 96 ± 10 |
| Sr | 337.4 | 6.7 | 360.3 | 26.9 | µg/g | 3.8 | 107 ± 8 |
| Zr | 186.5 | 1.5 | 194.8 | 19.0 | µg/g | 4.9 | 104 ± 10 |

## 1.12 SUPPLEMENTARY MATERIAL (REFERENCES)


Belt, S. T., Vare, L. L., Massé, G., Manners, H. R., Price, J. C., MacLachlan, S. E., Andrews, J. T., & Schmidt, S. (2010). Striking similarities in temporal changes to spring sea ice occurrence across the central Canadian Arctic Archipelago over the last 7000 years. *Quaternary Science Reviews*, *29*(25), 3489-3504. https://doi.org/https://doi.org/10.1016/j.quascirev.2010.06.041

Bringué, M., & Rochon, A. (2012). Late Holocene paleoceanography and climate variability over the Mackenzie Slope (Beaufort Sea, Canadian Arctic). *Marine Geology*, *291-294*, 83-96. https://doi.org/https://doi.org/10.1016/j.margeo.2011.11.004

Durantou, L., Rochon, A., Ledu, D., Massé, G., Schmidt, S., & Babin, M. (2012). Quantitative reconstruction of sea-surface conditions over the last 150 yr in the Beaufort Sea based on dinoflagellate cyst assemblages: the role of large-scale atmospheric circulation patterns. *Biogeosciences*, *9*(12), 5391-5406. https://doi.org/10.5194/bg-9-5391-2012

Gibb, O. T. (2009). Foraminiferal indicators of paleoceanographic and sea-ice conditions in the Amundsen Gulf and Viscount Melville Sound, Canadian Arctic Dalhousie University]. Halifax, Nova Scotia.

Jennings, A., Reilly, B., Andrews, J., Hogan, K., Walczak, M., Jakobsson, M., Stoner, J., Mix, A., Nicholls, K. W., O'Regan, M., Prins, M. A., & Troelstra, S. R. (2022). Modern and early Holocene ice shelf sediment facies from Petermann Fjord and northern Nares Strait, northwest Greenland. *Quaternary Science Reviews*, *283*, 107460. https://doi.org/https://doi.org/10.1016/j.quascirev.2022.107460

Kuzyk, Z. Z. A., Gobeil, C., & Macdonald, R. W. (2013). 210Pb and 137Cs in margin sediments of the Arctic Ocean: Controls on boundary scavenging. *Global Biogeochemical Cycles*, *27*(2), 422-439. https://doi.org/https://doi.org/10.1002/gbc.20041

Ledu, D., Rochon, A., de Vernal, A., Barletta, F., & St-Onge, G. (2010). Holocene sea ice history and climate variability along the main axis of the Northwest Passage, Canadian Arctic. *Paleoceanography*, *25*(2). https://doi.org/https://doi.org/10.1029/2009PA001817

Ledu, D., Rochon, A., de Vernal, A., & St-Onge, G. (2010). Holocene paleoceanography of the northwest passage, Canadian Arctic Archipelago. *Quaternary Science Reviews*, *29*(25-26), 3468-3488.

Letaïef, S., Montero-Serrano, J. C., & St-Onge, G. (2021). Sedimentary processes within the Canadian Arctic Archipelago: Relationships among sedimentological, geochemical, and magnetic sediment properties. *Geochemistry, Geophysics, Geosystems*, *22*(7), e2021GC009719.

Mudie, P. J., Rochon, A., Prins, M. A., Soenarjo, D., Troelstra, S. R., & Levac, E. (2006). Late Pleistocene-Holocene marine geology of Nares Strait region: Paleoceanography from foraminifera and dinoflagellate cysts, sedimentology and stable isotopes. *Polarforschung*, *74*(1-3), 169-183.

Ó Cofaigh, C., Dowdeswell, J., Jennings, A., Hogan, K., Kilfeather, A., Hiemstra, J., Noormets, R., Evans, J., McCarthy, D., & Andrews, J. (2013). An extensive and dynamic ice sheet on the West Greenland shelf during the last glacial cycle. *Geology*, *41*(2), 219-222.

Osterman, L. E., & Andrews, J. T. (1983). Changes in Glacial-Marine Sedimentation in Core HU77-159, Frobisher Bay, Baffin Island, N.W.T: A Record of Proximal, Distal, and Ice-Rafting Glacial-Marine Environments. In B. F. Molnia (Ed.), *Glacial-Marine Sedimentation* (pp. 451-493). Springer US. https://doi.org/10.1007/978-1-4613-3793-5_11

Pieńkowski, A. J., Gill, N. K., Furze, M. F., Mugo, S. M., Marret, F., & Perreaux, A. (2017). Arctic sea-ice proxies: Comparisons between biogeochemical and micropalaeontological reconstructions in a sediment archive from Arctic Canada. *The Holocene*, *27*(5), 665-682. https://doi.org/10.1177/0959683616670466

Richerol, T., Rochon, A., Blasco, S., Scott, D. B., Schell, T. M., & Bennett, R. J. (2008). Evolution of paleo sea-surface conditions over the last 600 years in the Mackenzie Trough, Beaufort Sea (Canada). *Marine Micropaleontology*, *68*(1), 6-20. https://doi.org/https://doi.org/10.1016/j.marmicro.2008.03.003

Shepard, F. P. (1954). Nomenclature based on sand-silt-clay ratios. *Journal of sedimentary Research*, *24*(3), 151-158.

Simon, Q., Thouveny, N., Bourlès, D. L., Nuttin, L., Hillaire-Marcel, C., & St-Onge, G. (2016). Authigenic 10Be/9Be ratios and 10Be-fluxes (230Thxs-normalized) in central Baffin Bay sediments during the last glacial cycle: Paleoenvironmental implications. *Quaternary Science Reviews*, *140*, 142-162. https://doi.org/https://doi.org/10.1016/j.quascirev.2016.03.027

Syvitski, J., Andrews, J. T., Schafer, C. T., & Stravers, J. A. (2022). Sediment fill of Baffin Island fjords: Architecture and rates. *Quaternary Science Reviews*, *284*, 107474. https://doi.org/https://doi.org/10.1016/j.quascirev.2022.107474

Wu, J., Stein, R., Fahl, K., Syring, N., Nam, S.-I., Hefter, J., Mollenhauer, G., & Geibert, W. (2020). Deglacial to Holocene variability in surface water characteristics and major floods in the Beaufort Sea. *Communications Earth & Environment*, *1*(1), 27. https://doi.org/10.1038/s43247-020-00028-z

# CHAPITRE 2
# ÉTABLISSEMENT DES NIVEAUX DE REFERENCE DES METAUX TRACES EXTRACTIBLES DANS LES SEDIMENTS MARINS DE SURFACE DE L'ARCTIQUE CANADIEN

## 2.1 RESUME EN FRANÇAIS DU DEUXIEME ARTICLE

Une évaluation spatiale complète de la distribution des métaux traces extractibles, y compris les éléments de terres rares (ETR), dans l'Arctique canadien a été réalisée à partir d'échantillons de sédiments terrestres et marins de surface afin d'évaluer l'état actuel de la contamination par les métaux. Les concentrations en éléments majeurs et en éléments traces ont été déterminées par digestion partielle à l'$HNO_3$-HCl et par des mesures au spectromètre de masse à plasma inductif à triple quadripôle. L'extraction partielle cible les fractions métalliques réactives et biodisponibles qui sont sensibles aux variations environnementales et aux contributions anthropiques. Les résultats ont révélé des variations régionales importantes dans les concentrations de métaux traces (p. ex. : Cr = 5−96 µg/g ; Zn = 9−139 µg/g ; ΣREE = 21−358 µg/g), avec un gradient ouest-est clair. Les concentrations les plus élevées de métaux non-ETR sont observées dans la mer de Beaufort et le golfe d'Amundsen, ce qui souligne l'influence du fleuve Mackenzie. À l'inverse, les ETR sont concentrés près des côtes caractérisées par les roches du Bouclier canadien dans le centre-sud et l'est de l'Arctique canadien. Les profils normalisés de distribution des terres rares montrent un enrichissement en terres rares légères par rapport aux terres rares lourdes. Les indices de pollution indiquent un enrichissement ou une contamination généralement faibles, bien que quelques échantillons présentent un enrichissement/une contamination modéré en arsenic dans le plateau de Beaufort et le détroit de Jones. D'après les recommandations canadiennes pour la qualité des sédiments, la plupart des échantillons présentaient des concentrations en métaux inférieures aux concentrations produisant des effets probables. Cependant, des

concentrations supérieures à ce seuil ont été mesurées pour l'arsenic (> 41,6 µg/g) et le nickel (> 42,8 µg/g) dans les golfes Amundsen et Coronation, le détroit de Jones et la baie de Baffin. Malgré des contaminations localisées, la répartition des métaux traces présente des concentrations naturelles influencées par la géologie et les processus sédimentaires régionaux. Cette base de référence géochimique offre de nouvelles perspectives sur des zones jusqu'alors non caractérisées, améliorant ainsi notre compréhension des sources et du devenir des métaux traces, ainsi que la précision de la surveillance environnementale dans l'Arctique canadien.

## 2.2 ESTABLISHING BASELINE LEVELS OF EXTRACTABLE TRACE METALS IN MARINE SURFACE SEDIMENT OF THE CANADIAN ARCTIC

A comprehensive spatial assessment of extractable trace metal, including rare earth element (REE), distribution in the Canadian Arctic was conducted based on terrestrial and marine surface sediment samples to evaluate the current state of metal contamination. Major and trace element concentrations were determined by $HNO_3$-HCl partial digestion and triple quadrupole inductively coupled plasma mass spectrometer measurements. Partial extraction targets reactive and bioavailable metal fractions that are sensitive to environmental variations and anthropogenic contributions. Results revealed significant regional variations in trace metal concentrations (Cr=5–96 μg/g; Zn=9–139 μg/g; ΣREE=21–358 μg/g), with a clear West-East gradient. The highest non-REE metal concentrations are observed in Beaufort Sea and Amundsen Gulf, highlighting the influence of the Mackenzie River. Conversely, the REEs are concentrated near the coasts underlain by Canadian Shield rocks in the south-central and eastern Canadian Arctic. Normalized REE distribution patterns show an enrichment in light REEs compared to heavy REEs. The pollution indices indicate generally low enrichment or contamination, although few samples exhibit moderate arsenic enrichment/contamination in the Beaufort Shelf and Jones Sound. Based on the Canadian sediment quality guidelines, most samples had metal concentrations below the Probable Effects Level. However, concentrations exceeding this threshold were measured for arsenic (> 41.6 μg/g) and nickel (> 42.8 μg/g) in the Amundsen and Coronation gulfs, Jones Sound and Baffin Bay. Despite localized contamination, the trace metal distribution exhibit natural concentrations influenced by the regional geology and sedimentary processes. This geochemical baseline offers new insights from previously uncharacterized areas, improving our understanding of the sources and fate of trace metals and the accuracy of environmental monitoring of the Canadian Arctic.

## 2.3 INTRODUCTION

The Canadian Arctic is undergoing rapid environmental changes, including permafrost thawing and reduced sea ice cover (Mudryk et al., 2018) driven by global climate warming or increasing anthropogenic pressures, such as enhanced northern maritime traffic (Chénier et al., 2017; ECCC, 2024) and the accumulation of contaminants via long-range transport (Macdonald et al., 2000b). As a result, changes in biogeochemical cycles are observed in Arctic marine environments (AMAP, 2005, 2011, 2018, 2021).

Trace metal(loid) concentrations (hereinafter referred to as trace metal) in sediments are controlled by multiple natural processes, including the weathering of exposed geological formations, aeolian dust deposition, rivers and groundwaters inflows, as well as grain size distribution, diagenesis, and biological uptake (Chapman et al., 1998). Although trace metal levels in CA sediments are mostly natural and influenced by the surrounding geology (Brice et al., 2025), the rapid changes disrupt these processes, accelerating the remobilization and redistribution of trace metals, which can result in increased concentrations in surficial sediments and potential ecotoxicological issues to benthic fauna.

In the 1990s, the Arctic Monitoring & Assessment Program (AMAP) concluded that trace metal pollution represents a potential ecotoxicological risk to the Arctic ecosystems and ultimately to local communities via country food (AMAP, 1998). Since then, the trace metals such as Pb, Cd and Hg have been monitored in the Arctic by the AMAP (AMAP, 2005, 2021) and the Canadian Northern Contaminants Program (Bidleman et al., 2003; Chételat and Braune, 2012; Jensen et al., 1997; Stow et al., 2017). These metals have shown different temporal and spatial trends in soils, sediments, water and biota. For example, Hg has been increasing in fishes in the Mackenzie River system since the 1990s (Stow et al., 2017). Pb levels have been decreasing in the environment since the phase-out of leaded gasoline, but in biota, the trend is less pronounced (AMAP, 2005).

In the CA, trace metal contamination in marine sediments has never been investigated in the channels of the archipelago, and existing studies from the Baffin Bay region are very

limited (Bartley et al., 2024; Campbell and Loring, 1980). Only the Beaufort Sea region has been extensively studied for metal pollution because of oil exploration, which can emit several metals such as Ba, Cd, Cr, Cu, Pb and V (e.g., Naidu et al., 2012; Trefry and Neff, 2019; Trefry et al., 2003). Besides some localized hot spots of metal contamination detected in sediment cores near drilling sites, no overall contamination or significant increase in metal concentrations was observed during and after offshore oil exploration. Enrichment in As, along with Fe and Mn, was found on the continental margin of the Alaskan Beaufort Sea, but diagenetic remobilization is likely the cause rather than anthropogenic inputs (Trefry & Neff, 2019). Trends in metal concentrations in the environment are not quite fully understood due to the multiple processes involved, including both natural and anthropogenic inputs, local to long-range atmospheric transport, biogeochemical reactions, among others, making metal pollution monitoring a challenge.

Long time neglected in environmental studies, REEs are now metals of concern along with legacy trace metal contaminants such as Hg, Pb and Cd (González et al., 2015). It includes the 15 lanthanides (from La to Lu), Y and some authors include Sc. In recent years, there has been an increasing interest in the exploitation of REEs for multiple purposes, such as energy transition, electronics devices, and other industrial sectors (US EPA, 2012). With increasing anthropogenic inputs into the environment, the risks of REE enrichment and contamination are expected to rise, making monitoring necessary (González et al., 2015). Canada has major REE reserves, and several exploration projects are already underway in many areas of the country, but the CA remains largely untouched for now (NRCAN, 2024). It is therefore essential to establish baseline trace metal including REE levels today.

In this context, to better understand trends and monitor changes associated with increasing anthropogenic perturbations, a geochemical baseline for marine surface sediments has been established across the CA. The primary objective of this study is to provide regional acid-extractable geochemical data from marine surface sediments (fraction <150 μm) – i.e. the mobile fraction available to benthic organisms – for a large region of the CA, where significant gaps remain. This baseline will then enable us to assess the current state of trace

metal contamination and identify the factors controlling their distribution. Finally, by improving our understanding of acid-extractable trace metal distribution, behavior, and the processes involved, we aim to estimate the level of ecotoxicological risks associated with ongoing and future changes in the marine environment.

## 2.4 METHODOLOGY

### 2.4.1 Regional setting

The CA region comprises an Arctic Ocean shelf that connects the Beaufort Sea to the Baffin Bay through the channels and straits of the Arctic Archipelago (Fig. 21a). The seafloor composition is heterogenous and characterized by different bedrock sources and sedimentary processes (Campbell and Loring, 1980; Gamboa et al., 2017; Letaïef et al., 2021). Brice et al. (2025) divided the CA into three geochemical clusters forming four sedimentary provinces, based on the chemical composition of marine surface sediment (fraction <150 μm) measured by Energy Dispersive X-Ray Fluorescence (ED-XRF; Fig. 21b). The first province is mainly located in central CA and consists of sediments derived from the limestone and dolostone of the Arctic platform, transported by small rivers and coastal erosion. These sediments are rich in Ca and Mg and have low trace metal content. The second sedimentary province (southeastern CA) includes sediments from Baffin Island fjords and bays, as well as Coronation and Queen Maud Gulfs. These sediments, derived from the Canadian Shield, are characterized by coarse grain size, Zr-Sr-Si-K-Al associations and low trace metal content. Major mainland rivers and sea ice transport supply the gulfs, while glacial and coastal erosion contributes to sediment deposition along Baffin Island coast. The last two provinces, one in the Beaufort/Mackenzie Shelf and Amundsen Gulf, and the other in Baffin Bay, were grouped into a single chemical cluster. The province in western CA is strongly influenced by the Mackenzie River (Bossé-Demers et al., 2025; Gamboa et al., 2017), which discharges fine-grained clay minerals, preformed metallic oxides, terrestrial organic carbon, and dissolved metals (Mn, Fe, V, Zn). Strong Mn enrichment is observed in surface sediments in the Amundsen Gulf and along Banks Island coasts. The last province (eastern

CA) includes sediments from Lancaster and Jones Sounds, the North Water Polynya (NOW) area, and Davis Strait. These sediments are mainly characterized by high marine organic carbon content, originating from the high productivity of the polynyas. Glacial erosion also contributes with inputs of sediments of mixed composition derived from surrounding bedrock.

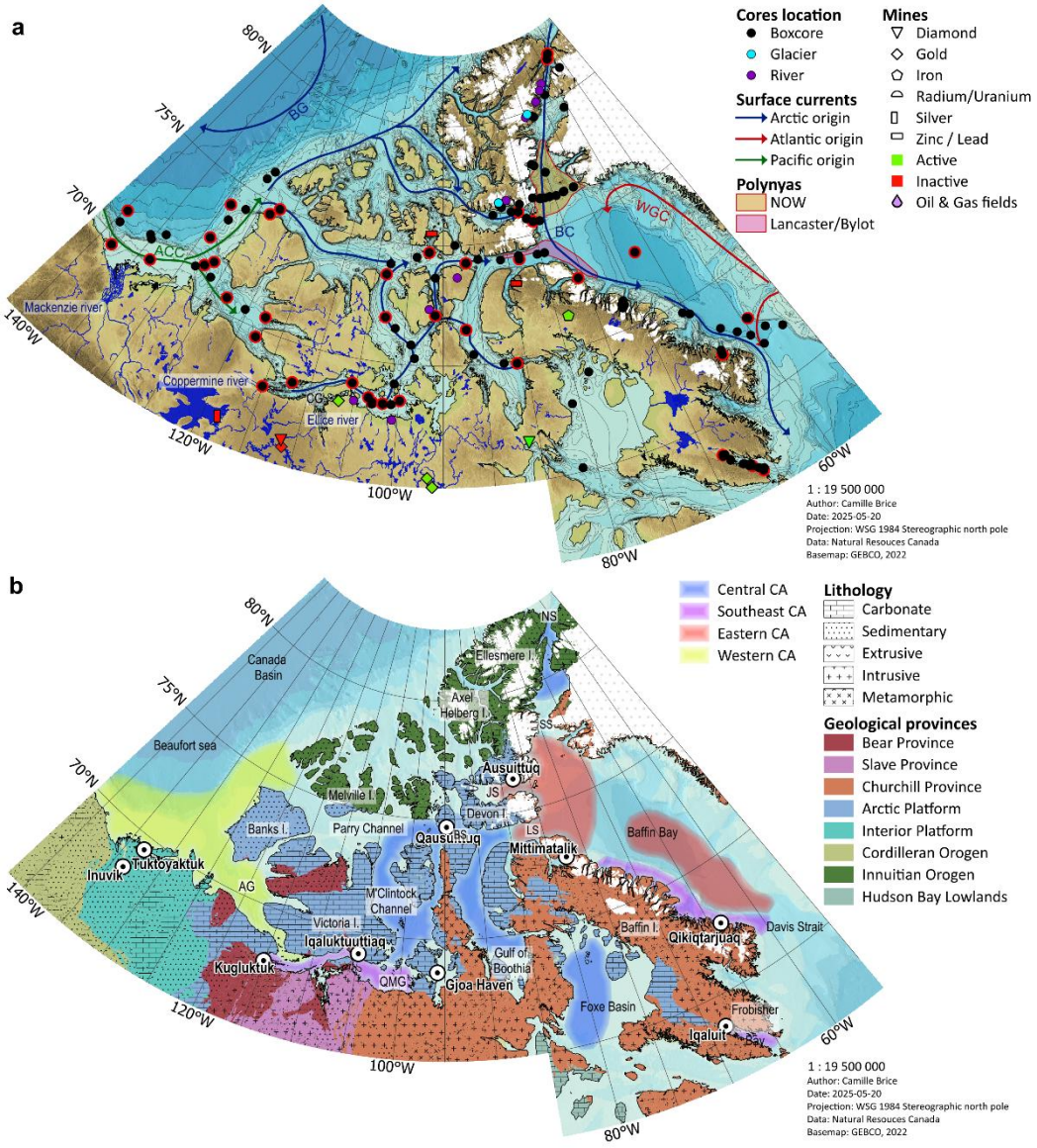


Figure 21. Maps showing the Canadian Arctic. (a) Map presenting the main geographical settings and the location of the surface sediment samples. Push cores used for geochemical background are circled in red. (b) Geological map with the sedimentary provinces.

### 2.4.2 Sampling

To establish the baseline, trace metal concentrations in the seafloor sediments of the CA were measured using 141 sediment samples. A total of 128 marine surface sediment samples (uppermost 1 cm) were collected across the region with a box corer device during the ArcticNet summer expeditions (2016-2019 and 2022) aboard the Canadian Coast Guard icebreaker Amundsen. Additionally, sediments from 10 rivers and 3 glacial tills were sampled as references of land inputs. To provide a regional geochemical background representative of pre-industrial times, the base (lowermost 1-2cm) of 16 push-cores subsampled from the box cores of different sedimentary provinces (Fig. 21b) were also analyzed.

### 2.4.3 Analytical methods

The grain size ($D_{90}$) and total organic carbon (TOC) data used in this study were obtained from Corminboeuf et al. (2021) and Brice et al. (2025). Briefly, grain size analysis was conducted using a Malvern PANalytical Mastersizer 3000 laser diffraction analyzer, following the instrumental protocol described in Belzile and Montero-Serrano (2022), after H2O2 pre-treatment, dispersion in sodium hexametaphosphate (20% v/v), and wet sieving at <2 mm. For TOC content and elemental analysis, the samples were first wet-sieved using a 150-µm Nitex® mesh and distilled water, and then oven-dried at <60 °C for 12 h and crushed with an agate mortar. The TOC content in the <150 µm sediment fraction were measured at the Geotop Light Stable Isotope Geochemistry Laboratory (Montreal, Quebec) with a Carlo-Erba NC 2500 elemental analyzer and following the acidification in solution method described in Hélie (2009).

The concentrations of six major elements (Mg, K, Ca, Ti, Mn, Fe), 14 trace metals (As, Cd, Cr, Co, Cu, Mo, Ni, Pb, Sb, Sc, Sr, Th, V, Zn) and REEs (14 lanthanides + Y) in sediments were determined using partial acid digestion following a slightly modified version of the US EPA Method 3051A (US EPA, 2007). Henceforth, we will use the term 'trace

metals' to refer to non-REE metals. This method primarily targets trace elements associated with reactive phases such as organic matter, sulfides, Fe-Mn (oxyhydr)oxides, carbonates, and hydrated aluminosilicates and does not attack refractory silicates and heavy minerals (Xu et al., 2012). For this purpose, about 50 mg of the dry <150 µm fraction was mixed with 2 mL of concentrated HCl and 6 mL of concentrated $HNO_3$, both of TraceMetalTM Grade (Thermo Fisher Scientific). Digestion was performed using CEM EasyPrep vessels and CEM Mars 5 microwave system under the following conditions: ramp time= 18 min, temperature = 175°C, hold time = 4 min, maximum pressure = 400 PSI, and power = 1600W (75%). The digested samples were diluted with Milli-Q water to a final concentration of 2% $HNO_3$ and <0.1% HCl. Trace metal concentrations were measured using an Agilent 8900 triple quadrupole inductively coupled plasma mass spectrometer (ICP-QQQ-MS) at the Laboratoire d'Analyses Environnementales (Université du Québec à Montréal). Falcon tubes and laboratory glassware were pre-cleaned with 10% $HNO_3$, and EasyPrep vessels were soaked in 0.2 M $HNO_3$ for 12h before analysis. For every eight samples, one procedural blank was analyzed following the same method. For surface samples, if the average value of blanks for an element exceeds the detection limit and is greater than 20 times the minimum sample value, it is subtracted from all sample values (Table 10). For samples used for geochemical background, which were processed at a different time, variable contamination was observed for Cr and to a lesser extent Al and Ca in the blanks (Table 11). Therefore, blank values were subtracted from the sample values measured within the same batch. Because Al and Ca concentrations in most sediment samples are on average 150 and 70 times higher than the contamination levels, respectively, these elements were retained, but Cr was excluded from the geochemical background. All the elements analyzed in the samples were above the detection limit. Quality control was ensured with replicates of certified reference materials TILL-3 (for surface samples) and TILL-2 (for geochemical background), which are characterized for partial extraction with concentrated HCl and $HNO_3$. Good recoveries (80-120%) were obtained for all elements, except for V, which showed recoveries between 133 and 147% (Table 12a). REEs are not certified for partial digestion in TILL-2 and TILL-3, but digestion protocol and analysis were compared with total digestion certified values to

assess reliability (Table 12b). Recoveries of 81-101% are observed for La, Ce, Nd, Sm and Eu, and of 34-67% for Tb, Er, Yb, Lu and Y. It reveals that the lighter REEs are almost all extracted, while only a fraction of the heavier REEs is extracted.

### 2.4.4 Data processing

A Spearman correlation matrix was performed on elemental data of surface sediments, using the R package "corrplot' (Wei et al., 2017) to compare major and trace element concentrations with $D_{90}$ sediment grain size and TOC content (data from Brice et al., 2025). Nonsignificant coefficients (p-value > 0.05) were not shown in the matrix. Before the multivariate statistical analysis, a centered log-ratio (clr) transformation was applied to the surface sediment data (Aitchison, 1982) using the R package "compositions" (van den Boogaart et al., 2023). K-means clustering analysis (R package "stats"; R Core Team, 2024) was performed on the chemical data to group samples with similar chemical composition within the CA. The quality of the cluster analysis was assessed using a silhouette plot ("factoextra" R package; Kassambara and Mundt, 2020), with negative values suggesting potentially incorrect or questionable assignments. Next, principal component analysis (PCA) was performed on the chemical data of surface sediments using the R package "FactoMineR" (Husson et al., 2016; Lê et al., 2008), with the goal of identifying elemental associations exhibiting similar patterns of relative variation. Geochemical distribution maps were generated using QGIS version 3.22.10.

The REEs were grouped into light REEs (LREE; La - Nd), medium REEs (MREE; Sm - Dy) and heavy REEs (HREE; Ho-Lu) and were represented by the element, La, Sm and Yb, respectively. The REE measurements were normalized to the Post-Archaean Australian Shale (PAAS; Pourmand et al., 2012) to facilitate interpration. Ce and Eu anomalies were calculated using the following equations (Barrat and Bayon, 2024; Barrat et al., 2023):

Eq.1 $$Ce/Ce^* = Ce_{PAAS} / (La_{PAAS} \times Pr_{PAAS})^{1/2}$$

Eq.2 $$Eu/Eu^* = Eu_{PAAS} / (Sm_{PAAS} \times Gd_{PAAS})^{1/2}$$

Tableau 8.

Canadian Sediment Quality Guidelines for the Protection of Aquatic Life (CCME, 1999). *Values from the Screening Quick Reference Table for Inorganics in Marine Sediments (Buchmann, 2008).

| Element | TEL (µg/g) | PEL (µg/g) |
|---|---|---|
| Cr | 52.3 | 160 |
| Ni* | 15.9 | 42.8 |
| Cu | 18.7 | 108 |
| Zn | 124 | 270 |
| As | 7.24 | 41.6 |
| Cd | 0.7 | 4.21 |
| Pb | 30.2 | 112 |

The Canadian Sediment Quality Guidelines (CSQGs) for the Protection of Aquatic Life (CCME, 1999) were used to provide an initial estimate of contaminant levels in the CA and their potential adverse effects on aquatic life. The guidelines establish two main levels: the threshold effect level (TEL), below which adverse effects are expected to occur only rarely, and the probable effect level (PEL), above which adverse effects are expected to occur frequently (Table 8). Since no guideline values for Ni are available in the CSQGs, National Oceanic and Atmospheric Administration (NOAA) guidelines were used instead (Buchmann, 2008). The CSQGs values represent total concentrations in surficial sediments (top 5 cm). While these guidelines help identify and assess potential contamination in sediments, they could be of limited value as they do not account for natural regional variations. To improve the assessment of metal contamination and associated ecological risks, pollution indices were applied on trace metal data, comparing current concentrations ($C_{sample}$) with pre-industrial background values ($C_{background}$). These indices include the enrichment factor (EF), the geo-accumulation index (Igeo), and the Ecological Risk Factor (ER). A regional geochemical background was established based on the composition of the basal sediment samples from 16 push cores across the CA. This background, estimated to predate industrial activities, was further subdivided into three local backgrounds according to the chemical clusters determined in Brice et al. (2025). To assess risk potential with ER a toxic response factor

(Tr) is assigned to each metal: 1 for Zn and Mn, 2 for V, 5 for Cu, Pb and Ni, 10 for As and 30 for Cd (Hakanson, 1980). Table 9 presents the calculations and classifications of these pollution indices. Because Cr background concentrations could not be determined, the PAAS value (Taylor and McLennan, 1985) was used as the background reference in the pollution index. It is important to note that both CSQGs and pollution indices do not account for environmental factors such as grain size, redox conditions, pH, bioavailability, or exposure time (MacDonald et al., 2000a).

Tableau 9.

Description of the pollution indices used in this study

| **Indice** | **Equation** | **Values** | **Sediment quality / Ecological risk** |
|---|---|---|---|
| EF (Sutherland, 2000) | $EF = \frac{(C_{metal}/C_{Sc})_{sample}}{(C_{metal}/C_{Sc})_{background}}$ | EF < 1 | No enrichment |
| | | EF = 1–3 | Minor enrichment |
| | | EF = 3–5 | Moderate enrichment |
| | | EF = 5–25 | Moderately severe enrichment |
| | | EF = 25–50 | Very severe enrichment |
| | | EF > 50 | Extremely severe enrichment |
| Igeo (Müller, 1969) | $Igeo = \log_2 * \frac{C_{sample}}{1.5 * C_{background}}$ | Igeo < 0 | Uncontaminated |
| | | 0 < Igeo < 1 | Uncontaminated to moderately contaminated |
| | | 1 < Igeo < 2 | Moderately contaminated |
| | | 2 < Igeo < 3 | Moderately to heavily contaminated |
| | | 3 < Igeo < 4 | Heavily contaminated |
| | | 4 < Igeo < 5 | Heavily to extremely contaminated |
| | | 5 > Igeo | Extremely contaminated |
| CF (Hakanson, 1980) | $CF = \frac{C_{sample}}{C_{background}}$ | CF < 1 | Low contamination |
| | | 1 < CF < 3 | Moderate contamination |
| | | 3 < CF < 6 | Considerable contamination |
| | | CF > 6 | Very high contamination |
| ER (Hakanson, 1980) | ER = Tr * CF<br><br>Tr = 1 (Mn, Zn), 2 (V), 5 (Co, Cu, Ni, Pb), 10 (As), 30 (Cd) | ER < 40 | Low risk |
| | | 40 < ER < 80 | Moderate risk |
| | | 80 < ER < 160 | Considerable risk |
| | | 160 < ER < 320 | High risk |
| | | ER > 320 | Very high risk |

## 2.5 RESULTS AND INTERPRETATIONS

### 2.5.1 Trace metals concentrations and spatial distribution

The chemical composition of surface sediments in the CA was highly variable. Trace metal concentration ranges are 5–96 µg/g for Cr, 1–39 for Co, 3–88 for Ni, 2–116 for Cu, 9–139 for Zn, 8–186 for V, 0.04–2 for Se, 0.8–60 for As, 0.01–0.44 for Cd and 2–38 for Pb (Fig. 22). Low trace metal concentrations were observed in the central CA channels and straits (e.g., M'Clintock Channel, Gulf of Boothia, Lancaster Sound) and in Nares Strait. The fjords of Baffin Island, Frobisher Bay and the Queen Maud Gulf (QMG) generally recorded low trace metal concentrations, but also the highest concentrations of REEs. The QMG, however, displayed higher Cr and Zn concentrations (40–60 and 60–130 µg/g, respectively) than sites located close to Baffin Island. In contrast, the western CA region, encompassing the Canadian Beaufort Sea, Mackenzie shelf-slope, Banks Island shelf-slope and the Amundsen Gulf, exhibited the highest concentrations of several trace metals, including Zn, Ni, Cr, Pb, Cd, As, and Co. Near the NOW, in eastern CA, Se concentrations were the highest, along with elevated levels of Cu, As, and Cr.

Fe concentrations, ranging from 0.3 to 4 wt.%, present a similar pattern to that of trace metals, with the highest values observed in western CA and around the NOW. However, a distinctly different trend is observed for Mn (68–11500 µg/g), Mo (0–26 µg/g) and Sb (0–2.7 µg/g). These elements generally exhibit low concentrations across the CA, with maximum values of approximately 2000 µg/g for Mn, 5.5 µg/g for Mo, and 0.9 µg/g for Sb. The highest concentrations are predominantly located in northern Davis Strait and, most notably, in Amundsen Gulf (Fig. 22).

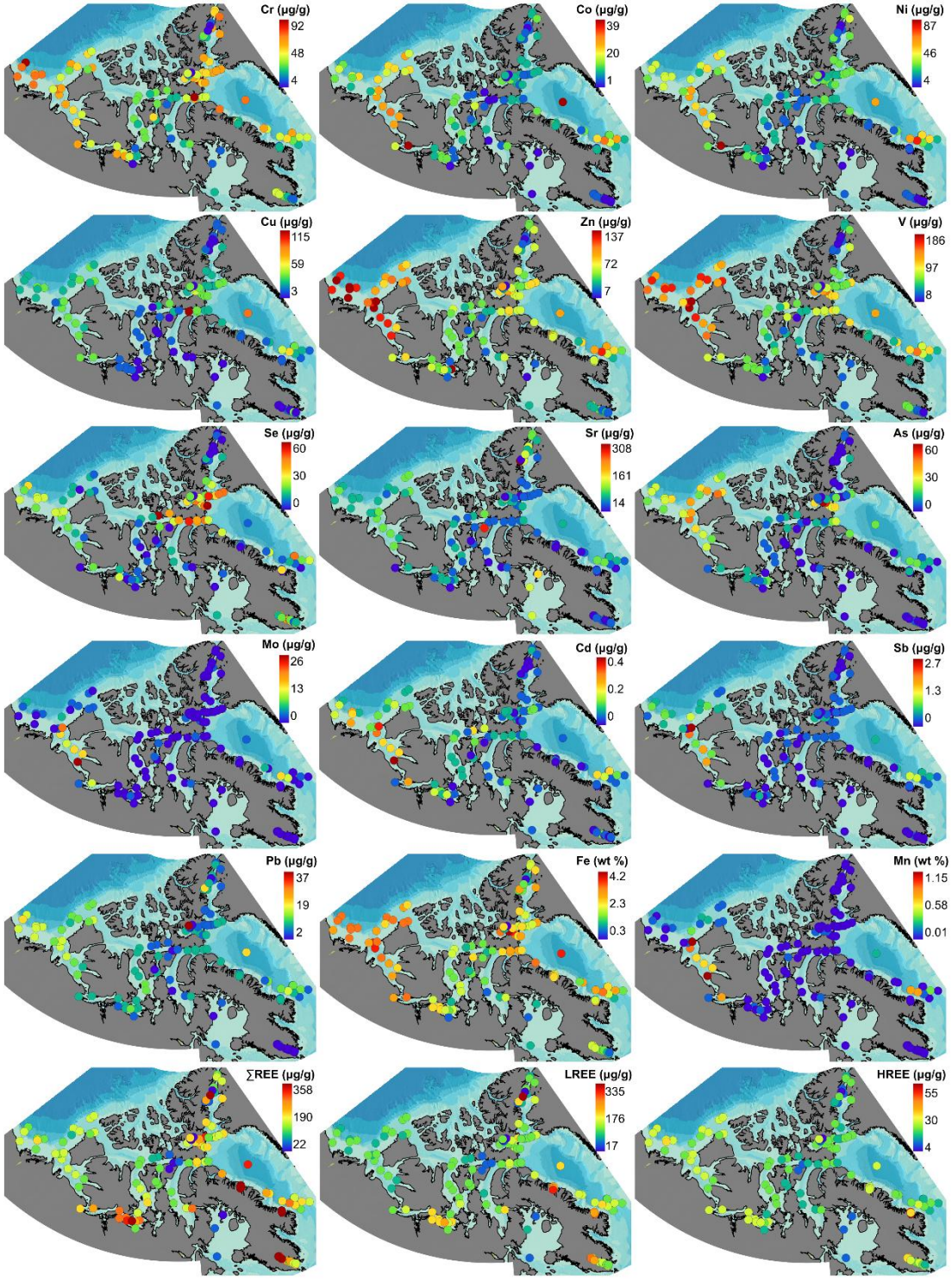


Figure 22. Maps presenting the trace metal concentrations and the distribution in the CA sediments.

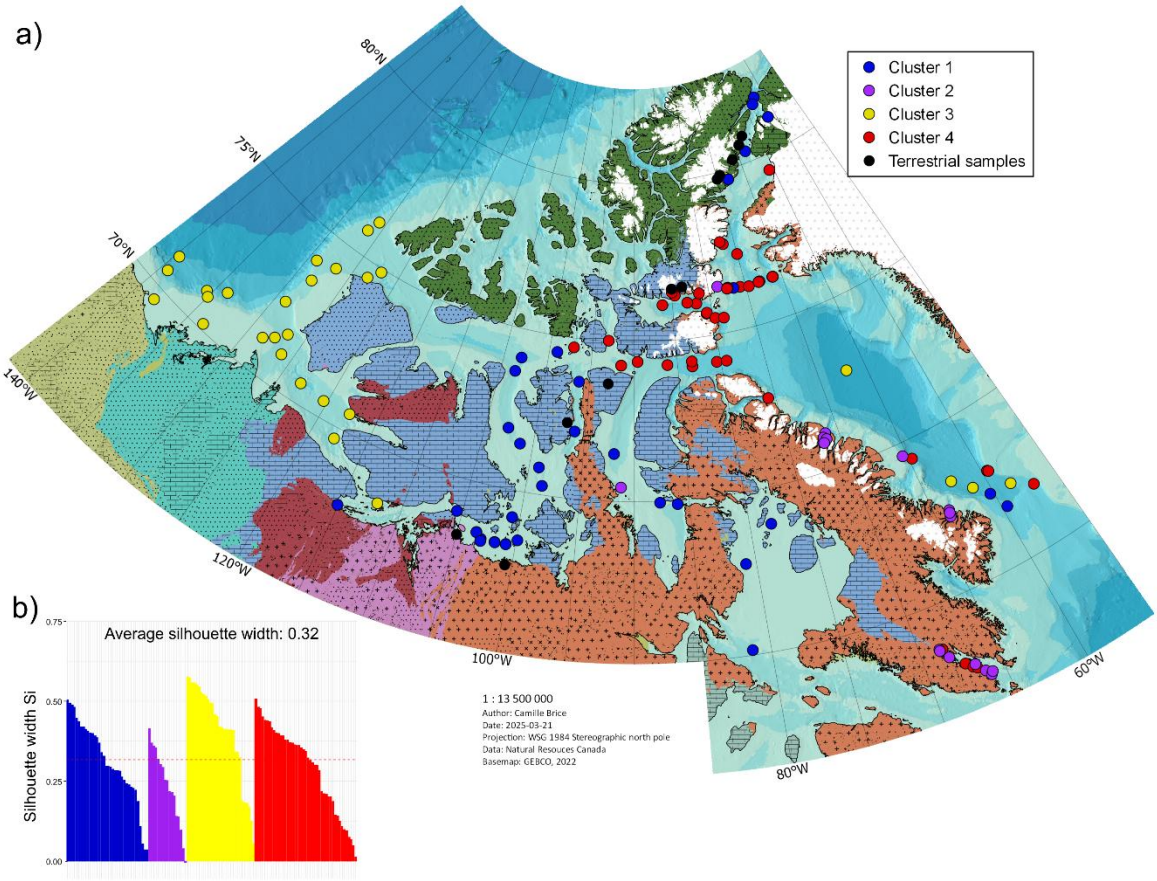


Figure 23. a) Map presenting the location of the clusters. a) Silhouette plot of the K-means clustering analysis applied of marine surface sediments.

K-means cluster analysis indicates that the dataset can be subdivided into four main clusters, regrouping 36, 17, 30 and 45 samples per cluster (Fig. 23). The spatial distribution of these clusters aligns closely with the sedimentary provinces previously described in Brice et al. (2025). Central CA straits and channels, and Nares Strait belong to cluster 1, while sites along the Baffin Island coast are associated with cluster 2. Cluster 3 is located in the Mackenzie/Beaufort Shelf and Amundsen Gulf region, whereas cluster 4 includes sites in Jones and Lancaster Sounds, as well as southern Smith Sound. PCA analysis performed on trace elements and TOC content revealed that the first two principal components (PC) explain 66% of the total variance (Fig. 24). Note that Mn was excluded from the PCA due to its dominant influence on the overall geochemical variability. As shown in the biplot, PC1 (46% of the total variance) highlights a clear opposition between trace metals and REEs. All metals

and TOC are located on the negative side of PC1, whereas all REEs and Th are associated with a positive PC1 scores. Grain size ($D_{90}$), represented by the size of the individual dots in the biplot, seems to be associated with a positive PC1 scores. The PC2, explaining 21% of the total variance, primarily reflects the variability of the trace metals. Se exhibits the strongest negative loading, followed by TOC, Cr and Cu. Most remaining trace metals are positioned on the positive side of PC2, while As and REEs remain unaffected by this component. PC scores reveal a clear spatial pattern (Fig. 30), with clusters distinctly separated across the biplot quadrants. The first two clusters are located on the positive side of PC1, with the cluster 1 in the positive PC2 quadrant. The other two clusters are more influenced by PC2, each positioned on opposite sides of this axis.

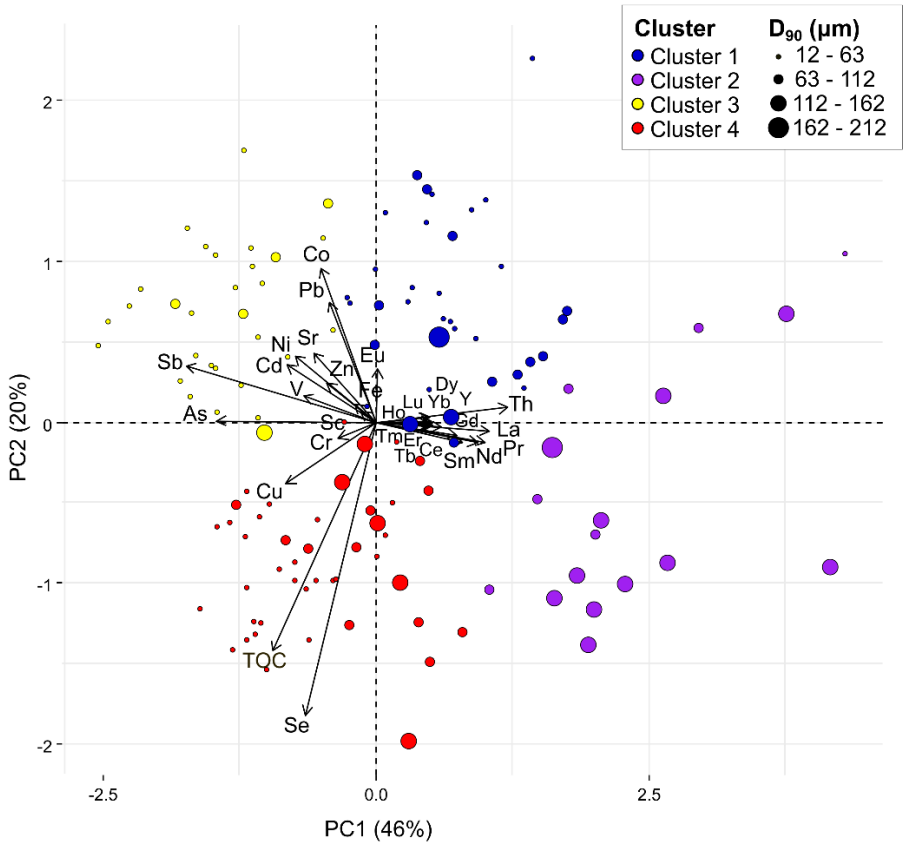


Figure 24. Principal component analysis applied on the marine surface sediments. Size of the individuals represents their associated grain size ($D_{90}$) composition.

### 2.5.2 REE distribution and pattern

The total REE content (ΣREE) ranges from 19 to 358 µg/g (Fig. 22). The lowest concentrations are observed in terrestrial samples and marine samples located on Ellesmere Island and in its fjords, respectively. In the marine environment, Lancaster Sound and Foxe Basin also exhibit among the lowest levels. Relatively low ΣREE (~90–190 µg/g) are observed in the western CA region, as well as in the central channels and straits, Nares Strait, and the NOW region. The highest concentrations are mainly found in the cluster 2 (QMG, Baffin Island bay and fjords), but interestingly also in terrestrial samples from Ellesmere Island. LREE concentrations, ranging from 17 to 335 µg/g, follow a similar distribution pattern as ΣREE. HREE concentrations (4–55 µg/g) show a slightly different spatial pattern, with highest concentrations in the Qikiqtarjuaq area and similar high content in the western CA region, Frobisher Bay and QMG.

The PAAS-normalized REE pattern of surface sediments of the CA generally show an enrichment in LREE, but with notable differences between the clusters (Fig. 25). Clusters 1 and 4 exhibit similar patterns with an LREE enrichment and no significant anomalies. Cluster 2 is characterized by a stronger LREE enrichment, along with pronounced negative Ce and Eu anomalies. More precisely, the fjords of Baffin Island exhibit significant negative Ce (0.5) and varying negative Eu (0.4-0.8) anomalies, whereas Frobisher Bay exhibits strong negative Eu anomalies (0.5), but no Ce anomaly (Fig. 31). Finally, cluster 3 displays enrichment in MREE and a positive Eu anomaly (1.2).

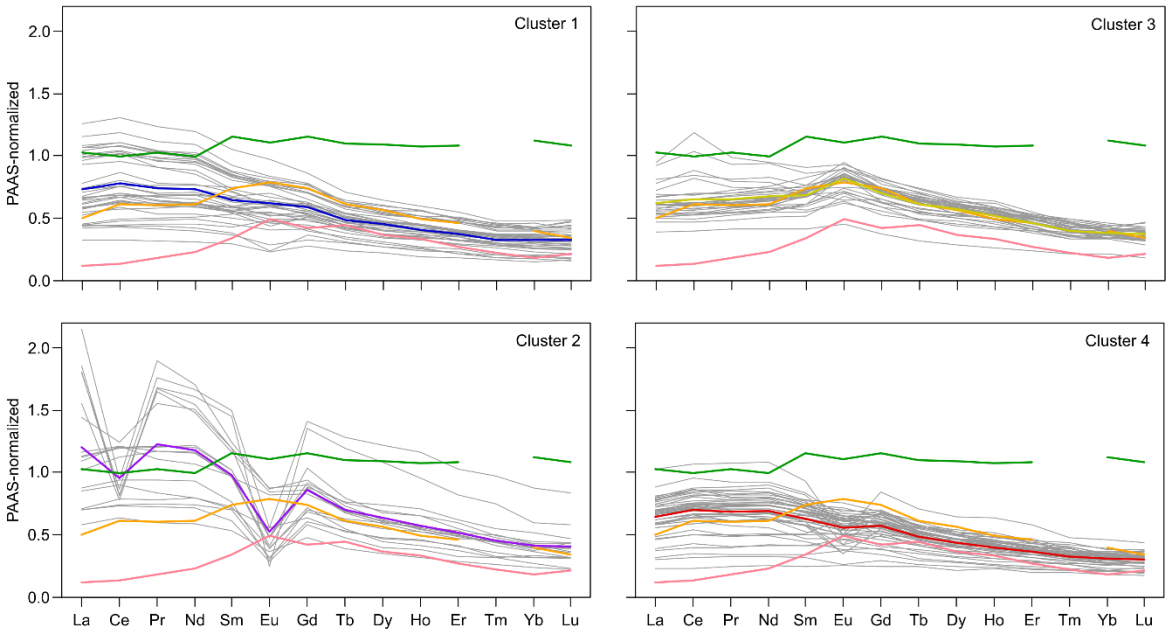


Figure 25. PAAS-normalized REE pattern of the marine surface sediments subdivided by clusters. Patterns in blue, purple, yellow and red represent the average of the associated cluster. The pattern in green is the average detrital silt pattern from (Freslon et al., 2014), the pattern in orange is the average organic matter pattern from (Bayon et al., 2015) and the pattern in pink is the average pattern from the Mackenzie Region (Bossé-Demers et al., 2025).

### 2.5.3 Sediment quality and pollution assessment

Trace metal concentrations were compared with the TEL and the PEL (Fig. 26), except for Co and V, which do not have guidelines. Zn, Cd and Pb concentrations are mostly or entirely below the TEL, indicating no risk of adverse biological effects. Cr content presents a normal distribution roughly centered just below the TEL, with no samples exceeding the PEL. Since third of the samples have concentrations above the TEL, adverse effects are possible, but the overall risk remains low. However, a few sediment samples exceed the PEL for Ni (n=21), Cu (n=1), and As (n=5). All sediments from Amundsen Gulf and half of those from the Canadian Beaufort Sea exceed the PEL for Ni, as well as most of the samples located north of Davis Strait (Fig. 22). This suggests probable risks of adverse biological effects in

these areas. The only sample exceeding the PEL for Cu is located in central Lancaster Sound. For As, the samples close to Banks Island and two samples in Jones Sound surpass the PEL.

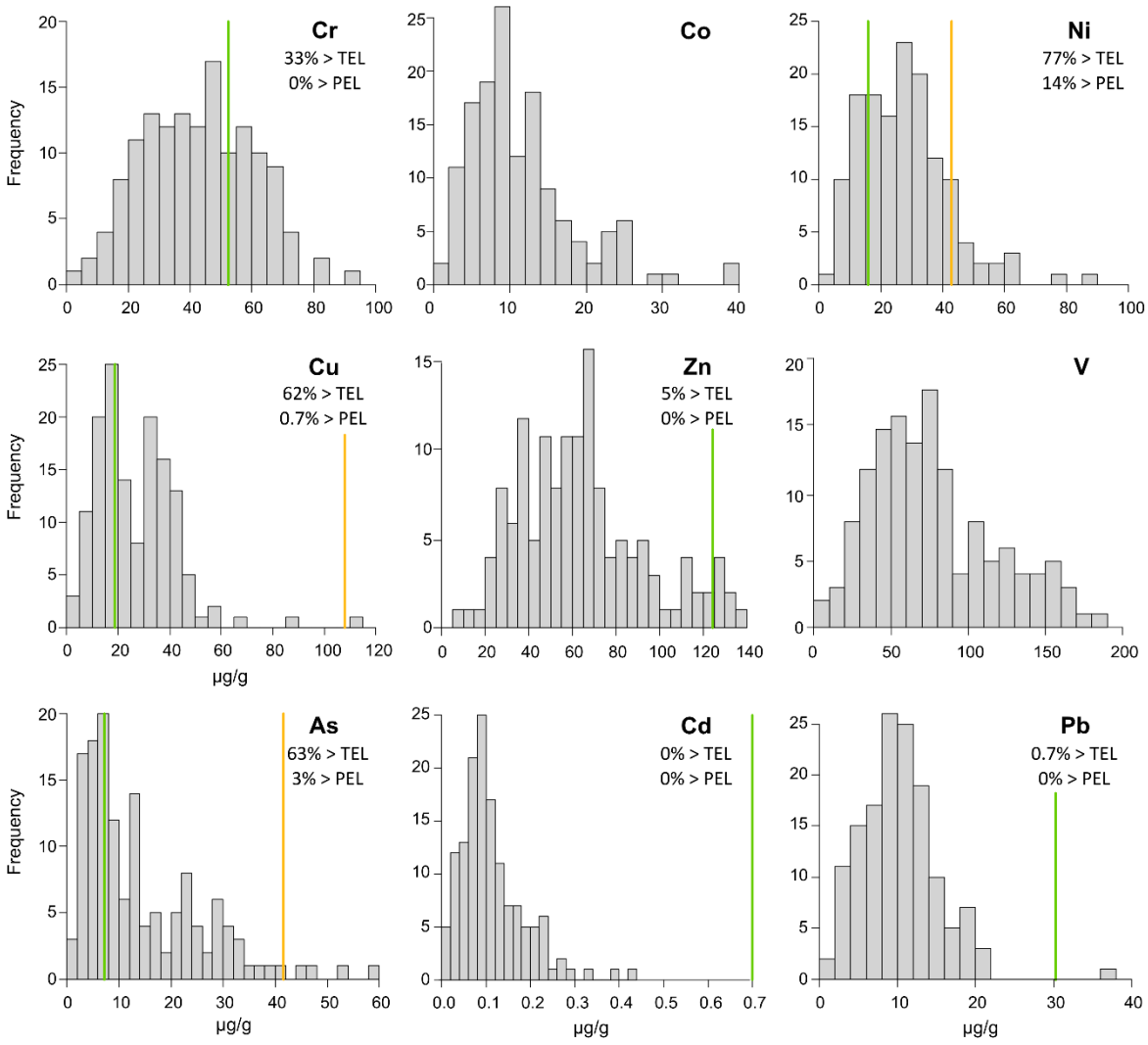


Figure 26. Barplots presenting trace metal concentrations in sampled sediments. Green lines represent the TEL values and orange lines represent the PEL values shown in Table 8.

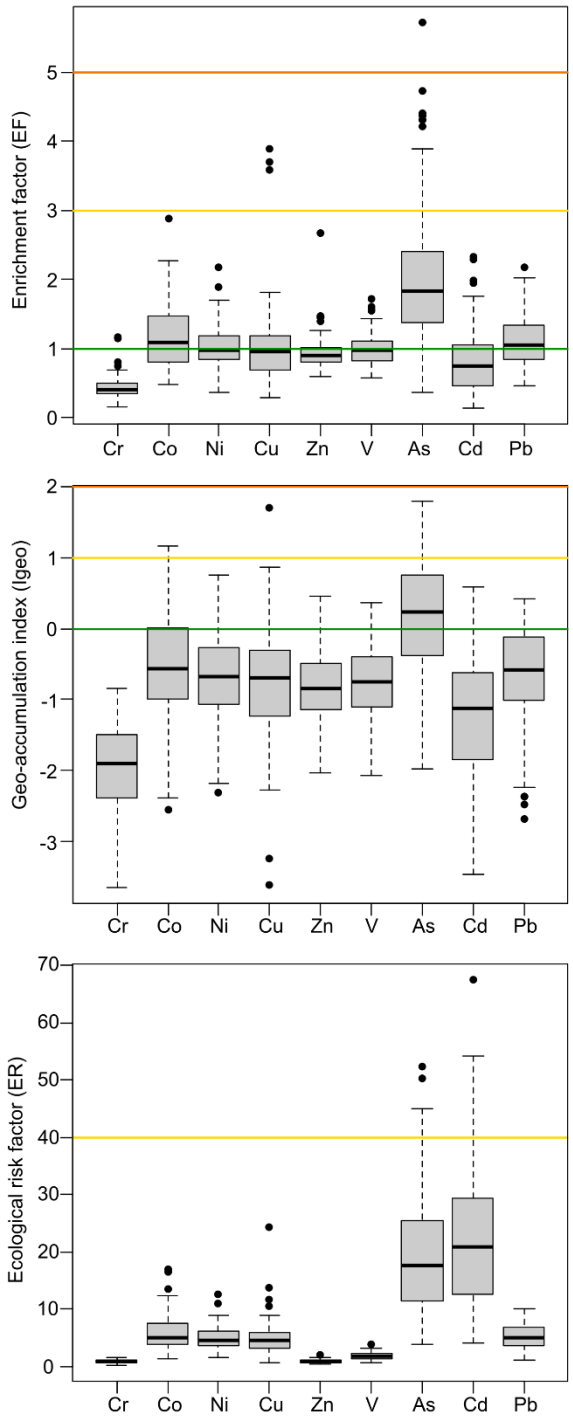


Figure 27. Boxplots of the three pollution indices used in this study. Green lines refer to the limit for "No enrichment" for the EF, "Uncontaminated" for the Igeo. Yellow lines refer to "Minor enrichment" and "Uncontaminated to moderately contaminated" and "Low risk" for the ER. Orange lines refer to "Moderate enrichment" and "Moderately contaminated".

EF results indicate no to minor enrichment for most metals, except for a few samples showing Cu enrichment and several samples exhibiting As enrichment (Fig. 27). Isolated samples from the coast of Banks, Victoria, Ellesmere and Baffin Islands display moderate As enrichment. In addition, two samples from Jones Sound and four from Coronation Gulf show As enrichment with one sample in Coronation Gulf reaching a moderately severe enrichment. Using Igeo, moderate contamination is observed in three samples for Co (Victoria Island coast and central Baffin Bay) and in one sample for Cu (Lancaster Sound). Multiple samples along Banks Island show moderate As contamination, as well as some in Lancaster Sound, two in Jones Sound, two in Nares Strait, and one in Coronation Gulf. No significant ecological risk was identified using ERI for most metals, except for Cd and As, which presented values above 40. Moderate risk was mainly observed in Amundsen Gulf and Lancaster Sound for Cd, while two isolated samples in the QMG and Canadian Beaufort Sea, and two samples in Jones Sound showed moderate risk for As.

## 2.6 DISCUSSION

### 2.6.1 Metal distribution and controlling factors

The four K-means clusters representing the distribution of extractable trace metal and REE concentrations in the sediment of the CA region closely align with the four sedimentary provinces previously defined based on total concentrations of major and selected trace elements (Brice et al., 2025). Our data highlight that lithologies remain the main controlling factor for the extractable fractions.

Trace metal concentrations are low in central CA and Nares Strait compared to the rest of the CA (Cluster 1; Fig. 22 & 24). The Ca-Mg-rich sediments composing this cluster are associated with detrital carbonates, a mineral phase that is not a major carrier of metals (e.g., Tribovillard et al., 2006). Additionally, the surrounding limestone and dolostone formations from the Arctic Platform are generally metal poor (Bédard et al., 2016).

The cluster 2 also presents low concentrations in trace metals, but high levels in REEs. The highest ΣREE are observed in the fjords of Baffin Island, in Frobisher Bay, and in the QMG, where sediments are supplied by the surrounding REE-rich Canadian Shield rocks (e.g., Lafrenière et al., 2023). LREE concentrations are particularly high compared to the rest of the CA, whereas HREE concentrations exhibit comparable values with other regions such as the Beaufort Sea Shelf. The LREE enrichment observed in cluster 2 reflects well the signature of the surrounding igneous/metamorphic rocks, which was observed by Grenier et al. (2022) in dissolved REEs in rivers of the Canadian Arctic Archipelago. Significant concentrations of Fe, Zn and Cr occur in some samples, likely deriving from mafic to ultramafic intrusions on Baffin Island (Liikane et al., 2015). Although mafic lithologies are frequently exposed in the area, the coarse nature of the sediments and their quartz- and feldspar-rich composition (Andrews et al., 2018) may limit metal scavenging.

High trace metal levels characterize the cluster 3. This region is strongly influenced by the Mackenzie River inputs, which provide fine-grained sediment composed of clay minerals, metallic oxides, and terrestrial organic matter, as well as dissolved and particulate trace metals (Bossé-Demers et al., 2025; Gamboa et al., 2017; Vonk et al., 2015; Wagemann et al., 1977). The cluster is thus spatially influenced by the Mackenzie River plume, which is propelled to the east by the coastal currents (Fig. 21a), and can be roughly separated into three zones. The Mackenzie Shelf, close to the river mouth, records the highest content Zn, V, Pb and Cr, while the Amundsen Gulf has the highest content of Ni, Co, Cd, Mo, and Sb (Fig. 22). Finally, the west Banks Island Shelf has among the highest As content as well as high V concentrations. Brice et al. (2025) concluded that trace metals were delivered to the seafloor primarily through adsorption onto organic matter, metallic oxides and aluminosilicates. Consistent with this, the present study found that high trace metal concentrations are mainly associated with easily mobilizable phases, such as amorphous authigenic metallic oxyhydroxides and labile organic matter, highlighting the role of reactive phases in trace metal accumulation in the CA. In cluster 3, the correlation plot reveals the association of TOC with Cr, Zn, V and Pb, while Mn is highly correlated with Co, Ni, Cu and Sb and Fe is correlated with Zn, V, As and Pb (Fig. 28). Given the distribution of the

elements, Zn, V, Pb and Cr seem to settle relatively rapidly on the shelf with terrestrial organic matter and detrital Fe oxides. Cr is also frequently derived and transported by terrigenous material inputs (Tribovillard et al., 2006). Highlighted by its correlation with Sc, Cr distribution seems indeed brought to the seafloor by the clastic fraction. The other metals are associated with Fe and Mn cycles and are most probably remobilized and entrained by the surface currents.

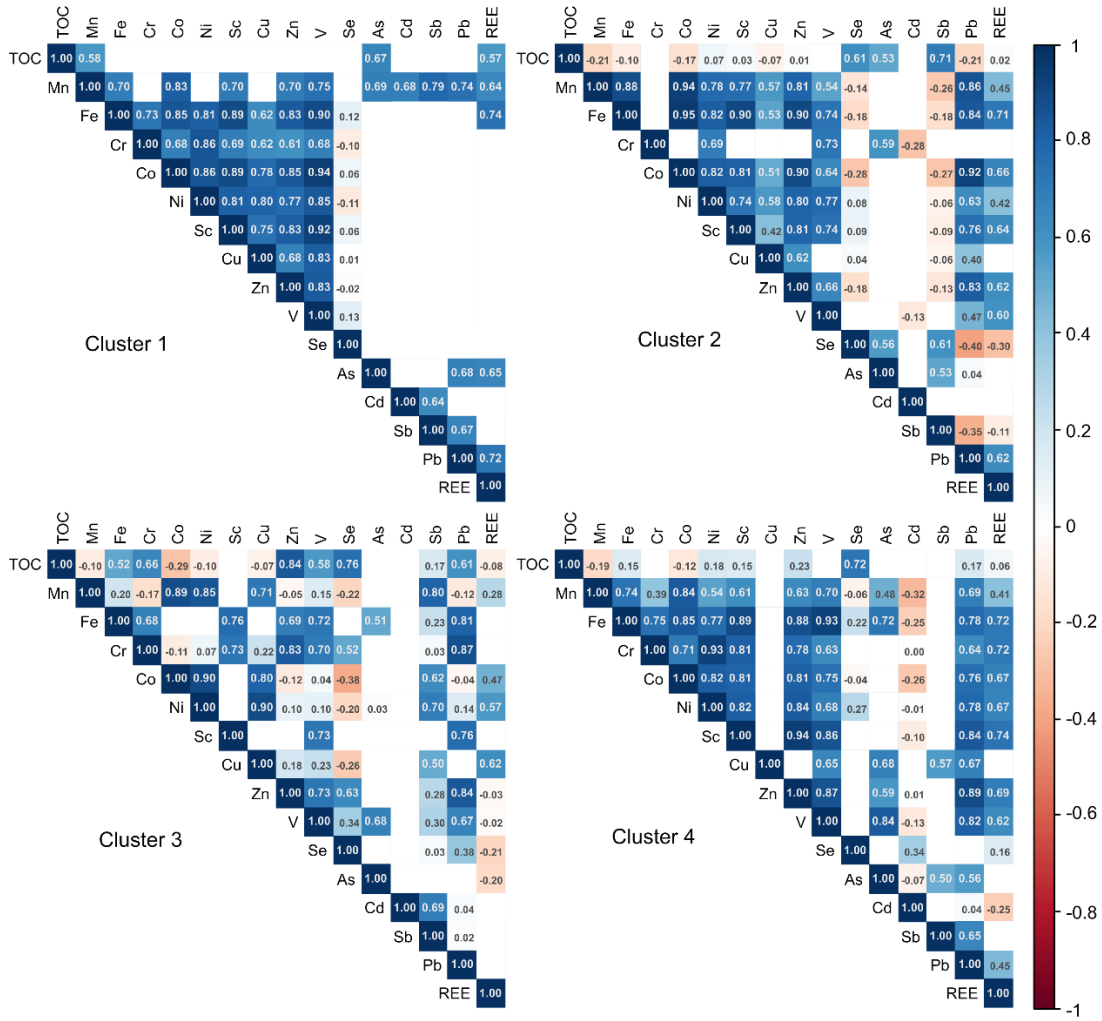


Figure 28. Spearman correlation plots of the marine samples subdivided into the four chemical clusters.

Strong surface enrichment of Mn is observed in Amundsen Gulf (Fig. 22) and is attributed to diagenetic processes that reduce, remobilize, and reprecipitate Mn farther from the Mackenzie River, where deeper oxygen penetration in sediments allowed authigenic Mn oxyhydroxide formation (Brice et al., 2025; Gamboa et al., 2017; Macdonald and Gobeil, 2012). Authigenic accumulation of Ni, Co, and particularly Mo and Sb seems thus driven by Mn behavior. Cd, which presents high values in Amundsen Gulf and Mackenzie Shelf, shows no correlation with any major host phases. This suggests that Cd is controlled by a mix of factors, including association with organic matter and oxides. Along the Banks Island coast, metal concentrations remain high (V > 100 μg/g; Zn > 75 μg/g; Cr > 34 μg/g), but it stands out for the As concentrations (30−45 μg/g). Also observed in the Canadian Beaufort Shelf by Trefry and Neff (2019), such surface enrichment is likely due to diagenetic processes associated with Mn and Fe oxides. The authors associate the high As content with the ferromanganese crust found in the area (Kuzyk et al., 2017; Macdonald and Gobeil, 2012). In our area, high Fe content confirms the co-enrichment of As in surface sediments with amorphous Fe oxyhydroxides, which are readily extractable (Fig. 22).

The cluster 4 is mainly defined by the TOC content, but also by the metals Se and Cu, and to a lesser extent Cr and As (Fig. 24). These trace metals are all used as micronutrients and are thus taken up by the phytoplankton in the photic zone (Duncan et al., 2015; Glabonjat et al., 2021). In the NOW area, the phytoplankton biomass is substantial (Klein et al., 2002), and upon the death of the organisms, scavenging of metals to the sediments by organic matter can be very high (Hargrave et al., 2002). In the sediments, remineralization of the biomass releases the metals, which can diffuse upward to the water or be captured by other phases like Fe oxyhydroxides (Rico et al., 2023) or sulfides, depending on the redox conditions in the sediments. Se presents a strong positive correlation with TOC (Fig. 28), suggesting that it remains linked to organic matter. The correlation of As and Cr with Fe indicates that they are likely captured by Fe-oxides/sulfides in this region. Terrigenous inputs from glacial erosion might also contribute to high As and Cr values found in this cluster.

### 2.6.2 REE spatial distribution

Marine sediment PAAS-normalized REE patterns are generally enriched in LREE, because of preferential scavenging of LREEs over HREEs in seawater (Sholkovitz et al., 1994). This general pattern is observed in most samples. However, the REE distribution across the CA and the observed patterns also appears to be strongly influenced by the underlying bedrock lithology. The highest concentrations of ΣREE and the strongest LREE enrichments (Fig. 29a), found in cluster 2, reflect the geochemical signatures of Precambrian igneous and metamorphic rocks that outcrop in Baffin Island (Fig. 21b). In contrast, the western CA, where younger Cenozoic to Paleozoic sedimentary rocks are prevalent, shows lower ΣREE contents. The lowest ΣREE concentrations are found in areas largely influenced by the Paleozoic carbonate rocks (Fig. 21b). Grenier et al. (2022) observed similar concentration variations and lanthanide profile in rivers are influenced by the Canadian Shield and carbonate rocks. The lithogenic control of REEs in the CA is also confirmed by the strong relationship of La (i.e., LREEs) versus Th present in the whole dataset (Fig. 29b). This relationship was also observed in sedimentary rocks in Greenland and Australia and was attributed to similar sedimentary behavior directly reflecting the Upper Continental Crust (UCC; McLennan et al., 1980). A ratio of La/Th= 2.8 and 3.6 was calculated for post-Archean and Archean sedimentary rocks, respectively (McLennan, 2001; McLennan et al., 1980), while a median ratio of 6.1 was calculated in our dataset. The strong correlation indicates that both LREEs and Th can be found in the same extractable phases, but the higher La/Th ratio reveals that a fraction of Th is in refractory phases. Relatively good correlations of La versus extractable Fe and total Al (Brice et al., 2025) in clusters 1, 2 and 4 (Fig. 32) suggests that LREEs are associated with Fe–Mn oxides and clays. The weak Th–Yb correlation likely reflects the dominance of refractory heavy minerals as the main hosting phase for HREEs.

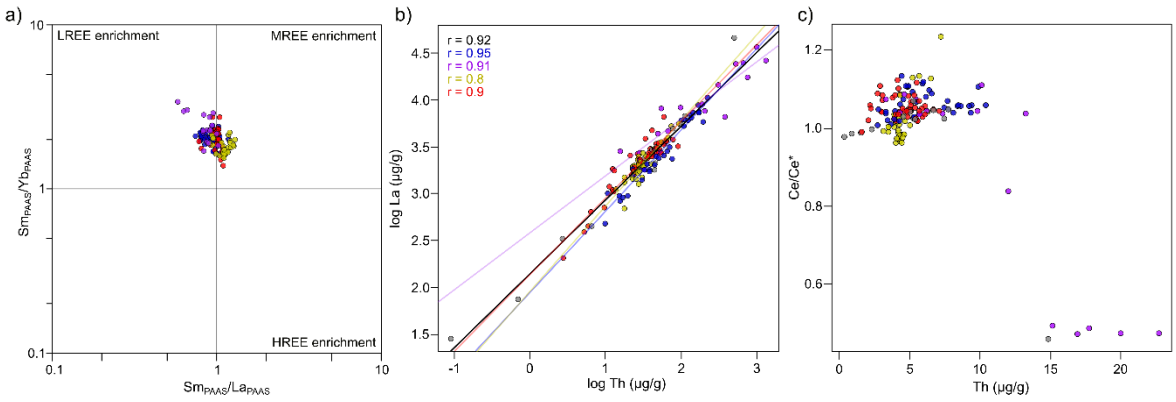


Figure 29. a) PAAS normalized plots of Sm/Yb versus Sm/La for marine sediments samples studied here. b) Relationship between log La concentration and log Th concentrations. c) Relationship between Ce anomalies and Th concentrations. Colors of the dots, the trendlines and the r-Spearman correlation values represent the associated clusters (blue for cluster 1, purple for cluster 2, yellow for cluster 3 and red for cluster 4). Black trendline and r value represent the average of all samples.

The distribution and pattern of REEs can also reveal information about their carrier phases across the region. Each type of carrier has a unique pattern, which can be identified in the samples depending on which phase is most dominant. The average pattern in western CA (cluster 3) present a MREE enrichment (Fig. 25 & 29a) that is very similar to the sedimentary organic matter pattern (Freslon et al., 2014), suggesting that the REEs in the region are bound to organic matter. However, the absence of correlation between REEs and TOC in cluster 3 (Fig. 28) highlights that the patterns are attributed to other processes. Bossé-Demers et al. (2025) established a leached Mackenzie River signature (Fig. 25), characterized by a significant MREE enrichment and consistent with REEs-metal oxides-humic complexes delivered by the river. The preferential scavenging of MREEs by leachable Fe-Mn (oxyhydr)oxides and organic matter likely accounts for this signature (Gutjahr et al., 2007; Lim et al., 2014). In cluster 2, because most sediments of this region are likely composed of refractory detrital components that are not extracted by the acid-extractable digestion, the concentrations and the patterns reflect only a fraction of the overall REE composition. The relatively strong LREE enrichment and negative Eu anomaly may result from the fact that the hosting phases of LREEs are efficiently extracted, whereas those of HREEs and Eu are not mobilized by our partial acid-digestion method. Indeed, LREEs are preferentially bound

to extractable phases such as metallic oxides and organic matter, while HREEs are mostly bound to zircons and Eu is typically an indicator of plagioclase (Lim et al., 2014; Sholkovitz, 1990). Both zircon and plagioclase are characteristic refractory minerals of this sedimentary province (Andrews et al., 2018). $LREE_{PAAS}$ exhibit values close to 1, thus similar to the PAAS and also to detrital silt from rivers (Bayon et al., 2015), suggesting that they are likely all extracted and are associated with detrital extractable phases such as preformed Fe-oxides (Fig. 28 & 32). This difference in partitioning can lead to fractionation during extraction, enhancing LREE enrichment.

Oxic conditions generally prevail in the CA bottom waters, consequently positive Ce anomalies are expected in sediments, because dissolved $Ce^{3+}$ oxidizes to $Ce^{4+}$, and tends to coprecipitate or be adsorbed onto Mn (oxyhydr)oxides (Sholkovitz et al., 1994; Ye et al., 2019). Positive anomalies (1.1-1.2) are indeed observed in deep-water samples of the Baffin Bay, where elevated Mn concentrations result from high scavenging (Colombo et al., 2020). In western CA, Ce anomalies range from 0.96 near to the Mackenzie River to 1.04 in the Amundsen Gulf and along the coasts of Banks Island (Fig. 31). The Mn-rich sediments in these regions suggest that scavenging by Mn (oxyhydr)oxides has barely any impact. The Ce signature is thus likely derived from the inputs of the Mackenzie River, such as shales within the watershed that typically exhibit a slight negative Ce anomaly (Fraser et al., 2012; Fraser and Hutchison, 2017; Hutchison, 2018; Strauss et al., 2020). As the influence of the Mackenzie River on the shelf diminishes with increasing distance from the delta (Bossé-Demers et al., 2025), Ce/Ce* becomes positive, probably due to the increasing influence of redox processes. In eastern CA, the strong negative Ce/Ce* observed in Baffin Island fjords are probably also inherited from the source rocks rather than caused by redox processes. Indeed, Ce/Ce* versus Th concentrations (Fig. 29c) shows that negative anomalies are associated with high Th concentrations.

### 2.6.3 State of pollution

Overall, extractable metal concentrations in the CA sediments fall within the natural range expected for the Arctic Ocean (Table 13; e.g., Budko et al., 2017; Budko et al., 2022; Cai et al., 2011; Campbell and Loring, 1980; Choudhary et al., 2020; Loring et al., 1998; Lu et al., 2013; Lu and Kang, 2018; Naidu et al., 2005; Trefry and Neff, 2019; Trefry et al., 2003; Zheng et al., 2022). However, several samples exceed the TEL values of the CSQG and NOAA guidelines for Cr, As, Ni, and Cu, indicating that these sediments may occasionally be associated with adverse biological effects (CCME, 1999). Furthermore, concentrations of Cu, As and Ni exceed the PEL in 27 sediment samples, suggesting that adverse effects are likely to occur frequently. It is important to note that the values in both the referenced studies and the CSQG and NOAA guidelines represent total concentrations, whereas our values reflect only extractable concentrations. As a result, total metal concentrations are likely higher, meaning that assessment based on SQGs may underestimate potential risks. Pollution indices, which are based solely on extractable concentrations, indicate moderate enrichment and/or contamination in As, Cu, and Co.

Only one sample, located in central Lancaster Sound, exhibits a Cu concentration above the PEL (115 μg/g; Fig. 22 & 28). However, this value has been classified as an outlier ($p < 0.05$) since it is inconsistent with both the surrounding data and the overall dataset. Given that this sample is an outlier, only two samples show moderate Cu enrichment, but no pollution was detected based on the Igeo index, and no values exceeded the PEL. This indicates that Cu concentrations do not pose an ecological risk. Mean and median Co concentrations in the CA are around 10 μg/g, which aligns well with the geochemical background values. Only two samples showed moderate pollution - one in Coronation Gulf and another in central Baffin Bay. In central Baffin Bay, Campbell and Loring (1980) also observed Co enrichment in deep central Baffin Bay muds compared to coastal and sound sediments. They concluded that the seafloor composition in deep Baffin Bay is more similar to the Atlantic Ocean deep-sea clays (Turekian and Imbrie, 1966) than to the CA shelf and coastal sediments. Indeed, overall high trace metal levels are observed in this sample, and to

a lesser degree, in samples near Davis Strait. Thus, when comparing deep Baffin Bay data with the regional background - established using shelf and coastal sediment data - pollution indices indicate higher-than-natural concentrations. In Coronation Gulf, a sample close to Victoria Island exhibits the highest content in Co (39 μg/g) and Ni (87 μg/g), which are three times the regional background values. Both Co and Ni are mainly delivered to sediments in association with Mn oxides, and to a lesser extent Fe-oxides (Audry et al., 2006; Stockdale et al., 2010). Indeed, throughout the CA, both trace metals show strong correlation with Mn and Fe, especially with Mn in cluster 3 (Fig. 28). In Coronation Gulf, which present high Fe-Mn concentrations, enhanced scavenging of Co and Ni by Fe-Mn oxides, coupled with surface enrichment during early diagenesis, are probably the main causes explaining the high values. In sediments, Co and Ni are mainly released to pore water during Mn oxides reductive dissolution and an important fraction undergo re-adsorption and/or re-precipitation with Mn oxides in the oxic zone, leading to surface enrichment (Heggie and Lewis, 1984; Meinhardt et al., 2016). The Co-Ni enrichment might also be favored by a source rich in these elements, such as the Franklin Igneous Province that comprises lithologies rich in trace metals (Beard et al., 2018; Bédard et al., 2016).

The majority of the samples present Ni concentrations above the TEL, and 21 exceeding the PEL. These higher concentrations are mainly found in the Mackenzie/Beaufort shelf, Amundsen Gulf and Davis Strait. In contrast, lower Ni levels have been reported in surficial sediments from the Russian and Norwegian Arctic (Budko et al., 2022; Choudhary et al., 2020; Holemann et al., 1999; Loring et al., 1998; Lu et al., 2013) and in the coastal Alaskan Beaufort Sea (Naidu et al., 2012; Trefry and Neff, 2019). However, similar Ni concentrations were measured in Baffin Bay by Campbell and Loring (1980). Higher Ni concentrations have been observed in deep waters of the Chukchi Sea (Lu and Kang, 2018; Wang et al., 2022; Zheng et al., 2022), where moderate ecological risk has been identified. The Ni concentrations measured in the CA are thus in agreement with the global Arctic baseline, which ranges from 17 to 49 μg/g (Gauthier et al., 2021). However, Lu and Kang (2018) reported that the labile Ni fractions account for ~40% of the total Ni in the Bering Strait sector, suggesting that our extractable concentrations might exceed global baseline

values. Nevertheless, when compared to the regional natural geochemical background, Ni extractable concentrations in surface sediments do not show enrichment or pollution (Fig. 26), highlighting natural Ni sources in the region.

More than half of the samples have As concentration above the TEL. However, with a median of 11 µg/g and a mean of 14 µg/g (Fig. 26), the values from this study are consistent with those reported for unpolluted sediments in other Arctic Ocean studies (Budko et al., 2022; Trefry and Neff, 2019; Trefry et al., 2003; Wang et al., 2022). In cluster 3, the affinity of As for Fe oxides leads to high deposition in the Mackenzie/Beaufort shelf and Amundsen Gulf, where three samples exceed the PEL. This is likely due to the natural surface enrichment during diagenesis in oxic conditions (Loring et al., 1998; Trefry and Neff, 2019). The release of As into pore water during the reductive dissolution of Fe oxides, followed by re-precipitation of Fe with co-associated As, can lead to the formation of a Fe–As enriched layer within the oxic zone (Trefry and Neff, 2019). This layer typically forms below the Mn oxide re-precipitation zone; however, this layer is not clearly observed along Banks Island. A shallower oxygen penetration depth compared to the Amundsen Gulf - where Mn enrichment is found - may promote Fe accumulation closer to the sediment surface. Although sediments along Banks Island exhibit natural As enrichment, the potential for biological effects remains high, as the measurements were derived from the labile fraction. Additionally, two samples from Jones Sound also exceed the PEL for As, with concentrations of 53 and 59 µg/g - the highest recorded in the dataset. These elevated values coincide with high Fe concentrations and relatively high V and TOC concentrations. Absorption and accumulation in phytoplankton and/or shuttling by Fe-(oxyhydr)oxides are hypothetical processes that can explain high deliveries of As to the sediments (Rico et al., 2023; Tribovillard et al., 2006). However, surface enrichment by diagenetic processes is not probable, as revealed by low Mn and Mo concentrations (Fig. 22). It is likely derived from a detrital input. As might be transported by glaciers meltwater draining Canadian Shield rocks surrounding eastern Jones Sound.

### 2.6.4 Ecotoxicological implications

Based on this study, surface metal concentrations in the CA are from natural sources and processes. However, climate change is expected to increase the risks associated with metal exposure in the Arctic due to geochemical changes in the environment (Macdonald et al., 2005). Reduced sea ice and rising temperatures impact oxygen levels in the water column and sediments, while the thawing of the permafrost affect the continental inputs to the Arctic Ocean (Biskaborn et al., 2019). An increase in material exported by rivers and coastal erosion, as well as an increase in reactive organic matter, Fe and trace elements, has already been observed and is expected to continue (O'Donnell et al., 2024; Skierszkan et al., 2024). Diagenetic reactions are affected by changing oxygen levels and organic matter inputs (Macdonald et al., 2015), and their modification can enable the remobilization of metals and affect their bioavailability and toxicity.

The Amundsen Gulf records the highest concentrations of Cd, Ni, Co, Mo, and Sb in our dataset (Fig. 22), making it a zone of interest. This surface enrichment is linked to high riverine inputs from the Mackenzie River and diagenetic Mn enrichment (Gamboa et al., 2017; Brice et al., 2025) and is thus sensitive to redox conditions. The Amundsen Gulf sedimentary dynamic is also influenced by small rivers from the mainland. An increase in permafrost thawing would most likely increase inputs of old reactive organic matter via these small rivers (Fouché et al., 2020), which could induce the reduction of Mn oxides closer to the surface and the release of associated metals. Labile Ni and Co present on the Amundsen Gulf seafloor, the most enriched area of the CA (Table 13), could be remobilized into the water column, making them readily accessible to benthic organisms. Although labile Cd concentrations remain below the TEL, significant flux to the water column through upward diffusion has been observed during early diagenesis (Gobeil et al., 1987). The dissolved Cd will contribute to the overall trace metals exposure to benthic organisms, mainly to invertebrates.

In sediments, As is closely associated with metallic oxides, particularly Fe-oxides (Chaillou et al., 2003; De Vitre et al., 1991; Tribovillard et al., 2006). Although adsorbed As is not generally considered readily accessible (Wang and Mulligan, 2006), changes in redox conditions, pH, bioturbation and microbial activity can lead to its mobilization. As observed with acid digestion, significant As levels were extracted along the Banks Island coast (Fig. 22). The As measured was most probably associated with authigenic amorphous Fe oxides, which are less stable than preformed Fe oxides derived from the Mackenzie River (Pierce and Moore, 1982). In addition to the release of As into interstitial waters due to oxide reduction, anaerobic conditions promote the reduction of arsenate ($As^{5+}$) to the more mobile arsenite ($As^{3+}$), as well as As methylation by microorganisms, leading to the formation of toxic and bio-accumulative organic species (Bright et al., 1996). In Jones Sound, the increasing rate of glacier melt, which is already ongoing for Belcher Glacier (Wychen et al., 2020), might result in increase in As inputs to the water column, resulting in a possible increased uptake by the phytoplankton as well as an accumulation in marine sediments.

## 2.7 CONCLUSION

A spatial geochemical survey was conducted across the CA to provide new data on seafloor sediment composition. Concentrations of trace metals and REEs, measured by partial acid digestion, revealed a spatial distribution exhibiting a west-east trend influenced by sourced bedrock, redox conditions, river inputs, ocean current and primary productivity. Four clusters were determined to describe the spatial variability: central CA (central channels and straits, and Nares Strait), eastern CA (Baffin Island coast), western CA (the Mackenzie/Beaufort Shelf and the Amundsen Gulf) and northeastern CA (the NOW region).

The Canadian Beaufort Sea and the Amundsen Gulf record the highest concentrations of trace metals in the CA. The discharge from the Mackenzie River is the principal source of these elements, but their distribution is then influenced by the metal's affinity with the carrier phases, i.e. organic matter and Fe-Mn oxides, and redox conditions. V, Zn, Pb and Cr are

rapidly scavenged onto the sediment by organic matter, whereas As, Ni, Co and Cd are mobilized and transported by coastal currents further away from the river. High As concentrations are observed in the Canadian Beaufort Sea, east of Banks Island, most likely associated with detrital and authigenic Fe oxides. The Amundsen Gulf has high concentrations of Ni, Co and Cd, and their association to Mn oxides seems to be the most plausible explanation.

The REE concentration of the CA sediments are primarily controlled by the bedrock. LREE are mainly found bound to metallic oxides that are acid-extractable while HREE seems associated with refractory phases. In eastern CA, the Precambrian lithologies of the Canadian Shield transfer their high concentrations, LREE-enriched signature and Ce negative anomaly to the sediments close to the coast. In Western CA, the sediment samples exhibit a notable MREE enrichment, characteristic of the leachable geochemical signature of the Mackenzie River. The rest of the CA are generally characterized by a small LREE enrichment and a small positive Ce anomaly reflecting typical marine sediment pattern.

No major ecological risks were identified in this study. The trace metals baseline of surface sediments exhibits high regional variability, leading to values that occasionally exceed sediment quality criteria. However, these values remain within the range of natural sources. Only Jones Sound presented two samples with high As concentrations exceeding the PEL, which were identified as polluted and enriched. Nevertheless, monitoring across the region should be continued to assess the direct and indirect impacts of human activities on the ecotoxicological risk of trace metals in CA marine sediments.

Overall, the findings from this study provide new insights into the sources and pathways of metals and highlight areas that may be particularly sensitive to contamination under future climate disturbances. These data will support policymakers in conducting environmental risk assessments and developing evidence-based regulatory frameworks for shipping and industrial activities within the CA. However, the present dataset represents only a snapshot of current metal concentrations in CA sediments. To strengthen long-term environmental protection and mitigation strategies, we recommend the continued

implementation of sustained monitoring programs in collaboration with local communities. Additionally, a more complete understanding of the geochemical behavior of metals in the Arctic marine environment will require future work on sediment core profiles, including sediment and pore water chemistry. A comprehensive ecological risk assessment should also incorporate trace metal partitioning in sediments and measurements of metal accumulation in benthic organisms

## 2.8 ACKNOWLEDGMENTS

The sediment samples analyzed in this study were collected aboard the Canadian research icebreaker CCGS Amundsen, with logistical and technical support provided by Amundsen Science. This research infrastructure is funded through the Canada Foundation for Innovation's Major Science Initiatives Fund. We acknowledge the captains, officers, crews, and scientific participants of the 2016, 2017, 2018, 2019, and 2022 ArcticNet expeditions onboard CCGS Amundsen for the recovery of the sediment samples used in this study. We thank Mathieu Babin (ISMER-UQAR) and Mathieu Moingt (UQAM) for providing technical support in the laboratory. This study was supported by ArcticNet (ArcticSeafloor project), EcotoQ (Programme d'accès aux infrastructures et formation), Québec-Océan, Geotop, the Northern Scientific Training Program (NSTP), the Fonds de recherche du Québec - Nature et technologies (FRQ) and the Natural Sciences and Engineering Research Council of Canada (NSERC) PhD scholarships provided to C. Brice, and NSERC Discovery Grants provided to J.-C. Montero-Serrano (RGPIN-2020-06600 and RGPNS-2020-06600). We thank Kelsey Koerner (ISMER-UQAR) for revising the English of the manuscript. Finally, we thank the two anonymous reviewers for their constructive feedback, which improved the quality of the manuscript, and Gui-Peng Yang (Ocean University of China) and Michel Boufadel (New Jersey Institute of Technology) for their editorial support.

## 2.9 REFERENCES


Aitchison, J. (1982). The Statistical Analysis of Compositional Data. *Journal of the Royal Statistical Society: Series B (Methodological)*, *44*(2), 139-160. https://doi.org/https://doi.org/10.1111/j.2517-6161.1982.tb01195.x

AMAP (1998). *AMAP Assessment Report: Arctic Pollution Issues.* Arctic Monitoring and Assessment Programme (AMAP), Oslo, Norway. xii+859 pp.

AMAP (2005). *AMAP Assessment 2002: Heavy Metals in the Arctic.* Arctic Monitoring and Assessment Programme (AMAP), Oslo, Norway. xvi + 265 pp.

AMAP (2011). *AMAP Assessment 2011: Mercury in the Arctic.* Arctic Monitoring and Assessment Programme (AMAP), Oslo, Norway. xiv + 193 pp.

AMAP (2018). *AMAP Assessment 2018: Biological Effects of Contaminants on Arctic Wildlife and Fish.* Arctic Monitoring and Assessment Programme (AMAP), Oslo, Norway. vii, 84.

AMAP (2021). *AMAP Assessment 2021: Mercury in the Arctic.* Arctic Monitoring and Assessment Programme (AMAP), Tromsø, Norway. 324 pp.

Andrews, J. T., Klein, A. J., Jenner, K. A., Jennings, A. E., & Campbell, C. (2018). The variability of Baffin Bay seafloor sediment mineralogy: the identification of discrete glacial sediment sources and application to Late Quaternary downcore analysis. *Canadian Journal of Earth Sciences*, *55*(6), 620-639. https://doi.org/10.1139/cjes-2017-0223

Audry, S., Blanc, G., Schäfer, J., Chaillou, G., & Robert, S. (2006). Early diagenesis of trace metals (Cd, Cu, Co, Ni, U, Mo, and V) in the freshwater reaches of a macrotidal estuary. *Geochimica et Cosmochimica Acta*, *70*(9), 2264-2282. https://doi.org/https://doi.org/10.1016/j.gca.2006.02.001

Barrat, J.-A., & Bayon, G. (2024). Practical guidelines for representing and interpreting rare earth abundances in environmental and biological studies. *Chemosphere*, *352*, 141487. https://doi.org/https://doi.org/10.1016/j.chemosphere.2024.141487

Barrat, J.-A., Bayon, G., & Lalonde, S. (2023). Calculation of cerium and lanthanum anomalies in geological and environmental samples. *Chemical Geology*, *615*, 121202. https://doi.org/https://doi.org/10.1016/j.chemgeo.2022.121202

Bayon, G., Toucanne, S., Skonieczny, C., André, L., Bermell, S., Cheron, S., Dennielou, B., Etoubleau, J., Freslon, N., Gauchery, T., Germain, Y., Jorry, S. J., Ménot, G., Monin, L., Ponzevera, E., Rouget, M. L., Tachikawa, K., & Barrat, J. A. (2015). Rare earth elements and neodymium isotopes in world river sediments revisited. *Geochimica et Cosmochimica Acta*, *170*, 17-38. https://doi.org/https://doi.org/10.1016/j.gca.2015.08.001

Beard, C. D., Scoates, J. S., Weis, D., Bédard, J. H., & Dell'Oro, T. A. (2018). Geochemistry and Origin of the Neoproterozoic Natkusiak Flood Basalts and Related Franklin Sills, Victoria Island, Arctic Canada. *Journal of Petrology*, *58*(11), 2191-2220. https://doi.org/10.1093/petrology/egy004

Bédard, J., Hayes, B., Hryciuk, M., Beard, C., Williamson, N., Dell'Oro, T., Rainbird, R., Prince, J., Baragar, W., Nabelek, P., Weis, D., Wing, B., Scoates, J., Naslund, H. R., Cousens, B., Williamson, M.-C., Hulbert, L.J., , Montjoie, R., Girard, É., Ernst, R., & Lissenberg, C. J. (2016). Geochemical database of Franklin sills, Natkusiak Basalts and Shaler Supergroup rocks, Victoria Island, Northwest Territories, and correlatives from Nunavut and the mainland. *Geological Survey of Canada*, *Open File 8009*(1). https://doi.org/doi:10.4095/297842

Belzile, C., Montero-Serrano, J.-C., 2022. Quantifying simulated fine sand fraction in muddy sediment using laser diffraction. *Canadian Journal of Earth Sciences 59*, 455-461.

Bidleman, T., Macdonald, R. W., & Stow, J. (2003). *Canadian Arctic Contaminants Report II: Sources, Occurence, Trends and Pathways in the Physicial Environment*. Ottawa, Canada: Department of Indian and Northen Affairs, Government of Canada

Biskaborn, B. K., Smith, S. L., Noetzli, J., Matthes, H., Vieira, G., Streletskiy, D. A., Schoeneich, P., Romanovsky, V. E., Lewkowicz, A. G., Abramov, A., Allard, M., Boike, J., Cable, W. L., Christiansen, H. H., Delaloye, R., Diekmann, B., Drozdov, D., Etzelmüller, B., Grosse, G., . . . Lantuit, H. (2019). Permafrost is warming at a global scale. *Nature Communications*, *10*(1), 264. https://doi.org/10.1038/s41467-018-08240-4

Bossé-Demers, T., Gobeil, C., Juhls, B., Lizotte, M., Fritz, M., Bröder, L., Matsuoka, A., Mareque, S., & Couture, R.-M. (2025). Distribution of rare earth elements and their signatures from the Mackenzie River delta to the abyssal Arctic Ocean. *Continental Shelf Research*, *289*, 105464. https://doi.org/https://doi.org/10.1016/j.csr.2025.105464

Brice, C., Montero-Serrano, J.-C., & Saint-Louis, R. (2025). Regional geochemical survey of Canadian Arctic sediments: insights into provenance, sediment dynamics and trace metal enrichment. *Applied Geochemistry*, *189*, 106432. https://doi.org/https://doi.org/10.1016/j.apgeochem.2025.106432

Bright, D. A., Dodd, M., & Reimer, K. J. (1996). Arsenic in subArctic lakes influenced by gold mine effluent: the occurrence of organoarsenicals and 'hidden' arsenic. *Science of The Total Environment*, *180*(2), 165-182. https://doi.org/https://doi.org/10.1016/0048-9697(95)04940-1

Buchmann, M. F. (2008). *NOAA Screening quick reference tables*. Seattle, WA: Office of Response and Retoriation Division, National Oceanic and Atmospheric Administration Retrieved from http://response.restoration.noaa.gov/cpr/sediment/squirt/squirt.html

Budko, D. F., Demina, L. L., Lisitzin, A. P., Kravchishina, M. D., & Politova, N. V. (2017). Occurrence forms of trace metals in recent bottom sediments from the White and Barents Seas. *Doklady Earth Sciences, 474*(1), 552-556. https://doi.org/10.1134/S1028334X17050014

Budko, D. F., Demina, L. L., Travkina, A. V., Starodymova, D. P., & Alekseeva, T. N. (2022). The Features of Distribution of Chemical Elements, including Heavy Metals and Cs-137, in Surface Sediments of the Barents, Kara, Laptev and East Siberian Seas. *Minerals*, *12*(3), 328. https://www.mdpi.com/2075-163X/12/3/328

Cai, M., Lin, J., Hong, Q., Wang, Y., & Cai, M. (2011). Content and distribution of trace metals in surface sediments from the northern Bering Sea, Chukchi Sea and adjacent Arctic areas. *Marine Pollution Bulletin*, *63*(5-12), 523-527.

Campbell, J. A., & Loring, D. H. (1980). Baseline levels of heavy metals in the waters and sediments of Baffin Bay. *Marine Pollution Bulletin*, *11*(9), 257-261. https://doi.org/https://doi.org/10.1016/0025-326X(80)90314-8

CCME. (1999). *Canadian Sediment Quality Guidelines for the Protection of Aquatic Life*. Winnipeg, MA: Canadian Council of Ministers of the Environment, Canadian environmental quality guidelines

Chaillou, G., Schäfer, J., Anschutz, P., Lavaux, G., & Blanc, G. (2003). The behaviour of arsenic in muddy sediments of the Bay of Biscay (France). *Geochimica et Cosmochimica Acta*, *67*(16), 2993-3003. https://doi.org/https://doi.org/10.1016/S0016-7037(03)00204-7

Chapman, P. M., Wang, F., Janssen, C., Persoone, G., & Allen, H. E. (1998). Ecotoxicology of metals in aquatic sediments: binding and release, bioavailability, risk assessment, and remediation. *Canadian Journal of Fisheries and Aquatic Sciences*, *55*(10), 2221-2243. https://doi.org/10.1139/f98-145

Chénier, R., Abado, L., Sabourin, O., & Tardif, L. (2017). Northern marine transportation corridors: Creation and analysis of northern marine traffic routes in Canadian waters. *Transactions in GIS*, *21*(6), 1085-1097. https://doi.org/https://doi.org/10.1111/tgis.12295

Chételat J., & Braune, B. (2012). *Canadian Arctic Contaminants Assessment Report III: Mercury in Canada's North*. Ottawa, Canada: Department of Aboriginal Affairs and Northern Development, Government of Canada

Choudhary, S., Nayak, G. N., & Khare, N. (2020). Source, mobility, and bioavailability of metals in fjord sediments of Krossfjord-Kongsfjord system, Arctic, Svalbard. *Environmental Science and Pollution Research*, *27*(13), 15130-15148. https://doi.org/10.1007/s11356-020-07879-1

Colombo, M., Jackson, S. L., Cullen, J. T., & Orians, K. J. (2020). Dissolved iron and manganese in the Canadian Arctic Ocean: On the biogeochemical processes controlling their distributions. *Geochimica et Cosmochimica Acta*, *277*, 150-174. https://doi.org/https://doi.org/10.1016/j.gca.2020.03.012

Corminboeuf, A., Montero-Serrano, J.-C., & St-Louis, R. (2021). Spatial and temporal distributions of polycyclic aromatic hydrocarbons in sediments from the Canadian Arctic Archipelago. *Marine Pollution Bulletin*, *171*, 112729. https://doi.org/https://doi.org/10.1016/j.marpolbul.2021.112729

De Vitre, R., Belzile, N., & Tessier, A. (1991). Speciation and adsorption of arsenic on diagenetic iron oxyhydroxides. *Limnology and Oceanography*, *36*(7), 1480-1485. https://doi.org/https://doi.org/10.4319/lo.1991.36.7.1480

Duncan, E. G., Maher, W. A., & Foster, S. D. (2015). Contribution of Arsenic Species in Unicellular Algae to the Cycling of Arsenic in Marine Ecosystems. *Environmental Science & Technology*, *49*(1), 33-50. https://doi.org/10.1021/es504074z

ECCC. (2024). *Marine Emissions Inventory Tool.* Environment and Climate Change Canada (Cross Sectoral Energy Division), Gatineau (QC). https://ec-meit.ca/app.html#

Fouché, J., Christiansen, C. T., Lafrenière, M. J., Grogan, P., & Lamoureux, S. F. (2020). Canadian permafrost stores large pools of ammonium and optically distinct dissolved organic matter. *Nature Communications*, *11*(1), 4500. https://doi.org/10.1038/s41467-020-18331-w

Fraser, T., Ferri, F., Fiess, K., & Pyle, L. (2012). Besa River Formation in Liard basin, southeast Yukon: Report on 2012 reconnaissance fieldwork. In K. E. MacFarlane, M. G. Nordling, & P. J. Sack (Eds.), *Yukon Exploration and Geology 2012* (pp. 37-46).

Fraser, T., & Hutchison, M. P. (2017). Lithogeochemical characterization of the Middle–Upper Devonian Road River Group and Canol and Imperial formations on Trail River, east Richardson Mountains, Yukon: age constraints and a depositional model for fine-grained strata in the Lower Paleozoic Richardson trough. *Canadian Journal of Earth Sciences*, *54*(7), 731-765. https://doi.org/10.1139/cjes-2016-0216

Freslon, N., Bayon, G., Toucanne, S., Bermell, S., Bollinger, C., Chéron, S., Etoubleau, J., Germain, Y., Khripounoff, A., Ponzevera, E., & Rouget, M.-L. (2014). Rare earth elements and neodymium isotopes in sedimentary organic matter. *Geochimica et Cosmochimica Acta*, *140*, 177-198. https://doi.org/https://doi.org/10.1016/j.gca.2014.05.016

Gamboa, A., Montero-Serrano, J.-C., St-Onge, G., Rochon, A., & Desiage, P.-A. (2017). Mineralogical, geochemical, and magnetic signatures of surface sediments from the Canadian Beaufort Shelf and Amundsen Gulf (Canadian Arctic). *Geochemistry, Geophysics, Geosystems*, *18*(2), 488-512. https://doi.org/https://doi.org/10.1002/2016GC006477

Gauthier, P. T., Blewett, T. A., Garman, E. R., Schlekat, C. E., Middleton, E. T., Suominen, E., & Crémazy, A. (2021). Environmental risk of nickel in aquatic Arctic ecosystems. *Science of The Total Environment*, *797*, 148921. https://doi.org/https://doi.org/10.1016/j.scitotenv.2021.148921

Glabonjat, R. A., Raber, G., Holm, H. C., Van Mooy, B. A. S., & Francesconi, K. A. (2021). Arsenolipids in Plankton from High- and Low-Nutrient Oceanic Waters Along a Transect in the North Atlantic. *Environmental Science & Technology*, *55*(8), 5515-5524. https://doi.org/10.1021/acs.est.0c06901

Gobeil, C., Silverberg, N., Sundby, B., & Cossa, D. (1987). Cadmium diagenesis in Laurentian Trough sediments. *Geochimica et Cosmochimica Acta*, *51*(3), 589-596. https://doi.org/https://doi.org/10.1016/0016-7037(87)90071-8

González, V., Vignati, D. A. L., Pons, M.-N., Montarges-Pelletier, E., Bojic, C., & Giamberini, L. (2015). Lanthanide ecotoxicity: First attempt to measure environmental risk for aquatic organisms. *Environmental Pollution*, *199*, 139-147. https://doi.org/https://doi.org/10.1016/j.envpol.2015.01.020

Grenier, M., Brown, K. A., Colombo, M., Belhadj, M., Baconnais, I., Pham, V., Soon, M., Myers, P. G., Jeandel, C., & François, R. (2022). Controlling factors and impacts of river-borne neodymium isotope signatures and rare earth element concentrations supplied to the Canadian Arctic Archipelago. *Earth and Planetary Science Letters*, *578*, 117341. https://doi.org/https://doi.org/10.1016/j.epsl.2021.117341

Gutjahr, M., Frank, M., Stirling, C. H., Klemm, V., van de Flierdt, T., & Halliday, A. N. (2007). Reliable extraction of a deepwater trace metal isotope signal from Fe–Mn oxyhydroxide coatings of marine sediments. *Chemical Geology*, *242*(3), 351-370. https://doi.org/https://doi.org/10.1016/j.chemgeo.2007.03.021

Hakanson, L. (1980). An ecological risk index for aquatic pollution control. A sedimentological approach. *Water Research*, *14*(8), 975-1001. https://doi.org/https://doi.org/10.1016/0043-1354(80)90143-8

Hargrave, B.T., Walsh, I.D., Murray, D.W., 2002. Seasonal and spatial patterns in mass and organic matter sedimentation in the North Water. *Deep Sea Research Part II: Topical Studies in Oceanography 49*, 5227-5244.

Heggie, D., & Lewis, T. (1984). Cobalt in pore waters of marine sediments. *Nature*, *311*(5985), 453-455. https://doi.org/10.1038/311453a0

Hélie, J. F. (2009). Elemental and stable isotopic approaches for studying the organic and inorganic carbon components in natural samples. *IOP Conference Series: Earth and Environmental Science*, *5*(1), 012005. https://doi.org/10.1088/1755-1307/5/1/012005

Holemann, J. A., Schirmacher, M., Kassens, H., & Prange, A. (1999). Geochemistry of Surficial and Ice-rafted Sediments from the Laptev Sea (Siberia). *Estuarine, Coastal and Shelf Science*, *49*(1), 45-59. https://doi.org/https://doi.org/10.1006/ecss.1999.0485

Husson, F., Josse, J., Le, S., Mazet, J., & Husson, M. F. (2016). Package 'factominer'. *An R package*, *96*(96), 698.

Hutchison, M. P. (2018). An appraisal of Devonian-Mississippian shale strata in Yukon's Liard basin. In K. E. MacFarlane (Ed.), *Yukon Exploration and Geology 2017* (pp. 69-88). Yukon Geological Survey.

Jensen, J., Adare, K., & Shearer, R. (1997). *Canadian Arctic Contaminants Assessment Report I*. Ottawa, Canada: Department of Indian and Northern Affairs, Government of Canada

Kassambara, A., & Mundt, F. (2020). Factoextra: Extract and Visualize the Results of Multivariate Data Analyses. R Package Version 1.0.7. https://CRAN.R-project.org/package=factoextra

Klein, B., LeBlanc, B., Mei, Z.-P., Beret, R., Michaud, J., Mundy, C. J., von Quillfeldt, C. H., Garneau, M.-È., Roy, S., Gratton, Y., Cochran, J. K., Bélanger, S., Larouche, P., Pakulski, J. D., Rivkin, R. B., & Legendre, L. (2002). Phytoplankton biomass, production and potential export in the North Water. *Deep Sea Research Part II: Topical Studies in Oceanography*, *49*(22), 4983-5002. https://doi.org/https://doi.org/10.1016/S0967-0645(02)00174-1

Kuzyk, Z. Z. A., Gobeil, C., Goñi, M. A., & Macdonald, R. W. (2017). Early diagenesis and trace element accumulation in North American Arctic margin sediments. *Geochimica et Cosmochimica Acta*, *203*, 175-200. https://doi.org/https://doi.org/10.1016/j.gca.2016.12.015

Lafrenière, M.-C., Lapierre, J.-F., Ponton, D. E., Guillemette, F., & Amyot, M. (2023). Rare earth elements (REEs) behavior in a large river across a geological and anthropogenic gradient. *Geochimica et Cosmochimica Acta*, *353*, 129-141. https://doi.org/https://doi.org/10.1016/j.gca.2023.05.019

Lê, S., Josse, J., & Husson, F. (2008). FactoMineR: An R Package for Multivariate Analysis. *Journal of Statistical Software*, *25*(1), 1 - 18. https://doi.org/10.18637/jss.v025.i01

Letaïef, S., Montero-Serrano, J. C., & St-Onge, G. (2021). Sedimentary processes within the Canadian Arctic Archipelago: Relationships among sedimentological, geochemical, and magnetic sediment properties. *Geochemistry, Geophysics, Geosystems*, *22*(7), e2021GC009719.

Liikane, D., St-Onge, M., Kjarsgaard, B., Rayner, N., Ernst, R., & Kastek, N. (2015). Frobisher suite mafic, ultramafic and layered mafic-ultramafic sills, southern Baffin Island, Nunavut. *Summary of Activities 2015, Canada-Nunavut Geoscience Office*, 21-32.

Lim, D., Jung, H. S., & Choi, J. Y. (2014). REE partitioning in riverine sediments around the Yellow Sea and its importance in shelf sediment provenance. *Marine Geology*, *357*, 12-24. https://doi.org/https://doi.org/10.1016/j.margeo.2014.07.002

Loring, D. H., Dahle, S., Naes, K., Dos Santos, J., Skei, J. M., & Matishov, G. G. (1998). Arsenic and other Trace Metals in Sediments from the Kara Sea and the Ob and Yenisey Estuaries, Russia. *Aquatic Geochemistry*, *4*(2), 233-252. https://doi.org/10.1023/A:1009691314353

Lu, Z. B., Cai, M., Wang, J., Yin, Z., & Yang, H. (2013). Levels and distribution of trace metals in surface sediments from Kongsfjorden, Svalbard, Norwegian Arctic. *Environmental Geochemistry and Health*, *35*(2), 257-269. https://doi.org/10.1007/s10653-012-9481-z

Lu, Z. B., & Kang, M. (2018). Risk assessment of toxic metals in marine sediments from the Arctic Ocean using a modified BCR sequential extraction procedure. *Journal of Environmental Science and Health, Part A*, *53*(3), 278-293. https://doi.org/10.1080/10934529.2017.1397443

MacDonald, D., Ingersoll, C. G., & Berger, T. A. (2000). Development and Evaluation of Consensus-Based Sediment Quality Guidelines for Freshwater Ecosystems. *Archives of Environmental Contamination and Toxicology*, *39*(1), 20-31. https://doi.org/10.1007/s002440010075

Macdonald, R. W., Barrie, L. A., Bidleman, T. F., Diamond, M. L., Gregor, D. J., Semkin, R. G., Strachan, W. M. J., Li, Y. F., Wania, F., Alaee, M., Alexeeva, L. B., Backus, S. M., Bailey, R., Bewers, J. M., Gobeil, C., Halsall, C. J., Harner, T., Hoff, J. T., Jantunen, L. M. M., . . . Yunker, M. B. (2000). Contaminants in the Canadian Arctic: 5 years of progress in understanding sources, occurrence and pathways. *Science of The Total Environment*, *254*(2), 93-234. https://doi.org/https://doi.org/10.1016/S0048-9697(00)00434-4

Macdonald, R. W., & Gobeil, C. (2012). Manganese Sources and Sinks in the Arctic Ocean with Reference to Periodic Enrichments in Basin Sediments. *Aquatic Geochemistry*, *18*(6), 565-591. https://doi.org/10.1007/s10498-011-9149-9

Macdonald, R. W., Harner, T., & Fyfe, J. (2005). Recent climate change in the Arctic and its impact on contaminant pathways and interpretation of temporal trend data. *Science of The Total Environment*, *342*(1), 5-86. https://doi.org/https://doi.org/10.1016/j.scitotenv.2004.12.059

Macdonald, R. W., Kuzyk, Z. Z. A., & Johannessen, S. C. (2015). The vulnerability of Arctic shelf sediments to climate change. *Environmental Reviews*, *23*(4), 461-479. https://doi.org/10.1139/er-2015-0040

McLennan, S. M. (2001). Relationships between the trace element composition of sedimentary rocks and upper continental crust. *Geochemistry, Geophysics, Geosystems*, *2*(4). https://doi.org/https://doi.org/10.1029/2000GC000109

McLennan, S. M., Nance, W. B., & Taylor, S. R. (1980). Rare earth element-thorium correlations in sedimentary rocks, and the composition of the continental crust. *Geochimica et Cosmochimica Acta*, *44*(11), 1833-1839. https://doi.org/https://doi.org/10.1016/0016-7037(80)90232-X

Meinhardt, A. K., März, C., Schuth, S., Lettmann, K. A., Schnetger, B., Wolff, J. O., & Brumsack, H. J. (2016). Diagenetic regimes in Arctic Ocean sediments: Implications for sediment geochemistry and core correlation. *Geochimica et Cosmochimica Acta*, *188*, 125-146. https://doi.org/https://doi.org/10.1016/j.gca.2016.05.032

Mudryk, L. R., Derksen, C., Howell, S., Laliberté, F., Thackeray, C., Sospedra-Alfonso, R., Vionnet, V., Kushner, P. J., & Brown, R. (2018). Canadian snow and sea ice: historical trends and projections. *The Cryosphere*, *12*(4), 1157-1176. https://doi.org/10.5194/tc-12-1157-2018

Müller, G. (1969). Index of geoaccumulation in sediments of the Rhine River. *Geojournal, 2*, 108-118.

Naidu, A., Kelley, J., Misra, D., & Venkatesan, M. (2005). *Trace metals and hydrocarbons in sediments of the Beaufort Lagoon, Northeast Arctic Alaska, exposed to long-term natural oil seepage, recent anthropogenic acivities and pristine conditions.* Final Report to Coastal Marine Institute, Univ. Alaska Fairbanks, Fairbanks, AK. Press.

Naidu, A. S., Blanchard, A. L., Misra, D., Trefry, J. H., Dasher, D. H., Kelley, J. J., & Venkatesan, M. I. (2012). Historical changes in trace metals and hydrocarbons in nearshore sediments, Alaskan Beaufort Sea, prior and subsequent to petroleum-related industrial development: Part I. Trace metals. *Marine Pollution Bulletin*, *64*(10), 2177-2189. https://doi.org/https://doi.org/10.1016/j.marpolbul.2012.07.037

NRCAN. (2024). *Rare earth elements facts*. Government of Canada. Retrieved 2024-11-27 from https://natural-resources.canada.ca/our-natural-resources/minerals-mining/mining-data-statistics-and-analysis/minerals-metals-facts/rare-earth-elements-facts/20522

O'Donnell, J. A., Carey, M. P., Koch, J. C., Baughman, C., Hill, K., Zimmerman, C. E., Sullivan, P. F., Dial, R., Lyons, T., Cooper, D. J., & Poulin, B. A. (2024). Metal mobilization from thawing permafrost to aquatic ecosystems is driving rusting of Arctic streams. *Communications Earth & Environment*, *5*(1), 268. https://doi.org/10.1038/s43247-024-01446-z

Pierce, M. L., & Moore, C. B. (1982). Adsorption of arsenite and arsenate on amorphous iron hydroxide. *Water Research*, *16*(7), 1247-1253. https://doi.org/https://doi.org/10.1016/0043-1354(82)90143-9

Pourmand, A., Dauphas, N., & Ireland, T. J. (2012). A novel extraction chromatography and MC-ICP-MS technique for rapid analysis of REE, Sc and Y: Revising CI-chondrite and Post-Archean Australian Shale (PAAS) abundances. *Chemical Geology*, *291*, 38-54. https://doi.org/https://doi.org/10.1016/j.chemgeo.2011.08.011

R Core Team. (2024). *R: A language and environment for statistical computing*. In R Foundation for Statistical Computing. https://www.R-project.org/

Rico, K. I., Schad, M., Picard, A., Kappler, A., Konhauser, K. O., & Mahmoudi, N. (2023). Resolving the fate of trace metals during microbial remineralization of phytoplankton biomass in precursor banded iron formation sediments. *Earth and Planetary Science Letters*, *607*, 118068. https://doi.org/https://doi.org/10.1016/j.epsl.2023.118068

Sholkovitz, E. R. (1990). Rare-earth elements in marine sediments and geochemical standards. *Chemical Geology*, *88*(3), 333-347. https://doi.org/https://doi.org/10.1016/0009-2541(90)90097-Q

Sholkovitz, E. R., Landing, W. M., & Lewis, B. L. (1994). Ocean particle chemistry: The fractionation of rare earth elements between suspended particles and seawater. *Geochimica et Cosmochimica Acta*, *58*(6), 1567-1579. https://doi.org/https://doi.org/10.1016/0016-7037(94)90559-2

Skierszkan, E. K., Schoepfer, V. A., Fellwock, M. D., Dockrey, J. W., Hayatifar, A., Bondici, V. F., McBeth, J. M., & Lindsay, M. B. J. (2024). Arsenic Mobilization from Thawing Permafrost. *ACS Earth and Space Chemistry*, *8*(4), 745-759. https://doi.org/10.1021/acsearthspacechem.3c00355

Stockdale, A., Davison, W., Zhang, H., & Hamilton-Taylor, J. (2010). The Association of Cobalt with Iron and Manganese (Oxyhydr)oxides in Marine Sediment. *Aquatic Geochemistry*, *16*(4), 575-585. https://doi.org/10.1007/s10498-010-9092-1

Stow, J., Tomlinson, S., Bourque, S. K., & Smith, S. (2017). *Contaminants in Canada's North: State of Knowledge and Regional Highlights: Canadian Arctic Contaminants Assessment Report 2017*. (066023890X). Ottawa, Canada: Department of Indigenous and Northern Affairs, Government of Canada

Strauss, J. V., Fraser, T., Melchin, M. J., Allen, T. J., Malinowski, J., Feng, X., Taylor, J. F., Day, J., Gill, B. C., & Sperling, E. A. (2020). The Road River Group of northern Yukon, Canada: early Paleozoic deep-water sedimentation within the Great American Carbonate Bank. *Canadian Journal of Earth Sciences*, *57*(10), 1193-1219. https://doi.org/10.1139/cjes-2020-0017

Taylor, S. R., & McLennan, S. M. (1985). *The continental crust: Its composition and evolution*. Blackwell Scientific Pub.,Palo Alto, CA. https://www.osti.gov/biblio/6582885

Trefry, J. H., & Neff, J. M. (2019). Effects of offshore oil exploration and development in the Alaskan Beaufort Sea: A three-decade record for sediment metals. *Integrated Environmental Assessment and Management*, *15*(2), 209-223. https://doi.org/https://doi.org/10.1002/ieam.4069

Trefry, J. H., Rember, R. D., Trocine, R. P., & Brown, J. S. (2003). Trace metals in sediments near offshore oil exploration and production sites in the Alaskan Arctic. *Environmental Geology*, *45*(2), 149-160. https://doi.org/10.1007/s00254-003-0882-2

Tribovillard, N., Algeo, T. J., Lyons, T., & Riboulleau, A. (2006). Trace metals as paleoredox and paleoproductivity proxies: An update. *Chemical Geology*, *232*(1), 12-32. https://doi.org/https://doi.org/10.1016/j.chemgeo.2006.02.012

Turekian, K. K., & Imbrie, J. (1966). The distribution of trace elements in deep-sea sediments of the Atlantic Ocean. *Earth and Planetary Science Letters*, *1*(4), 161-168. https://doi.org/https://doi.org/10.1016/0012-821X(66)90063-X

US EPA. (2007). Method 3051A (SW-846): Microwave Assisted Acid Digestion of Sediments, Sludges, and Oils. Washington, DC.

US EPA. (2012). Rare earth elements: A review of production, processing, recycling, and associated environmental issues. Cincinnati, OH

van den Boogaart, K. G., Tolosana-Delgado, R., & Bren, M. (2023). compositions: Compositional Data Analysis. https://CRAN.R-project.org/package=compositions

Vonk, J. E., Giosan, L., Blusztajn, J., Montlucon, D., Graf Pannatier, E., McIntyre, C., Wacker, L., Macdonald, R. W., Yunker, M. B., & Eglinton, T. I. (2015). Spatial variations in geochemical characteristics of the modern Mackenzie Delta sedimentary system. *Geochimica et Cosmochimica Acta*, *171*, 100-120. https://doi.org/https://doi.org/10.1016/j.gca.2015.08.005

Wagemann, R., Brunskill, G. J., & Graham, B. W. (1977). Composition and reactivity of some river sediments from the Mackenzie Valley, N.W.T., Canada. *Environmental Geology*, *1*(6), 349-358. https://doi.org/10.1007/BF02380503

Wang, J., Gough, W. A., Yan, J., & Lu, Z. (2022). Ecological Risk Assessment of Trace Metal in Pacific Sector of Arctic Ocean and Bering Strait Surface Sediments. *International Journal of Environmental Research and Public Health*, *19*(8), 4454. https://www.mdpi.com/1660-4601/19/8/4454

Wang, S., & Mulligan, C. N. (2006). Occurrence of arsenic contamination in Canada: Sources, behavior and distribution. *Science of The Total Environment*, *366*(2), 701-721. https://doi.org/https://doi.org/10.1016/j.scitotenv.2005.09.005

Wei, T., Simko, V., Levy, M., Xie, Y., Jin, Y., & Zemla, J. (2017). Package 'corrplot'. *Statistician*, *56*(316), e24.

Wychen, W. V., David, B., Will, K., Natalija, N., Luke, C., & and Gray, L. (2020). RADARSAT-2 Derived Glacier Velocities and Dynamic Discharge Estimates for the Canadian High Arctic: 2015–2020. *Canadian Journal of Remote Sensing*, *46*(6), 695-714. https://doi.org/10.1080/07038992.2020.1859359

Xu, G., Hannah, J. L., Bingen, B., Georgiev, S., & Stein, H. J. (2012). Digestion methods for trace element measurements in shales: Paleoredox proxies examined. *Chemical Geology*, *324-325*, 132-147. https://doi.org/https://doi.org/10.1016/j.chemgeo.2012.01.029

Ye, L., März, C., Polyak, L., Yu, X., & Zhang, W. (2019). Dynamics of manganese and cerium enrichments in Arctic Ocean sediments: a case study from the Alpha Ridge. *Frontiers in Earth Science*, *6*, 236.

Zheng, H., Ren, Q., Zheng, K., Qin, Z., Wang, Y., & Wang, Y. (2022). Spatial distribution and risk assessment of metal(loid)s in marine sediments in the Arctic Ocean and Bering Sea. *Marine Pollution Bulletin*, *179*, 113729. https://doi.org/https://doi.org/10.1016/j.marpolbul.2022.113729

## 2.10 SUPPLEMENTARY MATERIAL (FIGURES AND TABLES)

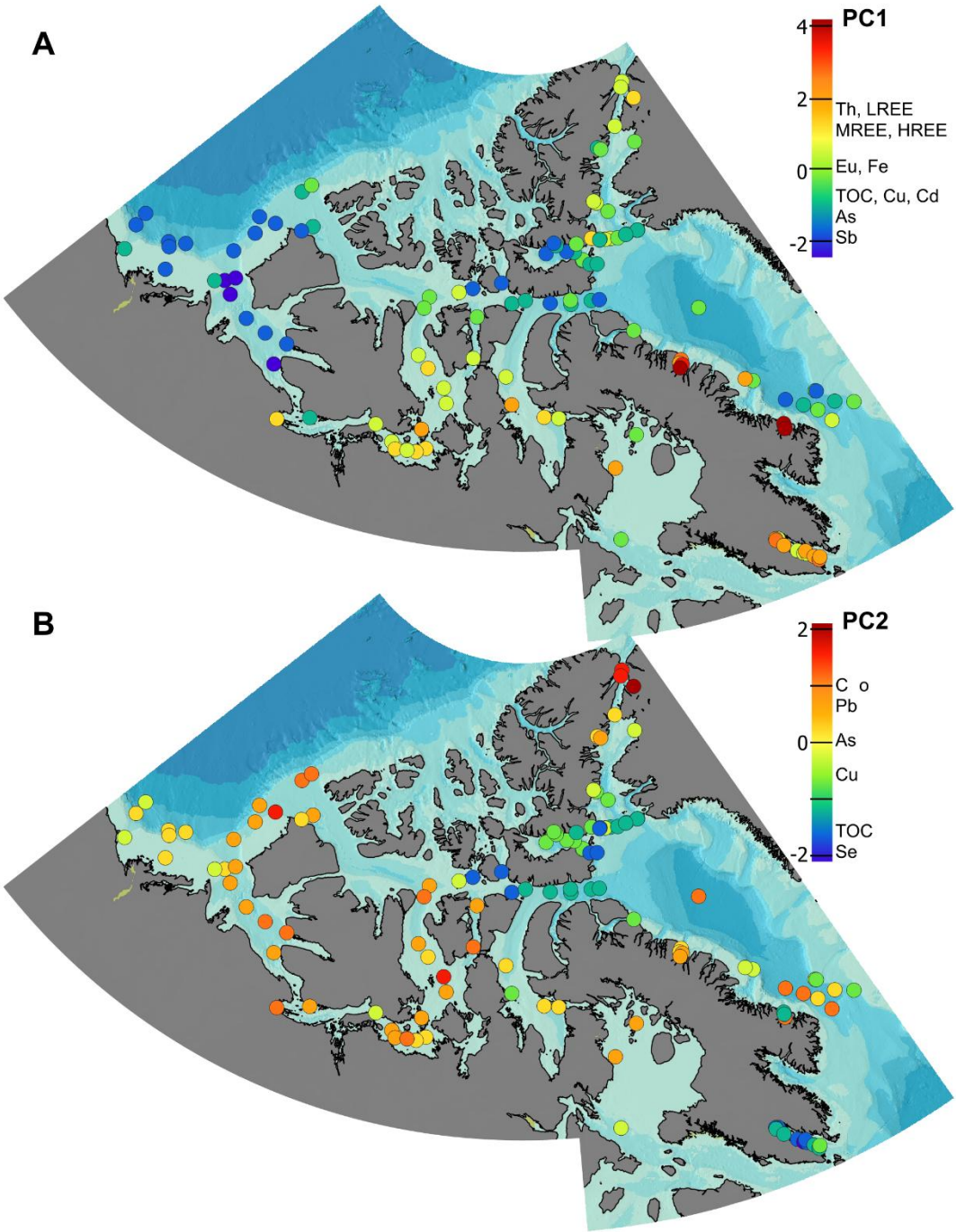


Figure 30. Maps presenting the PCA scores for the individuals for the (A) first principal component (PC1) and the (B) second principal component (PC2).

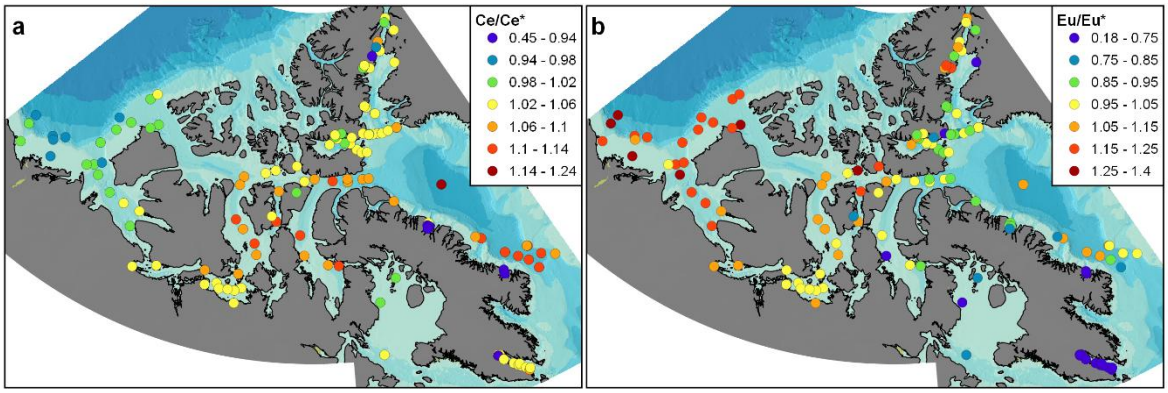


Figure 31. Distribution maps of the (a) Ce and (b) Eu anomalies calculated for the terrestrial and marine sediment samples.

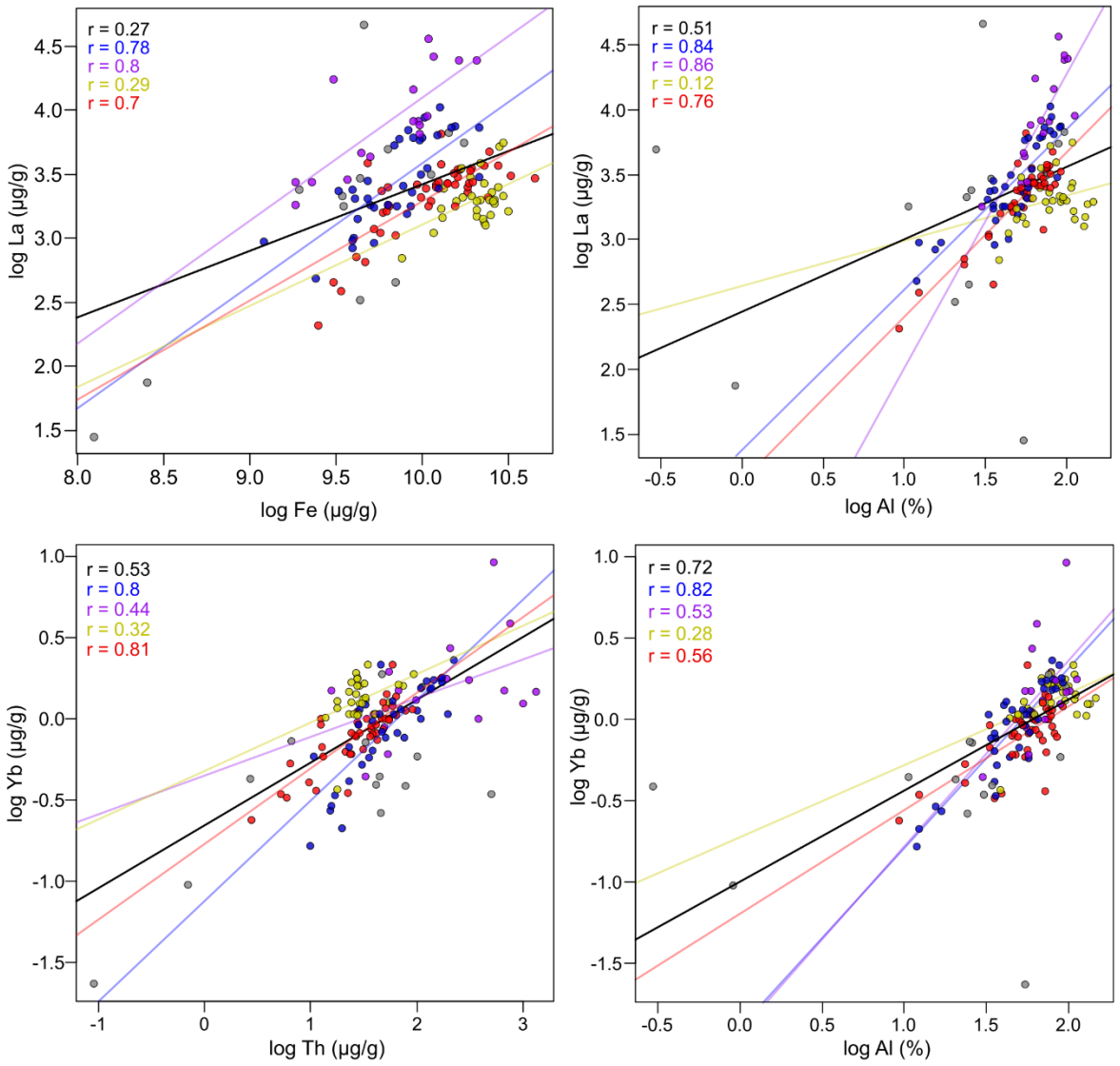


Figure 32. Log-log plots of La versus Fe (a), and Al (b) and Yb versus Th (c) and Al (d). Concentrations of Al are ED-XRF total concentrations from Brice et al. (2025).

Tableau 10.

ICP-QQQ blank results (µg/L) for the terrestrial and marine surface sediments. Cells in gray correspond to non-systematic contamination.

| Blanks | 24 Mg | 44 Ca | 39-39 K | 52 Cr | 55 Mn | 57 Fe | 59 Co | 60 Ni | 45-61 Sc |
|---|---|---|---|---|---|---|---|---|---|
| 1 | 1.937 | 6.900 | 2.056 | 1.1511 | 0.0476 | 8.7727 | 0.0044 | 0.1033 | 0.0020 |
| 2 | 2.410 | 5.281 | 6.169 | 0.2419 | 0.0511 | 5.9477 | 0.0022 | 0.0447 | 0.0018 |
| 3 | 4.076 | 29.443 | 1.556 | 0.7192 | 0.0133 | 3.5528 | 0.0025 | 0.0405 | 0.0008 |
| 4 | 6.177 | 182.885 | 6.884 | 1.2615 | 0.0386 | 8.5508 | 0.0072 | 0.0355 | 0.0060 |
| 5 | 4.220 | 89.030 | 3.365 | 0.5646 | 0.0250 | 4.0624 | 0.0054 | 0.0325 | 0.0029 |
| 6 | 3.412 | 89.095 | 3.814 | 0.1391 | 0.0246 | 1.6562 | 0.0045 | 0.0232 | 0.0032 |
| 7 | 7.186 | 290.562 | 10.533 | 0.1957 | 0.0729 | 3.9203 | 0.0117 | 0.0973 | 0.0113 |
| 8 | 3.922 | 147.853 | 5.930 | 0.1552 | 0.0371 | 2.9726 | 0.0066 | 0.0547 | 0.0048 |
| 9 | 2.440 | 78.534 | 3.933 | 0.0925 | 0.0229 | 1.6164 | 0.0044 | 0.0364 | 0.0025 |
| 10 | 2.773 | 93.849 | 3.544 | 0.0911 | 0.0217 | 1.4681 | 0.0055 | 0.0222 | 0.0023 |
| 11 | 2.315 | 78.393 | 2.874 | 0.0563 | 0.0171 | 1.1779 | 0.0052 | 0.0220 | 0.0024 |
| 12 | 2.223 | 72.920 | 3.367 | 0.0545 | 0.0204 | 1.3484 | 0.0053 | 0.0350 | 0.0011 |
| 13 | 0.655 | 8.941 | 1.231 | 0.0152 | 0.0104 | 0.1994 | 0.0000 | 0.0150 | 0.0000 |
| 14 | 0.812 | 8.010 | 1.332 | 0.0236 | 0.0053 | 0.2408 | 0.0000 | 0.0115 | 0.0000 |
| 15 | 1.771 | 62.290 | 3.024 | 0.0894 | 0.0245 | 1.3115 | 0.0043 | 0.0189 | 0.0000 |
| 16 | 2.830 | 86.518 | 3.514 | 0.1159 | 0.0269 | 1.4294 | 0.0050 | 0.0204 | 0.0002 |
| 17 | 2.044 | 37.866 | 2.268 | 0.0398 | 0.0189 | 0.9104 | 0.0017 | 0.0173 | 0.0000 |
| 18 | 1.829 | 18.300 | 1.519 | 0.0392 | 0.0120 | 0.6169 | 0.0022 | 0.0169 | 0.0000 |
| 19 | 1.834 | 4.399 | 1.084 | 0.0848 | 0.1002 | 0.4911 | 0.0011 | 0.0439 | 0.0000 |
| 20 | 1.744 | 5.763 | 1.187 | 0.0292 | 0.0185 | 0.3236 | 0.0009 | 0.0208 | 0.0000 |
| LOD | 0.001 | 0.008 | 0.001 | 0.0056 | 0.0045 | 0.0006 | 0.0003 | 0.0023 | 0.0049 |
| LOQ | 0.005 | 0.027 | 0.005 | 0.0185 | 0.0148 | 0.0021 | 0.0008 | 0.0075 | 0.0162 |
| Mean blanks | 2.831 | 45.619 | 3.459 | 0.2580 | 0.0304 | 2.5285 | 0.0040 | 0.0356 | 0.0021 |
| SD blanks | 1.633 | 72.094 | 2.375 | 0.3712 | 0.0229 | 2.5859 | 0.0028 | 0.0250 | 0.0028 |
| LOD/Mean | 0.001 | 0.000 | 0.000 | 0.0218 | 0.1470 | 0.0002 | 0.0642 | 0.0642 | 2.3824 |
| Above LOD? | Yes | Yes | Yes | Yes | Yes | Yes | Yes | Yes | No |
| Min value | 188.486 | 36.701 | 77.311 | 0.510 | 4.714 | 227.845 | 0.084 | 0.340 | |
| Min/Mean | 67 | 1 | 22 | 2 | 155 | 90 | 21 | 10 | |
| Blanks > min x 20? | No | Yes | No | Yes | No | No | No | Yes | |
| Correction | | 45.619 | | 0.258 | | | | 0.036 | |

Tableau 10 (suite)

| Blanks | 63 Cu | 47-63 Ti | 66 Zn | 51-67 V | 78-78 Se | 88 Sr | 75-91 As | 98 Mo | 89-105 Y |
|---|---|---|---|---|---|---|---|---|---|
| 1 | 0.1523 | 0.3627 | 0.3826 | 0.0162 | 0.0000 | 0.0464 | 0.0061 | 0.1298 | 0.0012 |
| 2 | 0.5316 | 0.4114 | 0.0184 | 0.0124 | 0.0000 | 0.0617 | 0.0076 | 0.0235 | 0.0021 |
| 3 | 0.3058 | 0.1264 | 0.0371 | 0.0124 | 0.0000 | 0.2034 | 0.0099 | 0.0757 | 0.0018 |
| 4 | 0.1832 | 0.2472 | 0.0130 | 0.0588 | 0.0008 | 1.3601 | 0.0340 | 0.1492 | 0.0114 |
| 5 | 0.0290 | 0.1456 | 0.0000 | 0.0298 | 0.0023 | 0.6429 | 0.0179 | 0.0674 | 0.0063 |
| 6 | 0.0390 | 0.1510 | 0.2037 | 0.0261 | 0.0000 | 0.6325 | 0.0194 | 0.0125 | 0.0054 |
| 7 | 0.0715 | 0.5010 | 0.4468 | 0.0898 | 0.0000 | 2.1196 | 0.0572 | 0.0018 | 0.0183 |
| 8 | 0.0449 | 0.3038 | 0.0789 | 0.0482 | 0.0000 | 1.1207 | 0.0212 | 0.0037 | 0.0097 |
| 9 | 0.1026 | 0.1548 | 0.3687 | 0.0222 | 0.0075 | 0.5781 | 0.0145 | 0.0035 | 0.0055 |
| 10 | 0.0535 | 0.1142 | 0.0738 | 0.0266 | 0.0000 | 0.6791 | 0.0196 | 0.0008 | 0.0057 |
| 11 | 0.0401 | 0.1594 | 0.0499 | 0.0220 | 0.0000 | 0.5804 | 0.0204 | 0.0000 | 0.0050 |
| 12 | 0.0890 | 0.1898 | 0.1298 | 0.0215 | 0.0000 | 0.5199 | 0.0196 | 0.0000 | 0.0048 |
| 13 | 0.0227 | 0.0821 | 0.1401 | 0.0018 | 0.0042 | 0.0631 | 0.0081 | 0.0009 | 0.0001 |
| 14 | 0.0489 | 0.1408 | 0.1690 | 0.0020 | 0.0012 | 0.0549 | 0.0102 | 0.0000 | 0.0002 |
| 15 | 0.0458 | 0.1235 | 0.1575 | 0.0175 | 0.0000 | 0.4885 | 0.0142 | 0.0001 | 0.0040 |
| 16 | 0.0432 | 0.1359 | 0.1173 | 0.0257 | 0.0000 | 0.6739 | 0.0208 | 0.0012 | 0.0049 |
| 17 | 0.1091 | 0.2305 | 0.1035 | 0.0099 | 0.0059 | 0.2818 | 0.0136 | 0.0000 | 0.0025 |
| 18 | 0.1255 | 0.1151 | 0.1689 | 0.0056 | 0.0028 | 0.1320 | 0.0098 | 0.0000 | 0.0009 |
| 19 | 15.5141 | 0.0873 | 0.1278 | 0.0014 | 0.0000 | 0.0177 | 0.0060 | 0.0085 | 0.0017 |
| 20 | 0.0765 | 0.1682 | 0.1219 | 0.0024 | 0.0000 | 0.0339 | 0.0046 | 0.0000 | 0.0010 |
| LOD (ug/L) | 0.0002 | 0.0102 | 0.0283 | 0.0003 | 0.0023 | 0.0002 | 0.0032 | 0.0023 | 0.0003 |
| LOQ (ug/L) | 0.0008 | 0.0336 | 0.0935 | 0.0011 | 0.0077 | 0.0006 | 0.0105 | 0.0075 | 0.0011 |
| Mean blanks | 0.1113 | 0.1975 | 0.1454 | 0.0226 | 0.0012 | 0.5145 | 0.0167 | 0.0239 | 0.0046 |
| SD blanks | 3.4462 | 0.1137 | 0.1236 | 0.0218 | 0.0022 | 0.5314 | 0.0119 | 0.0451 | 0.0044 |
| LOD/Mean | 0.0022 | 0.0516 | 0.1949 | 0.0142 | 1.8805 | 0.0003 | 0.1904 | 0.0952 | 0.0711 |
| Above LOD? | Yes | Yes | Yes | Yes | No | Yes | Yes | Yes | Yes |
| Min value | 0.3070 | 3.8180 | 0.6310 | 0.535 | | 1.512 | 0.072 | 0.012 | 0.174 |
| Min/Mean | 3 | 19 | 4 | 24 | | 3 | 4 | 1 | 38 |
| Blanks > min * 20? | Yes | Yes | Yes | No | | Yes | Yes | Yes | No |
| Correction | 0.111 | 0.198 | 0.145 | | | 0.515 | 0.017 | 0.024 | |

Tableau 10 (suite)

| Blanks | 111 Cd | 121 Sb | 153 Eu | 139-155 La | 140-156 Ce | 141-157 Pr | 146-162 Nd | 147-163 Sm | 157-173 Gd |
|---|---|---|---|---|---|---|---|---|---|
| 1 | 0.0000 | 0.0012 | 0.0003 | 0.0073 | 0.0216 | 0.0005 | 0.0026 | 0.0000 | 0.0007 |
| 2 | 0.0000 | 0.0008 | 0.0003 | 0.0109 | 0.0162 | 0.0016 | 0.0052 | 0.0004 | 0.0008 |
| 3 | 0.0000 | 0.0011 | 0.0003 | 0.0048 | 0.0110 | 0.0013 | 0.0047 | 0.0002 | 0.0003 |
| 4 | 0.0002 | 0.0005 | 0.0011 | 0.0309 | 0.0770 | 0.0098 | 0.0381 | 0.0066 | 0.0036 |
| 5 | 0.0000 | 0.0011 | 0.0008 | 0.0151 | 0.0376 | 0.0047 | 0.0188 | 0.0043 | 0.0013 |
| 6 | 0.0002 | 0.0035 | 0.0007 | 0.0146 | 0.0347 | 0.0048 | 0.0205 | 0.0031 | 0.0022 |
| 7 | 0.0005 | 0.0032 | 0.0022 | 0.0502 | 0.1237 | 0.0145 | 0.0638 | 0.0116 | 0.0062 |
| 8 | 0.0002 | 0.0023 | 0.0020 | 0.0264 | 0.0651 | 0.0081 | 0.0335 | 0.0055 | 0.0034 |
| 9 | 0.0015 | 0.0044 | 0.0008 | 0.0147 | 0.0335 | 0.0042 | 0.0180 | 0.0022 | 0.0014 |
| 10 | 0.0005 | 0.0083 | 0.0010 | 0.0159 | 0.0380 | 0.0048 | 0.0213 | 0.0024 | 0.0016 |
| 11 | 0.0000 | 0.0055 | 0.0009 | 0.0133 | 0.0326 | 0.0043 | 0.0165 | 0.0027 | 0.0008 |
| 12 | 0.0002 | 0.0053 | 0.0005 | 0.0184 | 0.0288 | 0.0035 | 0.0145 | 0.0032 | 0.0024 |
| 13 | 0.0009 | 0.0041 | 0.0000 | 0.0062 | 0.0022 | 0.0004 | 0.0011 | 0.0001 | 0.0001 |
| 14 | 0.0014 | 0.0031 | 0.0001 | 0.0066 | 0.0023 | 0.0004 | 0.0011 | 0.0000 | 0.0007 |
| 15 | 0.0000 | 0.0066 | 0.0006 | 0.0166 | 0.0270 | 0.0033 | 0.0141 | 0.0029 | 0.0025 |
| 16 | 0.0004 | 0.0087 | 0.0004 | 0.0202 | 0.0357 | 0.0042 | 0.0180 | 0.0039 | 0.0023 |
| 17 | 0.0000 | 0.0089 | 0.0003 | 0.0089 | 0.0147 | 0.0018 | 0.0071 | 0.0011 | 0.0009 |
| 18 | 0.0000 | 0.0066 | 0.0001 | 0.0056 | 0.0071 | 0.0010 | 0.0041 | 0.0006 | 0.0008 |
| 19 | 0.0000 | 0.0056 | 0.0001 | 0.0029 | 0.0011 | 0.0000 | 0.0003 | 0.0000 | 0.0007 |
| 20 | 0.0000 | 0.0020 | 0.0000 | 0.0039 | 0.0022 | 0.0002 | 0.0008 | 0.0000 | 0.0003 |
| LOD (ug/L) | 0.0006 | 0.0013 | 0.0004 | 0.0001 | 0.0002 | 0.0001 | 0.0005 | 0.0005 | 0.0003 |
| LOQ (ug/L) | 0.0018 | 0.0043 | 0.0012 | 0.0004 | 0.0007 | 0.0004 | 0.0016 | 0.0015 | 0.0011 |
| Mean blanks | 0.0003 | 0.0041 | 0.0006 | 0.0147 | 0.0306 | 0.0037 | 0.0152 | 0.0025 | 0.0016 |
| SD blanks | 0.0005 | 0.0027 | 0.0006 | 0.0112 | 0.0299 | 0.0037 | 0.0157 | 0.0029 | 0.0015 |
| LOD/Mean | 1.8380 | 0.3169 | 0.6031 | 0.0078 | 0.0065 | 0.0321 | 0.0311 | 0.1810 | 0.2051 |
| Above LOD? | No | Yes | Yes | Yes | Yes | Yes | Yes | Yes | Yes |
| Min value | | 0.004 | 0.009 | 0.295 | 0.591 | 0.070 | 0.251 | 0.045 | 0.039 |
| Min/Mean | | 1 | 15 | 20 | 19 | 19 | 17 | 18 | 23 |
| Blanks > min x 20? | | Yes | Yes | No | Yes | Yes | Yes | Yes | No |
| Correction | | 0.004 | 0.0006 | | 0.031 | 0.0037 | 0.015 | 0.003 | |

Tableau 10 (suite)

| Blanks | 174 Yb | 159-175 Tb | 163-179 Dy | 165-181 Ho | 166-182 Er | 169-185 Tm | 175-191 Lu | 208 Pb |
|---|---|---|---|---|---|---|---|---|
| 1 | 0.0000 | 0.0000 | 0.0004 | 0.0001 | 0.0001 | 0.0000 | 0.0000 | 0.0082 |
| 2 | 0.0004 | 0.0001 | 0.0006 | 0.0001 | 0.0002 | 0.0000 | 0.0001 | 0.0061 |
| 3 | 0.0003 | 0.0001 | 0.0006 | 0.0001 | 0.0001 | 0.0000 | 0.0000 | 0.0106 |
| 4 | 0.0006 | 0.0005 | 0.0021 | 0.0004 | 0.0010 | 0.0001 | 0.0001 | 0.0657 |
| 5 | 0.0004 | 0.0002 | 0.0013 | 0.0002 | 0.0006 | 0.0000 | 0.0000 | 0.0328 |
| 6 | 0.0007 | 0.0002 | 0.0014 | 0.0001 | 0.0002 | 0.0001 | 0.0000 | 0.0312 |
| 7 | 0.0016 | 0.0009 | 0.0044 | 0.0008 | 0.0015 | 0.0002 | 0.0004 | 0.1181 |
| 8 | 0.0006 | 0.0004 | 0.0023 | 0.0004 | 0.0011 | 0.0001 | 0.0002 | 0.0583 |
| 9 | 0.0003 | 0.0001 | 0.0007 | 0.0003 | 0.0006 | 0.0001 | 0.0001 | 0.0278 |
| 10 | 0.0004 | 0.0004 | 0.0020 | 0.0003 | 0.0005 | 0.0000 | 0.0002 | 0.0334 |
| 11 | 0.0005 | 0.0004 | 0.0012 | 0.0001 | 0.0004 | 0.0001 | 0.0002 | 0.0281 |
| 12 | 0.0005 | 0.0002 | 0.0010 | 0.0001 | 0.0004 | 0.0001 | 0.0001 | 0.0267 |
| 13 | 0.0000 | 0.0000 | 0.0003 | 0.0000 | 0.0001 | 0.0000 | 0.0000 | 0.0041 |
| 14 | 0.0000 | 0.0000 | 0.0003 | 0.0000 | 0.0001 | 0.0000 | 0.0001 | 0.0036 |
| 15 | 0.0007 | 0.0002 | 0.0007 | 0.0002 | 0.0006 | 0.0001 | 0.0001 | 0.0248 |
| 16 | 0.0007 | 0.0003 | 0.0012 | 0.0002 | 0.0005 | 0.0001 | 0.0001 | 0.0331 |
| 17 | 0.0002 | 0.0001 | 0.0006 | 0.0001 | 0.0002 | 0.0001 | 0.0000 | 0.0126 |
| 18 | 0.0003 | 0.0001 | 0.0003 | 0.0000 | 0.0002 | 0.0000 | 0.0000 | 0.0069 |
| 19 | 0.0001 | 0.0001 | 0.0001 | 0.0001 | 0.0000 | 0.0000 | 0.0000 | 0.0017 |
| 20 | 0.0001 | 0.0000 | 0.0000 | 0.0001 | 0.0000 | 0.0000 | 0.0000 | 0.0009 |
| LOD (ug/L) | 0.0003 | 0.0002 | 0.0002 | 0.0001 | 0.0004 | 0.0001 | 0.0002 | 0.0007 |
| LOQ (ug/L) | 0.0011 | 0.0007 | 0.0008 | 0.0004 | 0.0012 | 0.0005 | 0.0005 | 0.0022 |
| Mean blanks | 0.0004 | 0.0002 | 0.0011 | 0.0002 | 0.0004 | 0.0000 | 0.0001 | 0.0267 |
| SD blanks | 0.0004 | 0.0002 | 0.0010 | 0.0002 | 0.0004 | 0.0000 | 0.0001 | 0.0281 |
| LOD/Mean | 0.8164 | 0.9503 | 0.2158 | 0.6340 | 0.8751 | 3.0866 | 1.8254 | 0.0246 |
| Above LOD? | Yes | Yes | Yes | Yes | Yes | No | No | Yes |
| Min value | 0.014 | 0.005 | 0.028 | 0.006 | 0.016 | | | 0.132 |
| Min/Mean | 32 | 25 | 26 | 34 | 38 | | | 5 |
| Blanks > min x 20? | No | No | No | No | No | | | Yes |
| Correction | | | | | | | | 0.027 |

Tableau 11.

ICP-QQQ blank results (µg/L) for marine sediments used for the geochemical background.

| Blanks | 1 (2024-07-18) | 2 (2024-08-01) | 3 (2024-08-02) | LOD | LOQ |
|---|---|---|---|---|---|
| 24 Mg | 8.0094 | 11.5936 | 2.5385 | 0.0014 | 0.005 |
| 27 Al | 168.3574 | 270.1586 | 77.9201 | 0.2537 | 0.837 |
| 44 Ca | 278.8566 | 467.9925 | 118.6490 | 0.0081 | 0.027 |
| 39-39 K | 10.0400 | 15.8823 | 5.4889 | 0.0015 | 0.005 |
| 52 Cr | 6.6719 | 3.5730 | 6.2730 | 0.0056 | 0.019 |
| 55 Mn | 0.0633 | 0.1077 | 0.0196 | 0.0045 | 0.0148 |
| 57 Fe | 46.4382 | 23.7756 | 32.7090 | 0.0006 | 0.0021 |
| 59 Co | 0.0261 | 0.0236 | 0.0060 | 0.0003 | 0.0008 |
| 60 Ni | 0.0752 | 0.1952 | 0.0331 | 0.0023 | 0.0075 |
| 45-61 Sc | 0 | 0 | 0 | 0.0049 | 0.0162 |
| 63 Cu | 0.2781 | 0.2559 | 0.1316 | 0.0002 | 0.0008 |
| 47-63 Ti | 0.3107 | 0.4465 | 0.1648 | 0.0102 | 0.0336 |
| 66 Zn | 0.8937 | 0.6690 | 0.3080 | 0.0283 | 0.0935 |
| 51-67 V | 0.1182 | 0.1478 | 0.0790 | 0.0003 | 0.0011 |
| 78-78 Se | 0.0621 | 0.0770 | 0.0398 | 0.0032 | 0.0105 |
| 88 Sr | 0.0020 | 0.0000 | 0.0021 | 0.0023 | 0.0077 |
| 75-91 As | 2.0640 | 3.4491 | 0.9729 | 0.0002 | 0.0006 |
| 98 Mo | 1.4936 | 0.6009 | 1.2708 | 0.0023 | 0.0075 |
| 89-105 Y | 0.0155 | 0.0267 | 0.0071 | 0.0003 | 0.0011 |
| 111 Cd | 0.0023 | 0 | 0 | 0.0006 | 0.0018 |
| 121 Sb | 0.0173 | 0.0532 | 0.0084 | 0.0013 | 0.0043 |
| 153 Eu | 0.0679 | 0.0696 | 0.0673 | 0.0004 | 0.0012 |
| 139-155 La | 0.0504 | 0.0751 | 0.0218 | 0.0001 | 0.0004 |
| 140-156 Ce | 0.1085 | 0.1792 | 0.0461 | 0.0002 | 0.0007 |
| 141-157 Pr | 0.0129 | 0.0227 | 0.0061 | 0.0001 | 0.0004 |
| 146-162 Nd | 0.1034 | 0.1431 | 0.0779 | 0.0005 | 0.0016 |
| 147-163 Sm | 0.0093 | 0.0157 | 0.0033 | 0.0005 | 0.0015 |
| 157-173 Gd | 0.0045 | 0.0085 | 0.0021 | 0.0003 | 0.0011 |
| 174 Yb | 0.0008 | 0.0025 | 0.0001 | 0.0003 | 0.0011 |
| 159-175 Tb | 0.0004 | 0.0008 | 0.0000 | 0.0002 | 0.0007 |
| 163-179 Dy | 0.0067 | 0.0100 | 0.0051 | 0.0002 | 0.0008 |
| 165-181 Ho | 0.0002 | 0.0010 | 0.0001 | 0.0001 | 0.0004 |
| 166-182 Er | 0.0030 | 0.0041 | 0.0024 | 0.0004 | 0.0012 |
| 169-185 Tm | 0.0086 | 0.0087 | 0.0085 | 0.0001 | 0.0005 |
| 175-191 Lu | 0.0002 | 0.0004 | 0.0000 | 0.0002 | 0.0005 |
| 208 Pb | 0.0940 | 0.1641 | 0.0468 | 0.0007 | 0.0022 |

Tableau 12.

(a) Certified values for partial digestion with concentrated HCl and $HNO_3$

| | TILL-3 (n=8) | | | | TILL-2 (n=8) | | | |
|---|---|---|---|---|---|---|---|---|
| | Analyzed | Certified | Recovery | RSD | Analyzed | Certified | Recovery | RSD |
| Cr | 67.8 | 73 | 93% | 3% | Contamination | | | |
| Mn | 346.6 | 310 | 112% | 3% | 655.3 | 530 | 124% | 4% |
| Fe | 18080.8 | 20000 | 90% | 6% | 35909.3 | 32000 | 112% | 4% |
| Co | 10.5 | 11 | 96% | 2% | 12.6 | 13 | 97% | 4% |
| Ni | 31.8 | 32 | 99% | 2% | 32.0 | 31 | 103% | 4% |
| Cu | 21.7 | 23 | 95% | 6% | 149.8 | 149 | 101% | 4% |
| Zn | 39.4 | 43 | 92% | 5% | 105.1 | 116 | 91% | 4% |
| V | 43.8 | 33 | 133% | 3% | 55.9 | 38 | 147% | 4% |
| As | 80.8 | 84 | 96% | 3% | 23.5 | 22 | 107% | 3% |
| Mo | 0.2 | <2 | NA | 16% | | | | |
| Cd | 0.1 | <0.2 | NA | 2% | 0.3 | 0.3 | 103% | 14% |
| Pb | 15.7 | 16 | 98% | 2% | 22.1 | 21 | 105% | 3% |

(b) Certified values for total digestion (for REE)

| | TILL-3 (n=8) | | | | TILL-2 (n=8) | | | |
|---|---|---|---|---|---|---|---|---|
| | Analyzed | Certified | Recovery | RSD | Analyzed | Certified | Recovery | RSD |
| Y | 9.4 | 17 | 55% | 3% | 18.3 | 40 | 46% | 5% |
| La | 17.1 | 21 | 81% | 6% | 42.7 | 44 | 97% | 5% |
| Ce | 35.5 | 42 | 85% | 6% | 95.3 | 98 | 97% | 4% |
| Nd | 16.1 | 16 | 101% | 5% | 36.5 | 36 | 101% | 5% |
| Sm | 2.9 | 3.3 | 88% | 3% | 7.1 | 7.4 | 96% | 5% |
| Eu | 0.6 | <1 | NA | 3% | 1.0 | 1 | 100% | 5% |
| Yb | 0.8 | 1.5 | 55% | 4% | 1.6 | 3.7 | 42% | 8% |
| Tb | 0.3 | <0.5 | NA | 4% | 0.8 | 1.2 | 64% | 4% |
| Er | 0.9 | 1.4 | 67% | 4% | 1.8 | 3.7 | 50% | 6% |
| Lu | 0.1 | 0.2 | 60% | 5% | 0.2 | 0.6 | 34% | 9% |

Tableau 13

Trace metal concentrations measured in marine surface sediments across the Arctic.

* Extractable concentrations from partial $HNO_3$-HCl extraction.

| Zone | Reference | Cd | Cr | Pb | Cu | Co | Ni | As | Zn | V | Fe | Mn |
|---|---|---|---|---|---|---|---|---|---|---|---|---|
| | | min / max | | | | | | | | | | |
| Canadian arctic | This study * | 0.01 | 5 | 2 | 3 | 1 | 3 | 1 | 9 | 8 | 3286 | 68 |
| | | 0.44 | 96 | 38 | 116 | 39 | 88 | 60 | 139 | 186 | 42405 | 11501 |
| Baffin Bay | Campbell & Loring, 1980 | | 56 | 12 | 12 | 11 | 19 | | 34 | 63 | | 260 |
| | | | 109 | 32 | 81 | 42 | 94 | | 106 | 155 | | 9450 |
| Beaufort lagoon | Naidu et al., 2005 | 0.19 | 56 | 11 | 16 | | 27 | 7 | 48 | 87 | 21700 | 182 |
| | | 0.62 | 84 | 29 | 55 | | 54 | 20 | 111 | 136 | 35600 | 3132 |
| Beaufort shelf | Trefry & Neff, 2013; 2019 | 0.03 | 13 | 3 | 4 | | 6 | 1 | 2 | 25 | 7200 | 62 |
| | | 0.75 | 106 | 22 | 46 | | 48 | 116 | 136 | 174 | 69400 | 3390 |
| Bering / Chukchi Sea | Lu & Kang, 2017; Zheng et al., 2022 | 0.14 | 30 | 7 | 4 | | 9 | 2 | 22 | | | |
| | | 0.71 | 140 | 28 | 94 | | 164 | 38 | 391 | | | |
| Chukchi Sea | Cai et al., 2011 * | 0.09 | 9 | 1 | 3 | | | | 21 | 33 | | |
| | | 0.92 | 47 | 15 | 49 | | | | 168 | 187 | | |
| Barents Sea | Budko et al., 2017; 2022 | 0.04 | 20 | 4 | 3 | 2 | 7 | 4 | 40 | 27 | 15300 | 130 |
| | | 0.5 | 101 | 23 | 31 | 25 | 45 | 29 | 108 | 210 | 54000 | 490 |
| Kara Sea | Budko et al., 2022; Loring et al.,1998 | 0.01 | 13 | 6 | 2 | 0 | 4 | 4 | 8 | 22 | 5600 | 90 |
| | | 0.45 | 149 | 23 | 96 | 31 | 72 | 140 | 213 | 210 | 69100 | 27100 |
| Laptev & East Siberian Seas | Budko et al., 2022 | 0.11 | 72 | 13 | 18 | 10 | 21 | 19 | 106 | 63 | 38500 | 420 |
| | | 0.56 | 106 | 26 | 36 | 29 | 60 | 59 | 206 | 199 | 56000 | 9100 |
| Laptev Sea | Holemann et al., 1999 | 0.07 | 78 | 16 | 21 | 18 | 36 | 17 | 111 | 128 | 42000 | 500 |
| | | 0.09 | 106 | 26 | 31 | 26 | 56 | 41 | 121 | 208 | 56000 | 1500 |
| Krossfjorden, Svalbard | Choudhary et al., 2020 | 0.2 | 12 | 9 | 19 | 12 | 18 | | 50 | | | |
| | | 0.65 | 20 | 15 | 24 | 17 | 27 | | 83 | | | |
| Kongsfjorden, Svalbard | Lu et al., 2013 | 0.13 | 54 | 11 | 21 | 12 | 22 | | 50 | | | 300 |
| | | 0.63 | 82 | 37 | 37 | 22 | 35 | | 199 | | | 683 |
| **UCC** | Taylor & McLennan, 1985; McLennan, 2001 | 0.098 | 35 | 20 | 25 | 10 | 20 | 2 | 71 | 60 | 35000 | 600 |
| **PAAS** | | | 110 | 20 | 50 | 23 | 55 | | 85 | 150 | 50 500 | 850 |
| **TEL** | CCME, 1999 | 0.7 | 52 | 30 | 19 | | 16 | 7 | 124 | | | |
| **PEL** | | 4.21 | 160 | 112 | 108 | | 43 | 42 | 271 | | | |

## 2.11 SUPPLEMENTARY MATERIAL (REFERENCES)


Brice, C., Montero-Serrano, J.-C., & Saint-Louis, R. (2025). Regional geochemical survey of Canadian Arctic sediments: insights into provenance, sediment dynamics and trace metal enrichment. *Applied Geochemistry, 189*, 106432. https://doi.org/https://doi.org/10.1016/j.apgeochem.2025.106432

Budko, D. F., Demina, L. L., Lisitzin, A. P., Kravchishina, M. D., & Politova, N. V. (2017). Occurrence forms of trace metals in recent bottom sediments from the White and Barents Seas. *Doklady Earth Sciences, 474*(1), 552-556. https://doi.org/10.1134/S1028334X17050014

Budko, D. F., Demina, L. L., Travkina, A. V., Starodymova, D. P., & Alekseeva, T. N. (2022). The Features of Distribution of Chemical Elements, including Heavy Metals and Cs-137, in Surface Sediments of the Barents, Kara, Laptev and East Siberian Seas. *Minerals, 12*(3), 328. https://www.mdpi.com/2075-163X/12/3/328

Cai, M., Lin, J., Hong, Q., Wang, Y., & Cai, M. (2011). Content and distribution of trace metals in surface sediments from the northern Bering Sea, Chukchi Sea and adjacent Arctic areas. *Marine Pollution Bulletin, 63*(5-12), 523-527.

Campbell, J. A., & Loring, D. H. (1980). Baseline levels of heavy metals in the waters and sediments of Baffin Bay. *Marine Pollution Bulletin, 11*(9), 257-261. https://doi.org/https://doi.org/10.1016/0025-326X(80)90314-8

Choudhary, S., Nayak, G. N., & Khare, N. (2020). Source, mobility, and bioavailability of metals in fjord sediments of Krossfjord-Kongsfjord system, Arctic, Svalbard. *Environmental Science and Pollution Research, 27*(13), 15130-15148. https://doi.org/10.1007/s11356-020-07879-1

Holemann, J. A., Schirmacher, M., Kassens, H., & Prange, A. (1999). Geochemistry of Surficial and Ice-rafted Sediments from the Laptev Sea (Siberia). *Estuarine, Coastal and Shelf Science, 49*(1), 45-59. https://doi.org/https://doi.org/10.1006/ecss.1999.0485

Loring, D. H., Dahle, S., Naes, K., Dos Santos, J., Skei, J. M., & Matishov, G. G. (1998). Arsenic and other Trace Metals in Sediments from the Kara Sea and the Ob and Yenisey Estuaries, Russia. *Aquatic Geochemistry, 4*(2), 233-252. https://doi.org/10.1023/A:1009691314353

Lu, Z. B., Cai, M., Wang, J., Yin, Z., & Yang, H. (2013). Levels and distribution of trace metals in surface sediments from Kongsfjorden, Svalbard, Norwegian Arctic. *Environmental Geochemistry and Health, 35*(2), 257-269. https://doi.org/10.1007/s10653-012-9481-z

Lu, Z. B., & Kang, M. (2018). Risk assessment of toxic metals in marine sediments from the Arctic Ocean using a modified BCR sequential extraction procedure. Journal of *Environmental Science and Health, Part A, 53*(3), 278-293. https://doi.org/10.1080/10934529.2017.1397443

McLennan, S. M. (2001). Relationships between the trace element composition of sedimentary rocks and upper continental crust. *Geochemistry, Geophysics, Geosystems, 2*(4). https://doi.org/https://doi.org/10.1029/2000GC000109

Naidu, A., Kelley, J., Misra, D., & Venkatesan, M. (2005). Trace metals and hydrocarbons in sediments of the Beaufort Lagoon, Northeast Arctic Alaska, exposed to long-term natural oil seepage, recent anthropogenic acivities and pristine conditions. Final Report to Coastal Marine Institute, Univ. Alaska Fairbanks, Fairbanks, AK. Press.

Taylor, S. R., & McLennan, S. M. (1985). *The continental crust: Its composition and evolution*. Blackwell Scientific Pub.,Palo Alto, CA. https://www.osti.gov/biblio/6582885

Trefry, J. H., Dunton, K. H., Trocine, R. P., Schonberg, S. V., McTigue, N. D., Hersh, E. S., & McDonald, T. J. (2013). Chemical and biological assessment of two offshore drilling sites in the Alaskan Arctic. *Marine Environmental Research, 86*, 35-45. https://doi.org/https://doi.org/10.1016/j.marenvres.2013.02.008

Trefry, J. H., & Neff, J. M. (2019). Effects of offshore oil exploration and development in the Alaskan Beaufort Sea: A three-decade record for sediment metals. Integrated *Environmental Assessment and Management, 15*(2), 209-223. https://doi.org/https://doi.org/10.1002/ieam.4069

Zheng, H., Ren, Q., Zheng, K., Qin, Z., Wang, Y., & Wang, Y. (2022). Spatial distribution and risk assessment of metal(loid)s in marine sediments in the Arctic Ocean and Bering Sea. *Marine Pollution Bulletin, 179*, 113729. https://doi.org/https://doi.org/10.1016/j.marpolbul.2022.113729

# CHAPITRE 3
# CARACTÉRISATION CHIMIQUE ET ÉVALUATION DE LA CONTAMINATION DANS LES SÉDIMENTS CÔTIERS DE SURFACE DES COMMUNAUTÉS DE L'ARCTIQUE CANADIEN

## 3.1 RESUME EN FRANÇAIS DU TROISIEME ARTICLE

L'état actuel de la contamination par les métaux a été étudié dans les environnements côtiers à proximité de six communautés de l'Arctique canadien. Des sédiments côtiers de surface ont été prélevés au cours des étés 2022-2023 et analysés afin de déterminer leur granulométrie et leurs concentrations en éléments majeurs et traces. La composition élémentaire a d'abord été déterminée par fluorescence X à dispersion d'énergie afin de déterminer les concentrations totales. Une sélection d'échantillons a ensuite été soumise à une digestion partielle à l'acide et analysée par spectrométrie de masse à plasma inductif à triple quadripôle afin de quantifier les concentrations extractibles à l'acide. Les résultats obtenus à Tuktoyaktuk, Resolute Bay, Grise Fiord et Qikiqtarjuaq indiquent des niveaux naturels de métaux, mais des effets biologiques néfastes occasionnels sur la faune aquatique sont à prévoir à Tuktoyaktuk en raison de la teneur naturellement élevée en métaux du fleuve Mackenzie. Les sédiments de Pond Inlet présentent des compositions élémentaires variables qui sont influencées par les lithologies le long de la côte et d'éventuelles sources anthropiques localisées. Près de Kugluktuk, les résultats ont révélé des concentrations totales élevées de V et de Cr (< 50-1160 et < 100-1700 µg/g), qui proviennent probablement de matériaux érodés provenant d'intrusions ultramafiques transportés par la rivière Coppermine, ainsi que des décharges et eaux usées municipales. Cependant, les concentrations en métaux extractibles par l'acide sont nettement inférieures (Cr < 180 µg/g, V < 640 µg/g), ce qui suggère que les niveaux élevés de métaux sont probablement liés aux phases détritiques et que leur mobilité et leur biodisponibilité sont très limitées. Cette étude souligne l'importance de distinguer la

concentration totale en métaux de la fraction biodisponible et de comprendre la dynamique locale des sédiments, afin d'aider les communautés du Nord à gérer leur environnement côtier et à préserver la qualité des ressources alimentaires locales.

## 3.2 CHEMICAL CHARACTERIZATION AND CONTAMINATION ASSESSMENT IN SURFACE COASTAL SEDIMENTS OF CANADIAN ARCTIC COMMUNITIES

The current state of metal contamination was studied in the coastal environments near six communities in the Canadian Arctic. Coastal surface sediments were collected during summers 2022-2023 and analyzed for grain size and major and trace element concentrations. The elemental composition was first determined via energy dispersive X-ray fluorescence to determine the total concentrations. A selection of samples was then subjected to partial acid digestion and analyzed via triple quadrupole inductively coupled plasma–mass spectrometry to quantify the acid-extractable concentrations. The results from Tuktoyaktuk, Resolute Bay, Grise Fiord and Qikiqtarjuaq indicate natural metal levels, but occasional adverse biological effects on aquatic fauna are expected to occur in Tuktoyaktuk due to naturally elevated metal content in the Mackenzie River. Sediments from Pond Inlet present variable elemental compositions that are influenced by the lithologies along the coast and possible localized anthropogenic sources. Near Kugluktuk, results revealed high total concentrations of V and Cr (< 50-1160 and < 100-1700 μg/g), which probably originated from eroded material from ultramafic intrusions carried by the Coppermine River, and municipal landfills and sewage. However, the acid-extractable metal concentrations are significantly lower (Cr < 180 μg/g, V < 640 μg/g), suggesting that the high metal levels are probably related to detrital phases and that their mobility and bioavailability are very limited. This study highlights the importance of discriminating the total metal concentration from the bioavailable fraction and understanding local sediment dynamics, to support Northern communities in managing their coastal environment and preserving the quality of country food resources.

## 3.3 INTRODUCTION

The Canadian Arctic (CA) is a vast territory, but less than 1% of Canada's population resides there. Pressures from urban and industrial centers are thus very limited. However, the CA, similar to other Arctic regions, is subject to anthropogenic metal(loid) contamination

(AMAP, 2005, 2011, 2021a, 2021b). The long-range atmospheric transport of contaminants emitted worldwide has been identified as the main concern for the Arctic (Macdonald et al., 2000; Macdonald et al., 2005). Consequently, pollution has been monitored in the last decades through aerosols measurements (Becagli et al., 2020; Li & Cornett, 2011; Li et al., 2003; Li et al., 2009) and atmospheric deposition in lakes (Bindler et al., 2001; Korosi et al., 2018; Michelutti et al., 2009) and in snow and ice (Krachler et al., 2005; Macdonald et al., 2017). Closer pollution sources within the Arctic and pan-Arctic regions also contribute to high metal levels in the environment. It includes legacy sources, such as closed mines or former oil exploration platforms (Langer et al., 2023), and new sources, such as increasing commercial shipping and industrial development. In northern Canada, metal contamination has been measured in sediments near mines (Pelletier et al., 2020) and offshore drilling sites (Naidu et al., 2012; Trefry & Neff, 2019). Overall, trace metal enrichments were measured in Ba, Pb, Cr, Cu Hg and V, close to the sites but decreased with distance. However, these legacy contaminants that accumulate in sediments, soil and biomass can also be remobilized through wildfires (Sutton et al., 2024) and permafrost thaw (Miner et al., 2021; O'Donnell et al., 2024). The particulate matter emitted by ships represents a significant source of contaminants in the Arctic that require monitoring (Conca et al., 2019). This has raised emerging concerns for the CA, where increasing maritime traffic along corridors near communities and protected areas poses environmental risks (Chénier et al., 2017; Dawson et al., 2018).

On a local scale, trace metal contamination in northern communities has drawn less attention. They are sparse and have low populations compared with southern cities; therefore, they are considered a lower priority. However, in addition to long-range and regional sources, local sources have substantial impacts. Traditional fishing and harvesting of marine resources by the local people make them more vulnerable to metal pollution. Previous studies have detected chemical contaminant issues linked to local human activities in the Arctic, including pharmaceuticals and perfluorinated alkyl substances (Gunnarsdóttir et al., 2013; Stroski et al., 2020), and polycyclic aromatic hydrocarbons and trace metals (Bartley et al., 2024; Corminboeuf et al., 2021; Pedersen et al., 2015; Samuelson, 1998). These studies, along with

others, have identified the management of solid waste and sewage as major contributors to contamination in the Arctic. In similar settings, trace metal contamination linked to paints, sewage and fossil fuel combustion has been observed in coastal sediments and soil near small localized human settlements in Antarctica (Guerra et al., 2011; Santos et al., 2005).

Despite these observations and concerns from northern Canadian communities, the full extent of trace metal contamination remains largely unknown, although much efforts were directed to the study of some priority metal contaminants, in particular mercury (AMAP, 2021b). Coastal sediments near communities have accumulated past and present metal inputs from both local and regional sources, as well as from natural and anthropogenic sources. They can thus provide a good indicator of the current state of metal pollution. In this context, the marine coastal environments of six Canadian arctic communities (Tuktoyaktuk, Kugluktuk, Resolute, Grise Fiord, Pond Inlet and Qikiqtarjuaq) were investigated. Additionally, sediments from Milne Inlet, which is close to Pond Inlet, were also studied to evaluate the impact of the activity of the Mary River Mine on the community. The surface sediment samples were analyzed via an energy dispersive X-ray fluorescence (ED-XRF) for total concentration measurements, which provide information on major elements and some trace elements and allow a comprehension of the nature and sources of coastal metal contamination in sediments. The samples were subsequently analyzed by triple quadrupole inductively coupled plasma–mass spectrometry (ICP-QQQ) following partial acid digestion, which attacks and dissolves most phases with which the trace metals are bound. This technique quantify the metal content that is more mobile and bioavailable, hereby referred to as extractable concentrations, and thus provide information on the metal fraction originating from human sources and/or that are sensible to environmental disturbances. Some silicates, aluminosilicates and heavy minerals are partially attacked by this digestion, but most remain undissolved and are not measured (Xu et al., 2012). When combined with ED-XRF analysis, which provides concentration data linked to these minerals, this approach offers a comprehensive framework for studying sediment dynamics and metal contamination.

The purpose of this study is primarily to assess metallic pollution in surface sediments of northern Canadian communities by determining and understanding the distribution of major and trace elements. The findings will help identify areas that may pose ecotoxicological risks to marine fauna and, consequently, to potentially affect country food resources. In addition, the study seeks to improve our understanding of the sources, transport mechanisms, and bioavailability of these elements.

## 3.4 METHODOLOGY

### 3.4.1 Sampling sites

Surface sediment samples were collected along the coasts of Tuktoyaktuk (n=12), Kugluktuk (n=49), Resolute (n=11), Grise Fiord (n=11), Pond Inlet (n=30) and Qikiqtarjuaq (n=7). Samples were also collected in Milne Inlet, near Ragged Island (n=6) and Mary River port (n=4; Fig. 33 & 34). Approximately the first 5 cm of sediments were sampled using a Petite Ponar grab deployed manually. Based on sedimentation rates measured near Iqaluit (Bartley et al., 2024), and Kugluktuk and Pond Inlet (Letaief et al., 2021), the homogenized sediment samples represent at most the last 10-15 years. In Kugluktuk and Pond Inlet, sampling was conducted in August 2022 and 2023, respectively, with the assistance of local guides. Sampling near Qikiqtarjuaq was done during Leg 2 of the 2022 Amundsen Expeditions, while samples from Grise Fjord and Resolute Bay were collected during Leg 3 of the 2023 Amundsen Expeditions. Surface sediment samples from the Tuktoyaktuk Harbor and from Milne Inlet were acquired through separate research initiatives led by Alfred Wegener Institute (van Crimpen et al., 2025) and ISMER-UQAR (Dhifallah et al., 2022), respectively.

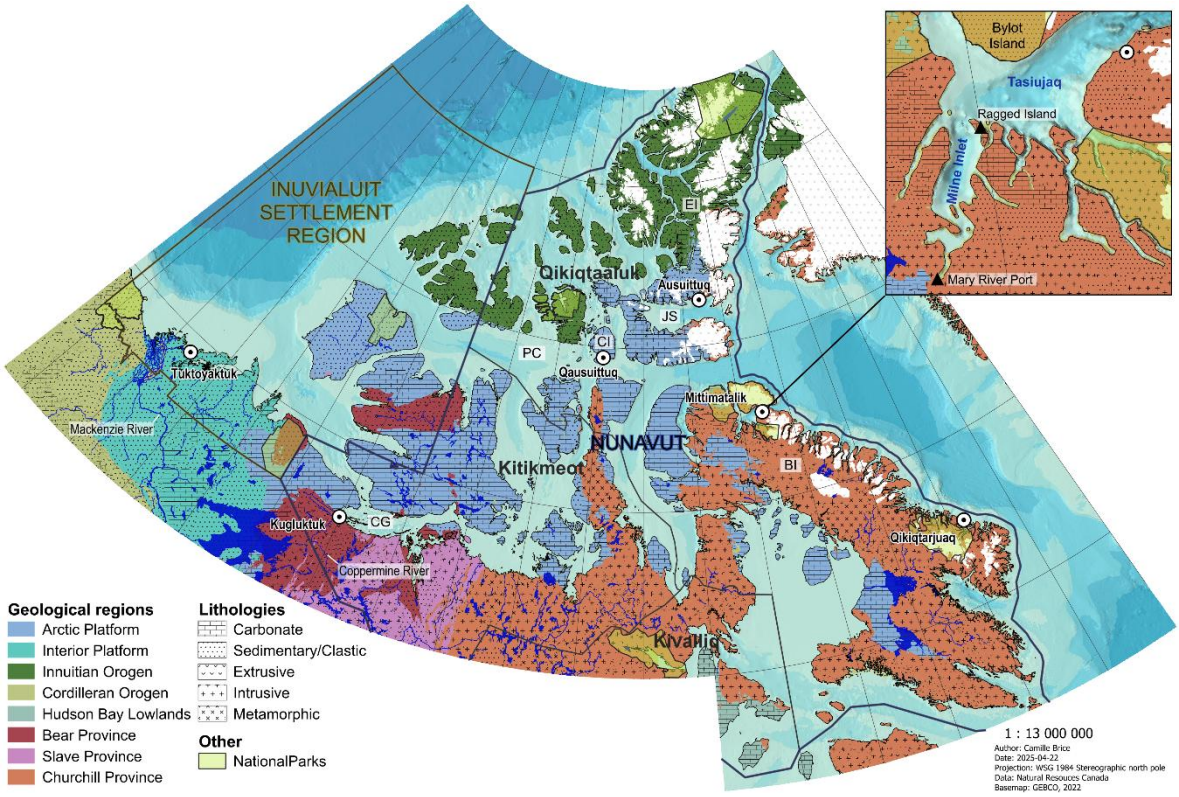


Figure 33. Geological map on the Canadian Arctic showing the locations of the Inuit communities, identified by their name in Inuktitut, and Milne Inlet investigated in this study. BI: Baffin Island; CG: Coronation Gulf; CI: Cornwallis Island; EI: Ellesmere Island; JS: Jones Sound; PC: Parry Channel.

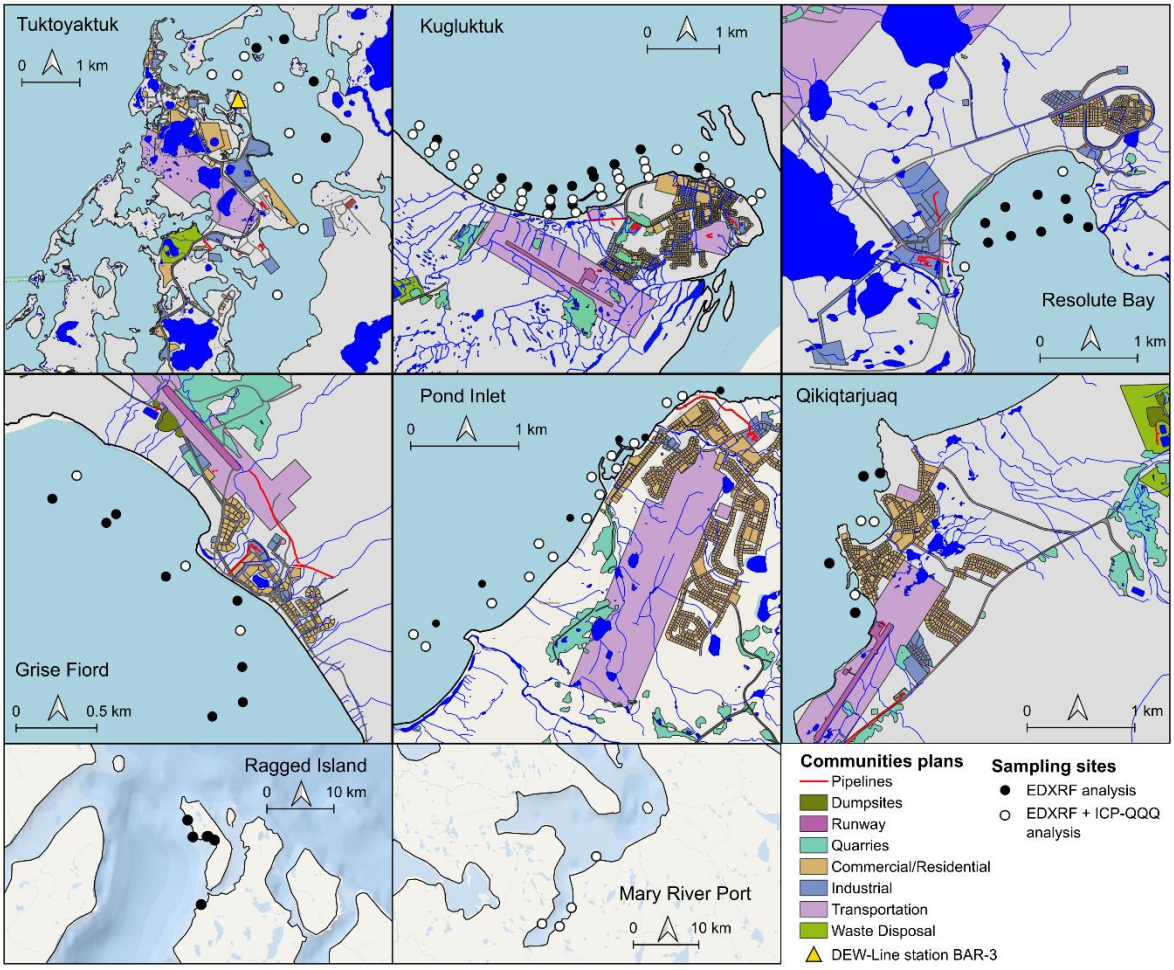


Figure 34. Maps of the six Inuit communities, Ragged Island, and Mary River Port, showing the locations of sediment samples analyzed in this study alongside the respective community plans. Black dots indicate samples analyzed by energy-dispersive X-ray fluorescence (ED-XRF) only, while white dots represent samples analyzed by both ED-XRF and partial acid digestion followed by triple quadrupole inductively coupled plasma mass spectrometry (ICP-QQQ).

Tuktoyaktuk is an Inuvialuit hamlet of 937 people (Statistics Canada, 2023) situated in the Northwest Territories, in the Inuvik region (Fig. 33). It sits on the Mackenzie River delta, in Kugmallit Bay. Tuktoyaktuk used to be a home base for workers in oil exploration between 1970 and 1986. During this time, Esso, Dome, Imperial, Gulf, etc. operated large oil exploration projects in the Beaufort Sea (Adams, 1998). The hamlet was also the location of the Distant Early Warning (DEW) Line site BAR-3 (Fig. 34) between the late 1950s and

1993. Many of the oil companies and the BAR-3 site disposed of their waste in the municipal landfill (Adams, 1998). BAR-3 is notably qualified as a high priority for action by the Federal Contaminated Sites Inventory (Government of Canada, 2022). The solid waste facility is located 3 km south of the hamlet (Fig. 34). Before 1984, the sewage lagoon was next to the landfill but was relocated 3 km south of it. The natural harbor of Tuktoyaktuk is sheltered by Tuktoyaktuk Island and originated from a river valley formed during the last deglaciation and flooded afterward with relative sea level rise. The hamlet is experiencing high coastal erosion rates because of exposure to storm surges and permafrost thaw (Whalen et al., 2022). The geology of the region is dominated by sandstone and siltstone from the interior platform, whereas the surficial geology is characterized by glaciofluvial material with numerous thermokarst lakes and peatlands (Harrison et al., 2011).

Kugluktuk is located on the western side of the Coppermine River delta, on the Canadian mainland shore of the Coronation Gulf (Fig. 33). Located in the Kitikmeot region, it is Nunavut's westernmost community. Its population is approximately 1400 people according to the 2021 Census of Population (Statistics Canada, 2023). Sewage and solid waste disposal sites are located west of the airport, upstream of streams connected to the coast (Fig. 34). The wastewater system is composed of a wastewater stabilization pond (WSP) discharged once every summer into an engineered constructed wetland before it reaches the Coronation Gulf. The hamlet lies on mafic igneous sills (i.e., diorite, gabbro) intruding sedimentary rocks of the Hornby Bay and Amundsen Basins (Dredge, 2001; Rainbird et al., 2020). Surficial sediments, which are discontinuous around the community, consist mainly of marine sand and silt deposits (Smith, 2013). The Coppermine River discharges great sediment loads to the coast, along with important dissolved metal concentrations (Coulombe-Pontbriand et al., 1998). The high sediment transport capacity during high flow has a great influence on the shoreline of Kugluktuk.

Resolute Bay, or Qausuittuq in Inuktitut, is located on Cornwallis Island, facing the Parry Channel (Fig. 33). It is in the Qikiqtaaluk region. It is the second northernmost community of Canada, after Grise Fiord and had a population of 183 in 2021 (Statistics

Canada, 2023). According to the 2024-2025 Integrated Community Sustainability Plans, the sewage treatment plant needs to be replaced (ICSP, 2024). Resolute houses an Arctic training facility for Canadian armed forces and a research station for the Polar Continental Shelf Program from Natural Resources Canada. The Polaris Mine, an underground lead–zinc mining site, was located on Little Cornwallis Island, approximately 100 km from the community (Donald, 2005). It was in operation between 1982 and 2002. The carbonates of the Arctic platform mainly compose the rocks around Resolute Bay.

Grise Fiord, or Ausuittuq in Inuktitut, is the northernmost community in both Nunavut and Canada. It is located at the southern tip of Ellesmere Island, on the northern shore of Jones Sound. This small hamlet of 144 residents (Statistics Canada, 2023) is surrounded by mountains. It has a single-cell WSP located between the airport and the coast, approximately 670 m northwest of the community (Fig. 34). The WSP discharges wastewater into a tundra wetland before reaching Jones Sound (Centre for Water Resources Studies, 2015). The local geology is characterized by Proterozoic granite and tonalite from the Ellesmere-Inglefield belt (Harrison et al., 2011; Harrison et al., 2014), with Paleozoic carbonates, such as dolostone and limestone, dominating the area north of the intrusive rocks.

Pond Inlet, Mittimatalik in Inuktitut, is situated on northern Baffin Island in the Qikiqtaaluk region. It lies on the southern shore of Tasiujaq (Eclipse Sound), which separates Baffin Island from Bylot Island, and is bordered by the Sirmilik National Park (Fig. 33). The population of Pond Inlet in 2021 was 1555 residents (Statistics Canada, 2023). Pond Inlet is the most visited community by cruise ships in Nunavut (ECCC, 2024). The solid waste and sewage infrastructures are located approximately 1.4 km east of the hamlet. The community has a single-cell WSP discharging annually directly in the Tasiujaq (Centre for Water Resources Studies, 2015). Northern Baffin Island is shaped by the Archean basement of the Rae Craton, which mainly comprises tonalitic-monzogranitic gneiss hosting subsequent quartzofeldspathic intrusions. The Pond Inlet area is characterized by monzogranite to granodiorite intrusions containing potassic feldspar crystals and mafic minerals such as garnet, biotite, orthopyroxene, hornblende and magnetite. Glacial till and other Quaternary

deposits cover the bedrock outside of the community (Skipton et al., 2018). Tasiujaq is continuously supplied with sediment carried from glaciers on both northern Baffin and Bylot Islands.

In addition to the presence of the hamlet in the region, the Mary River Mine and its shipping port are installed in Milne Inlet, approximately 80 km west of Pond Inlet (Fig. 33). The outer inlet is composed of Proterozoic carbonates and clastic rocks and the inner inlet, where the port is located, is composed of Archean gneiss (Harrison et al., 2011). The Mary River Mine, 100 km southeast of the port, sits on the Mary River Group and features Archean mafic to intermediate volcanic rocks with iron formations. The mine is an open pit that extracts high-grade iron ore since 2014 and is operated by Baffinland Iron Mines Corporation (Rodon & Bouchard, 2024). Iron is transported via a tote road to the Milne Inlet port facility and is then shipped to European destinations. Shipping together with tourism results in the Tasiujaq region recording the highest maritime traffic of the Canadian Arctic (ECCC, 2024).

Qikiqtarjuaq is located on Broughton Island, next to the coast of Baffin Island, and is part of the Qikiqtaaluk region (Fig. 33). It is a small hamlet of approximately 600 inhabitants (Statistics Canada, 2023) that sits at the entrance of the Auyuittuq National Park. Qikiqtarjuaq is equipped with a WSP and a wetland located 3 km northeast of the hamlet (Fig. 34). The regional geology is mainly composed of metamorphosed granitic rocks from the Cumberland batholith of the Rae Craton (Sanborn-Barrie et al., 2013).

### 3.4.2 Laboratory analysis

Grain size analysis was performed on the <2 mm fraction following the instrumental conditions outlined in Belzile and Montero-Serrano (2022). For this purpose, an aliquot of the bulk fraction of each sediment sample was treated with 5 to 10 mL of 30% $H_2O_2$ to remove organic matter. The dry residues were then diluted with ~30 mL of sodium hexametaphosphate (20% v/v), sieved at <2 mm, and disaggregated via an in-house rotator for 12 hours prior to the particle size measurements. The samples were measured with a Malvern PANalytical Mastersizer 3000 laser diffraction grain size analyzer equipped with a

HydroLV module. The grain size composition (clay, silt, and sand) and statistical parameters ($D_{90}$) were extracted via GRADISTAT software version 9.1 (Blott & Pye, 2001).

For elemental geochemistry analysis, all sediment samples were initially wet-sieved through a 150-µm Nitex® mesh using distilled water. This process was performed to minimize spatial biases in elemental concentrations associated with bulk grain size variations. Some samples from Kugluktuk and Pond Inlet were excluded from the analysis because their sediment particle sizes exceeded 150 µm. Ultimately, 45 samples from Kugluktuk and 22 from Pond Inlet contained sufficient fractions of particles smaller than <150 µm and were retained for further analysis. These samples were then oven dried (<60°C) for 12 h, followed by crushing and homogenization with an agate mortar.

The <150 µm sediment fractions were measured for eight major elements (Mg, Al, Si, K, Ca, Ti, Mn and Fe) and five trace elements (V, Cr, Zn, Sr and Zr) with a Malvern PANalytical Epsilon 3-XL ED-XRF. For this, the loss on ignition (LOI) was initially determined gravimetrically by weighing an aliquot of 2 g before and after heating it for 4 h at 950°C. Following the LOI, ~1.1 g of ignited sample was mixed with 5.5 g of lithium tetraborate (CLAISSE, pure, 99% $Li_2B_4O_7$, and 1% LiBr) and fused with a CLAISSE M4 Fluxer automated fusion furnace to form glass disks. The glass disks were analyzed for elemental geochemistry, and the acquired ED-XRF spectra were treated with the Malvern PANalytical Omnian standardless software package calibration. The acquired data are expressed as dry weight percentage mass (wt.%) for major elements and micrograms per gram (µg/g) for trace elements. Procedural blanks were prepared with synthesized silicon oxide powder (99.999% $SiO_2$; American Elements; SI-OX-05M-P.325M). The blank concentrations were less than the detection limit (DL) for most major and trace elements, except for Al (~0.56%; Table 14). The Al contamination, probably derived from the ceramic crucibles used for LOI determination, was corrected by subtracting the mean Al values of the procedural blank concentrations in the sediment samples. The accuracy of the overall method, including digestion and glass disk preparation, was assessed by analyzing the USGS-certified materials SDC-1 and BCR-2 (Table 15). The results obtained for these reference

materials are in good agreement with reference values from the GeoREM database (http://georem.mpch-mainz.gwdg.de/). Except for Zr in the analysis of SDC-1, the recovery values (accuracy) for all the measured elements were between 91 and 116%, which corresponds to the usual acceptable deviation limits (Thompson et al., 2002). The reproducibility of ED-XRF, determined through replicate analyses of USGS standards SDC-1 and BCR-2 performed every 9 samples, showed a relative standard deviation (RSD, 1σ) of <1% for major elements and <13% for trace elements. Cr yielded less satisfactory results with the certified materials, showing values of 126 ± 14% for SDC-1 and 226 ± 59% for BCR-2. These suboptimal results are likely due to the certified values being below the DL, which is 100 μ/g.

Based on the data obtained by ED-XRF, a selection of sediment samples from all the communities were made for trace element measurement (Fig. 34). The concentration of seven major (Mg, Al, K, Ca, Ti, Mn and Fe), 11 trace elements (Cr, Co, Ni, Sc, Cu, Zn, V, As, Sr, Cd and Pb) and rare earth elements (14 lanthanides + Y) in the sediments was determined by ICP-QQQ after partial acid digestion based on a slightly modified version of the US EPA Method 3051A (US EPA, 2007). This digestion method primarily targets trace metals associated with reactive components like organic matter, sulfides, Fe-Mn (oxyhydr)oxides, carbonates, and hydrated aluminosilicates, while leaving refractory silicates and heavy minerals unaffected (Xu et al., 2012). Briefly, approximately 50 mg of the dry <150 μm sediment fraction was mixed with 2 mL and 6 mL of concentrated TraceMetal Grade (ThermoScientific) HCl and $HNO_3$, respectively. The samples were then digested using CEM EasyPrep vessels and CEM Mars 5 microwave system under the following conditions: ramp time = 18 min, temperature = 175°C, hold time = 4 min, maximum pressure = 400 PSI, and power = 1600 W (75%). The digested samples were diluted with Milli-Q water to a final concentration of 2% $HNO_3$ and <0.1% HCl. Next, the concentrations of trace metals were determined using an Agilent 8900 triple quadrupole inductively coupled plasma mass spectrometer (ICP-QQQ) at the Laboratoire d'Analyses Environnementales (LAE, Université du Québec à Montréal). The Falcon tubes and laboratory glassware were precleaned with 10% $HNO_3$, and EasyPrep vessels were soaked in 0.2 M $HNO_3$ for 12 h prior

to digestion analysis. For every 8 samples, one procedural blank was analyzed following the same method (Table 16). To account for background contamination, blank concentrations were subtracted from the sample values measured within the same batch. Quality control was assessed with the certified reference material TILL-3. Good recovery rates (80–120%, n =4) were obtained for all the elements (Table 17a), except for Co (78%) and Cu (77%). Rare earth elements and Y (REY) are not certified for partial acid digestion, but they have been used with moderation. Recoveries were determined with certified values of total concentration to provide an estimate (Table 17b).

### 3.4.3 Data processing

A centered log-ratio transformation was performed on the data (Aitchison, 1982) using the R package 'compositions' (van den Boogaart et al., 2023) before performing a K-means clustering analysis, utilizing the R package 'stats' (R Core Team, 2024). The clustering quality was validated through a silhouette plot generated by the R package 'factoextra'(Kassambara & Mundt, 2020), with negative values indicating questionable or incorrect assignments. Subsequently, a robust principal component analysis (rPCA) was carried out using the R package 'robCompositions' to identify elemental groupings with analogous relative variation patterns (Filzmoser P, 2018; Templ M, 2011). Spatial interpolation was performed with empirical Bayesian kriging (EBK) with ArcGIS Pro (Krivoruchko, 2012). The Canadian Sediment Quality Guidelines (CSQGs) for the Protection of Aquatic Life (CCME, 1999) were used to provide a first estimate of the contaminant level and the associated risk of adverse effects on aquatic life. The CSQGs characterize the metal concentrations into two main levels: the threshold effect limit (TEL) and the probable effect limit (PEL). Adverse biological effects are expected to occur only rarely below the TEL, occasionally between the limits, and frequently above the PEL. Because no data are available for Ni in the CSQGs, NOAA guidelines were used (Buchmann, 2008). Notably, the PELNOAA for Ni is set to a lower level than the average shale concentration (Turekian & Wedepohl, 1961). The natural values used for comparison are the upper continental crust (UCC; Taylor & McLennan, 1985), the Post-Archean Australian shale (PAAS; Pourmand et al., 2012; Taylor &

McLennan, 1985) and the median composition of the surface sediments of the Canadian Arctic obtained via ED-XRF (Brice et al., 2025) and partial acid digestion (Brice et al., 2026). Finally, a Spearman correlation matrix was applied to the elemental data using the R package 'corrplot' (Wei et al., 2017) to analyze the relationships between major and trace metals acquired by ED-XRF and $D_{90}$ sediment grain size data. Coefficients with p-values exceeding 0.05 were excluded from the matrix.

## 3.5 RESULTS AND DISCUSSION

Element concentrations obtained by ED-XRF and ICP-QQQ, as well as reference values are presented in Table 18.

### 3.5.1 General sedimentological and geochemical characteristics of coastal sediments

In Tuktoyaktuk, harbor sediments are silty and exhibit a uniform grayish-brown color (Munsell color 2.5Y5/2). They are compositionally similar to PAAS, as shown by the Al-Si-Ca and the Herron (1988) diagrams (Fig. 35). Trace metal and Al concentrations (6.9–9.5 wt.%) are higher than in most other communities (Fig. 36). V ranges from 169 to 264 µg/g, with concentrations decreasing from the inner harbor toward the coast, a trend also observed for Cr and Fe. Zn concentrations are elevated, with most samples exceeding the TEL, and the highest concentrations occur near the hamlet and Tuktoyaktuk Island (Fig. 43). Eight samples were analyzed for acid-extractable metals; all exceeded the TEL for Cr, As, Cu, and Zn (Fig. 36). None surpassed the PEL, except Ni, which exceeded it in all samples but remained below the PAAS benchmark.

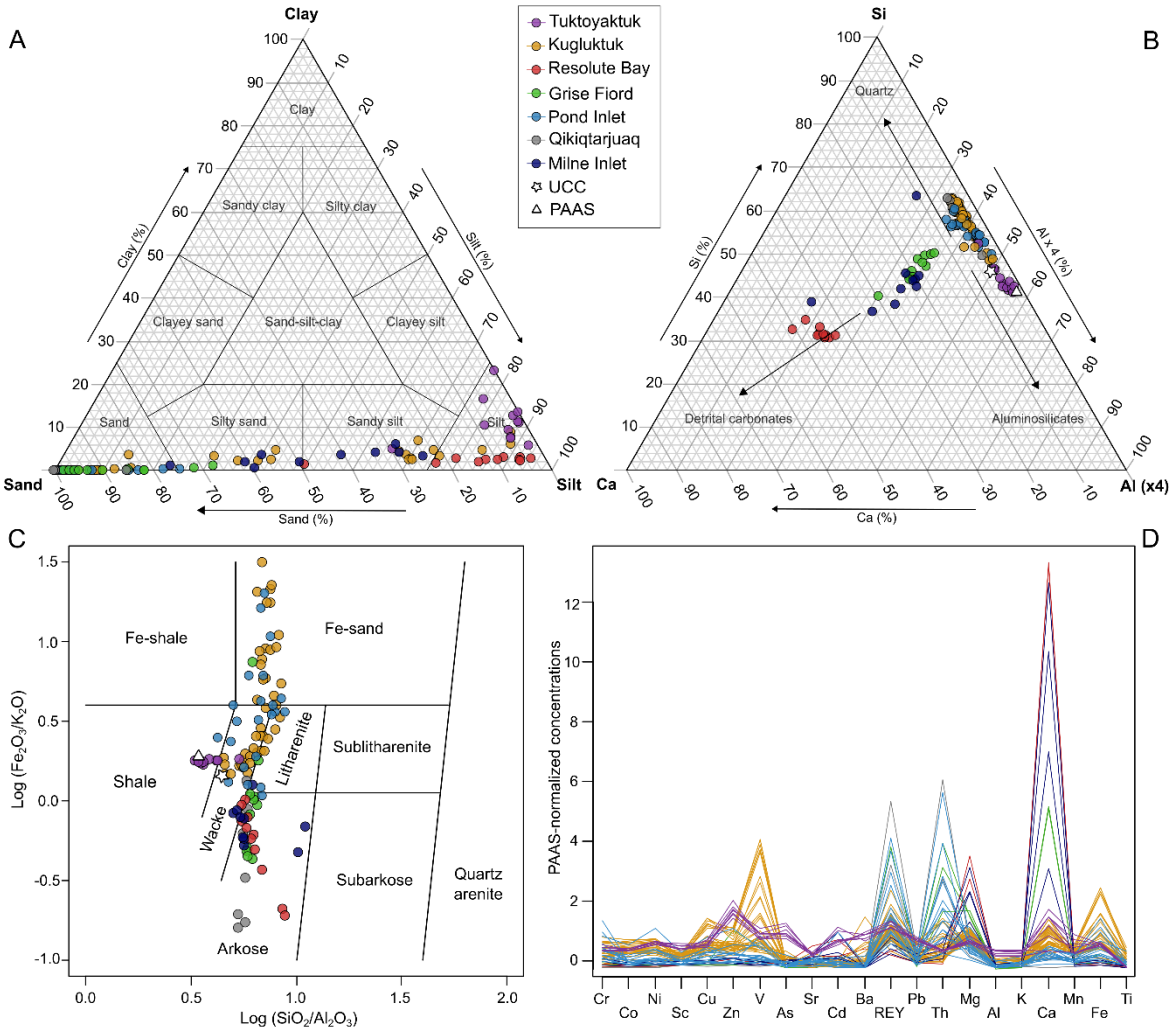


Figure 35. (A) Ternary diagram illustrating the sand–silt–clay composition of the <150 µm fraction in coastal sediments,classified according to Shepard's sediment texture classification (Shepard, 1954). (B) Si–Ca–Al ternary diagram shows the overall composition of surface sediments from the Inuit communities in comparison with Post-Archaean Australian Shale (PAAS; Taylor & McLennan, 1985; Pourmand et al., 2012) and upper continental crust (UCC; Taylor, 1985). (C) Herron (1988) geochemical classification diagram. (D) diagram of acid-extracted concentrations normalized to PAAS.

Sediments along the Kugluktuk coast show high variability in sedimentological and chemical properties. A bimodal grain size distribution is observed, with silty sand and sand near the river mouth and silt dominating elsewhere (Fig. 35A & 44). Similarly, colors are ranging from black (2.5Y2.5/1) near the river mouth to dark brown (10Y3/4) elsewhere, with

very dark grayish brown (2.5Y3/2) with rust along the coast, west of the community. The sediments are composed of clastic material classified from wacke and litharenite to Fe-sand (Fig. 35C), which reflects large variations in total Fe content (1.8–20 wt.%). Wide concentration ranges are also observed in Ti (0.3–5 wt.%), Mn (0.04–1 wt%), V (<50–1160 µg/g), Cr (<50–1700 µg/g) and Zr (120−1790 µg/g), while Zn, Sr, Mg, Al, Si, K and Ca show much narrower ranges. The concentrations obtained through partial acid digestion and ICP-QQQ measurements are generally lower (Fig. 36), but enrichment compared to PAAS is detected for V and Fe (Fig. 35C). Extractable V and Fe range from 59 to 637 µg/g and 2 to 14 wt.%, respectively, indicating their notable mobility. In contrast, extractable Cr concentrations vary between 19 and 114 µg/g, suggesting that Cr is primarily bound to stable mineral phases (e.g., chromite, pyroxenes), which have limited bioavailability and minimal impact on benthic organisms. Extractable Mn (0.03–0.07 wt.%) is markedly lower than total Mn and exhibits an opposing spatial distribution (Fig. 44), highlighting different Mn-bearing minerals phases. Most values for trace metals fall within natural background levels and below PEL thresholds, except Ni, which exceeds the PEL in some samples.

Silty light yellowish brown (2.5Y6/3) sediments collected in Resolute Bay are the richest in Ca (16–18 wt.%) and Mg (5–7 wt. %) of the dataset and the poorest in Al (2–3 wt.%), Fe (0.1–0.6 wt.%), Ti (0.08–0.15 wt.%) and Mn (0.01 – 0.02 wt. %) (Fig. 35). All samples presented V, Cr, Zn and Mn values below the ED-XRF DL (Fig. 36). Because the sediments from Resolute Bay presented very low metal concentrations, only two samples were retained for partial acid digestion analysis. The two samples presented low concentrations of all the metals, and all the values were below the TEL, indicating that there was no ecological risk in the bay.

In Grise Fiord, sediments are sandy, with colors transitioning from very dark gray (2.5Y3/1) near the coast to olive brown (2.5Y4/3) farther offshore. They are relatively enriched in Ca (6–12 wt. %) and Mg (3–5 wt. %; Fig. 35). Aside from one sample, the concentrations of Cr and Zn were below the ED-XRF DL, and the V levels were low (<78 µg/g; Fig. 36). The Fe, Ti and Mn contents are also low, with ranges of 0.8–3 wt.%,

0.3–1 wt.%, and 0.02–0.05 wt. %, respectively. However, the northernmost sample, located close to the runway and dumpsite (Fig. 34), presented relatively high concentrations of several metals. The concentrations are 355 µg/g for V, 127 µg/g for Zn, 3620 µg/g for Zr, 7.1 wt.% for Fe, 3.7 wt.% for Ti and 0.1 wt.% for Mn. Of the 11 ED-XRF-analyzed samples, three – including the metal-rich sample – underwent further analysis using partial acid digestion. Although metal concentrations were generally low, the highest levels still occurred in the sample near the runway. Only the total concentration of Zn exceeded the TEL. All three samples showed an enrichment in extractable REY and Th (Fig. 35D).

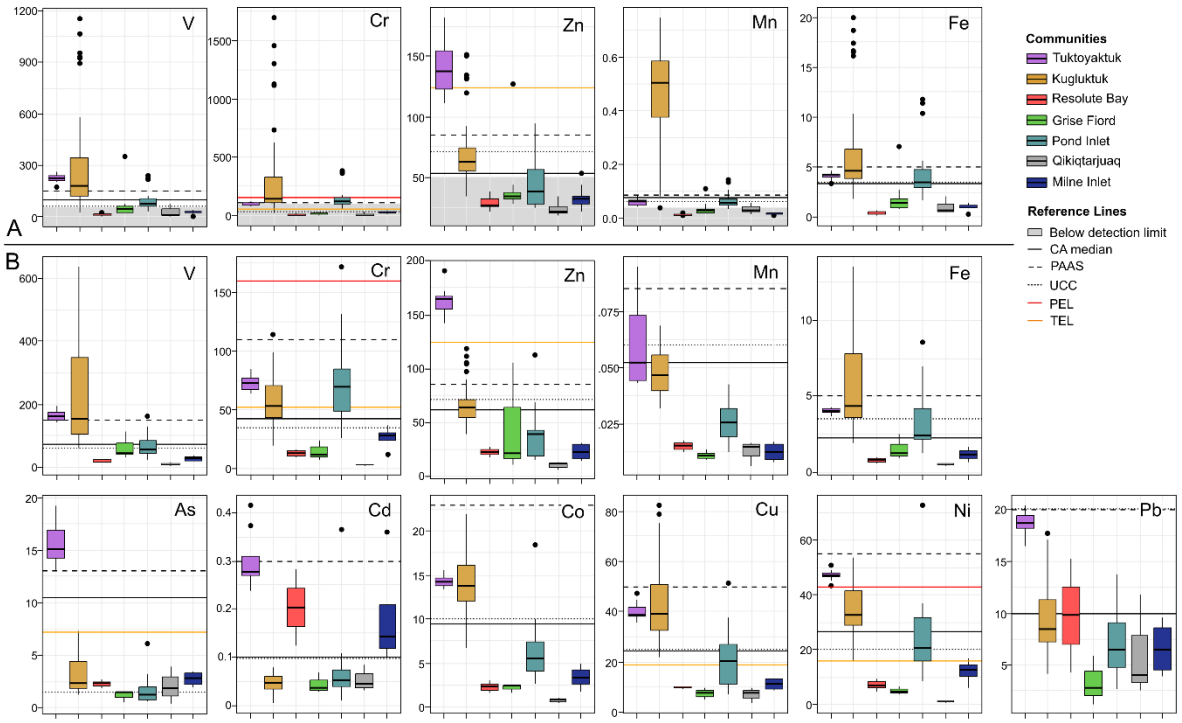


Figure 36. Boxplots showing total (A) and acid-extractable (B) concentrations of trace elements (µg/g), as well as Fe and Mn (wt.%), in coastal sediment from six Inuit communities and Milne Inlet.

In Pond Inlet, coastal sediments are composed of clastic sands with heterogeneous compositions, ranging from wacke and litharenite to Fe-sands (Fig. 35). Most sediments are grayish brown (2.5Y5/2), although some samples display very dark grayish brown (2.5Y3/2) and very dark gray (2.5Y3/1) colors, often with rust. Overall, the total metal concentrations

measured are comparable to the UCC, PAAS and CA median values (Fig. 36). The median concentrations are 25% for Si, 4.6% for Al, 3.5% for Fe, 1.8% for Ca, 0.06% for Mn, 74 µg/g for V and 123 µg/g for Cr. Of trace elements, only Zr presented higher values, with a median of 893 µg/g (compared with 210 µg/g for PAAS and 190 µg/g for UCC). However, three samples presented significantly higher contents of Fe (10–12 wt.%), Mn (0.11–0.14 wt.%), V (221–242 µg/g), Cr (359–385 µg/g) and Zr (3930–4170 µg/g). The samples are located at different sites along the coast (Fig. 45), indicating that there is no common point source. Partial acid digestion revealed an enrichment in REY and Th (Fig. 35D) and the same spatial distribution for Fe, Cr and V, but smaller values, comparable to PAAS. The samples from the eastern end of the coast presented the highest values, where Cr exceeded the PEL. Additionally, another sample in the harbor presented higher-than-average concentrations of multiple elements. The highest values were recorded for Co (18 µg/g), Ni (73 µg/g), Cu (51 µg/g), Zn (112 µg/g), As (6.1 µg/g) and Pb (114 µg/g). Only Ni is present at concentrations above the PEL.

In Milne Inlet, the sediments consist of silty sand to sandy silt rich in detrital carbonates (Fig. 35). The concentrations acquired with ED-XRF revealed values below the DL for V, Cr and Mn for all the samples. The total Zn concentration above the DL (53 µg/g) was recorded for only one sample. The four sediment samples collected near Milne Port were also analyzed using partial acid digestion. The concentrations of acid-extractable metals were low and comparable to natural background values (Fig. 36). However, the samples were collected quite far from the port, with the closest located approximately 3 km away. If metal contamination is present, it may be highly localized and therefore not captured in these samples.

The coastal sediments from Qikiqtarjuaq are predominantly characterized by a mix of Si (20–33 wt.%), Al (4.5–7.5 wt. %) and K (1.8–4.1 wt. %) that suggest arkosic sands. Sediments are grey (2.5Y5/1) to greyish brown (2.5Y5/2). It contains low concentrations of Mg (0.3–1.6 wt.%) and Ca (1.1–1.3 wt. %) as well as Fe and Mn (Fig. 35 & 36). The concentrations of Cr and Zn were below the DL, and only two samples had V concentrations

above the DL, but they remained low (63–75 µg/g). The three samples analyzed using partial acid digestion presented trace metal concentrations well below the TEL (Fig. 36). However, a notable enrichment in REY + Th is observed in all samples (Fig. 35D).

### 3.5.2 Spatial geochemical characterization of the Canadian Arctic communities

K-means clustering applied to ED-XRF data from all sites identified four distinct clusters (Fig. 37), enabling characterization of the spatial distribution of major and trace elements and differentiation between natural and anthropogenic sources (e.g., Sakan et al., 2011). To further explore these patterns, a rPCA was conducted (Fig. 38A & 39). Mn was excluded due to its high variability, which masked trends in other chemical elements. Distribution maps of Mn total concentrations are presented in the supplementary material (Fig. 46). The first two robust principal components (rPC) explain 85% of the total variance. rPC1 is defined by high loadings of Cr, V, Ti, Fe, and Zr on the negative axis, while the remaining elements are associated with the positive axis. This component effectively separates cluster 4 from the other groups. The rPC2 places Zr on the positive axis and V, Zn, K, and Al on the negative axis, and probably reflects variations in grain size. A second rPCA was performed on the acid-extractable concentrations, and the resulting biplot is visualized using the same cluster structure (Fig. 38B & 40). In this rPCA, rPC1, which explains 59% of the total variance, separates As, Cd, Sr and Ba from the other trace elements, while rPC2 (accounting for 17% of the variance) mainly separates Th, REY, As and Pb from Ba, suggesting distinct geochemical behaviors within the acid-leachable fraction.

Cluster 1, found along the coast of Grise Fiord, Pond Inlet and Qikiqtarjuaq, is defined by a mix of geochemical associations, such as Ca-Mg-Sr-LOI, Si-Al-K and Zr. It regroups communities presenting coarse-grain sediments (Fig. 35) overlying the Canadian Shield bedrocks (Fig. 33). Cluster 2, found in Resolute Bay, Milne Inlet, and parts of Grise Fiord, overlaps with Cluster 1 in the biplot, suggesting similar geochemical signatures. However, it is primarily defined by Ca-Mg-Sr-LOI, indicative of carbonate-rich sediments mainly derived from the Arctic Platform. Samples corresponding to cluster 3 are coming from

coastal Tuktoyaktuk and Kugluktuk and are primarily characterized by Zn and Al-K, with secondary associations of Fe-Ti-V and Si. This cluster reflects fluvial inputs and the presence of clay-rich lithogenic material. Cluster 4 appears on the opposite side of rPC1 relative to the other groups and includes samples with elevated metal concentrations near Kugluktuk and Pond Inlet. Its distinct position in both rPCA biplots, combined with its strong association with trace metals, suggests a potential anthropogenic influence, particularly since these patterns cannot be fully explained by local geology.

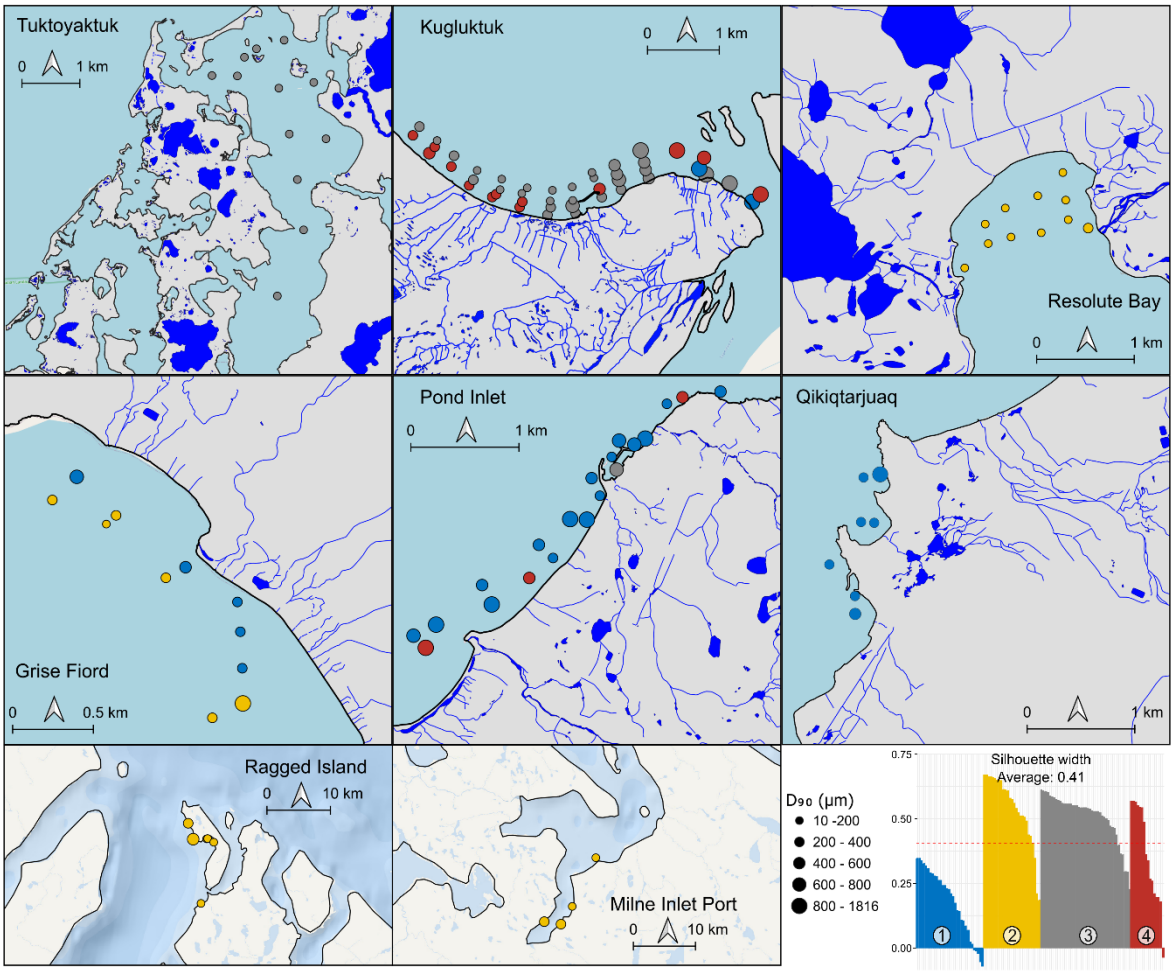


Figure 37. Spatial distribution maps of the identified clusters and corresponding silhouette plot (bottom right) obtained from energy-dispersive X-ray fluorescence (ED-XRF) and loss on ignition (LOI) data.

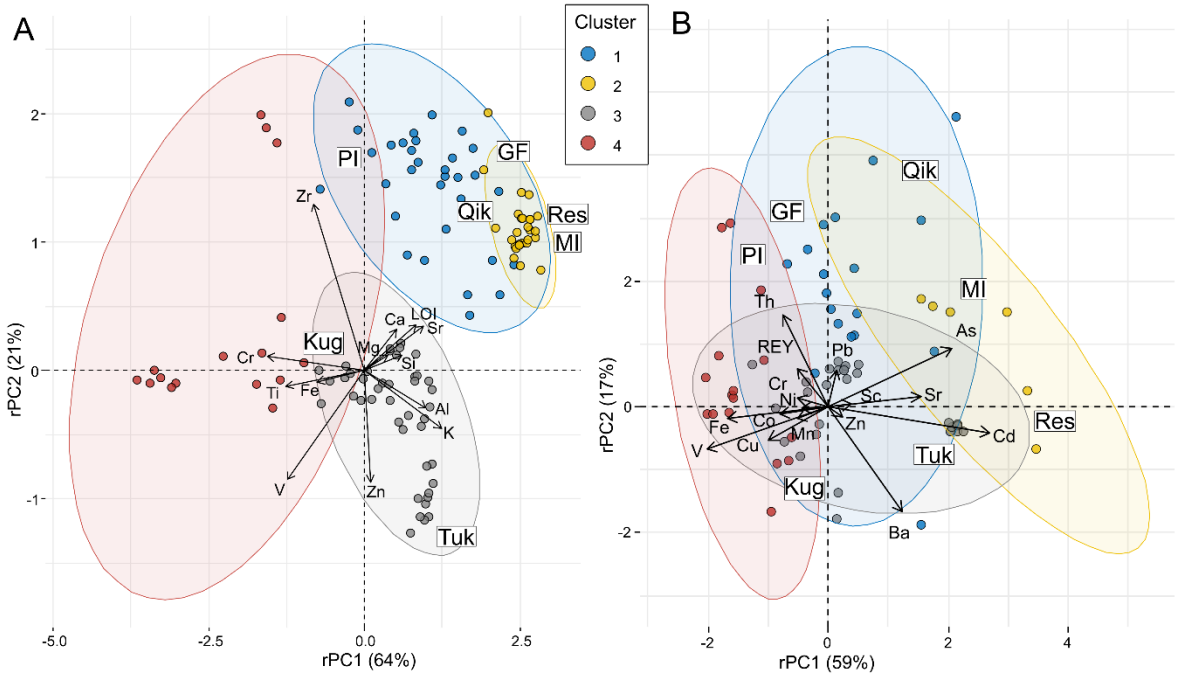


Figure 38. Biplots of the first and second robust principal components analysis (rPCA) obtained from the total (A) and acid-extractable (B) elemental concentrations. Clusters are indicated in different colors. The labels Tuk (Tuktoyaktuk), Kug (Kugluktuk), Res (Resolute Bay), GF (Grise Fiord), PI (pond Inlet), Qik (Qikiqtarjuaq) and MI (Milne Inlet) indicate the general regrouping of the sites.

### 3.5.2.1 Natural sources: cluster 1, 2 and 3

*Cluster 1 – Precambrian igneous/metamorphic rocks influences*

Grise Fiord is surrounded by numerous glaciers that erode a combination of Proterozoic granites and Paleozoic carbonates (Fig. 33). This glacial activity most likely contributes to coastal inputs of quartz, plagioclase, K-feldspar, calcite, dolomite, and other minerals, which are reflected in the sediment composition of the coastal Grise Fiord. Elemental associations such as Al-K-Si, Ca-Mg and Fe-Ti-Mn-Zr are commonly observed (Fig. 38A & 41), resulting in the classification of the samples in the clusters 1 and 2. As seen in the Si-Al-Ca ternary plot (Fig. 35B), samples from Grise Fiord are richer in detrital carbonates than Qikiqtarjuaq

and Pond Inlet, both belonging to cluster 1. Samples from cluster 1 are located in close proximity to the coastline and are characterized by a higher sand content compared to those from Cluster 2, indicating a more proximal depositional environment influenced by higher hydrodynamic energy.

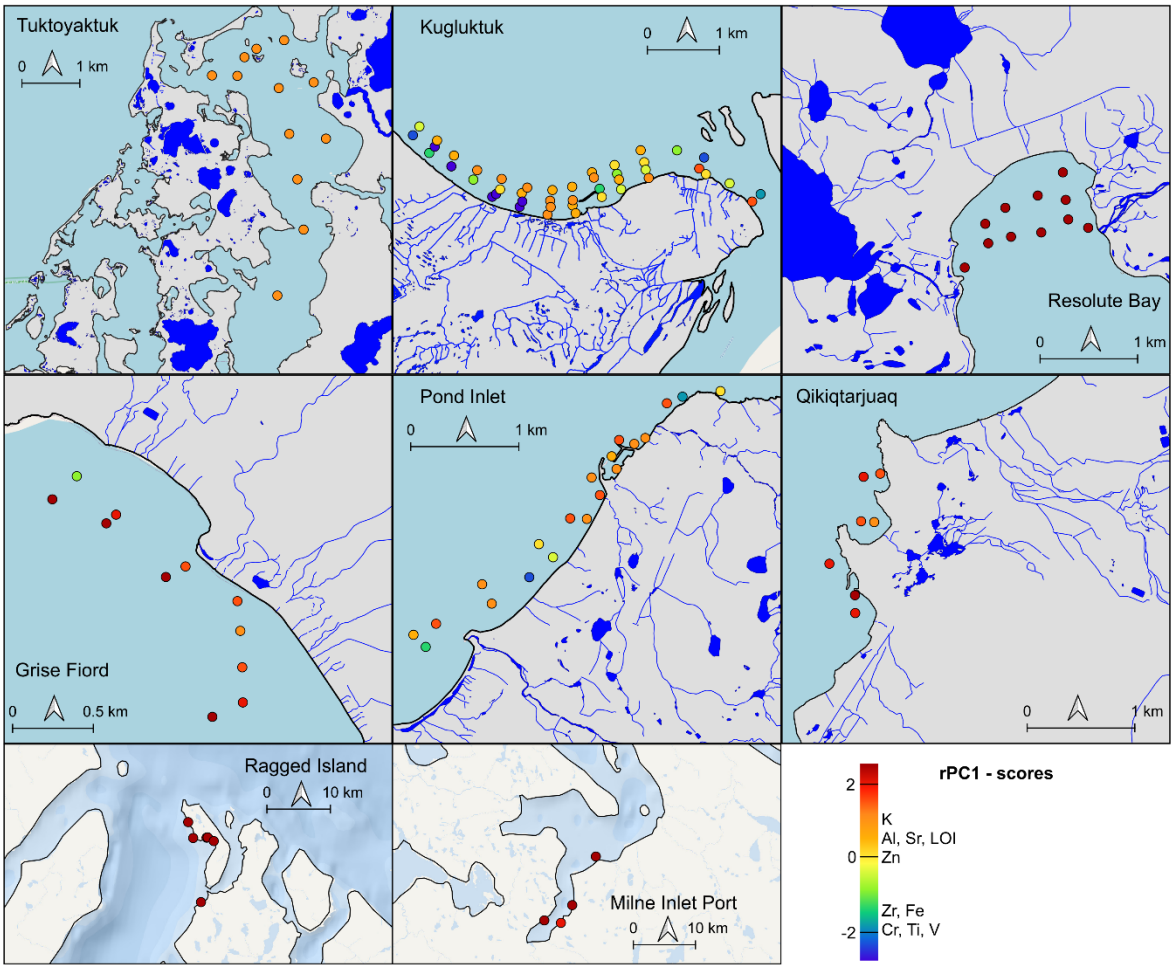


Figure 39. Maps first robust principal component scores (rPC1) derived from energy-dispersive X-ray fluorescence (ED-XRF) data.

The coastal sediments of Pond Inlet are derived from the underlying Archean mafic-intermediate basement and garnet-bearing monzogranite-granodiorite intrusions of the region (Fig. 33). The coarse sandy sediments, which display Al-Si-K-Sr-Ca and Fe-Ti-Mn-Zr elemental associations (Fig. 38A & 41), likely reflect the presence of felsic and mafic

minerals, respectively (Andrews et al., 2018; Boyd & Piper, 1976). Significant variations in sediment composition, combined with the absence of a clear spatial pattern, suggest that the sediments originate from a mix of outcropping felsic and mafic rocks. This variability results in localized shifts in the dominance of specific elemental associations (Fig. 39 & 40).

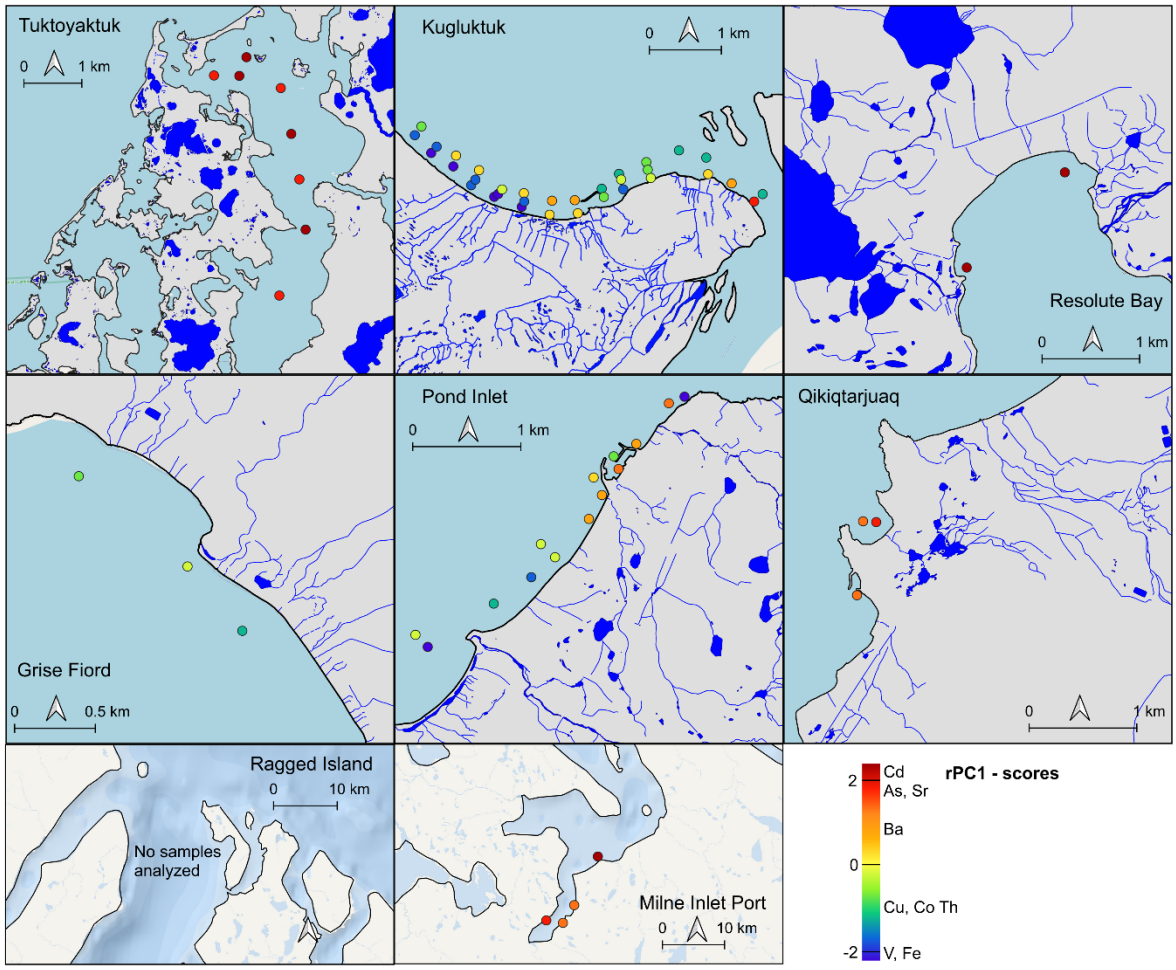


Figure 40. Maps first robust principal component scores (rPC1) derived from acid-extraction data.

The Al-K-Si-rich fine sand found in the coastal sediments of Qikiqtarjuaq suggests that the sediments are more likely composed of minerals such as quartz and K-feldspar. Zr-Ti-Fe-Mn-Mg correlations (Fig. 41) likely reflects the presence of mafic minerals. This texture and composition are consistent with the regional geology, as the Qikiqtarjuaq region is

predominantly underlain by granodiorite and monzogranite (Harrison et al., 2011; Sanborn-Barrie et al., 2013). The coarse nature of the surface sediments aligns with the typical seabed texture observed in the region (Misiuk et al., 2018).

The generally high REY + Th concentrations characterizing cluster 1 supports the predominant influence of the Precambrian lithologies on the sediment composition, as observed by Brice et al. (2026) for sediments along the Baffin Island coast. Conversely, low trace metal levels highlight that the nature of the sediments does not appear to favor high scavenging or enrichment of metals. However, although it has been classified in cluster 1, the northernmost sample in coastal Grise Fiord stands out due to its elevated total metal concentrations. In this sample, Fe-Ti-Mn-Zr concentrations are substantially higher, while Al-K-Si and Ca-Mg concentrations decrease proportionally (Fig. 39 & 46). The V and Zn concentrations are also high compared to surrounding samples, which mostly fall < DL values. This sample exhibits marked chemical differences relative to the general coastal composition. These findings suggest the presence of a localized source with limited spatial impact, possibly linked to the nearby dumpsite and/or airport. Nonetheless, drawing definitive conclusions is challenging based on a single anomalous sample.

*Cluster 2 – Carbonate rocks influences*

The seabed of the Resolute Bay is primarily composed of coarse silt rich in carbonate material (Ca–Mg), derived from the limestones and dolostones that underlie much of Cornwallis Island (Harrison et al., 2011). According to the biplot obtained by the rPCA applied on the acid-extractable metals concentrations (Fig. 38B), the sediments from Resolute Bay are characterized by high Cd contents. Indeed, the two samples analyzed by acid digestion exhibit Cd levels higher than those of most communities, but lower than the PAAS and significantly lower than the TEL (Fig. 36). Therefore, no anomalies or potential ecotoxicological risks are indicated.

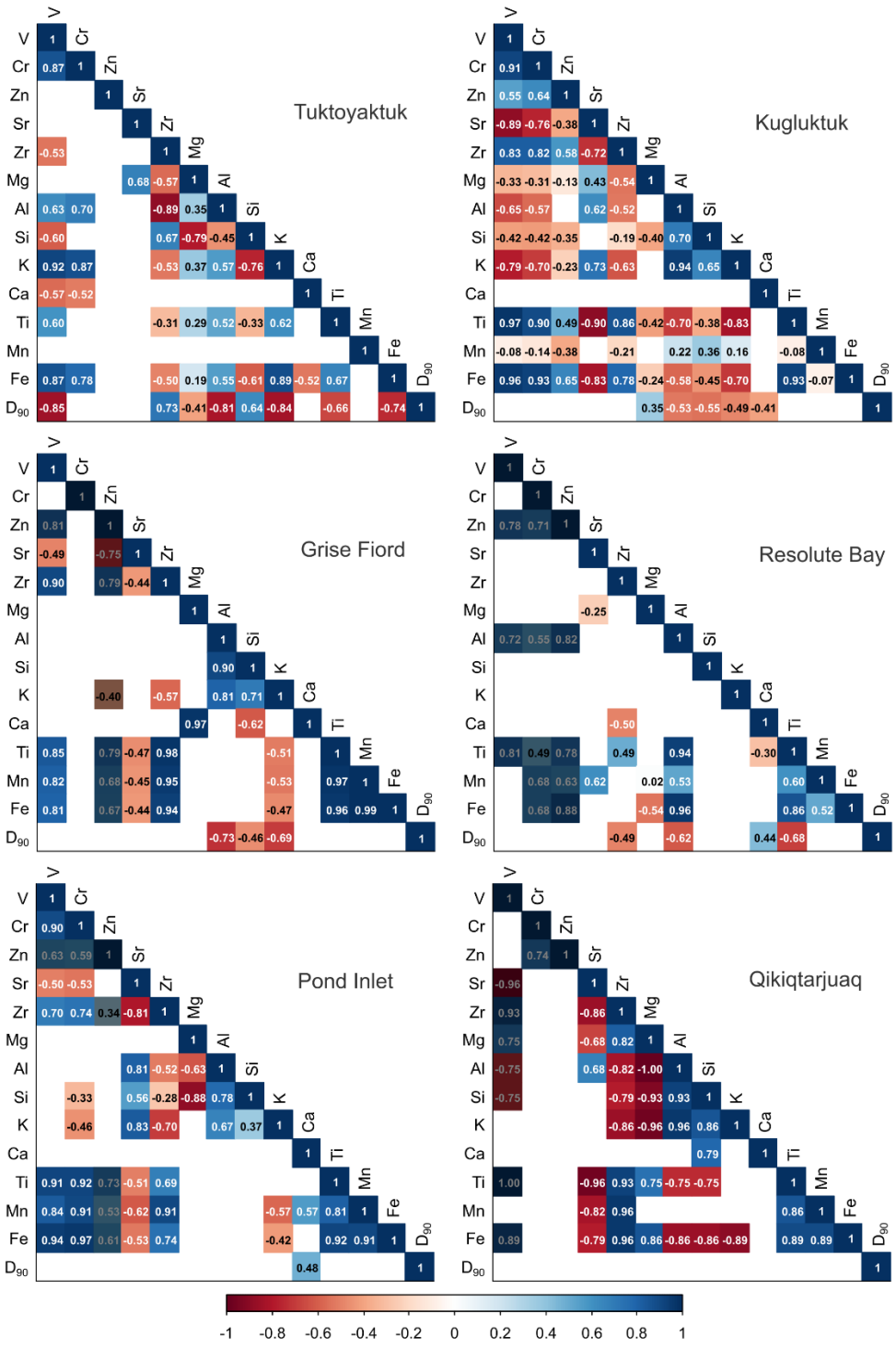


Figure 41. Spearman correlation matrix performed on the energy-dispersive X-ray fluorescence (ED-XRF) data from the six communities. Elements with most values < DL are darkened.

In Milne Inlet, coarse silt sediments are enriched in Ca and Mg and display relatively low concentrations of Fe, Al, K, and Si, indicating a predominant contribution from carbonate source rocks. Although the inner inlet is underlain by gneiss of the Rae Craton, the surface sediments deposited on the seafloor are predominantly sourced from the Arctic Platform carbonates, which are exposed in the outer inlet and to the south of the inlet (Harrison et al., 2011). The presence of carbonate-rich sediments in the inner inlet highlights the transport of fine sediments by sea ice. According to satellite imagery, in spring, sediment-laden sea ice originating from the outer inlet breaks up and drifts into the inner inlet, where it melts and likely releases its sediment load onto the seafloor. Importantly, no geochemical signature indicative of mafic rocks from the Mary River Group was detected in the analyzed sediments.

Overall, low total and acid-extractable metal concentrations are found in the carbonate-rich sediments from Resolute Bay, Grise Fiord and Milne Inlet. These findings are consistent with results from a regional geochemical survey conducted in central CA (Brice et al., 2025; Brice et al., 2026).

*Cluster 3 – Main rivers and sedimentary/igneous rocks influences*

The Tuktoyaktuk Harbor is located within the Mackenzie Delta (Fig. 33), where the Mackenzie River serves as the primary source of sediment. The dominant sedimentary contribution from the river has been documented at a regional scale across the Mackenzie Shelf (Bossé-Demers et al., 2025; Gamboa et al., 2017). The seafloor is composed of fine silt enriched in Al and metals (V, Zn, As, Cd, Co, Ni, Pb) indicative of the presence of aluminosilicates, Fe-Mn oxides, and associated trace metals. Good positive correlations between Fe, Al, K, V and Cr (Fig. 41) suggest a terrigenous origin for Fe inputs, with clay minerals and Fe oxides acting as key carriers of trace metal. Acid digestion results show that Fe and Mn are predominantly present as mobile (oxyhydr)oxides, Zn is entirely extractable, and approximately two-thirds of V and Cr are in extractable forms. The total and acid-extractable concentrations of trace metals are relatively high compared to most communities, with values exceeding the TEL in Cr, Zn, As, Cu and the PEL in Ni. However, these results are comparable with the PAAS, and consistent with measurements from the Mackenzie River

Delta sedimentary system (Vonk et al., 2015). These findings suggest that land-derived inputs from the Mackenzie River are the primary source of trace metals to the study site. However, due to potential contamination risks, the harbor should be avoided for fishing and harvesting activities.

In Kugluktuk, the coast is subdivided into clusters 3 and 4, with cluster 3 encompassing most of the samples (Fig. 37). This cluster is characterized by geochemical associations such as Sr-Si-Al-K and Fe-Ti (Fig. 38A & 41), which are indicative of lithogenic materials including quartz, clay minerals (Si-Al), feldspars (Ca-Al-K-Si-Sr), and mafic minerals (Fe-Ti). These sediments likely originate from coastal erosion of local sedimentary rocks and mafic sills, as well as fluvial inputs from the Coppermine River, as supported by the grain size distribution along the coast (Fig. 44). The Coppermine River drains a large catchment area underlain by the Bear and Slave Provinces, which are predominantly composed of intrusive rocks (43%) and sedimentary rocks (34%; Brown et al., 2020). Although the concentrations of several metals in the river exceed the Drinking Water and Freshwater Aquatic Life Guidelines (Coulombe-Pontbriand et al., 1998), only moderate levels are observed in total metals ($Fe_{MED}$= 4 wt.%, $Cr_{MED}$=141 µg/g, and $V_{MED}$=165 µg/g) and in some extractable metals ($Co_{MED}$= 13 µg/g, $Ni_{MED}$=32 µg/g, $Cu_{MED}$=37 µg/g). These values are comparable to PAAS and remain below the PEL. Sediments from cluster 3 in Kugluktuk differ from those in Tuktoyaktuk by their elevated Mn concentrations (Fig. 36A). While total metal concentrations in Kugluktuk are consistent with regional values previously reported for the Coronation Gulf (Brice et al., 2025), acid-extractable concentrations are substantially lower (Brice et al., 2026). This suggests that the Mn in Kugluktuk coastal sediments seems not primarily associated with authigenic oxides, in contrast to the conclusions drawn for the Gulf.

#### 3.5.2.2 Anthropogenic contributions: cluster 4

*Pond Inlet*

Sediment samples classified within cluster 4 are found at three different locations along the coast of Pond Inlet (Fig. 37). This cluster 4 is characterized by elevated concentrations of Zr, Ti, Fe, Cr and V, suggesting the presence of heavy minerals and/or potential anthropogenic influences. As previously discussed, the coastal sediments in Pond Inlet exhibit a heterogeneous chemical composition, which is attributed to the presence of both felsic and mafic rock outcrops in the area. In the rPCA biplot (Fig. 38A), all three samples are located near the Zr and REY-Th, which suggest contributions from igneous and metamorphic rocks of the Rae Craton (Skipton et al., 2025). Two of these samples, located on the western side near streams mouths, exhibit relatively low acid-extractable concentrations of Fe, Cr and V, supporting the hypothesis of a natural geogenic origin. In contrast, the third sample, collected from the eastern end of the sampling zone, displays a distinct geochemical signature, with significantly higher total and acid-extractable concentrations of Fe, Cr, and especially V (Fig. 45). Given the absence of known natural sources in the eastern sector that could account for such elevated concentrations, this anomaly may point to a localized anthropogenic source, specifically, the fuel pipeline situated on the coast adjacent to the sample site (Fig. 34). This pipeline, used for the annual resupply of fuel to nearby storage tanks by marine tankers, ruptured on June 11, 2024, releasing approximately 7,000 liters of diesel into the ocean (CBC News, 2024). According to Nunavut's Petroleum Products Division, the pipeline may have experienced problems for several months prior to the incident. Although the spill occurred a year after the sediment sampling, the results may suggest that the pipeline poses a long-term, localized contamination risk. In the case of a diesel spill, elevated concentrations of Fe, Cr, and particularly V are typically expected in sediments, along with Ni. However, in this case, Ni concentrations were not elevated (Celo et al., 2015; Karnaeva et al., 2021; Salazar-Coria et al., 2007). Another sample, collected from the harbor, was classified in cluster 3 and presented the highest concentrations of coastal Pond Inlet for Zn, As, Co, Cu, Ni and Pb

(Fig. 36 & 45). While trace metal concentrations in this sample remain within natural background levels, the relatively elevated values and high extractability suggest a potential anthropogenic influence, likely due to the operation of multiple boat engines within the harbor.

*Kugluktuk*

In Kugluktuk, the samples classified within cluster 4 have distinct chemical signatures from those of cluster 3. They exhibit significantly higher concentrations of Fe-Ti-V-Cr-Zr and most of them show significantly lower Mn concentrations (Fig. 44). This cluster includes three samples located at the mouth of the Coppermine River, a group of nine samples distributed along the coast west of the community, and a single isolated sample near the barge dock (Fig. 37). The highest recorded values of Fe (6–20 wt.%), Cr (611–1700 µg/g), V (408–1160 µg/g), and Ti (2–5 wt.%), as well as of the trace metals Zn, Ni, Pb, Cu, and Co are all observed in the western strip.

The high total concentrations in Fe, Ti and Zr, along with their strong positive correlations (Fig. 38 & 41), suggest an enrichment in heavy minerals within cluster 4 (Fitzpatrick & Chittleborough, 2002). V and Cr also show strong covariation with these elements, indicating that they are likely associated with the same heavy mineral phases. In contrast, Mn shows a different geochemical behavior, with generally lower concentrations in cluster 4 (Fig. 44) and no significant correlations with Fe, Ti and Zr across all samples (Fig. 41). However, two distinct linear Fe-Mn relationships are observed, which align almost perfectly with the cluster groupings (Fig. 47). This pattern suggests that although Fe and Mn covary, they are influenced by two different geochemical processes: one promoting Fe enrichment in cluster 4, and another favoring Mn enrichment in cluster 3.

The acid-extractable concentrations are significantly lower than total concentrations, particularly for Cr and Mn. Extractable Mn show a single linear trend with Fe (Fig. 47). Although the western coastal strip and the river mouth remain the areas with the highest extractable concentrations for Fe, Ti, V, and Cr, their extractions are lower than those in

cluster 3 (Fig. 48). This geochemical pattern supports the hypothesis of heavy mineral enrichment. Heavy minerals, such as crystalline oxides and silicates, are resistant to partial acid digestion, resulting in low extraction recoveries (Krasnodębska-Ostręga et al., 2001). The particularly low extractable concentrations of Cr suggest it is primarily hosted in chromite, a refractory mineral known to resist even to microwave hydrofluoric acid digestion (Kelly et al., 2003). Fe and V exhibit strong positive correlations and high extraction recoveries (Fig. 47 & 48), indicating that V is likely associated with readily accessible Fe oxides. In contrast, Mn shows a distinct behavior: its extraction recovery is approximately 47% in cluster 4, compared to only ~8% in cluster 3. This stark contrast suggests that Mn is hosted in different dominant mineral phases across the two clusters, a pattern also supported by the Fe-Mn correlation trends (Fig. 47). In cluster 3, Mn may be primarily bound within silicate minerals (e.g., Spessartina, a Mn-rich garnet), whereas in cluster 4, it likely occurs in both resistant heavy minerals and more labile Fe-Mn oxides.

In the light of these observations, cluster 4 is likely enriched in heavy minerals such as rutile (Ti), zircon (Zr), ilmenite (Ti–Fe), and chromite (Cr). Ferromagnesian minerals may also contribute to high V concentrations, as V can substitute for $Fe^{3+}$ in their crystal structures (Kelley et al., 2017). Mn displays a good correlation with these heavy mineral–associated elements in cluster 4, suggesting that part of the Mn may also be hosted to iron-bearing phases such as goethite. The enrichment of heavy mineral observed both the western coastal strip and at the mouth of the Coppermine River is likely the result of hydrodynamic sorting processes (Chen et al., 2014). Due to their high density, these minerals tend to settle rapidly as water velocity decreases. In Kugluktuk, the river mouth represents a transitional zone where the fluvial currents meet coastal waters, leading to reduced flow and enhanced sediment deposition. In addition, the longshore current likely transports suspended heavy particles westward, while the breakwater near the barge dock seems to promote their accumulation downcurrent. This interpretation is supported by the grain size distribution (Fig. 44), which reflects hydrodynamic sorting influenced by both river discharge and coastal currents transport. Overall, the presence of heavy minerals capable of carrying and scavenging trace metals in sediments at the river mouth and along the western coastal strip

likely explains several key findings of this study. Furthermore, the Muskox Intrusion - an ultramafic to mafic intrusion located upstream along the Coppermine River - may play a significant role in this enrichment. Indeed, as part of the Mackenzie Large Igneous Province, the intrusion contains layers enriched in Fe, Cu, Ti, V, and Ni, as well as chromite-bearing horizons (Scoates & Scoates, 2024). Material derived from the Muskox Intrusion, transported by the Coppermine River, could therefore partly account for the elevated trace metal concentrations in the river water (Coulombe-Pontbriand et al., 1998), as well as the abundance of heavy minerals and associated trace metal enrichment observed in the coastal sediments.

While the hydrodynamic conditions and the upstream ultramafic Muskox Intrusion can explain the deposition of heavy minerals at the mouth of the Coppermine River, they do not fully explain for the significant enrichment of both heavy minerals and trace metals observed in the western coastal strip, where total V and Cr concentrations exceed those at the river mouth (Fig. 42). Grain size distribution data suggest that the breakwater near the barge dock may be altering local sedimentation dynamics, potentially creating favorable conditions for the accumulation of heavy minerals. This hypothesis is further supported by empirical Bayesian kriging interpolation maps, which show distinct hotspots for Fe, V, and Cr in the western strip (Fig. 42), suggesting the possible influence of an additional localized source. One such source may be anthropogenic input from sewage lagoons and waste disposal sites located upstream of small streams that discharge into the bay (Fig. 34). The wastewater system in Kugluktuk is composed of a constructed lagoon designed to retain wastewater for approximately one year to allow for contaminant removal. The lagoon is then discharged annually in summer into a constructed wetland and, ultimately, into coastal waters (Stroski et al., 2020). However, reported leaks in the lagoon system (ICSP, 2024), raise concerns about unregulated discharges. Thus, the combination of anthropogenic inputs and natural heavy mineral enrichment, which serve as excellent metal carriers, could contribute to localized contamination in the western strip.

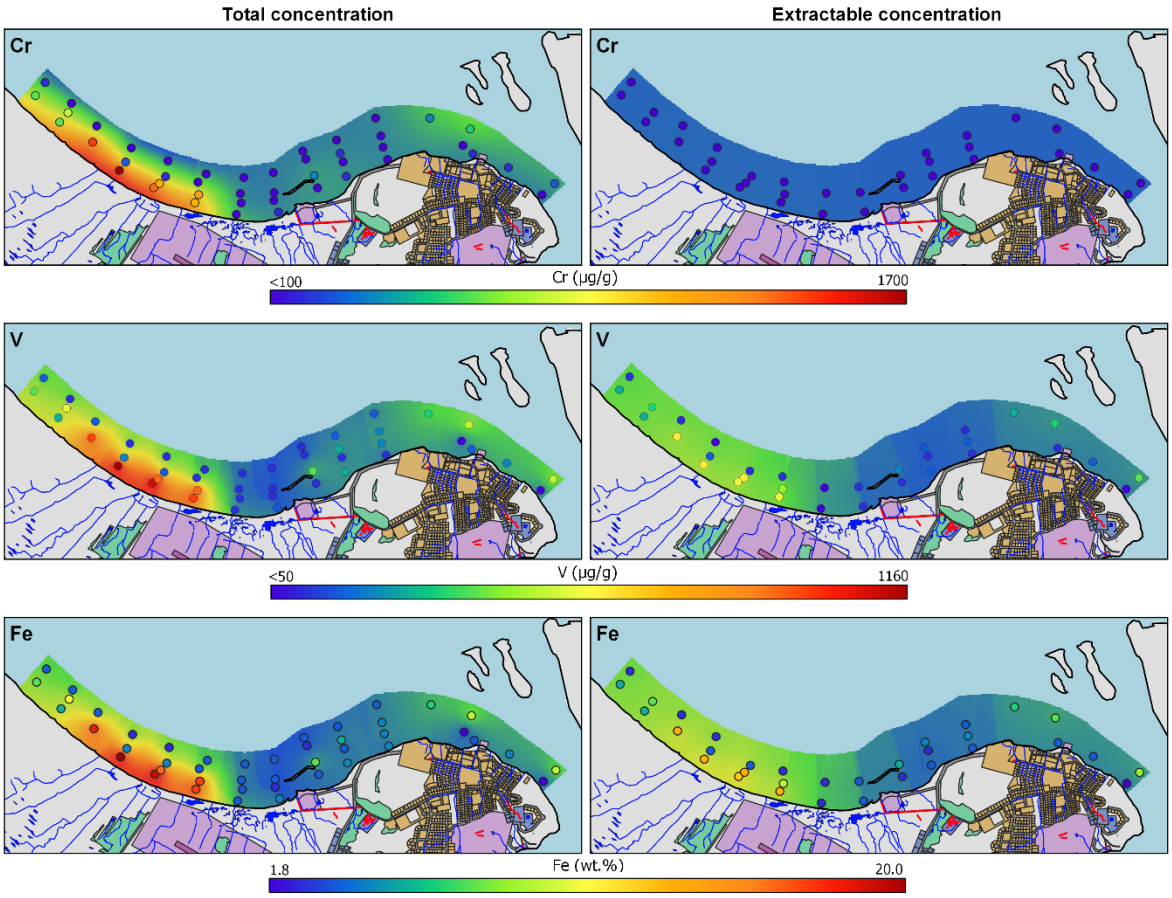


Figure 42. Maps of Kugluktuk showing the total (left) and acid-extractable (right) concentrations of Cr, V and Fe measured in the sediment samples. Empirical Bayesian kriging spatial interpolation was applied to the data in ArcGIS for visual purposes.

Besides V, which exhibited high concentrations in both total and acid-extractable forms, the other trace metals showed extractable concentrations comparable to natural background values. Although Ni exceeded the PEL in some samples, concentrations remained below the PAAS, indicating a low level of ecotoxicological risk. The high extractable V concentrations are likely due to its strong association with readily accessible Fe oxides, which act as effective scavengers in sediments. In contrast, other trace metals may not be easily retained in the solid phase due to differing geochemical behaviors that favor partitioning into the dissolved phase. To fully evaluate potential environmental impacts in

the western strip, including bioavailability and ecological risk, further investigations involving benthic organisms are recommended.

## 3.6 CONCLUSION

This study assessed trace metal contamination in coastal sediments from six Canadian Inuit communities, as well as Milne Inlet, the location of the Mary River Mine port. The results reveal varying degrees of metal enrichment across sites, influenced by both natural geological processes and potential anthropogenic inputs.

Pond Inlet and Qikiqtarjuaq are primarily influenced by coarse-grained clastic sediments derived from surrounding Precambrian Canadian Shield rocks. While sediments in Qikiqtarjuaq show very low trace metal concentrations, those in Pond Inlet display more heterogeneous chemical compositions, reflecting the influence of both felsic and mafic lithologies. Some samples from Pond Inlet show elevated trace metal concentrations, likely linked to local geological variability. Enrichment in REY and Th is characteristic of Canadian Shield-derived sediments. In contrast, carbonate-rich and trace-element-poor sediments dominate in Resolute Bay and Milne Inlet, reflecting the influence of the Arctic Platform. Grise Fiord sediments show a mixed provenance derived from both siliciclastic material from the Canadian Shield and carbonate input from the Arctic Platform. This spatial variability highlights the strong control of regional geology on sediment composition and trace metal distribution across the eastern CA.

Elevated trace metal concentrations are found in coastal sediments from both Tuktoyaktuk and Kugluktuk. In the Tuktoyaktuk harbor, the Mackenzie River delivers fine silts enriched in aluminosilicates and metal oxides, which act as carriers for trace metals. Several metals exceed the TEL, suggesting the potential for occasional adverse biological effects. However, these concentrations remain comparable to the regional background values reported for the Mackenzie Delta and Shelf. In Kugluktuk, coastal sediments are primarily

derived from the erosion of intrusive mafic and sedimentary rocks as well as inputs from the Coppermine River. These sediments exhibit moderate trace metal concentrations overall, reflecting both natural geological sources and localized depositional processes.

Suspected anthropogenic contributions were identified in three communities. In Grise Fiord, a single sediment sample exhibited anomalously high concentrations of Fe, Mn, Ti, V, and Zn, which are approximately four times higher than the other samples, warranting further investigation to confirm its origin. In Pond Inlet, several samples exceeded natural background concentrations for trace metals, with potential contamination linked to a nearby fuel pipeline spill and boating activity within the harbor. Along the coast of Kugluktuk, sediments revealed significant enrichment in trace metals, particularly at the mouth of the Coppermine River and along a coastal strip west of the community. While these results are likely influenced by natural inputs from upstream mafic–ultramafic intrusions, the pronounced accumulation of V and Cr in the western strip also suggest a possible anthropogenic source, potentially amplified by the preferential deposition of heavy minerals.

Overall, this study highlights the complex interplay between natural geological processes and anthropogenic influences in shaping trace metal distributions in coastal sediments from Canadian Inuit communities. To accurately assess pollution levels and potential ecological risks to the coastal ecosystems in these communities, further investigations are needed, particularly focusing on metal mobility, bioavailability, metal content in biota and expanded spatial sampling.

## 3.7 ACKNOWLEDGEMENTS

We thank the communities of Kugluktuk, Qaussuittuq, Aussuittuq, Mittimatalik and Qikiqtarjuaq that approved our project and welcomed us. We are thankful to R. Hala (Kugluktuk) and M. Amarualik (Pond Inlet) for their help on the field. We thank Mathieu Babin (ISMER-UQAR) and Mathieu Moingt (UQAM) for providing technical support in the

laboratory. This study was supported by ArcticNet (ArcticSeafloor project), EcotoQ (Programme d'accès aux infrastructures et formation), Québec-Océan, Geotop, the Northern Scientific Training Program (NSTP), the Fonds de recherche du Québec - Nature et technologies (FRQNT) and the Natural Sciences and Engineering Research Council of Canada (NSERC) PhD scholarships provided to C. Brice, and NSERC Discovery Grants provided to J.-C. Montero-Serrano (RGPIN-2020-06600 and RGPNS-2020-06600).

## 3.8 REFERENCES

Adams, M. A. (1998). *Environmental Impact of Arctic Municipal Landfills as Contaminant Point Sources: Case Study: Tuktoyaktuk Solid Waste Site* Royal Military College of Canada]. Kingston, Ontario.

Aitchison, J. (1982). The Statistical Analysis of Compositional Data. *Journal of the Royal Statistical Society: Series B (Methodological)*, *44*(2), 139-160. https://doi.org/https://doi.org/10.1111/j.2517-6161.1982.tb01195.x

AMAP (2005). *AMAP Assessment 2002: Heavy Metals in the Arctic.* Arctic Monitoring and Assessment Programme (AMAP), Oslo, Norway. xvi + 265 pp.

AMAP (2011). *AMAP Assessment 2011: Mercury in the Arctic.* Arctic Monitoring and Assessment Programme (AMAP), Oslo, Norway. xiv + 193 pp.

AMAP. (2021a). *AMAP Assessment 2020: POPs and Chemicals of Emerging Arctic Concern: Influence of Climate Change*. Arctic Monitoring and Assessment Programme (AMAP), Tromsø, Norway. vii + 134pp.

AMAP (2021b). *AMAP Assessment 2021: Mercury in the Arctic.* Arctic Monitoring and Assessment Programme (AMAP), Tromsø, Norway. 324 pp.

Andrews, J. T., Klein, A. J., Jenner, K. A., Jennings, A. E., & Campbell, C. (2018). The variability of Baffin Bay seafloor sediment mineralogy: the identification of discrete glacial sediment sources and application to Late Quaternary downcore analysis. *Canadian Journal of Earth Sciences*, *55*(6), 620-639. https://doi.org/10.1139/cjes-2017-0223

Bartley, M. C., Tremblay, T., De Silva, A. O., Michelle Kamula, C., Ciastek, S., & Kuzyk, Z. Z. A. (2024). Sedimentary records of contaminant inputs in Frobisher Bay, Nunavut. *Environmental Science and Ecotechnology*, *18*, 100313. https://doi.org/https://doi.org/10.1016/j.ese.2023.100313

Becagli, S., Caiazzo, L., Di Iorio, T., di Sarra, A., Meloni, D., Muscari, G., Pace, G., Severi, M., & Traversi, R. (2020). New insights on metals in the Arctic aerosol in a climate changing world. *Science of The Total Environment*, *741*, 140511. https://doi.org/https://doi.org/10.1016/j.scitotenv.2020.140511

Bindler, R., Renberg, I., John Anderson, N., Appleby, P. G., Emteryd, O., & Boyle, J. (2001). Pb isotope ratios of lake sediments in West Greenland: inferences on pollution sources. *Atmospheric Environment*, *35*(27), 4675-4685. https://doi.org/https://doi.org/10.1016/S1352-2310(01)00115-7

Blott, S. J., & Pye, K. (2001). GRADISTAT: a grain size distribution and statistics package for the analysis of unconsolidated sediments. *Earth surface processes and Landforms*, *26*(11), 1237-1248.

Bossé-Demers, T., Gobeil, C., Juhls, B., Lizotte, M., Fritz, M., Bröder, L., Matsuoka, A., Mareque, S., & Couture, R.-M. (2025). Distribution of rare earth elements and their signatures from the Mackenzie River delta to the abyssal Arctic Ocean. *Continental Shelf Research*, *289*, 105464. https://doi.org/https://doi.org/10.1016/j.csr.2025.105464

Boyd, R. W., & Piper, D. J. (1976). Baffin Bay continental shelf clay mineralogy. *Atlantic Geology*, *12*(1), 17-18.

Brice, C., Montero-Serrano, J.-C., & Saint-Louis, R. (2025). Regional geochemical survey of Canadian Arctic sediments: insights into provenance, sediment dynamics and trace metal enrichment. *Applied Geochemistry*, *189*, 106432. https://doi.org/https://doi.org/10.1016/j.apgeochem.2025.106432

Brice, C., Montero-Serrano, J.-C., St-Louis, R., & Rosabal, M. (2026). Establishing baseline levels of extractable trace metals in marine surface sediment of the Canadian Arctic. *Marine Pollution Bulletin, 223*, 119043. https://doi.org/https://doi.org/10.1016/j.marpolbul.2025.119043

Brown, K. A., Williams, W. J., Carmack, E. C., Fiske, G., François, R., McLennan, D., & Peucker-Ehrenbrink, B. (2020). Geochemistry of Small Canadian Arctic Rivers with Diverse Geological and Hydrological Settings. *Journal of Geophysical Research: Biogeosciences*, *125*(1), e2019JG005414. https://doi.org/https://doi.org/10.1029/2019JG005414

Buchmann, M. F. (2008). *NOAA Screening quick reference tables*. Seattle, WA: Office of Response and Retoriation Division, National Oceanic and Atmospheric Administration Retrieved from http://response.restoration.noaa.gov/cpr/sediment/squirt/squirt.html

CBC News. (2024). Pond Inlet pipeline problems may have begun months before large spill detected. *CBC News*. https://www.cbc.ca/news/canada/north/pond-inlet-fuel-spill-update-1.7253483#:~:text=North-,Pond%20Inlet%20pipeline%20problems%20may%20have%20begun%20months%20before%20large,had%20spilled%20into%20the%20ocean.

CCME. (1999). *Canadian Sediment Quality Guidelines for the Protection of Aquatic Life*. Winnipeg, MA: Canadian Council of Ministers of the Environment, Canadian environmental quality guidelines

Celo, V., Dabek-Zlotorzynska, E., & McCurdy, M. (2015). Chemical Characterization of Exhaust Emissions from Selected Canadian Marine Vessels: The Case of Trace Metals and Lanthanoids. *Environmental Science & Technology*, *49*(8), 5220-5226. https://doi.org/10.1021/acs.est.5b00127

Centre for Water Resources Studies. (2015). *Treatment Performance of Municipal Wastewater Stabilization Ponds in Nunavut*. Dalhousie University.

Chen, J.-B., Gaillardet, J., Bouchez, J., Louvat, P., & Wang, Y.-N. (2014). Anthropophile elements in river sediments: Overview from the Seine River, France. *Geochemistry, Geophysics, Geosystems*, *15*(11), 4526-4546. https://doi.org/https://doi.org/10.1002/2014GC005516

Chénier, R., Abado, L., Sabourin, O., & Tardif, L. (2017). Northern marine transportation corridors: Creation and analysis of northern marine traffic routes in Canadian waters. *Transactions in GIS*, *21*(6), 1085-1097. https://doi.org/https://doi.org/10.1111/tgis.12295

Conca, E., Abollino, O., Giacomino, A., Buoso, S., Traversi, R., Becagli, S., Grotti, M., & Malandrino, M. (2019). Source identification and temporal evolution of trace elements in PM10 collected near to Ny-Ålesund (Norwegian Arctic). *Atmospheric Environment*, *203*, 153-165. https://doi.org/https://doi.org/10.1016/j.atmosenv.2019.02.001

Corminboeuf, A., Montero-Serrano, J.-C., & St-Louis, R. (2021). Spatial and temporal distributions of polycyclic aromatic hydrocarbons in sediments from the Canadian Arctic Archipelago. *Marine Pollution Bulletin*, *171*, 112729. https://doi.org/https://doi.org/10.1016/j.marpolbul.2021.112729

Coulombe-Pontbriand, M., Reid, R., & Jackson, F. (1998). Coppermine River - overview of the hydrology and water quality. *Indian and Northern Affairs. Water Resources Division.*, 43.

Dawson, J., Pizzolato, L., Howell, S. E. L., Copland, L., & Johnston, M. E. (2018). Temporal and Spatial Patterns of Ship Traffic in the Canadian Arctic from 1990 to 2015. *Arctic*, *71*(1), 15-26. https://www.jstor.org/stable/26387327

Dhifallah, F., Rochon, A., Simard, N., McKindsey, C. W., Gosselin, M., & Howland, K. L. (2022). Dinoflagellate communities in high-risk Canadian Arctic ports. *Estuarine, Coastal and Shelf Science*, *266*, 107731. https://doi.org/https://doi.org/10.1016/j.ecss.2021.107731

Donald, B. J. (2005). *Polaris Mine : a case study of reclamation in the high Arctic* [Text]. Proceedings of the British Columbia Mine Reclamation Symposium, https://open.library.ubc.ca/soa/cIRcle/collections/59367/items/1.0042473

Dredge, L. A. (2001). *Where the River Meets the Sea: Geology and Landforms of the Lower Coppermine River Valley and Kugluktuk, Nunavut*. Geological Survey of Canada. https://books.google.ca/books?id=O0niQgAACAAJ

ECCC. (2024). *Marine Emissions Inventory Tool* https://ec-meit.ca/app.html#

Filzmoser P, H. K., Templ M. (2018). *Applied Compositional Data Analysis. With Worked Examples in R*. Springer International Publishing. Springer Nature Switzerland AG, Cham, Switzerland. https://doi.org/doi:10.1007/978-3-319-96422-5

Fitzpatrick, R. W., & Chittleborough, D. J. (2002). Titanium and Zirconium Minerals. In *Soil Mineralogy with Environmental Applications* (p. 667-690). https://doi.org/https://doi.org/10.2136/sssabookser7.c22

Gamboa, A., Montero-Serrano, J.-C., St-Onge, G., Rochon, A., & Desiage, P.-A. (2017). Mineralogical, geochemical, and magnetic signatures of surface sediments from the Canadian Beaufort Shelf and Amundsen Gulf (Canadian Arctic). *Geochemistry, Geophysics, Geosystems*, *18*(2), 488-512. https://doi.org/https://doi.org/10.1002/2016GC006477

Government of Canada. (2022). *Federal contaminated sites inventory*. https://www.tbs-sct.gc.ca/fcsi-rscf/home-accueil-eng.aspx

Guerra, R., Fetter, E., Ceschim, L. M. M., & Martins, C. C. (2011). Trace metals in sediment cores from Deception and Penguin Islands (South Shetland Islands, Antarctica). *Marine Pollution Bulletin*, *62*(11), 2571-2575. https://doi.org/https://doi.org/10.1016/j.marpolbul.2011.08.012

Gunnarsdóttir, R., Jenssen, P. D., Erland Jensen, P., Villumsen, A., & Kallenborn, R. (2013). A review of wastewater handling in the Arctic with special reference to pharmaceuticals and personal care products (PPCPs) and microbial pollution. *Ecological Engineering*, *50*, 76-85. https://doi.org/https://doi.org/10.1016/j.ecoleng.2012.04.025

Harrison, J. C., St-Onge, M., Petrov, O., Strelnikov, S., Lopatin, B., Wilson, F., Tella, S., Paul, D., Lynds, T., Shokalsky, S., Hults, C. K., Bergman, S., Jepsen, H., & Solli, A. (2011). *Geological map of the Arctic / Carte géologique de l'Arctique* [ "A" Series Map 2159A, 2011, 2159 sheets, 2151:2155,2000,2000]. Natural Resources Canada.

Harrison, J. C., Thorsteinsson, R., Frisch, T., Mayr, U., Gilbert, C., Lynds, T., & Ford, A. (2014). *Geology, Tectonic assemblage map of Grise Fiord, eastern Devon and southern Ellesmere islands, Nunavut*. Geological Survey of Canada.

Herron, M. M. (1988). Geochemical classification of terrigenous sands and shales from core or log data. *Journal of sedimentary Research*, *58*(5), 820-829. https://doi.org/10.1306/212f8e77-2b24-11d7-8648000102c1865d

ICSP. (2024). *Integrated Community Sustainability Plan (ICSP) Webtool*. https://www.buildingnunavut.com/en/index.asp

Karnaeva, A., Kulikova, O., Mazlova, E., & Buryak, A. (2021). Aged diesel and heavy metal pollution in the Arctic tundra (Yamal Peninsula, Russia). *Science of The Total Environment*, *792*, 148471. https://doi.org/https://doi.org/10.1016/j.scitotenv.2021.148471

Kassambara, A., & Mundt, F. (2020). Factoextra: Extract and Visualize the Results of Multivariate Data Analyses. R Package Version 1.0.7. https://CRAN.R-project.org/package=factoextra

Kelley, K. D., Scott, C., Polyak, D. E., & Kimball, B. E. (2017). *Vanadium* [Professional Paper 1802U]. U. S. Geological Survey. https://pubs.usgs.gov/publication/pp1802U

Kelly, W. R., Murphy, K. E., Becker, D. A., & Mann, J. L. (2003). Determination of Cr in certified reference material HISS-1, marine sediment, by cold plasma isotope dilution ICP-MS and INAA: comparison of microwave versus closed (Carius) tube digestion. *Journal of Analytical Atomic Spectrometry*, *18*(2), 166-169.

Korosi, J. B., Griffiths, K., Smol, J. P., & Blais, J. M. (2018). Trends in historical mercury deposition inferred from lake sediment cores across a climate gradient in the Canadian High Arctic. *Environmental Pollution*, *241*, 459-467. https://doi.org/https://doi.org/10.1016/j.envpol.2018.05.049

Krachler, M., Zheng, J., Koerner, R., Zdanowicz, C., Fisher, D., & Shotyk, W. (2005). Increasing atmospheric antimony contamination in the northern hemisphere: snow and ice evidence from Devon Island, Arctic Canada. *Journal of Environmental Monitoring*, *7*(12), 1169-1176.

Krasnodębska-Ostręga, B., Emons, H., & Golimowski, J. (2001). Selective leaching of elements associated with Mn – Fe oxides in forest soil, and comparison of two sequential extraction methods. *Fresenius' Journal of Analytical Chemistry*, *371*(3), 385-390. https://doi.org/10.1007/s002160100982

Krivoruchko, K. (2012). Empirical bayesian kriging. *ArcUser Fall*, *6*(10), 1145.

Langer, M., von Deimling, T. S., Westermann, S., Rolph, R., Rutte, R., Antonova, S., Rachold, V., Schultz, M., Oehme, A., & Grosse, G. (2023). Thawing permafrost poses environmental threat to thousands of sites with legacy industrial contamination. *Nature Communications*, *14*(1), 1721. https://doi.org/10.1038/s41467-023-37276-4

Li, C., & Cornett, J. (2011). Increased zinc concentrations in the Canadian Arctic air. *Atmospheric Pollution Research*, *2*(1), 45-48. https://doi.org/https://doi.org/10.5094/APR.2011.006

Li, C., Cornett, J., & Ungar, K. (2003). Long-term decrease of cadmium concentrations in the Canadian Arctic air. *Geophysical Research Letters*, *30*(5). https://doi.org/https://doi.org/10.1029/2002GL016723

Li, C., Cornett, J., Willie, S., & Lam, J. (2009). Mercury in Arctic air: The long-term trend. *Science of The Total Environment*, *407*(8), 2756-2759. https://doi.org/https://doi.org/10.1016/j.scitotenv.2008.12.010

Macdonald, K. M., Sharma, S., Toom, D., Chivulescu, A., Hanna, S., Bertram, A. K., Platt, A., Elsasser, M., Huang, L., Tarasick, D., Chellman, N., McConnell, J. R., Bozem, H., Kunkel, D., Lei, Y. D., Evans, G. J., & Abbatt, J. P. D. (2017). Observations of atmospheric chemical deposition to high Arctic snow. *Atmos. Chem. Phys.*, *17*(9), 5775-5788. https://doi.org/10.5194/acp-17-5775-2017

Macdonald, R. W., Barrie, L. A., Bidleman, T. F., Diamond, M. L., Gregor, D. J., Semkin, R. G., Strachan, W. M. J., Li, Y. F., Wania, F., Alaee, M., Alexeeva, L. B., Backus, S. M., Bailey, R., Bewers, J. M., Gobeil, C., Halsall, C. J., Harner, T., Hoff, J. T., Jantunen, L. M. M., . . . Yunker, M. B. (2000). Contaminants in the Canadian Arctic: 5 years of progress in understanding sources, occurrence and pathways. *Science of The Total Environment*, *254*(2), 93-234. https://doi.org/https://doi.org/10.1016/S0048-9697(00)00434-4

Macdonald, R. W., Harner, T., & Fyfe, J. (2005). Recent climate change in the Arctic and its impact on contaminant pathways and interpretation of temporal trend data. *Science of The Total Environment*, *342*(1), 5-86. https://doi.org/https://doi.org/10.1016/j.scitotenv.2004.12.059

Michelutti, N., Simonetti, A., Briner, J. P., Funder, S., Creaser, R. A., & Wolfe, A. P. (2009). Temporal trends of pollution Pb and other metals in east-central Baffin Island inferred from lake sediment geochemistry. *Science of The Total Environment*, *407*(21), 5653-5662. https://doi.org/https://doi.org/10.1016/j.scitotenv.2009.07.004

Miner, K. R., D'Andrilli, J., Mackelprang, R., Edwards, A., Malaska, M. J., Waldrop, M. P., & Miller, C. E. (2021). Emergent biogeochemical risks from Arctic permafrost degradation. *Nature Climate Change*, *11*(10), 809-819. https://doi.org/10.1038/s41558-021-01162-y

Misiuk, B., Lecours, V., & Bell, T. (2018). A multiscale approach to mapping seabed sediments. *PLOS ONE*, *13*(2), e0193647. https://doi.org/10.1371/journal.pone.0193647

Naidu, A. S., Blanchard, A. L., Misra, D., Trefry, J. H., Dasher, D. H., Kelley, J. J., & Venkatesan, M. I. (2012). Historical changes in trace metals and hydrocarbons in nearshore sediments, Alaskan Beaufort Sea, prior and subsequent to petroleum-related industrial development: Part I. Trace metals. *Marine Pollution Bulletin*, *64*(10), 2177-2189. https://doi.org/https://doi.org/10.1016/j.marpolbul.2012.07.037

O'Donnell, J. A., Carey, M. P., Koch, J. C., Baughman, C., Hill, K., Zimmerman, C. E., Sullivan, P. F., Dial, R., Lyons, T., Cooper, D. J., & Poulin, B. A. (2024). Metal mobilization from thawing permafrost to aquatic ecosystems is driving rusting of Arctic streams. *Communications Earth & Environment*, *5*(1), 268. https://doi.org/10.1038/s43247-024-01446-z

Pedersen, K. B., Lejon, T., Jensen, P. E., & Ottosen, L. M. (2015). Chemometric Analysis for Pollution Source Assessment of Harbour Sediments in Arctic Locations. *Water, Air, & Soil Pollution*, *226*(5), 150. https://doi.org/10.1007/s11270-015-2416-4

Pelletier, N., Chételat, J., Cousens, B., Zhang, S., Stepner, D., Muir, D. C. G., & Vermaire, J. C. (2020). Lead contamination from gold mining in Yellowknife Bay (Northwest Territories), reconstructed using stable lead isotopes. *Environmental Pollution*, *259*, 113888. https://doi.org/https://doi.org/10.1016/j.envpol.2019.113888

Pourmand, A., Dauphas, N., & Ireland, T. J. (2012). A novel extraction chromatography and MC-ICP-MS technique for rapid analysis of REE, Sc and Y: Revising CI-chondrite and Post-Archean Australian Shale (PAAS) abundances. *Chemical Geology*, *291*, 38-54. https://doi.org/https://doi.org/10.1016/j.chemgeo.2011.08.011

Rainbird, R. H., Rooney, A. D., Creaser, R. A., & Skulski, T. (2020). Shale and pyrite Re-Os ages from the Hornby Bay and Amundsen basins provide new chronological markers for Mesoproterozoic stratigraphic successions of northern Canada. *Earth and Planetary Science Letters*, *548*, 116492. https://doi.org/https://doi.org/10.1016/j.epsl.2020.116492

Rodon, T., & Bouchard, K. (2024). Between a rock and a hard place: the Social Acceptability of the Mary River mining project in Nunavut. *Mineral Economics*. https://doi.org/10.1007/s13563-024-00462-x

Sakan, S., Đorđević, D., Dević, G., Relić, D., Anđelković, I., & Đuričić, J. (2011). A study of trace element contamination in river sediments in Serbia using microwave-assisted aqua regia digestion and multivariate statistical analysis. *Microchemical Journal*, *99*(2), 492-502. https://doi.org/https://doi.org/10.1016/j.microc.2011.06.027

Salazar-Coria, L., Amezcua-Allieri, M. A., Tenorio-Torres, M., & González-Macías, C. (2007). Polyaromatic hydrocarbons (PAHs) and metal evaluation after a diesel spill in Oaxaca, Mexico. *Bulletin of Environmental Contamination and Toxicology*, *79*(4), 462-467. https://doi.org/10.1007/s00128-007-9240-5

Samuelson, G. M. (1998). WATER AND WASTE MANAGEMENT ISSUES IN THE CANADIAN ARCTIC: IQALUIT, BAFFIN ISLAND. *Canadian Water Resources Journal / Revue canadienne des ressources hydriques*, *23*(4), 327-338. https://doi.org/10.4296/cwrj2304327

Sanborn-Barrie, M., Young, M. D., & Whalen, J. B. (2013). *Geology, Qikiqtarjuaq, Baffin Island, Nunavut*. Natural Resources Canada.

Santos, I. R., Silva-Filho, E. V., Schaefer, C. E. G. R., Albuquerque-Filho, M. R., & Campos, L. S. (2005). Heavy metal contamination in coastal sediments and soils near the Brazilian Antarctic Station, King George Island. *Marine Pollution Bulletin*, *50*(2), 185-194. https://doi.org/https://doi.org/10.1016/j.marpolbul.2004.10.009

Scoates, J. S., & Scoates, R. F. J. (2024). The Muskox intrusion: Overview of a major open-system layered intrusion and its role as a sub-volcanic magma reservoir in the Mackenzie large igneous province. *Lithos*, *474-475*, 107560. https://doi.org/https://doi.org/10.1016/j.lithos.2024.107560

Skipton, D., Saumur, B.-M., St-Onge, M. R., Wodicka, N., Bros, E. R., Currie, L. D., Weller, O. M., & Haggart, J. W. (2018). *Bedrock geology, Pond Inlet, Nunavut, part of NTS 38-B.* Natural Resources Canada.

Skipton, D., Wodicka, N., Weller, O., Jackson, S., St-Onge, M., Saumur, B., & Petts, D. (2025). Polyphase Metamorphism of the Northern Rae Craton (Baffin Island, Arctic Canada) and Trace Element Behaviour in Monazite: Insights From Phase Equilibria Modelling and Geochronology. *Journal of Metamorphic Geology*, *43*(3), 287-314. https://doi.org/https://doi.org/10.1111/jmg.12808

Smith, I. R. (2013). Reconnaissance assessment of landscape hazards and potential impacts of future climate change in Kugluktuk, western Nunavut. *Summary of activities 2013. Canada-Nunavut Geoscience Office.* , 149-158.

Statistics Canada. (2023). *Census Profile. 2021 Census of Population*. Ottawa: Statistics Canada Catalogue number 98-316-X2021001. Released November 15, 2023. Retrieved from https://www12.statcan.gc.ca/census-recensement/2021/dp-pd/prof/index.cfm?Lang=E

Stroski, K. M., Luong, K. H., Challis, J. K., Chaves-Barquero, L. G., Hanson, M. L., & Wong, C. S. (2020). Wastewater sources of per- and polyfluorinated alkyl substances (PFAS) and pharmaceuticals in four Canadian Arctic communities. *Science of The Total Environment*, *708*, 134494. https://doi.org/https://doi.org/10.1016/j.scitotenv.2019.134494

Sutton, O. F., McCarter, C. P. R., & Waddington, J. M. (2024). Globally-significant arsenic release by wildfires in a mining-impacted boreal landscape. *Environmental Research Letters*, *19*(6), 064024. https://doi.org/10.1088/1748-9326/ad461a

Taylor, S. R., & McLennan, S. M. (1985). *The continental crust: Its composition and evolution*. Blackwell Scientific Publication (312 pp.). https://www.osti.gov/biblio/6582885

Templ M, H. K., Filzmoser P. (2011). robCompositions: an R-package for robust statistical analysis of compositional data. In *Compositional Data Analysis: Theory and Applications* (pp. 341-355). John Wiley and Sons. https://doi.org/10.1002/9781119976462.ch25

Trefry, J. H., & Neff, J. M. (2019). Effects of offshore oil exploration and development in the Alaskan Beaufort Sea: A three-decade record for sediment metals. *Integrated Environmental Assessment and Management*, *15*(2), 209-223. https://doi.org/https://doi.org/10.1002/ieam.4069

Turekian, K. K., & Wedepohl, K. H. (1961). Distribution of the Elements in Some Major Units of the Earth's Crust. *GSA Bulletin*, *72*(2), 175-192. https://doi.org/10.1130/0016-7606(1961)72[175:Doteis]2.0.Co;2

US EPA. (2007). *Method 3051A (SW-846): Microwave Assisted Acid Digestion of Sediments, Sludges, and Oils*. Washington, DC.

van Crimpen, F. C. J., Madaj, L., van Genuchten, J. M., Tesi, T., Whalen, D., Scharffenberg, K., Bröder, L., Fritz, M., & Vonk, J. E. (2025). Shallow coastal zones are key mediators in Arctic land-ocean carbon fluxes. *Communications Earth & Environment, 6*(1), 909. https://doi.org/10.1038/s43247-025-02846-5

van den Boogaart, K. G., Tolosana-Delgado, R., & Bren, M. (2023). compositions: Compositional Data Analysis. https://CRAN.R-project.org/package=compositions

Vonk, J. E., Giosan, L., Blusztajn, J., Montlucon, D., Graf Pannatier, E., McIntyre, C., Wacker, L., Macdonald, R. W., Yunker, M. B., & Eglinton, T. I. (2015). Spatial variations in geochemical characteristics of the modern Mackenzie Delta sedimentary system. *Geochimica et Cosmochimica Acta*, *171*, 100-120. https://doi.org/https://doi.org/10.1016/j.gca.2015.08.005

Wei, T., Simko, V., Levy, M., Xie, Y., Jin, Y., & Zemla, J. (2017). Package 'corrplot'. *Statistician*, *56*(316), e24.

Whalen, D., Forbes, D. L., Kostylev, V., Lim, M., Fraser, P., Nedimović, M. R., & Stuckey, S. (2022). Mechanisms, volumetric assessment, and prognosis for rapid coastal erosion of Tuktoyaktuk Island, an important natural barrier for the harbour and community. *Canadian Journal of Earth Sciences*, *59*(11), 945-960. https://doi.org/10.1139/cjes-2021-0101

Xu, G., Hannah, J. L., Bingen, B., Georgiev, S., & Stein, H. J. (2012). Digestion methods for trace element measurements in shales: Paleoredox proxies examined. *Chemical Geology*, *324-325*, 132-147. https://doi.org/https://doi.org/10.1016/j.chemgeo.2012.01.029

## 3.9 SUPPLEMENTARY MATERIAL (FIGURES AND TABLES)

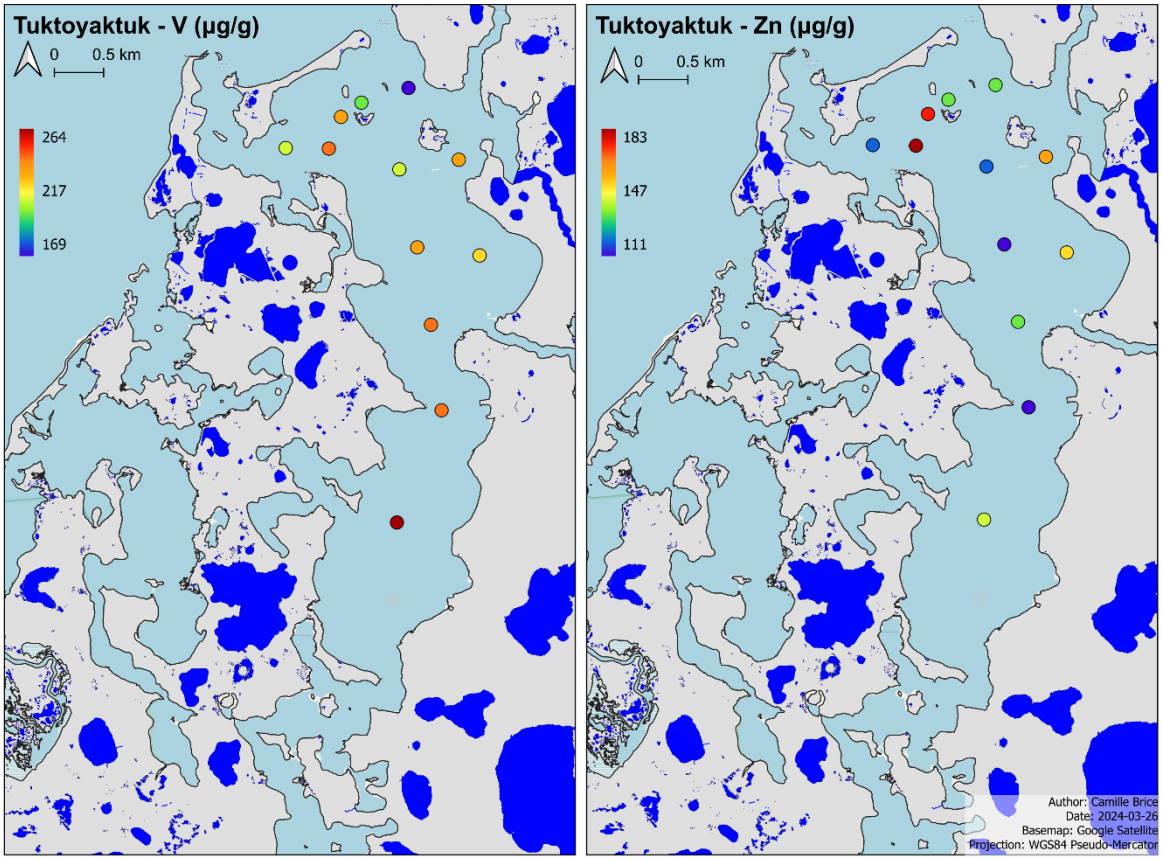


Figure 43. Maps of Tuktoyaktuk Harbor showing the spatial distribution of total V and Zn concentrations in surface sediments.

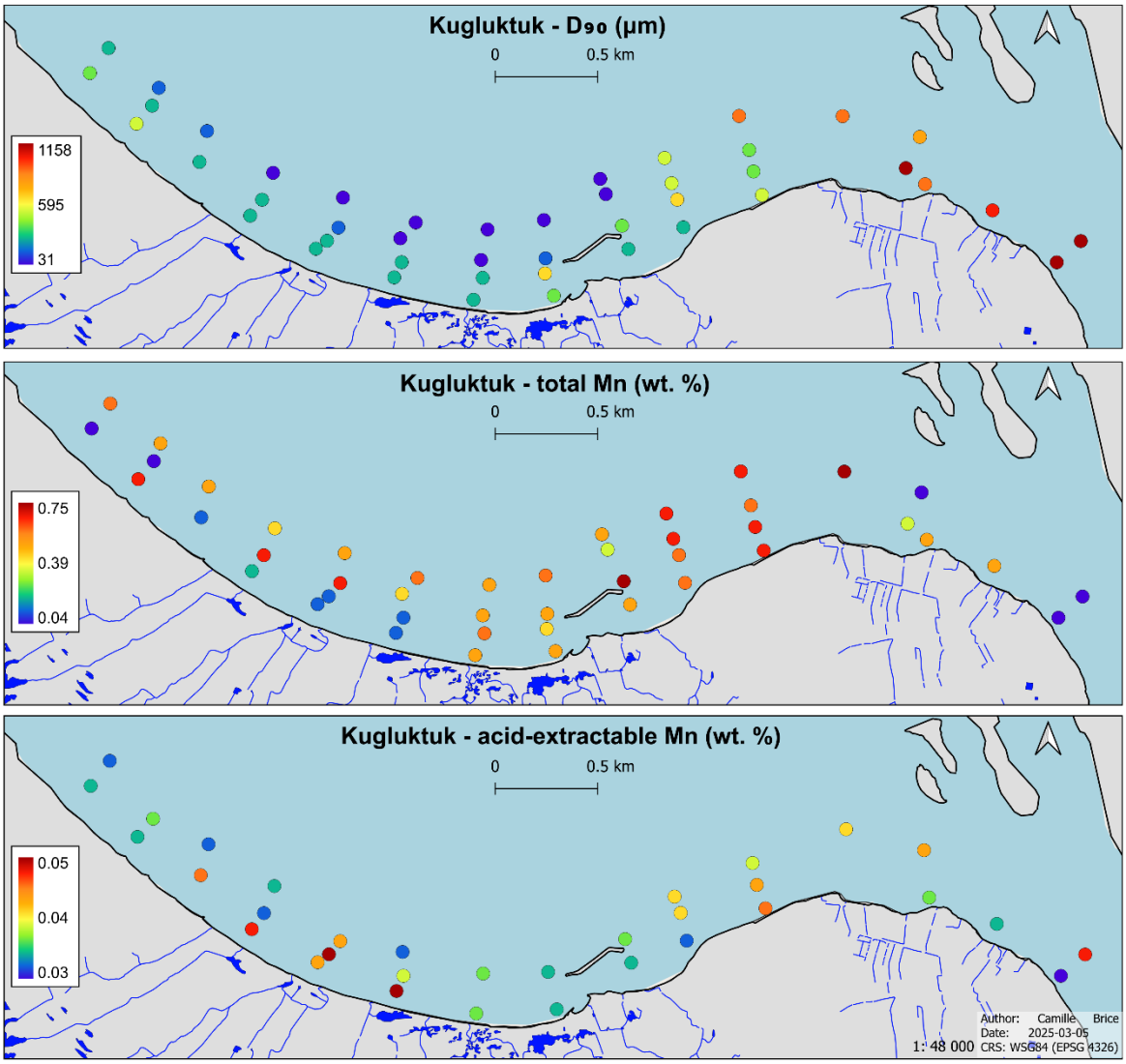


Figure 44. Maps of Kugluktuk showing the spatial distribution of grain size ($D_{90}$), total Mn and acid-extractable Mn in surface sediments.

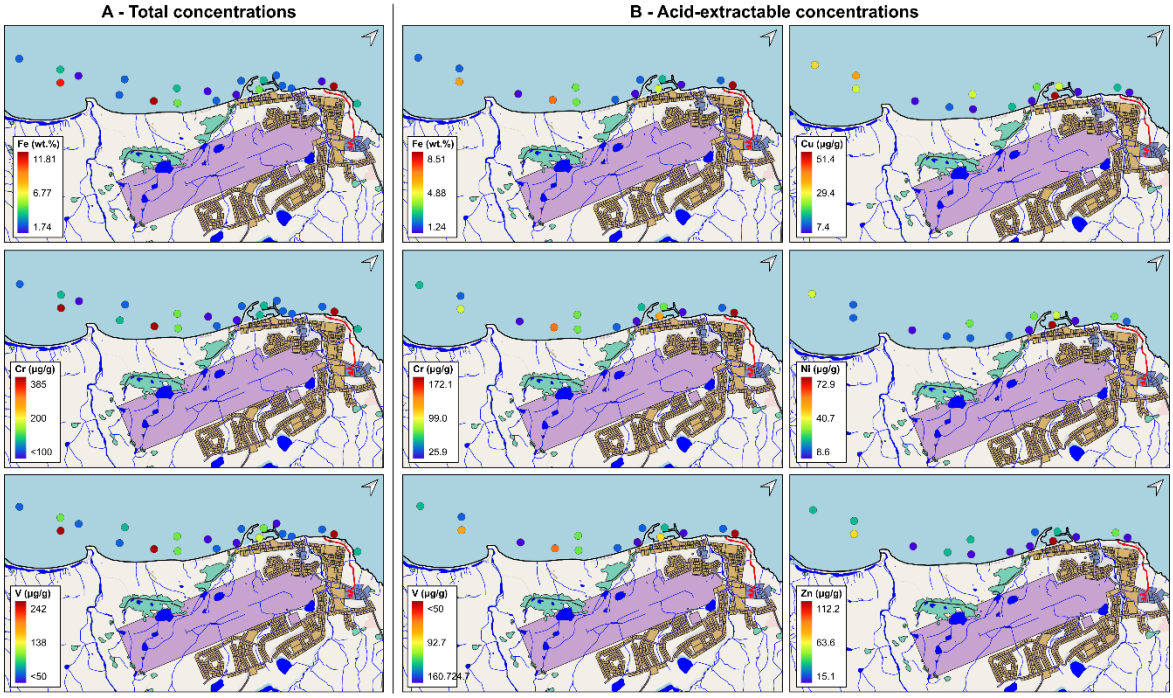


Figure 45. Maps of Pond Inlet showing the spatial distribution of the total (A) and acid-extractable (B) metal concentrations in surface sediments.

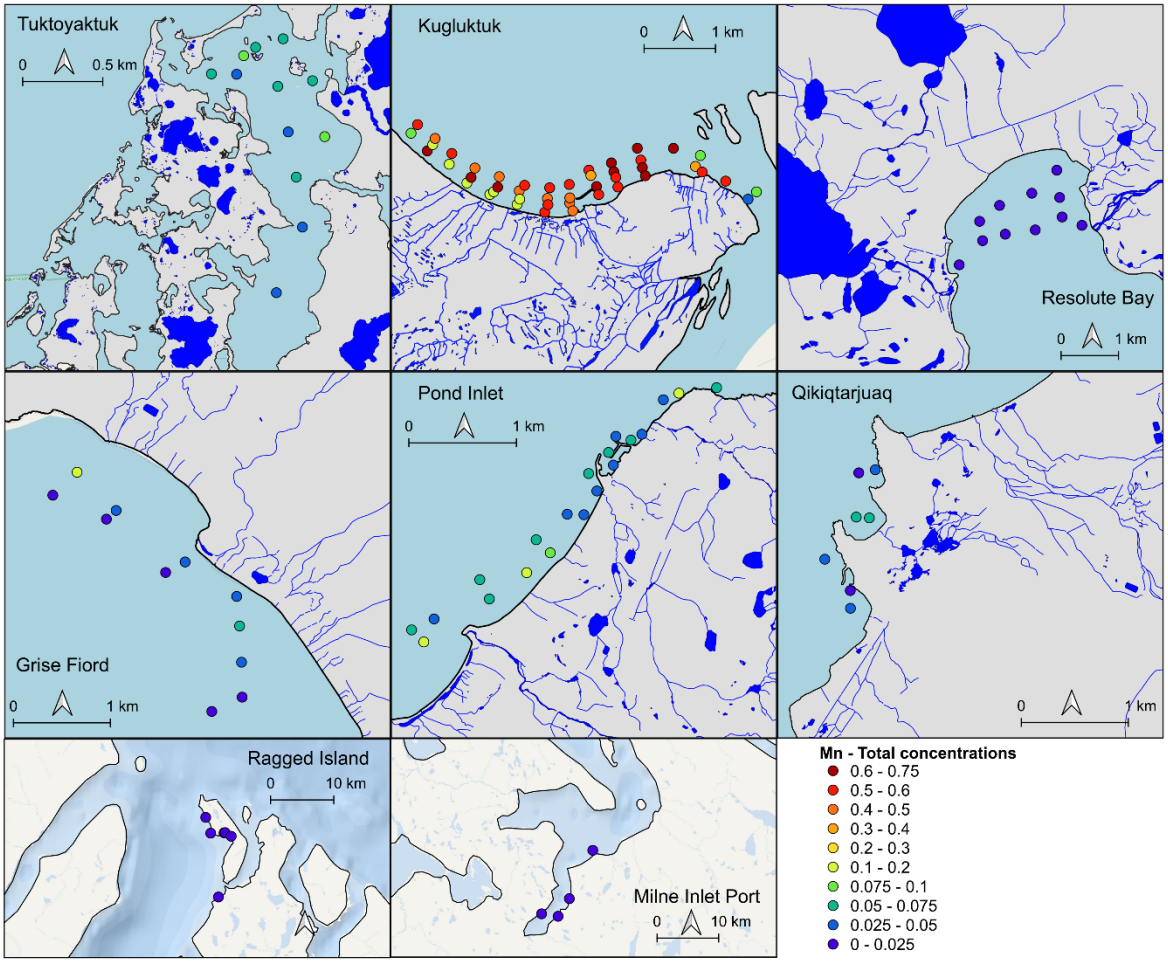


Figure 46. Spatial distribution maps of Mn total concentrations.

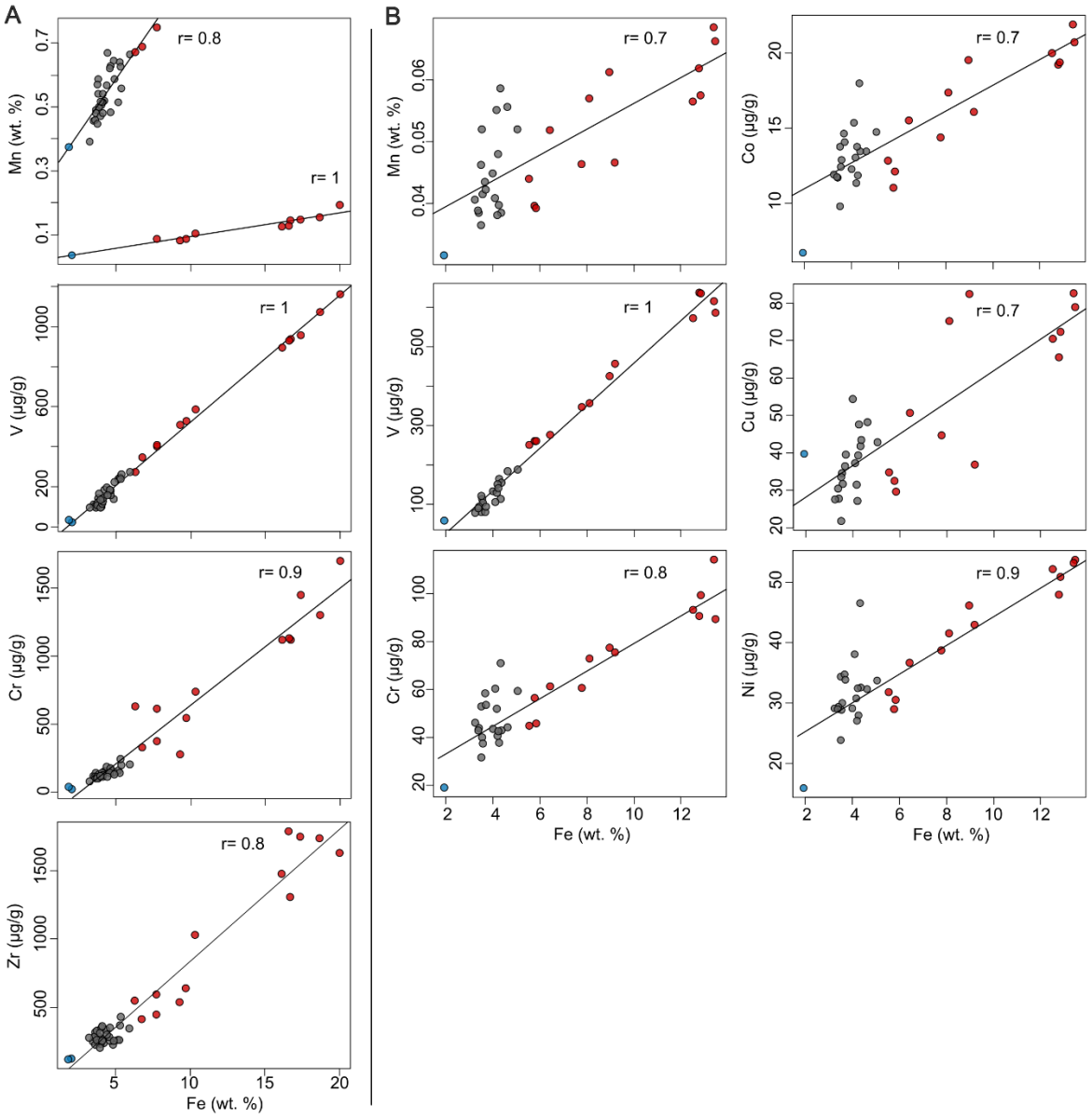


Figure 47. Scatter plots showing the correlation of Fe and other elements for (A) total and (B) acid-extractable concentrations. Spearman correlation coefficients (r) were calculated. Data are categorized by cluster: cluster 1 (blue), cluster 3 (gray) and cluster 4 (red).

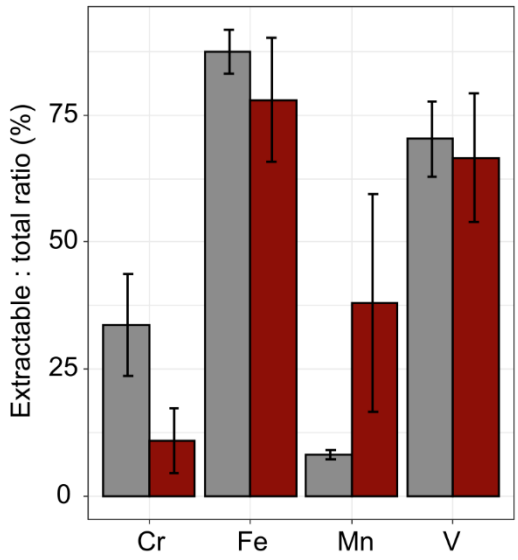


Figure 48. Acid-extraction recoveries (%) obtained for coastal sediments of Kugluktuk, calculated with energy-dispersive X-ray fluorescence (ED-XRF) results. Data are categorized by cluster: cluster 3 (gray) and cluster 4 (red).

Tableau 14.

Blank values derived from the energy-dispersive X-ray fluorescence (ED-XRF) analysis.

| Blanks | L.O.I. | $Al_2O_3$ | $SiO_2$ | $K_2O$ | CaO | $TiO_2$ | MnO | $Fe_2O_3$ | V | Cr | Zn | Sr | Zr |
|---|---|---|---|---|---|---|---|---|---|---|---|---|---|
| | | | | (wt. %) | | | | | | | (µg/g) | | |
| 1 | 0.95 | 1.77 | 97.3 | 0.009 | 0 | 0.001 | 0 | 0 | 0.4 | 60.4 | 10.2 | 4.7 | 11.2 |
| 2 | 1.01 | 0.71 | 98.3 | 0 | 0 | 0.001 | 0 | 0 | 0.9 | 9.1 | 8 | 2 | 6.4 |
| 3 | 0.96 | 0.85 | 98.2 | 0 | 0 | 0.001 | 0 | 0 | 0.2 | 10.7 | 10.2 | 2.1 | 5.2 |
| 4 | 0.98 | 0.87 | 98.1 | 0 | 0 | 0.001 | 0 | 0 | 0 | 12.2 | 0 | 0 | 3.9 |
| 5 | 0.98 | 1.49 | 97.5 | 0 | 0 | 0.001 | 0 | 0 | 1.7 | 11.8 | 13.3 | 2.7 | 7.3 |
| 6 | 0.72 | 1.29 | 98.0 | 0 | 0 | 0.001 | 0 | 0 | 2.1 | 14.3 | 7 | 2.6 | 5.8 |
| 7 | 0.73 | 0.43 | 98.8 | 0.013 | 0 | 0.001 | 0 | 0 | 0 | 6.9 | 12.3 | 2.8 | 9.6 |
| Mean | 0.90 | 1.06 | 98.0 | 0.003 | 0.0 | 0.001 | 0 | 0 | 0.76 | 17.9 | 8.7 | 2.4 | 7.1 |
| SD | 0.12 | 0.47 | 0.5 | 0.006 | 0.0 | 0.000 | 0 | 0 | 0.85 | 18.9 | 4.4 | 1.4 | 2.6 |
| DL | | 0.05 | 0.05 | 0.05 | 0.05 | 0.05 | 0.05 | 0.05 | 50 | 100 | 50 | 50 | 30 |
| < DL ? | | No | NA | Yes | Yes | Yes | Yes | Yes | Yes | Yes | Yes | Yes | Yes |
| Samples min. | | 3.94 | | | | | | | | | | | |
| Samples mean | | 8.70 | | | | | | | | | | | |
| Blank/mean | | 12% | | | | | | | | | | | |
| Blank/min. | | 27% | | | | | | | | | | | |
| Correction | | 0.56 | | | | | | | | | | | |

Tableau 15.

Certified values for ED-XRF analysis based on the reference standards SDC-1 (Canadian Soil) and BCR-1 (Basalt), along with the corresponding recovery percentages for each element analyzed in this study.

| | **Certified value** | **Uncertainty** | **Average** | **Unit** | **RSD (1σ; %)** | **Accuracy (σ; %)** |
|---|---|---|---|---|---|---|
| *SDC-1* | | | | | | |
| MgO | 1.69 | 0.1 | 1.54 | % | 2.3 | 91 ± 2 |
| $Al_2O_3$ | 15.8 | 0.3 | 15.8 | % | 0.2 | 100 ± 0.3 |
| $SiO_2$ | 65.8 | 0.4 | 66.9 | % | 0..2 | 102 ±0.2 |
| CaO | 1.4 | 0.1 | 1.4 | % | 0.4 | 98 ± 0.5 |
| $TiO_2$ | 1.0 | 0.0 | 1.2 | % | 0.3 | 114 ± 0.5 |
| MnO | 0.1 | NA | 0.1 | % | 1.4 | 99 ± 2 |
| $Fe_2O_3$ | 6.8 | NA | 6.8 | % | 0.3 | 101 ± 0.4 |
| V | 102.0 | 12.0 | 99.3 | µg/g | 11.3 | 98 ± 13 |
| Cr | 64.0 | 7.0 | 79.4 | µg/g | 9.4 | 126 ± 14 |
| Zn | 103.0 | 8.0 | 103.9 | µg/g | 5.6 | 101 ± 7 |
| Sr | 180.0 | 9.0 | 212.2 | µg/g | 1.4 | 116 ± 2 |
| Zr | 290.0 | 30.0 | 383.8 | µg/g | 1.1 | 132 ± 2 |
| *BCR-2* | | | | | | |
| MgO | 3.6 | 0.0 | 3.5 | % | 1.2 | 97 ± 1 |
| $Al_2O_3$ | 13.5 | 0.1 | 14.0 | % | 0.3 | 104 ± 0.3 |
| $SiO_2$ | 54.0 | 0.2 | 54.4 | % | 0.2 | 101 ± 0.2 |
| CaO | 7.1 | 0.1 | 7.3 | % | 0.3 | 102 ± 0.3 |
| $TiO_2$ | 2.3 | 0.0 | 2.5 | % | 0.5 | 111 ± 0.5 |
| MnO | 0.2 | 0.0 | 0.2 | % | 1.1 | 99 ± 1 |
| $Fe_2O_3$ | 13.8 | 0.2 | 14.0 | % | 0.4 | 102 ± 0.4 |
| V | 417.6 | 4.5 | 460.6 | µg/g | 5.0 | 110 ± 5.5 |
| Cr* | 18.0 | 0.4 | 40.3 | µg/g | 35.2 | 224 ± 59.3 |
| Zn | 129.5 | 1.8 | 132.0 | µg/g | 4.3 | 102 ± 4.4 |
| Sr | 337.4 | 6.7 | 379.9 | µg/g | 1.7 | 113 ± 1.9 |
| Zr | 186.5 | 1.5 | 211.5 | µg/g | 4.9 | 113 ± 3.2 |

Tableau 16

ICP-QQQ blank measurements for coastal sediments (µg/L).

| Blanks | 1 | 2 | 3 | 4 | 5 | 6 | 7 | 8 | 9 | LOD | Mean | SD |
|---|---|---|---|---|---|---|---|---|---|---|---|---|
| Mg | 4.03 | 5.32 | 1.17 | 0.41 | 2.23 | 1.38 | 5.63 | 1.57 | 2.20 | 0.0014 | 2.66 | 1.88 |
| Al | 83.6 | 73.7 | 4.7 | 1.5 | 41.9 | 31.5 | 142.9 | 19.5 | 41.4 | 0.2537 | 48.9 | 44.9 |
| Ca | 130.5 | 103.7 | 0.0 | 0.0 | 60.9 | 32.4 | 229.5 | 24.4 | 64.2 | 0.0081 | 71.7 | 73.8 |
| K | 6.12 | 4.50 | 1.63 | 0.90 | 2.87 | 1.96 | 8.17 | 1.75 | 3.05 | 0.0015 | 3.44 | 2.40 |
| Cr | 0.49 | 0.44 | 0.31 | 0.17 | 0.12 | 0.08 | 0.16 | 0.07 | 0.08 | 0.0056 | 0.21 | 0.16 |
| Mn | 0.03 | 0.03 | 0.00 | 0.00 | 0.01 | 0.01 | 0.03 | 0.00 | 0.01 | 0.0045 | 0.01 | 0.01 |
| Fe | 5.59 | 4.76 | 2.35 | 1.02 | 1.65 | 0.83 | 3.97 | 0.71 | 1.57 | 0.0006 | 2.49 | 1.82 |
| Co | 0.01 | 0.01 | 0.01 | 0.01 | 0.01 | 0.01 | 0.01 | 0.01 | 0.00 | 0.0003 | 0.01 | 0.00 |
| Ni | 0.02 | 0.01 | 0.01 | 0.00 | 0.01 | 0.00 | 0.02 | 0.00 | 0.05 | 0.0023 | 0.01 | 0.02 |
| Sc | 0.00 | 0.00 | 0.00 | 0.00 | 0.00 | 0.00 | 0.00 | 0.00 | 0.00 | 0.0049 | 0.00 | 0.00 |
| Cu | 0.20 | 0.17 | 0.16 | 0.15 | 0.13 | 0.11 | 0.08 | 0.07 | 0.07 | 0.0002 | 0.13 | 0.05 |
| Ti | 0.63 | 0.44 | 0.25 | 0.68 | 0.48 | 0.63 | 0.34 | 0.42 | 0.41 | 0.0102 | 0.48 | 0.14 |
| Zn | 0.56 | 0.85 | 0.46 | 0.44 | 0.32 | 0.30 | 0.48 | 0.31 | 0.32 | 0.0283 | 0.45 | 0.18 |
| V | 0.04 | 0.04 | 0.01 | 0.01 | 0.02 | 0.01 | 0.06 | 0.01 | 0.02 | 0.0003 | 0.02 | 0.02 |
| As | 0.02 | 0.02 | 0.00 | 0.00 | 0.01 | 0.01 | 0.03 | 0.00 | 0.01 | 0.0032 | 0.01 | 0.01 |
| Se | 0.01 | 0.00 | 0.00 | 0.00 | 0.00 | 0.00 | 0.00 | 0.00 | 0.00 | 0.0023 | 0.00 | 0.00 |
| Sr | 1.03 | 0.80 | 0.05 | 0.02 | 0.51 | 0.29 | 1.73 | 0.24 | 0.50 | 0.0002 | 0.57 | 0.55 |
| Mo | 0.18 | 0.16 | 0.14 | 0.11 | 0.09 | 0.09 | 0.11 | 0.13 | 0.13 | 0.0023 | 0.13 | 0.03 |
| Pd | 0.01 | 0.01 | 0.01 | 0.01 | 0.01 | 0.01 | 0.00 | 0.01 | 0.00 | 0.0026 | 0.01 | 0.00 |
| Y | 0.01 | 0.01 | 0.00 | 0.00 | 0.00 | 0.00 | 0.01 | 0.00 | 0.00 | 0.0003 | 0.00 | 0.00 |
| Cd | 0.00 | 0.00 | 0.00 | 0.00 | 0.00 | 0.00 | 0.00 | 0.00 | 0.00 | 0.0006 | 0.00 | 0.00 |
| Pb | 0.05 | 0.04 | 0.01 | 0.01 | 0.03 | 0.02 | 0.08 | 0.01 | 0.03 | 0.0007 | 0.03 | 0.02 |
| Eu | 0.07 | 0.07 | 0.07 | 0.07 | 0.07 | 0.07 | 0.07 | 0.07 | 0.07 | 0.0004 | 0.07 | 0.00 |
| La | 0.02 | 0.02 | 0.00 | 0.00 | 0.01 | 0.01 | 0.04 | 0.01 | 0.01 | 0.0001 | 0.01 | 0.01 |
| Ce | 0.05 | 0.04 | 0.00 | 0.00 | 0.03 | 0.02 | 0.09 | 0.01 | 0.03 | 0.0002 | 0.03 | 0.03 |
| Pr | 0.01 | 0.01 | 0.00 | 0.00 | 0.00 | 0.00 | 0.01 | 0.00 | 0.00 | 0.0001 | 0.00 | 0.00 |
| Nd | 0.08 | 0.07 | 0.05 | 0.05 | 0.06 | 0.06 | 0.09 | 0.06 | 0.06 | 0.0005 | 0.07 | 0.01 |
| Sm | 0.00 | 0.00 | 0.00 | 0.00 | 0.00 | 0.00 | 0.01 | 0.00 | 0.00 | 0.0005 | 0.00 | 0.00 |
| Gd | 0.00 | 0.00 | 0.00 | 0.00 | 0.00 | 0.00 | 0.00 | 0.00 | 0.00 | 0.0003 | 0.00 | 0.00 |
| Yb | 0.00 | 0.00 | 0.00 | 0.00 | 0.00 | 0.00 | 0.00 | 0.00 | 0.00 | 0.0003 | 0.00 | 0.00 |
| Tb | 0.00 | 0.00 | 0.00 | 0.00 | 0.00 | 0.00 | 0.00 | 0.00 | 0.00 | 0.0002 | 0.00 | 0.00 |
| Dy | 0.01 | 0.00 | 0.00 | 0.00 | 0.00 | 0.00 | 0.01 | 0.00 | 0.00 | 0.0002 | 0.00 | 0.00 |
| Ho | 0.00 | 0.00 | 0.00 | 0.00 | 0.00 | 0.00 | 0.00 | 0.00 | 0.00 | 0.0001 | 0.00 | 0.00 |
| Er | 0.00 | 0.00 | 0.00 | 0.00 | 0.00 | 0.00 | 0.00 | 0.00 | 0.00 | 0.0004 | 0.00 | 0.00 |
| Tm | 0.01 | 0.01 | 0.01 | 0.01 | 0.01 | 0.01 | 0.01 | 0.01 | 0.01 | 0.0001 | 0.01 | 0.00 |
| Lu | 0.00 | 0.00 | 0.00 | 0.00 | 0.00 | 0.00 | 0.00 | 0.00 | 0.00 | 0.0002 | 0.00 | 0.00 |
| Th | 0.00 | 0.00 | 0.00 | 0.00 | 0.00 | 0.00 | 0.00 | 0.00 | 0.00 | 0.0031 | 0.00 | 0.00 |

Tableau 17

a) Certified values for partial acid digestion of the certified reference material TILL-3 using concentrated HCl and $HNO_3$, along with the corresponding recovery percentages for each element analyzed in this study. b) Certified values for total digestion of the certified reference material TILL-3, along with the corresponding recovery percentages for REY analyzed in this study.

| | ***a) TILL-3*** | | | | | ***b) TILL-3*** | | | |
|---|---|---|---|---|---|---|---|---|---|
| | Analyzed | Certified | Recovery | RSD | | Analyzed | Certified | Recovery | RSD |
| Cr | 58.6 | 73 | 80% | 3% | Y | 8.2 | 17 | 48% | 4% |
| Mn | 310.4 | 310 | 100% | 2% | La | 14.6 | 21 | 70% | 8% |
| Fe | 17458 | 20000 | 87% | 2% | Ce | 30 | 42 | 72% | 7% |
| Co | 8.6 | 11 | 78% | 1% | Nd | 13.4 | 16 | 84% | 7% |
| Ni | 26.5 | 32 | 83% | 2% | Sm | 2.6 | 3.3 | 79% | 1% |
| Cu | 17.8 | 23 | 77% | 10% | Eu | 0.6 | <1 | NA | 7% |
| Zn | 47.2 | 43 | 110% | 46% | Yb | 0.7 | 1.5 | 47% | 3% |
| V | 37.5 | 33 | 114% | 2% | Tb | 0.3 | <0.5 | NA | 4% |
| As | 69.1 | 84 | 82% | 3% | Er | 0.8 | 1.4 | 57% | 6% |
| Ag | 1.3 | 1.6 | 80% | 4% | Lu | 0.1 | 0.2 | 50% | 7% |
| Ba | 44.2 | 43 | 103% | 5% | | | | | |
| Pb | 15.7 | 16 | 98% | 2% | | | | | |

Tableau 18.

Table presenting the concentration ranges and medians acquired by ED-XRF (XRF) and acid digestion (AD) for the six communities and Milne Inlet (Milne port and Ragged Island). Values in bold are median concentrations. The reference values are the upper continental crust (UCC), post-Archean Australian shale (PAAS) and median concentrations for regional studies in the CA. The sediment quality guidelines are the threshold effect level (TEL) and the probable effect level (PEL).

| | Analysis (n) | As | Cd | Co | Cr | Cu | Fe | Mn | Ni | Pb | V | Zn |
|---|---|---|---|---|---|---|---|---|---|---|---|---|
| Kugluktuk | XRF (49) | | | | <100–1700 | | 1.9–20 | <0.04–0.75 | | | <50–1160 | <50–152 |
| | | | | | **141** | | **4.6** | **0.51** | | | **182** | **62** |
| | AD (33) | 1.2–7 | 0.01–0.1 | 7–22 | 19–114 | 23–83 | 1.9–13.5 | 0.03–0.07 | 16–54 | 4–18 | 59–637 | 39–118 |
| | | **2.3** | **0.05** | **14** | **53** | **39** | **4.3** | **0.05** | **33** | **9** | **154** | **64** |
| Pond Inlet | XRF (22) | | | | <100–385 | | 1.7–11.8 | <0.04–0.14 | | | <50–242 | <50–95 |
| | | | | | **123** | | **3.5** | **0.06** | | | **74** | **<50** |
| | AD (15) | 0.6–6 | 0.01–0.4 | 3–18 | 26–172 | 7–51 | 1.2–8.5 | 0.01–0.04 | 9–73 | 3–14 | 25–161 | 15–112 |
| | | **1.2** | **0.05** | **6** | **70** | **20** | **2.4** | **0.03** | **21** | **7** | **54** | **39** |
| Qikiqtarjuaq | XRF (7) | | | | <100 | | 0.5–2.1 | <0.04–0.06 | | | <50–75 | <50 |
| | | | | | **<100** | | **0.6** | **0.04** | | | **<50** | **<50** |
| | AD (3) | 0.4–4 | 0.03–0.08 | 0.4–1 | 2.2–3.5 | 3–10 | 0.5–0.6 | 0.01–0.02 | 0.4–1.7 | 2–12 | 9–14 | 6–13 |
| | | **1.9** | **0.05** | **0.8** | **3** | **8** | **0.6** | **0.02** | **1.7** | **4** | **9** | **11** |
| Resolute Bay | XRF (11) | | | | <100 | | 0.1–0.7 | <0.04 | | | <50 | <50 |
| | | | | | **<100** | | **0.4** | **<0.04** | | | **<50** | **<50** |
| | AD (2) | 1.9–2.7 | 0.13–0.3 | 1.6–3 | 9–16 | 9.2–10.5 | 0.6–1.0 | 0.01–0.02 | 5–10 | 4–15 | 15–24 | 17–27 |
| Grise Fiord | XRF (11) | | | | <100 | | 0.8–7.1 | <0.04–0.11 | | | <50–355 | <50–127 |
| | | | | | **<100** | | **1.4** | **<0.04** | | | **<50** | **<50** |
| | AD (3) | 0.5–1.5 | 0.03–0.07 | 1.6–2.5 | 7–24 | 5–10 | 1–2.5 | 0.009–0.013 | 4–7 | 1–6 | 33–113 | 11–106 |
| | | **1.4** | **0.04** | **2** | **12** | **8** | **1.3** | **0.011** | **5** | **3** | **42** | **21** |
| Tuktoyaktuk | XRF (12) | | | | <100–124 | | 3.4–4.6 | 0.04–0.09 | | | 169–264 | 111–183 |
| | | | | | **100** | | **4.2** | **0.06** | | | **228** | **138** |
| | AD (8) | 13–19 | 0.2–0.4 | 13–16 | 64–85 | 35–48 | 3.7–4.3 | 0.04–0.1 | 43–51 | 16–20 | 143–196 | 143–191 |
| | | **15** | **0.3** | **14** | **73** | **39** | **4.0** | **0.05** | **47** | **19** | **162** | **164** |

| | | | | | | | | | | | | |
|---|---|---|---|---|---|---|---|---|---|---|---|---|
| Milne Inlet | XRF (4) | | | | <100 | | 0.2–1.4 | <0.04 | | | <50 | <50 |
| | | | | | **<100** | | **1.0** | **<0.04** | | | **<50** | **<50** |
| | AD (4) | 1.9–3.5 | 0.1–0.4 | 2–5 | 12–37 | 9–14 | 0.7–1.7 | 0.01–0.02 | 6–17 | 4–10 | 19–36 | 14–31 |
| | | **2.8** | **0.1** | **3** | **28** | **11** | **1.2** | **0.013** | **13** | **7** | | **23** |
| Ragged Island | XRF (6) | | | | <100 | | 0.9–1.3 | <0.04 | | | <50 | <50–53 |
| | | | | | **<100** | | **1.1** | **<0.04** | | | **<50** | **<50** |
| CA | XRF (128) | | | | <100–135 | | 1.1–5.8 | <0.04–1.6 | | | <50–306 | <50–114 |
| | | | | | **<100** | | **3.4** | **0.07** | | | **98** | **53** |
| | AD (128) | 2–59 | 0.02–0.4 | 2–39 | 13–92 | 3–115 | 0.9–4.2 | 0.01–1.15 | 7–87 | 2–222 | 25–186 | 20–137 |
| | | **11** | **0.1** | **10** | **43** | **25** | **2.3** | **0.05** | **27** | **10** | **71** | **62** |
| UCC | | 1.5 | 0.098 | 10 | 35 | 25 | 3.50 | 0.060 | 20 | 20 | 60 | 71 |
| PAAS | | 10* | 0.3* | 23 | 110 | 50 | 5.06 | 0.085 | 55 | 20 | 150 | 85 |
| TEL | | 7.24 | 0.7 | | 52.3 | 18.7 | | | 15.9 | 30.2 | | 124 |
| PEL | | 41.6 | 4.21 | | 160 | 108 | | | 42.8 | 112 | | 270 |

# CONCLUSION GÉNÉRALE

L'étude géochimique des fonds marins de l'Arctique canadien a permis de répondre à l'objectif principal de cette thèse, soit d'apporter de nouvelles connaissances sur l'état actuel de la contamination métallique de la région. Cette étude vient d'une part combler d'importantes lacunes dans les connaissances sur la composition chimique du fond marin dans des secteurs jusqu'alors non caractérisés. D'autre part, l'analyse de la composition chimique des sédiments marins a permis d'identifier les facteurs naturels contrôlant la répartition des éléments majeurs et traces, de mieux comprendre le comportement des ETM en milieu marin arctique, ainsi que d'identifier les zones présentant un risque écotoxicologique (Figure 49). Elle met également en évidence les zones particulièrement sensibles à une potentielle contamination dans un contexte de changements climatiques futurs. Cette étude repose sur l'analyse des propriétés sédimentologiques et chimiques d'échantillons de sédiments marins de surface et de sédiments terrestres, collectés dans une vaste zone s'étendant de la mer de Beaufort à la baie de Baffin. Les principaux résultats et conclusions associés aux trois objectifs spécifiques sont présentés dans cette section. Une discussion portant sur les limites de l'étude et les perspectives de recherche futures suivra.

*Objectif 1 : documenter la dynamique sédimentaire et évaluer l'applicabilité d'indices de pollution*

Dans ce premier chapitre, l'objectif était de fournir les connaissances préalables nécessaires pour une évaluation complète de la contamination métallique des sédiments marins. Ainsi, à partir d'analyses géochimiques au ED-XRF, la dynamique sédimentaire de l'Arctique canadien a pu être mieux définie. De plus, l'application du facteur d'enrichissement et de l'indice de géo-accumulation a également été étudiée afin de déterminer les avantages et les limites de ces outils dans l'évaluation de la pollution des sédiments dans l'AC.

Les données géochimiques ED-XRF ont mis à l'évidence une forte variabilité régionale de la composition des fonds marins qui est principalement influencée par la géologie. Combinés à des analyses statistiques multivariées, les résultats ont permis de catégoriser les sédiments marins l'Arctique canadien selon trois groupes chimiques distincts correspondant à quatre provinces géographiques. Le premier groupe est composé d'échantillons ayant été collectés dans les chenaux et détroits du centre de l'AC, ainsi que le détroit de Nares. Ce groupe chimique se caractérise par des sédiments ayant une forte teneur en carbonates détritiques dont la provenance est les calcaires et dolomies composant la Plateforme arctique. L'érosion côtière et la glace de mer sont les processus dominants responsables du transport des sédiments dans ce groupe. Les échantillons du deuxième groupe proviennent des zones côtières du golfe de la Reine-Maud ainsi que des fjords et baies de l'île de Baffin. Ils sont composés de sédiments grossiers riches en matériaux silicoclastiques. La composition de ces sédiments est influencée par les différentes rivières drainant le nord du Canada et l'île de Baffin et par les glaciers de l'île de Baffin, qui érodent les roches ignées et métamorphiques du Bouclier canadien. Le troisième groupe, quant à lui, se caractérise par des sédiments riches en carbone organique, en oxydes de Fe-Mn et en aluminosilicates fins. Il est présent dans deux régions distinctes de l'AC : à l'est et à l'ouest. L'ouest, incluant le plateau du Mackenzie, le sud de la mer de Beaufort et le golfe d'Amundsen, est fortement influencé par la rivière Mackenzie, qui décharge une grande quantité de sédiments riches en carbone organique d'origine terrestre ainsi qu'en Al, Fe, V et Zn d'origine lithogénique. L'est de l'Arctique canadien, pour sa part, est principalement influencé par la production primaire associée aux polynies et par les apports glaciaires provenant des glaciers des îles Devon et Ellesmere.

Les concentrations les plus élevées en métaux traces (V, Zn et Cr) sont observées dans la région du plateau du Mackenzie. Le fleuve Mackenzie semble être le principal contributeur de métaux dans cette zone, en déversant d'importantes quantités d'oxydes de Fe-Mn d'origine lithogénique, de minéraux argileux et de métaux associés issus de l'altération des schistes qui dominent la composition du bassin versant. Les données indiquent que les

minéraux argileux fins et les oxydes de Fe constituent les principales phases porteuses des métaux traces, suivis par la MO.

À travers l'AC, les indices de pollution suggèrent que les métaux traces proviennent majoritairement de sources naturelles et présentent un faible risque écologique pour les organismes benthiques vivant à l'interface eau-sédiment. Toutefois, les EF et les Igeo calculés à partir de différents fonds géochimiques révèlent des divergences significatives, soulignant la nécessité d'interpréter ces indices avec précaution. L'utilisation des fonds géochimiques généraux, tels que la croûte continentale supérieure (UCC) ou schiste moyen (AS), peut être pertinente lorsque les échantillons de sédiments présentent une composition chimique régionale similaire. Cependant, ce n'est pas le cas pour la majorité des sédiments de l'AC, qui présentent une grande variabilité lithologique. Par ailleurs, la normalisation des concentrations métalliques à l'aide d'un élément conservatif dans le calcul de l'EF a également montré certaines limites. Il est donc recommandé de valider les EF en utilisant différents éléments normalisateurs conservateurs, afin de minimiser les risques de mauvaises interprétations.

En résumé, dans l'AC, le portrait spatial géochimique combiné à l'utilisation d'indices de pollution s'est révélée une approche précieuse pour mieux comprendre la répartition des métaux, les processus naturels contrôlant leur enrichissement ou leur appauvrissement, ainsi que pour évaluer la contamination métallique potentiellement liée aux activités humaines. Cette étude a permis d'identifier le fleuve Mackenzie comme la principale source de contribution d'ETM dans l'ouest de l'AC, sans qu'aucune contribution anthropique significative n'ait été détectée. De plus, les caractéristiques des sources sédimentaires, notamment le socle rocheux, ainsi que la nature des sédiments, incluant leur minéralogie et leur granulométrie, ont été identifiées comme des facteurs clés régissant l'accumulation des ETM dans les sédiments marins de l'AC. Finalement, l'utilisation des indices de pollution s'est avérée pertinente dans le cadre de cette étude. Toutefois, l'établissement d'un fond géochimique régional, basé sur les provinces sédimentaires, s'est révélé essentiel pour garantir une interprétation fiable et adaptée de ces indices.

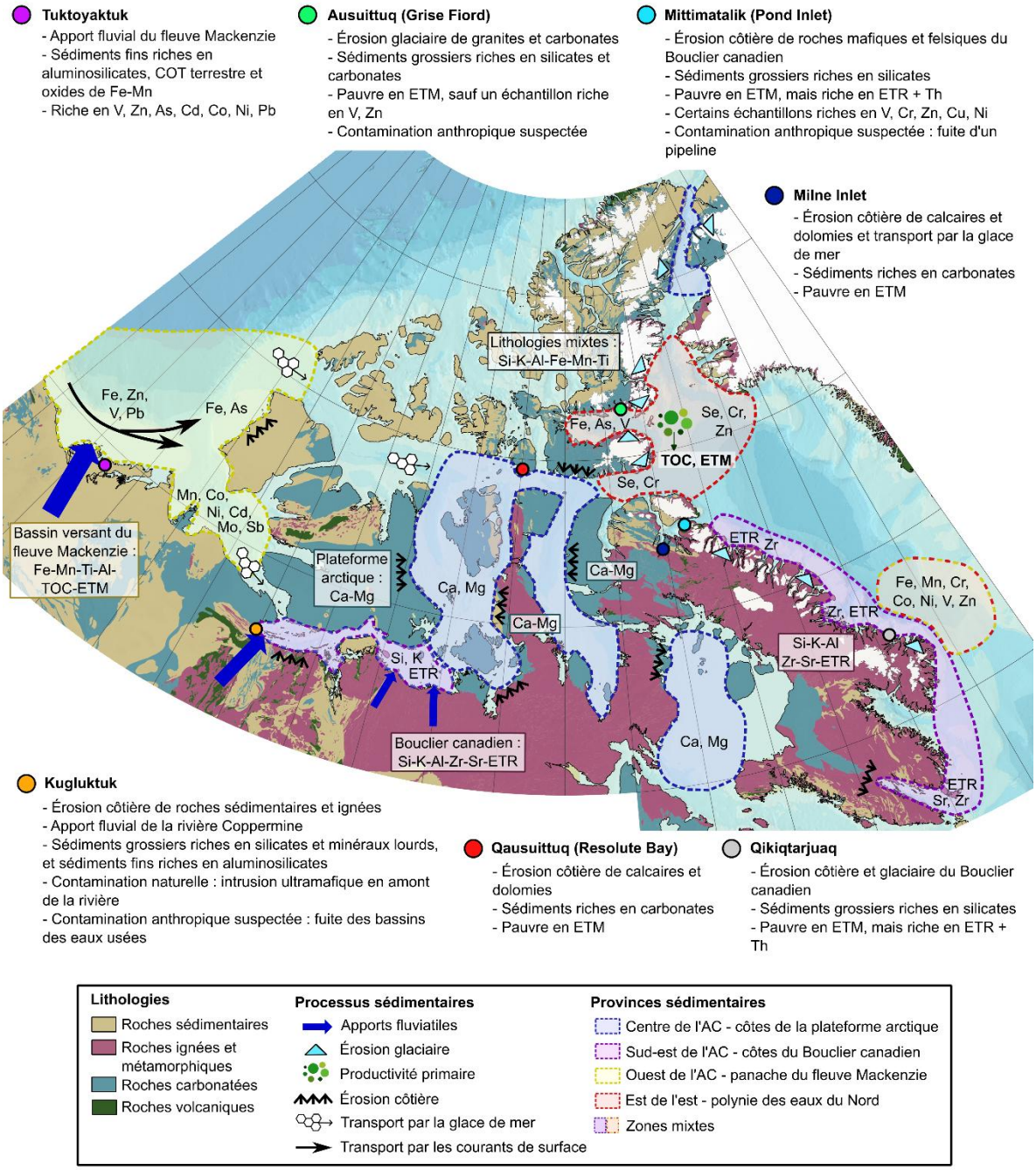


Figure 49. Figure synthétisant les sources, processus de transport et zones d'accumulation principaux des éléments majeurs et traces dans les sédiments marins de l'Arctique canadien.

*Objectif 2 : Établir les concentrations de référence des ETM dans la fraction extractible à l'acide des sédiments dans l'Arctique canadien*

À partir des nouvelles connaissances tirées du premier chapitre, le deuxième objectif visait à compléter le levé géochimique de l'Arctique canadien en fournissant une base de référence des concentrations modernes des ETM. Ainsi, les mêmes échantillons ont été analysés, cette fois-ci, par digestion partielle à l'acide et spectromètre de masse à triple quadrupôle (ICP-QQQ). Cette nouvelle méthode a permis d'obtenir les concentrations dites extractibles de la majorité des ETM dans les sédiments. La contamination par plusieurs métaux (As, Cd, Co, Cr, Cu, Ni, Pb, V, Zn) a été évaluée avec les indices pollutions et les recommandations canadiennes pour la qualité des sédiments (CCME, 1999). Basée sur les conclusions du Chapitre 1, un fond géochimique régional subdivisé selon les provinces sédimentaires a été établi pour l'utilisation des indices de pollution. De plus, les éléments des terres rares ont également été étudiés.

Tout comme les résultats au ED-XRF, cette étude géochimique révèle une distribution spatiale suivant une tendance ouest-est influencée par la lithologie, les conditions rédox, les apports fluviaux, la dérive de la glace de mer, les courants océaniques et la productivité primaire. Le plateau du Mackenzie, le sud de la mer de Beaufort et le golfe d'Amundsen présentent les concentrations les plus élevées en métaux traces dans l'AC. Le principal apport de ces éléments provient du fleuve Mackenzie, mais leur répartition est ensuite influencée par l'affinité des métaux avec les phases porteuses et par les conditions d'oxydoréduction. Le V, Zn, Pb et Cr sont rapidement retirés de la colonne d'eau et transportés vers les sédiments à l'embouchure de la rivière, principalement par l'intermédiaire de la matière organique. En revanche, l'As, Ni, Co et Cd sont plus mobiles et sont transportés plus loin de la rivière par les courants côtiers. Les fortes concentrations en As observées dans le sud de la mer de Beaufort, à l'est de l'île Banks, semblent associées aux cycles du Fe. Cette région, plus éloignée de l'embouchure de la rivière Mackenzie et moins riche en COT, favorise probablement la déposition d'oxydes de Fe détritiques et/ou la formation d'oxydes authigéniques (Magen, 2008), ce qui expliquerait l'accumulation d'As. Le golfe d'Amundsen

présente des concentrations élevées en Ni, Co et Cd, dont l'association avec les oxydes de Mn constitue l'explication la plus plausible. De plus, les conditions diagenétiques dans cette région favorisent l'enrichissement du Mn et, par conséquent, de ces métaux à la surface des sédiments.

Tout comme les autres métaux traces, la concentration en ETR dans les sédiments de l'AC est principalement contrôlée par la lithologie. Les ETR légers (La-Nd) se trouvent principalement liés aux oxydes métalliques, extractibles par acide, tandis que les ETR lourds semblent associées aux zircons et autres phases réfractaires. Dans l'est de l'AC, les lithologies précambriennes du Bouclier canadien transmettent aux sédiments côtiers leurs fortes concentrations, une signature enrichie en ETR légers et une anomalie négative en Ce. Dans l'ouest de l'AC, les échantillons présentent la signature labile du fleuve Mackenzie (Bossé-Demers et al., 2025), avec un enrichissement en ETR moyens (Sm-Dy). Le reste de l'AC est généralement caractérisé par un léger enrichissement en ETR légers et une petite anomalie positive en Ce, reflétant un profil typique des sédiments marins.

Aucun risque écologique majeur n'a été identifié dans cette étude. Les concentrations en métaux traces dans les sédiments de surface présentent une forte variabilité régionale, ce qui entraîne occasionnellement des dépassements des critères de qualité des sédiments. Cependant, ces dépassements restent généralement dans la gamme de concentrations associées à des sources naturelles observées à travers les régions arctiques. Seul le détroit de Jones présente deux échantillons dont les concentrations en As dépassant la CEP, et qui ont été classés comme pollués et enrichis. Bien que l'origine de ces concentrations élevées semble naturelle, elle n'est pas totalement expliquée à ce stade.

*Objectif 3 : Évaluation de la contamination métallique le long des côtes des communautés inuites*

Un portrait exhaustif de l'état actuel de la contamination métallique dans l'Arctique canadien à l'échelle régionale a été établi à partir des Chapitres 1 et 2, ainsi que de plusieurs autres études (ex., Campbell & Loring, 1980; Naidu et al., 2012; Trefry & Neff, 2019; Trefry

et al., 2003). Dans ce troisième chapitre, l'objectif était d'évaluer l'état de la contamination à une échelle locale, soit à l'échelle des communautés inuites vivant dans l'AC.

À l'aide d'analyses géochimiques de la fraction totale par ED-XRF et de la fraction extractible à l'acide par ICP-QQQ, cette étude a évalué la contamination en métaux traces dans les sédiments côtiers de six communautés inuites canadiennes, ainsi qu'à Milne Inlet, site du port de la mine Mary River. Les résultats révèlent des degrés variables d'enrichissement en métaux selon les sites, influencés à la fois par des processus géologiques naturels et par de potentielles sources anthropiques.

Les communautés de Pond Inlet et de Qikiqtarjuaq sont principalement influencées par des sédiments clastiques grossiers dérivés des roches précambriennes du Bouclier canadien environnant. Tandis que les sédiments de Qikiqtarjuaq présentent des concentrations très faibles en métaux traces, ceux de Pond Inlet affichent une composition plus hétérogène, en raison de la présence conjointe de roches felsiques et mafiques, certains échantillons montrant des teneurs élevées en métaux traces. L'enrichissement en ETR et en Th observé dans ces communautés est caractéristique des sédiments dérivés du Bouclier canadien. Des sédiments riches en carbonates et pauvres en ETM prédominent à Resolute Bay et à Milne Inlet. Les sédiments de Grise Fiord reflètent une influence mixte du Bouclier canadien et de la Plate-forme arctique, contenant à la fois du matériel silicoclastique et carbonaté. Des concentrations plus élevées en métaux traces ont été observées à Tuktoyaktuk et à Kugluktuk. Dans le port de Tuktoyaktuk, le fleuve Mackenzie apporte des silts fins enrichis en aluminosilicates et en oxydes métalliques, qui transportent les métaux traces. Plusieurs métaux y dépassent la CSE, ce qui suggère un potentiel d'effets biologiques occasionnels. Toutefois, ces concentrations demeurent comparables aux valeurs de fond régionales rapportées pour le delta du Mackenzie et le sud de la mer de Beaufort. Les sédiments côtiers de Kugluktuk, issus de l'érosion de roches intrusives mafiques, de roches sédimentaires et des apports de la rivière Coppermine, présentent globalement des concentrations modérées en métaux traces.

Des contributions anthropiques sont suspectées dans trois communautés. À Grise Fiord, un échantillon unique présente des teneurs anormalement élevées en Fe, Mn, Ti, V et Zn, environ quatre fois supérieures à celles des autres échantillons. Des analyses complémentaires sont nécessaires pour confirmer l'origine de cette anomalie. À Pond Inlet, certains échantillons dépassent les concentrations naturelles en métaux, avec une contamination potentiellement liée à des déversements d'hydrocarbures à proximité d'un pipeline et à l'activité des embarcations dans le port. Les sédiments côtiers de Kugluktuk révèlent un enrichissement significatif en minéraux lourds et en métaux traces, notamment à l'embouchure de la rivière Coppermine et le long de la côte à l'ouest de la communauté. Bien que ces enrichissements soient probablement liés à la présence en amont d'intrusions mafiques à ultramafiques, l'accumulation marquée de V et de Cr à l'ouest de Kugluktuk suggère également une possible contribution anthropique, possiblement amplifiée par le dépôt préférentiel de minéraux lourds.

*Perspectives*

Ce projet a permis de générer de nouvelles connaissances sur les processus naturels complexes qui contrôlent la distribution des métaux traces dans l'AC, contribuant ainsi à une meilleure compréhension du système géochimique régional. Cette compréhension approfondie facilite ou va faciliter l'identification des apports anthropiques potentiels dans un environnement dominé par des sources naturelles. Cependant, cette étude ne constitue qu'une étape dans l'évaluation globale de la contamination métallique dans l'AC. Des recherches complémentaires, incluant des analyses temporelles ainsi que des investigations ciblées dans les zones à risque, seront nécessaires pour dresser un portrait plus complet et dynamique de l'état de la contamination métallique dans cette région sensible.

L'étude des sédiments marins de surface via les deux méthodes d'analyses de cette thèse offre une excellente vue d'ensemble de la répartition spatiale des métaux dans la zone d'étude et renseigne sur le comportement de ceux-ci. L'utilisation d'indices de pollution sur les données de concentrations totales et extractibles ont permis de facilement quantifier le niveaux de contamination à travers l'Arctique canadien. Par contre, les conclusions tirées de

ces analyses sont limitées pour évaluer les risques écotoxicologiques. Ainsi, à partir de ces mêmes échantillons, une analyse par extraction séquentielle (Tessier et al., 1979) permettrait d'obtenir les concentrations de métaux associés à chaque phase porteuse et apporterait ainsi des interprétations plus robustes sur leur mobilité et biodisponibilité. L'étude de carottes sédimentaires à travers l'Arctique pourrait complémenter les données de sédiments de surface. L'analyse de la distribution verticale des concentrations des éléments majeurs et traces dans les sédiments et dans les eaux interstitielles des carottes viendrait combler les lacunes sur notre compréhension des processus diagenétiques s'effectuant dans l'AC. Par exemple, les travaux de Kuzyk et al. (2017) sur la diagenèse précoce dans l'ouest de l'AC ont permis de mieux comprendre l'enrichissement localisé de certains métaux dans la région. Les informations provenant des extractions séquentielles et des profils verticaux permettront d'interpréter de manière fiable les résultats des indices de pollution. En effet, les indices de pollution peuvent mener à des conclusions erronées lorsque le contexte géographique et les conditions biogéochimiques du milieu ne sont pas maitrisés. Une étude spatiale exhaustive associée à une compréhension du partitionnement des métaux dans les sédiments et de la diagénèse offre un portrait complet permettant de saisir la nature d'une contamination dans un milieu, s'il y a lieu.

L'analyse de carottes sédimentaires peut également renseigner sur les variations temporelles des concentrations des ETM et aider à retracer leur accumulation dans le milieu marin à travers le temps. Finalement, les concentrations mesurées dans les eaux interstitielles représentent la fraction la plus biodisponible pour les organismes (Ankley et al., 1994) et corrèlent avec la toxicité mesurée dans ceux-ci (ex. Alves et al., 2018). Elles constituent donc une information essentielle pour l'évaluation des risques écotoxicologiques. Pour prédire la toxicité des ETM, il faut également mesurer leur accumulation dans les organismes, qui dépend entre autres de la concentration dans le milieu, de la biodisponibilité et des comportements de l'organisme (Simpson & Batley, 2007). Ainsi, la mesure des concentrations dans les organismes benthiques combinés à la mesure dans les sédiments pourrait apporter ces informations.

Une meilleure couverture spatiale de l'échantillonnage est nécessaire pour permettre une évaluation représentative de la qualité des sédiments côtiers à proximité des communautés inuites. En effet, comme l'a démontré le cas de Kugluktuk, des contaminations métalliques importantes peuvent se manifester de manière très localisée. Dans cette communauté, la densité adéquate de l'échantillonnage a permis de détecter ces enrichissements. En revanche, dans d'autres localités, l'échantillonnage demeure incomplet, ce qui limite la capacité à détecter d'éventuelles contaminations. C'est notamment le cas à Grise Fiord, où un seul échantillon a révélé des concentrations anormalement élevées en certains métaux. En l'absence d'échantillons supplémentaires dans cette zone, il est difficile de déterminer s'il s'agit d'une anomalie isolée ou du reflet d'un phénomène plus étendu. Ce manque d'échantillons dans la zone d'étude restreint donc la portée des interprétations et souligne l'importance d'un maillage spatial plus dense pour les futures campagnes d'échantillonnage.

Cette thèse de doctorat a fourni des données inédites sur les éléments des terres rares dans l'Arctique canadien. Or, les informations tirées des analyses n'ont pas permis d'adéquatement caractériser les ETR. L'extraction partielle a limité la compréhension du comportement des ETR dans les sédiments marins, car les ETR lourds n'ont été que faiblement extraits alors que les ETR légers ont été presqu'entièrement extraits. Ainsi, les profils des lanthanides normalisés, fréquemment utilisés pour analyser les sources, le fractionnement et le transport des ETR, présentent des résultats artificiellement définis par la méthodologie. Une extraction totale permettrait donc d'obtenir les profils réels des ETR, et ainsi cela permettra de distinguer l'influence des activités humaines sur les concentrations et la distribution des ETR.

Finalement, une surveillance à long terme de la région en collaboration avec les membres des communautés est fortement recommandée afin de suivre l'évolution des impacts anthropiques sur le milieu marin de l'AC. Ce travail collaboratif permettra l'établissement d'une base de référence des concentrations en métaux dans les sédiments, ainsi que le suivi régulier de ces concentrations dans le temps. Il en découlera une meilleure

compréhension des tendances temporelles d'accumulation des métaux en lien avec les émissions anthropiques et les variations des conditions naturelles. Cette approche est essentielle pour anticiper les effets potentiels des changements environnementaux et des activités humaines croissantes dans cette région particulièrement vulnérable.

# ANNEXE I – LISTE DES ECHANTILLONS

Tableau 19.

Liste des échantillons de sédiments utilisés pour les chapitres 1 et 2 de cette étude.

| Expédition | Station | Nom de la carotte | Type | Long. | Lat. | Prof. eau (m) |
|---|---|---|---|---|---|---|
| AMD1603 | Lakeman-08 | AMD1603-0416-01-BC | Boxcore | -122.167 | 74.885 | 505 |
| AMD1603 | 405 | AMD1603-0416-02-BC | Boxcore | -123.028 | 70.608 | 628 |
| AMD1603 | 0416-03 | AMD1603-0416-03-BC | Boxcore | -120.348 | 70.513 | 330 |
| AMD1603 | 0416-04 | AMD1603-0416-04-BC | Boxcore | -117.856 | 69.653 | 415 |
| AMD1603 | 0416-05 | AMD1603-0416-05-BC | Boxcore | -115.071 | 67.864 | 60 |
| AMD1603 | 0416-07 | AMD1603-0416-07-BC | Boxcore | -102.725 | 71.869 | 245 |
| AMD1603 | 1402 | AMD1603-1402-BC | Boxcore | -117.632 | 70.546 | 400 |
| AMD1603 | 165 | AMD1603-165-BC | Boxcore | -75.761 | 72.709 | 645 |
| AMD1603 | 177 | AMD1603-177-BC | Boxcore | -63.801 | 67.475 | 385 |
| AMD1603 | Lakeman-05 | AMD1603-2016-805-18-BC | Boxcore | -129.127 | 74.007 | 420 |
| AMD1603 | 554 | AMD1603-2016-805-20-BC | Boxcore | -126.476 | 75.741 | 373 |
| AMD1603 | 301 | AMD1603-301-BC | Boxcore | -83.319 | 74.121 | 740 |
| AMD1603 | 304 | AMD1603-304-BC | Boxcore | -91.521 | 74.246 | 314 |
| AMD1603 | 307 | AMD1603-307-BC | Boxcore | -103.014 | 74.102 | 350 |
| AMD1603 | 310E | AMD1603-310E-BC | Boxcore | -99.076 | 70.832 | 216 |
| AMD1603 | 310W | AMD1603-310W-BC | Boxcore | -101.272 | 71.459 | 163 |
| AMD1603 | 311 | AMD1603-311-BC | Boxcore | -98.534 | 70.280 | 170 |
| AMD1603 | 312 | AMD1603-312-BC | Boxcore | -100.697 | 69.166 | 66 |
| AMD1603 | 314 | AMD1603-314-BC | Boxcore | -105.475 | 68.971 | 89 |
| AMD1603 | 316 | AMD1603-316-BC | Boxcore | -112.100 | 68.400 | 182 |
| AMD1603 | 407 | AMD1603-407-BC | Boxcore | -126.090 | 71.009 | 390 |
| AMD1603 | 408 | AMD1603-408-BC | Boxcore | -127.574 | 71.303 | 205 |
| AMD1603 | 411 | AMD1603-411-BC | Boxcore | -126.731 | 71.623 | 435 |
| AMD1603 | 420 | AMD1603-420-BC | Boxcore | -128.491 | 71.066 | 43 |
| AMD1603 | 421 | AMD1603-421-BC | Boxcore | -133.891 | 71.399 | 1135 |
| AMD1603 | 434 | AMD1603-434-BC | Boxcore | -133.544 | 70.174 | 46 |
| AMD1603 | 435 | AMD1603-435-BC | Boxcore | -139.657 | 71.076 | 290 |
| AMD1603 | 472 | AMD1603-472-BC | Boxcore | -138.227 | 69.611 | 124 |
| AMD1603 | 482 | AMD1603-482-BC | Boxcore | -139.384 | 70.524 | 821 |
| AMD1603 | 525 | AMD1603-525-BC | Boxcore | -128.952 | 72.392 | 347 |
| AMD1603 | 535 | AMD1603-535-BC | Boxcore | -128.192 | 73.416 | 289 |
| AMD1603 | 545 | AMD1603-545-BC | Boxcore | -126.823 | 74.178 | 315 |
| AMD1603 | 575 | AMD1603-575-BC | Boxcore | -125.874 | 76.156 | 318 |
| AMD1603 | 585 | AMD1603-585-BC | Boxcore | -123.222 | 74.513 | 382 |
| AMD1603 | BRG | AMD1603-BRG-BC | Boxcore | -135.462 | 70.992 | 664 |
| AMD1603 | FURZE04 | AMD1603-FURZE04-BC | Boxcore | -103.389 | 73.648 | 245 |

| | | | | | | |
|---|---|---|---|---|---|---|
| AMD1603 | FURZE07 | AMD1603-FURZE07-BC | Boxcore | -97.195 | 74.706 | 318 |
| AMD1603 | GSCLander2 | AMD1603-GSCLander2-BC | Boxcore | -135.000 | 70.875 | 200 |
| AMD1603 | QMG2 | AMD1603-QMG2-BC | Boxcore | -100.803 | 68.316 | 53 |
| AMD1603 | QMG3 | AMD1603-QMG3-BC | Boxcore | -102.944 | 68.314 | 56 |
| AMD1603 | QMG4 | AMD1603-QMG4-BC | Boxcore | -103.418 | 68.490 | 82 |
| AMD1603 | QMGM | AMD1603-QMGM-BC | Boxcore | -101.765 | 68.310 | 107 |
| AMD1702 | OF-B2 (OF-23) | AMD1702-01BC | Boxcore | -67.333 | 62.999 | 442 |
| AMD1702 | OF-S23 | AMD1702-03BC | Boxcore | -66.939 | 62.818 | 507 |
| AMD1702 | OF-B6 | AMD1702-04BC | Boxcore | -66.705 | 62.745 | 493 |
| AMD1702 | FB2-2-5d | AMD1702-05BC | Boxcore | -68.420 | 63.663 | 82 |
| AMD1702 | BELL12 | AMD1702-07BC | Boxcore | -68.624 | 63.687 | 141 |
| AMD1702 | A16 | AMD1702-08BC | Boxcore | -68.626 | 63.639 | 140 |
| AMD1702 | BELL11 | AMD1702-09BC | Boxcore | -68.182 | 63.359 | 118 |
| AMD1702 | OF-S22 | AMD1702-10BC | Boxcore | -66.746 | 62.866 | 289 |
| AMD1702 | OF-B9 | AMD1702-11BC | Boxcore | -66.282 | 62.566 | 375 |
| AMD1702 | OF-B14 | AMD1702-12BC | Boxcore | -66.021 | 62.386 | 411 |
| AMD1702 | OF-B5 | AMD1702-13BC | Boxcore | -65.882 | 62.463 | 278 |
| AMD1702 | DISKO FAN 1 | AMD1702-14BC | Boxcore | -59.565 | 67.992 | 947 |
| AMD1702 | DISKO FAN 3 | AMD1702-15BC | Boxcore | -59.564 | 67.992 | 1012 |
| AMD1702 | DISKO FAN 5 | AMD1702-16BC | Boxcore | -59.485 | 67.964 | 873 |
| AMD1702 | 8.1 | AMD1702-17BC | Boxcore | -64.732 | 69.407 | 1054 |
| AMD1702 | 176 | AMD1702-18BC | Boxcore | -65.403 | 69.597 | 267 |
| AMD1702 | BB2 | AMD1702-19BC | Boxcore | -67.015 | 72.751 | 2373 |
| AMD1702 | 101 | AMD1702-20BC | Boxcore | -77.516 | 76.357 | 378 |
| AMD1702 | 105 | AMD1702-21BC | Boxcore | -75.758 | 76.317 | 331 |
| AMD1702 | 115 | AMD1702-22BC | Boxcore | -71.254 | 76.331 | 668 |
| AMD1702 | 129 | AMD1702-23BC | Boxcore | -76.647 | 76.331 | 521 |
| AMD1702 | TS-233 | AMD1702-24BC | Boxcore | -76.686 | 77.755 | 396 |
| AMD1702 | 111 | AMD1702-25BC | Boxcore | -73.207 | 76.308 | 593 |
| AMD1702 | 108 | AMD1702-26BC | Boxcore | -74.606 | 76.264 | 448 |
| AMD1702 | Belcher Glacier | AMD1702-27BC | Boxcore | -80.752 | 75.702 | 623 |
| AMD1702 | 323 | AMD1702-28BC | Boxcore | -80.467 | 74.156 | 792 |
| AMD1702 | 301-1 | AMD1702-29BC | Boxcore | -83.318 | 74.277 | 715 |
| AMD1702 | 304 | AMD1702-30BC | Boxcore | -91.515 | 74.246 | 315 |
| AMD1702 | 5.10 | AMD1702-31BC | Boxcore | -99.076 | 74.489 | 223 |
| AMD1702 | 3.9 | AMD1702-32BC | Boxcore | -96.161 | 73.654 | 262 |
| AMD1702 | QMGM | AMD1702-33BC | Boxcore | -101.741 | 68.302 | 114 |
| AMD1702 | QMG4 | AMD1702-34BC | Boxcore | -103.430 | 68.484 | 71 |
| AMD1702 | QMG3 | AMD1702-35BC | Boxcore | -102.941 | 68.244 | 46 |
| AMD1702 | QMG1 | AMD1702-36BC | Boxcore | -99.898 | 68.492 | 40 |
| AMD1702 | QMG2 | AMD1702-37BC | Boxcore | -100.807 | 68.306 | 95 |
| AMD1702 | 312 | AMD1702-38BC | Boxcore | -100.695 | 69.170 | 65 |
| AMD1702 | 3.7 | AMD1702-39BC | Boxcore | -96.065 | 72.089 | 474 |
| AMD1702 | 3.4 | AMD1702-40BC | Boxcore | -91.993 | 71.475 | 270 |
| AMD1702 | 3.5 | AMD1702-41BC | Boxcore | -91.236 | 70.436 | 224 |
| AMD1702 | 5.11W | AMD1702-42BC | Boxcore | -87.666 | 69.954 | 184 |
| AMD1702 | 5.11 | AMD1702-43BC | Boxcore | -86.084 | 69.882 | 298 |
| AMD1702 | 3.10-2 | AMD1702-45BC | Boxcore | -78.162 | 68.878 | 52 |
| AMD1702 | 3.10 | AMD1702-46BC | Boxcore | -80.847 | 67.797 | 96 |
| AMD1702 | 1.1 | AMD1702-47BC | Boxcore | -81.353 | 65.155 | 418 |
| AMD1803 | QMGM | AMD1803-01BC | Boxcore | -101.741 | 68.299 | 112 |
| AMD1803 | 1.4 | AMD1803-02BC | Boxcore | -78.740 | 76.480 | 124 |

| | | | | | | |
|---|---|---|---|---|---|---|
| AMD1803 | 101 | AMD1803-03BC | Boxcore | -77.409 | 76.382 | 373 |
| AMD1803 | 115 | AMD1803-04BC | Boxcore | -71.176 | 76.331 | 662 |
| AMD1803 | 1.5 | AMD1803-05BC | Boxcore | -63.910 | 67.284 | 609 |
| AMD1803 | Garnier River | AMD1803-Garnier River | River | -92.912 | 73.658 | 0 |
| AMD1803 | River in Le Feuvre Inlet, Prince of Wales | AMD1803-River in Le Feuvre Inlet, Prince of Wales | River | -96.917 | 72.341 | 0 |
| AMD1803 | Simpson River | AMD1803-Simpson River | River | -100.568 | 67.676 | 0 |
| AMD1803 | Tingmeak River | AMD1803-Tingmeak River | River | -104.986 | 68.268 | 0 |
| AMD1902 | 2.6 | AMD1902-01BC | Boxcore | -73.065 | 76.318 | 575 |
| AMD1902 | 122 | AMD1902-02BC | Boxcore | -75.014 | 77.341 | 647 |
| AMD1902 | 6.2 | AMD1902-03BC | Boxcore | -65.764 | 79.514 | 378 |
| AMD1902 | 134 | AMD1902-04BC | Boxcore | -68.453 | 80.356 | 377 |
| AMD1902 | Rob1 | AMD1902-05BC | Boxcore | -62.247 | 81.802 | 716 |
| AMD1902 | 6.4 | AMD1902-06BC | Boxcore | -63.217 | 81.626 | 796 |
| AMD1902 | 251b | AMD1902-08BC | Boxcore | -61.557 | 81.042 | 1135 |
| AMD1902 | 6.1 | AMD1902-09BC | Boxcore | -73.659 | 79.786 | 205 |
| AMD1902 | 6.1 | AMD1902-10BC | Boxcore | -73.095 | 79.692 | 245 |
| AMD1902 | Talbot Inlet | AMD1902-11BC | Boxcore | -77.075 | 77.843 | 515 |
| AMD1902 | 2.5 | AMD1902-12BC | Boxcore | -77.505 | 76.356 | 379 |
| AMD1902 | 293 | AMD1902-13BC | Boxcore | -80.689 | 75.728 | 627 |
| AMD1902 | 2.2 | AMD1902-14BC | Boxcore | -81.849 | 76.064 | 770 |
| AMD1902 | 2.3 | AMD1902-15BC | Boxcore | -83.023 | 76.129 | 827 |
| AMD1902 | 2.4 | AMD1902-16BC | Boxcore | -86.300 | 76.126 | 674 |
| AMD1902 | 1.4 | AMD1902-17BC | Boxcore | -84.571 | 76.395 | 139 |
| AMD1902 | 1.4 | AMD1902-18BC | Boxcore | -84.931 | 76.500 | 125 |
| AMD1902 | 297 | AMD1902-19BC | Boxcore | -81.314 | 76.370 | 451 |
| AMD1902 | 296 | AMD1902-20BC | Boxcore | -79.753 | 75.523 | 556 |
| AMD1902 | 2.7 | AMD1902-21BC | Boxcore | -78.675 | 75.482 | 521 |
| AMD1902 | 302 | AMD1902-22BC | Boxcore | -86.170 | 74.234 | 553 |
| AMD1902 | 303 | AMD1902-23BC | Boxcore | -89.616 | 74.368 | 294 |
| AMD1902 | Wel02 | AMD1902-25BC | Boxcore | -93.112 | 75.013 | 247 |
| AMD1902 | Ellesmere South Central River | AMD1902-Ellesmere South Central River | River | -83.504 | 76.646 | 0 |
| AMD1902 | Eugenie Glacier | AMD1902-Eugenie Glacier | Glacier | -74.859 | 79.810 | 0 |
| AMD1902 | Eugenie River | AMD1902-Eugenie River | River | -74.996 | 79.792 | 0 |
| AMD1902 | Near Eugenie Glacier | AMD1902-Near Eugenie Glacier | Glacier | -74.356 | 79.893 | 0 |
| AMD1902 | Near Hans Island River | AMD1902-Near Hans Island River | River | -68.001 | 80.846 | 0 |
| AMD1902 | RISG (Near 1.4) | AMD1902-RISG (Near 1.4) | River | -84.931 | 76.610 | 0 |
| AMD1902 | River Ellesmere East | AMD1902-River Ellesmere East | River | -69.191 | 80.611 | 0 |
| AMD1902 | River near 135 | AMD1902-River near 135 | River | -71.263 | 80.246 | 0 |
| AMD1902 | Sydkap Glacier | AMD1902-Sydkap Glacier | Glacier | -84.939 | 76.605 | 0 |
| AMD2202 | KEBABB A3 | AMD2202-01BC | Boxcore | 66.73346 | -59.604 | 872.2 |
| AMD2202 | 195 | AMD2202-04BC | Boxcore | 66.8909 | -56.929 | 655.2 |
| AMD2202 | KEBABB B6 | AMD2202-06BC | Boxcore | 67.28777 | -58.447 | 1134 |
| AMD2202 | KEBABB B3 | AMD2202-07BC | Boxcore | 67.32643 | -60.272 | 1074 |
| AMD2202 | KEBABB C3 | AMD2202-09BC | Boxcore | 67.75013 | -61.262 | 1558 |
| AMD2202 | KEBABB D1 | AMD2202-10BC | Boxcore | 67.39527 | -63.853 | 463.9 |
| AMD2202 | KEBABB D3 | AMD2202-11BC | Boxcore | 68.24121 | -62.594 | 1540 |
| AMD2202 | Scott Inlet sill | AMD2202-12BC | Boxcore | 71.15239 | -71.259 | 459.2 |

| | | | | | | |
|---|---|---|---|---|---|---|
| AMD2202 | SI_coring1 | AMD2202-13BC | Boxcore | 71.04059 | -71.557 | 672 |
| AMD2202 | SI_coring2 | AMD2202-14BC | Boxcore | 70.96636 | -71.323 | 660.9 |
| AMD2202 | SI_coring 3 | AMD2202-15BC | Boxcore | 70.8746 | -71.661 | 682.1 |
| AMD2202 | 323_east | AMD2202-16BC | Boxcore | 74.13701 | -79.339 | 788 |
| AMD2202 | 115 | AMD2202-17BC | Boxcore | 76.32894 | -71.222 | 652.4 |
| AMD2202 | 111 | AMD2202-18BC | Boxcore | 76.30665 | -73.215 | 589.2 |

Tableau 20.

Liste des échantillons de sédiments utilisés pour le chapitre 3 de cette étude.

| Communauté | Nom éch. | Lat. | Long. | Prof. eau approx. | Date |
|---|---|---|---|---|---|
| Kugluktuk | KUG2022-01 | 67.825878 | -115.080487 | 2.5 | 2022-08-21 |
| | KUG2022-02 | 67.82680697 | -115.077702 | 2.5 | 2022-08-21 |
| | KUG2022-03 | 67.82814497 | -115.087924 | 2.5 | 2022-08-21 |
| | KUG2022-05 | 67.82928902 | -115.095739 | 2.5 | 2022-08-21 |
| | KUG2022-06 | 67.829991 | -115.097968 | 2.5 | 2022-08-21 |
| | KUG2022-09 | 67.82881502 | -115.114622 | 1 | 2022-08-21 |
| | KUG2022-10 | 67.82984499 | -115.115613 | 2 | 2022-08-21 |
| | KUG2022-11 | 67.82740703 | -115.123739 | 2 | 2022-08-21 |
| | KUG2022-12 | 67.82861603 | -115.124446 | 2 | 2022-08-21 |
| | KUG2022-13 | 67.82645401 | -115.130111 | 3 | 2022-08-21 |
| | KUG2022-14 | 67.82747501 | -115.13084 | 3 | 2022-08-21 |
| | KUG2022-15 | 67.82441997 | -115.138741 | 2 | 2022-08-21 |
| | KUG2022-16 | 67.82539001 | -115.13976 | 2 | 2022-08-21 |
| | KUG2022-17 | 67.82424102 | -115.148047 | 3 | 2022-08-21 |
| | KUG2022-18 | 67.82519597 | -115.146975 | 5 | 2022-08-21 |
| | KUG2022-19 | 67.825217 | -115.157229 | 5 | 2022-08-21 |
| | KUG2022-20 | 67.82588303 | -115.156362 | 5 | 2022-08-21 |
| | KUG2022-21 | 67.82647203 | -115.166297 | 5 | 2022-08-21 |
| | KUG2022-22 | 67.82681803 | -115.165007 | 5 | 2022-08-21 |
| | KUG2022-23 | 67.82791497 | -115.173903 | 5 | 2022-08-21 |
| | KUG2022-24 | 67.82861201 | -115.172527 | 5 | 2022-08-21 |
| | KUG2022-26 | 67.83026299 | -115.179778 | 4 | 2022-08-21 |
| | KUG2022-27 | 67.831932 | -115.187075 | 3 | 2022-08-21 |
| | KUG2022-28 | 67.83272099 | -115.185267 | 4 | 2022-08-21 |
| | KUG2022-29 | 67.83414599 | -115.192474 | 4 | 2022-08-21 |
| | KUG2022-30 | 67.83523598 | -115.190311 | 4 | 2022-08-21 |
| | KUG2022-31 | 67.83349799 | -115.184491 | 8 | 2022-08-23 |
| | KUG2022-32 | 67.83161298 | -115.178904 | 6 | 2022-08-23 |
| | KUG2022-33 | 67.82978598 | -115.171255 | 5 | 2022-08-23 |
| | KUG2022-34 | 67.82739303 | -115.163687 | 10 | 2022-08-23 |

| | | | | | |
|---|---|---|---|---|---|
| | KUG2022-35 | 67.82870304 | -115.163159 | 12 | 2022-08-23 |
| | KUG2022-36 | 67.82692398 | -115.156518 | 8 | 2022-08-23 |
| | KUG2022-37 | 67.827618 | -115.154733 | 8 | 2022-08-23 |
| | KUG2022-38 | 67.82598001 | -115.147168 | 4 | 2022-08-23 |
| | KUG2022-39 | 67.82731298 | -115.14641 | 4 | 2022-08-23 |
| | KUG2022-40 | 67.82605 | -115.139701 | 5 | 2022-08-23 |
| | KUG2022-41 | 67.82772596 | -115.139891 | 5 | 2022-08-23 |
| | KUG2022-42 | 67.82885701 | -115.13271 | 5 | 2022-08-23 |
| | KUG2022-43 | 67.82952304 | -115.133368 | 6 | 2022-08-23 |
| | KUG2022-44 | 67.82933 | -115.125094 | 5 | 2022-08-23 |
| | KUG2022-45 | 67.83043298 | -115.125907 | 5 | 2022-08-23 |
| | KUG2022-46 | 67.83078502 | -115.116115 | 4 | 2022-08-23 |
| | KUG2022-47 | 67.83227004 | -115.117282 | 4 | 2022-08-23 |
| | KUG2022-48 | 67.832263 | -115.105292 | 4 | 2022-08-23 |
| | KUG2022-49 | 67.83135499 | -115.096348 | 4 | 2022-08-23 |
| Qikiqtarjuaq | AMD2202-3.41 | 67.56399097 | -64.02568596 | 6.3 | 2022-10-02 |
| | AMD2202-3.43 | 67.55996397 | -64.02699304 | 12.5 | 2022-10-02 |
| | AMD2202-3.44 | 67.56003102 | -64.02985898 | 9.5 | 2022-10-02 |
| | AMD2202-3.47 | 67.55388197 | -64.03118097 | 4.3 | 2022-10-02 |
| | AMD2202-3.48 | 67.55239896 | -64.03113202 | 4.9 | 2022-10-02 |
| | AMD2202-3.49 | 67.56373004 | -64.02930996 | 7.4 | 2022-10-02 |
| | AMD2202-3.54 | 67.556503 | -64.03675603 | 7.9 | 2022-10-02 |
| Pond Inlet | PI2023-01 | 72.70304301 | -77.95186202 | 2.5 | 2023-08-24 |
| | PI2023-05 | 72.702582 | -77.96241098 | 8 | 2023-08-24 |
| | PI2023-08 | 72.70203902 | -77.96676002 | 25 | 2023-08-24 |
| | PI2023-11 | 72.69916696 | -77.97276498 | 1.5 | 2023-08-24 |
| | PI2023-13 | 72.69867998 | -77.97581197 | 1.5 | 2023-08-24 |
| | PI2023-14 | 72.699001 | -77.98004801 | 7 | 2023-08-24 |
| | PI2023-15 | 72.69660202 | -77.98075 | 2 | 2023-08-24 |
| | PI2023-16 | 72.69765403 | -77.98209697 | 4 | 2023-08-24 |
| | PI2023-17 | 72.69444603 | -77.98537203 | 1.5 | 2023-08-24 |
| | PI2023-18 | 72.69589903 | -77.98766901 | 5 | 2023-08-24 |
| | PI2023-19 | 72.69247301 | -77.98899796 | 1.5 | 2023-08-24 |
| | PI2023-20 | 72.69251701 | -77.99364698 | ND | 2023-08-24 |
| | PI2023-21 | 72.68930398 | -77.99840396 | 1.5 | 2023-08-24 |
| | PI2023-22 | 72.69038902 | -78.002337 | 3 | 2023-08-24 |
| | PI2023-23 | 72.68764998 | -78.00500404 | 2 | 2023-08-24 |
| | PI2023-25 | 72.68546498 | -78.01544404 | 1 | 2023-08-24 |
| | PI2023-26 | 72.68706802 | -78.01811602 | 8 | 2023-08-24 |
| | PI2023-28 | 72.68379699 | -78.03091401 | 4 | 2023-08-24 |
| | PI2023-29 | 72.68188298 | -78.03379202 | 3 | 2023-08-24 |
| | PI2023-30 | 72.68288503 | -78.03720203 | 2 | 2023-08-24 |
| | PI2023-32 | 72.68056098 | -78.050585 | ND | 2023-08-24 |
| | PI2023-34 | 72.67524996 | -78.06836897 | ND | 2023-08-24 |
| Grise Fiord | AMD2303-3.01 | 76.42347897 | -82.93858403 | ND | 2023-09-27 |
| | AMD2303-3.02 | 76.42134402 | -82.92929504 | ND | 2023-09-27 |

| | | | | | |
|---|---|---|---|---|---|
| | AMD2303-3.03 | 76.41847003 | -82.91288503 | ND | 2023-09-27 |
| | AMD2303-3.04 | 76.41654597 | -82.90062801 | ND | 2023-09-27 |
| | AMD2303-3.05 | 76.41489398 | -82.89993399 | ND | 2023-09-27 |
| | AMD2303-3.06 | 76.41287101 | -82.89947902 | ND | 2023-09-27 |
| | AMD2303-3.07 | 76.41011998 | -82.90654496 | ND | 2023-09-27 |
| | AMD2303-3.08 | 76.41788397 | -82.91752802 | ND | 2023-09-27 |
| | AMD2303-3.09 | 76.42086097 | -82.93160602 | ND | 2023-09-27 |
| | AMD2303-3.10 | 76.42219604 | -82.94435296 | ND | 2023-09-27 |
| | AMD2303-3.15 | 76.41092003 | -82.89933401 | ND | 2023-09-26 |
| Resolute | AMD2303-3.32 | 74.69229603 | -94.85077098 | ND | 2023-10-04 |
| | AMD2303-3.33 | 74.69016703 | -94.85949897 | ND | 2023-10-04 |
| | AMD2303-3.35 | 74.68904 | -94.87077196 | ND | 2023-10-04 |
| | AMD2303-3.36 | 74.68677999 | -94.85828402 | ND | 2023-10-04 |
| | AMD2303-3.37 | 74.68977098 | -94.84977001 | ND | 2023-10-04 |
| | AMD2303-3.38 | 74.68638302 | -94.86878201 | ND | 2023-10-04 |
| | AMD2303-3.40 | 74.68797399 | -94.84889603 | ND | 2023-10-04 |
| | AMD2303-3.41 | 74.68578698 | -94.876704 | ND | 2023-10-04 |
| | AMD2303-3.43 | 74.68355304 | -94.88487803 | ND | 2023-10-04 |
| | AMD2303-3.44 | 74.68757199 | -94.87774403 | ND | 2023-10-04 |
| | AMD2303-3.45 | 74.68720403 | -94.84196898 | ND | 2023-10-04 |
| Tuktoyaktuk | TH-02 | 69.450680 | -132.997670 | ND | 2022-08-06 |
| | TH-05 | 69.447853 | -133.011964 | ND | 2022-08-16 |
| | TH-07 | 69.447794 | -133.000797 | ND | 2022-08-16 |
| | TH-09 | 69.445909 | -132.982545 | ND | 2022-08-16 |
| | TH-10 | 69.446791 | -132.967168 | ND | 2022-08-16 |
| | TH-12 | 69.438826 | -132.977931 | ND | 2022-08-16 |
| | TH-13 | 69.438093 | -132.961779 | ND | 2022-08-16 |
| | TH-16 | 69.431792 | -132.974372 | ND | 2022-08-16 |
| | TH-18 | 69.424020 | -132.971630 | ND | 2022-08-16 |
| | TH-20 | 69.413809 | -132.983186 | ND | 2022-08-16 |
| | TH-23 | 69.453310 | -132.980190 | ND | 2022-08-19 |
| | TH-24 | 69.451980 | -132.992380 | ND | 2022-08-19 |
| Milne Inlet | MI2017-2C | 71.9401 | -80.7481 | 18.5 | 2017-08-13 |
| | MI2017-3B | 72.0098 | -80.6387 | 17 | 2017-08-19 |
| | MI2017-6 | 71.9146 | -80.8004 | 14 | 2017-08-19 |
| | MI2017-9A | 71.9182 | -80.8775 | 16 | 2017-08-13 |
| Ragged Island | RI-2B | 72.48022 | -80.01427 | 10.0 | 2019-08-17 |
| | RI-2C | 72.48051 | -80.00948 | 20.0 | 2019-08-17 |
| | RI-3C | 72.38992 | -80.04044 | 17.6 | 2019-08-18 |
| | RI-6 | 72.50188 | -80.09983 | 38.0 | 2019-08-16 |
| | RI-7 | 72.47541 | -79.98116 | 18,1 - 25 | 2019-08-22 |
| | RI-9 | 72.47968 | -80.07672 | 15,6 - 22 | 2019-08-25 |

## RÉFÉRENCES BIBLIOGRAPHIQUES


Aarkrog, A. (2003). Input of anthropogenic radionuclides into the World Ocean. *Deep Sea Research Part II: Topical Studies in Oceanography*, *50*(17), 2597-2606. https://doi.org/https://doi.org/10.1016/S0967-0645(03)00137-1

Acquavita, A., Floreani, F., & Covelli, S. (2021). Occurrence and speciation of arsenic and mercury in alluvial and coastal sediments. *Current Opinion in Environmental Science & Health*, *22*, 100272. https://doi.org/https://doi.org/10.1016/j.coesh.2021.100272

Aitchison, J. (1982). The Statistical Analysis of Compositional Data. *Journal of the Royal Statistical Society: Series B (Methodological)*, *44*(2), 139-160. https://doi.org/https://doi.org/10.1111/j.2517-6161.1982.tb01195.x

Alkire, M. B., Jacobson, A. D., Lehn, G. O., Macdonald, R. W., & Rossi, M. W. (2017). On the geochemical heterogeneity of rivers draining into the straits and channels of the Canadian Arctic Archipelago. *Journal of Geophysical Research: Biogeosciences*, *122*(10), 2527-2547. https://doi.org/https://doi.org/10.1002/2016JG003723

Alloway, B. J. (2012). *Heavy metals in soils: trace metals and metalloids in soils and their bioavailability* (Vol. 22). Springer Science & Business Media.

Alves, C. M., Ferreira, C. M. H., & Soares, H. M. V. M. (2018). Relation between different metal pollution criteria in sediments and its contribution on assessing toxicity. *Chemosphere*, *208*, 390-398. https://doi.org/https://doi.org/10.1016/j.chemosphere.2018.05.072

AMAP (1998). *AMAP Assessment Report: Arctic Pollution Issues.* Arctic Monitoring and Assessment Programme (AMAP), Oslo, Norway. xii+859 pp.

AMAP (2005). *AMAP Assessment 2002: Heavy Metals in the Arctic.* Arctic Monitoring and Assessment Programme (AMAP), Oslo, Norway. xvi + 265 pp.

AMAP (2011). *AMAP Assessment 2011: Mercury in the Arctic.* Arctic Monitoring and Assessment Programme (AMAP), Oslo, Norway. xiv + 193 pp.

AMAP (2021). *AMAP Assessment 2021: Mercury in the Arctic.* Arctic Monitoring and Assessment Programme (AMAP), Tromsø, Norway. 324 pp.

Andreae, M. O. (1979). Arsenic speciation in seawater and interstitial waters: The influence of biological-chemical interactions on the chemistry of a trace element. *Limnology and Oceanography*, *24*(3), 440-452. https://doi.org/https://doi.org/10.4319/lo.1979.24.3.0440

Ankley, G. T., Thomas, N. A., Di Toro, D. M., Hansen, D. J., Mahony, J. D., Berry, W. J., Swartz, R. C., Hoke, R. A., Garrison, A. W., Allen, H. E., & Zarba, C. S. (1994). Assessing potential bioavailability of metals in sediments: A proposed approach. *Environmental Management*, *18*(3), 331-337. https://doi.org/10.1007/BF02393863

Antcibor, I., Eschenbach, A., Zubrzycki, S., Kutzbach, L., Bolshiyanov, D., & Pfeiffer, E. M. (2014). Trace metal distribution in pristine permafrost-affected soils of the Lena River delta and its hinterland, northern Siberia, Russia. *Biogeosciences*, *11*(1), 1-15. https://doi.org/10.5194/bg-11-1-2014

Astakhov, A. S., Sattarova, V. V., Xuefa, S., Limin, H., Aksentov, K. I., Alatortsev, A. V., Kolesnik, O. N., & Mariash, A. A. (2019). Distribution and sources of rare earth elements in sediments of the Chukchi and East Siberian Seas. *Polar Science, 20*, 148-159. https://doi.org/https://doi.org/10.1016/j.polar.2019.05.005

Azizur Rahman, M., Hasegawa, H., & Peter Lim, R. (2012). Bioaccumulation, biotransformation and trophic transfer of arsenic in the aquatic food chain. *Environmental Research*, *116*, 118-135. https://doi.org/https://doi.org/10.1016/j.envres.2012.03.014

Barrat, J.-A., & Bayon, G. (2024). Practical guidelines for representing and interpreting rare earth abundances in environmental and biological studies. *Chemosphere*, *352*, 141487. https://doi.org/https://doi.org/10.1016/j.chemosphere.2024.141487

Barrat, J.-A., Bayon, G., & Lalonde, S. (2023). Calculation of cerium and lanthanum anomalies in geological and environmental samples. *Chemical Geology*, *615*, 121202. https://doi.org/https://doi.org/10.1016/j.chemgeo.2022.121202

Bartley, M. C., Tremblay, T., De Silva, A. O., Michelle Kamula, C., Ciastek, S., & Kuzyk, Z. Z. A. (2024). Sedimentary records of contaminant inputs in Frobisher Bay, Nunavut. *Environmental Science and Ecotechnology*, *18*, 100313. https://doi.org/https://doi.org/10.1016/j.ese.2023.100313

Basu, N., Abass, K., Dietz, R., Krümmel, E., Rautio, A., & Weihe, P. (2022). The impact of mercury contamination on human health in the Arctic: A state of the science review. *Science of The Total Environment*, *831*, 154793. https://doi.org/https://doi.org/10.1016/j.scitotenv.2022.154793

Belzile, C., & Montero-Serrano, J.-C. (2022). Quantifying simulated fine sand fraction in muddy sediment using laser diffraction. *Canadian Journal of Earth Sciences*, *59*(7), 455-461. https://doi.org/10.1139/cjes-2022-0011

Belzile, N. (1988). The fate of arsenic in sediments of the Laurentian Trough. *Geochimica et Cosmochimica Acta*, *52*(9), 2293-2302. https://doi.org/https://doi.org/10.1016/0016-7037(88)90131-7

Belzile, N., & Lebel, J. (1986). Capture of arsenic by pyrite in near-shore marine sediments. *Chemical Geology*, *54*(3), 279-281. https://doi.org/https://doi.org/10.1016/0009-2541(86)90142-7

Belzile, N., & Tessier, A. (1990). Interactions between arsenic and iron oxyhydroxides in lacustrine sediments. *Geochimica et Cosmochimica Acta*, *54*(1), 103-109. https://doi.org/https://doi.org/10.1016/0016-7037(90)90198-T

Bergamaschi, L., Rizzio, E., Valcuvia, M. G., Verza, G., Profumo, A., & Gallorini, M. (2002). Determination of trace elements and evaluation of their enrichment factors in Himalayan lichens. *Environmental Pollution*, *120*(1), 137-144. https://doi.org/https://doi.org/10.1016/S0269-7491(02)00138-0

Bernhoft, R. A. (2013). Cadmium Toxicity and Treatment. *The Scientific World Journal*, *2013*(1), 394652. https://doi.org/https://doi.org/10.1155/2013/394652

Bini, C., & Bech, J. (2014). *PHEs, environment and human health*. Springer.

Birch, G. F. (2020). An assessment of aluminum and iron in normalisation and enrichment procedures for environmental assessment of marine sediment. *Science of The Total Environment*, *727*, 138123. https://doi.org/https://doi.org/10.1016/j.scitotenv.2020.138123

Blott, S. J., & Pye, K. (2001). GRADISTAT: a grain size distribution and statistics package for the analysis of unconsolidated sediments. *Earth surface processes and Landforms*, *26*(11), 1237-1248.

Boës, X., Rydberg, J., Martinez-Cortizas, A., Bindler, R., & Renberg, I. (2011). Evaluation of conservative lithogenic elements (Ti, Zr, Al, and Rb) to study anthropogenic element enrichments in lake sediments. *Journal of Paleolimnology*, *46*(1), 75-87. https://doi.org/10.1007/s10933-011-9515-z

Bossé-Demers, T., Gobeil, C., Juhls, B., Lizotte, M., Fritz, M., Bröder, L., Matsuoka, A., Mareque, S., & Couture, R.-M. (2025). Distribution of rare earth elements and their signatures from the Mackenzie River delta to the abyssal Arctic Ocean. *Continental Shelf Research*, *289*, 105464. https://doi.org/https://doi.org/10.1016/j.csr.2025.105464

Breit, G. N., & Wanty, R. B. (1991). Vanadium accumulation in carbonaceous rocks: A review of geochemical controls during deposition and diagenesis. *Chemical Geology*, *91*(2), 83-97. https://doi.org/https://doi.org/10.1016/0009-2541(91)90083-4

Brown, R. J. E. (1972). Permafrost in the Canadian Arctic Archipelago. *Zeitschrift fur Geomorphologie*, *13*, 102-130. https://cir.nii.ac.jp/crid/1570572699166533888

Bruggmann, S., McManus, J., Archer, C., Vance, D., & Severmann, S. (2024). Nickel's behaviour in marine sediments under aerobic to anaerobic diagenetic conditions. *Chemical Geology*, *662*, 122234. https://doi.org/https://doi.org/10.1016/j.chemgeo.2024.122234

Bruggmann, S., Severmann, S., & McManus, J. (2023). Geochemical conditions regulating chromium preservation in marine sediments. *Geochimica et Cosmochimica Acta*, *348*, 239-257. https://doi.org/https://doi.org/10.1016/j.gca.2023.03.003

Bruland, K. W., & Rue, E. L. (2001). Analytical methods for the determination of concentrations and speciation of iron. In D. R. Turner & K. A. Hunter (Eds.), *The biogeochemistry of iron in seawater* (pp. 255-289). Wiley.

Bryan, A. L., Dickson, A. J., Dowdall, F., Homoky, W. B., Porcelli, D., & Henderson, G. M. (2021). Controls on the cadmium isotope composition of modern marine sediments. *Earth and Planetary Science Letters*, *565*, 116946. https://doi.org/https://doi.org/10.1016/j.epsl.2021.116946

Buck, K. N., Ross, J. R. M., Russell Flegal, A., & Bruland, K. W. (2007). A review of total dissolved copper and its chemical speciation in San Francisco Bay, California. *Environmental Research*, *105*(1), 5-19. https://doi.org/https://doi.org/10.1016/j.envres.2006.07.006

Budko, D. F., Demina, L. L., Lisitzin, A. P., Kravchishina, M. D., & Politova, N. V. (2017). Occurrence forms of trace metals in recent bottom sediments from the White and Barents Seas. *Doklady Earth Sciences*, *474*(1), 552-556. https://doi.org/10.1134/S1028334X17050014

Budko, D. F., Demina, L. L., Travkina, A. V., Starodymova, D. P., & Alekseeva, T. N. (2022). The Features of Distribution of Chemical Elements, including Heavy Metals and Cs-137, in Surface Sediments of the Barents, Kara, Laptev and East Siberian Seas. *Minerals*, *12*(3), 328. https://www.mdpi.com/2075-163X/12/3/328

Cai, M., Lin, J., Hong, Q., Wang, Y., & Cai, M. (2011). Content and distribution of trace metals in surface sediments from the northern Bering Sea, Chukchi Sea and adjacent Arctic areas. *Marine Pollution Bulletin*, *63*(5-12), 523-527.

Callender, E. (2005). Heavy metals in the Environment - Historical Trends. In B. S. Lollar (Ed.), *Environmental geochemistry* (Vol. 9).

Calvert, S. E., & Pedersen, T. F. (1993). Geochemistry of Recent oxic and anoxic marine sediments: Implications for the geological record. *Marine Geology*, *113*(1), 67-88. https://doi.org/https://doi.org/10.1016/0025-3227(93)90150-T

Campbell, J. A., & Loring, D. H. (1980). Baseline levels of heavy metals in the waters and sediments of Baffin Bay. *Marine Pollution Bulletin*, *11*(9), 257-261. https://doi.org/https://doi.org/10.1016/0025-326X(80)90314-8

Canadian Ice Services. (2023). *Annual Arctic Ice Atlas, Winter 2022-2023*. Ottawa: Government of Canada

CCME. (1999). *Canadian Sediment Quality Guidelines for the Protection of Aquatic Life*. Winnipeg, MA: Canadian Council of Ministers of the Environment, Canadian environmental quality guidelines

CCME. (2014). *Canadian Water Quality Guidelines: Cadmium. Scientific Criteria Document.* . Winnipeg, MB: Canadian Council of Ministers of the Environment

Chaillou, G., Schäfer, J., Anschutz, P., Lavaux, G., & Blanc, G. (2003). The behaviour of arsenic in muddy sediments of the Bay of Biscay (France). *Geochimica et Cosmochimica Acta*, *67*(16), 2993-3003. https://doi.org/https://doi.org/10.1016/S0016-7037(03)00204-7

Chapman, P. M., Wang, F., Janssen, C., Persoone, G., & Allen, H. E. (1998). Ecotoxicology of metals in aquatic sediments: binding and release, bioavailability, risk assessment, and remediation. *Canadian Journal of Fisheries and Aquatic Sciences*, *55*(10), 2221-2243. https://doi.org/10.1139/f98-145

Chen, Q., & and Taylor, D. (2018). Transboundary atmospheric pollution in Southeast Asia: current methods, limitations and future developments. *Critical Reviews in Environmental Science and Technology*, *48*(16-18), 997-1029. https://doi.org/10.1080/10643389.2018.1493337

Chen, Y.-M., Gao, J.-b., Yuan, Y.-Q., Ma, J., & Yu, S. (2016). Relationship between heavy metal contents and clay mineral properties in surface sediments: Implications for metal pollution assessment. *Continental Shelf Research*, *124*, 125-133. https://doi.org/https://doi.org/10.1016/j.csr.2016.06.002

Choudhary, S., Nayak, G. N., & Khare, N. (2020). Source, mobility, and bioavailability of metals in fjord sediments of Krossfjord-Kongsfjord system, Arctic, Svalbard. *Environmental Science and Pollution Research*, *27*(13), 15130-15148. https://doi.org/10.1007/s11356-020-07879-1

Choudhary, S., Nayak, G. N., & Khare, N. (2023). Sedimentary processes, metal enrichment and potential ecological risk of metals in lacustrine sediments of Svalbard, Arctic. *Environmental Science and Pollution Research*, *30*(49), 106967-106981. https://doi.org/10.1007/s11356-022-23600-w

Colombo, M., Jackson, S. L., Cullen, J. T., & Orians, K. J. (2020). Dissolved iron and manganese in the Canadian Arctic Ocean: On the biogeochemical processes controlling their distributions. *Geochimica et Cosmochimica Acta*, *277*, 150-174. https://doi.org/https://doi.org/10.1016/j.gca.2020.03.012

Colombo, M., Rogalla, B., Li, J., Allen, S. E., Orians, K. J., & Maldonado, M. T. (2021). Canadian Arctic Archipelago Shelf-Ocean Interactions: A Major Iron Source to Pacific Derived Waters Transiting to the Atlantic. *Global Biogeochemical Cycles*, *35*(10), e2021GB007058. https://doi.org/https://doi.org/10.1029/2021GB007058

Croffie, M. E. T., Williams, P. N., Fenton, O., Fenelon, A., Metzger, K., & Daly, K. (2020). Optimising Sample Preparation and Calibrations in ED-XRF for Quantitative Soil Analysis. *Agronomy, 10*(9), 1309. https://www.mdpi.com/2073-4395/10/9/1309

Darby, D. A. (2003). Sources of sediment found in sea ice from the western Arctic Ocean, new insights into processes of entrainment and drift patterns. *Journal of Geophysical Research: Oceans*, *108*(C8). https://doi.org/https://doi.org/10.1029/2002JC001350

Darby, D. A., Myers, W. B., Jakobsson, M., & Rigor, I. (2011). Modern dirty sea ice characteristics and sources: The role of anchor ice. *Journal of Geophysical Research: Oceans*, *116*(C9). https://doi.org/https://doi.org/10.1029/2010JC006675

de Kemp, E. A., Gilbert, C., & James, D. T. (2006). *Geology of Nunavut*. Geological Survey of Canada, Canada-Nunavut Geoscience Office.

De Vitre, R., Belzile, N., & Tessier, A. (1991). Speciation and adsorption of arsenic on diagenetic iron oxyhydroxides. *Limnology and Oceanography*, *36*(7), 1480-1485. https://doi.org/https://doi.org/10.4319/lo.1991.36.7.1480

Denton, G. R., Wood, H. R., Concepcion, L. P., Siegrist, H. G., Eflin, V. S., Narcis, D. K., & Pangelinan, G. T. (1997). *Analysis of in-place contaminants in marine sediments from four harbor locations on Guam*. Water and Environmental Research Institute of the Western Pacific ….

Desaules, A. (2012). Critical evaluation of soil contamination assessment methods for trace metals. *Science of The Total Environment*, *426*, 120-131. https://doi.org/https://doi.org/10.1016/j.scitotenv.2012.03.035

Deschamps, C.-E., Montero-Serrano, J.-C., & St-Onge, G. (2018). Sediment Provenance Changes in the Western Arctic Ocean in Response to Ice Rafting, Sea Level, and Oceanic Circulation Variations Since the Last Deglaciation. *Geochemistry, Geophysics, Geosystems*, *19*(7), 2147-2165. https://doi.org/https://doi.org/10.1029/2017GC007411

Dudarev, A. A., & Odland, J. O. (2022). Forty-Year Biomonitoring of Environmental Contaminants in Russian Arctic: Progress, Gaps and Perspectives. *International Journal of Environmental Research and Public Health*, *19*(19), 11951. https://www.mdpi.com/1660-4601/19/19/11951

Duffus, J. H. (2002). "Heavy metals" a meaningless term? (IUPAC Technical Report). *Pure and Applied Chemistry*, *74*(5), 793-807. https://doi.org/doi:10.1351/pac200274050793

Duncan, E. G., Maher, W. A., & Foster, S. D. (2015). Contribution of Arsenic Species in Unicellular Algae to the Cycling of Arsenic in Marine Ecosystems. *Environmental Science & Technology*, *49*(1), 33-50. https://doi.org/10.1021/es504074z

Dupont, C. L., Buck, K. N., Palenik, B., & Barbeau, K. (2010). Nickel utilization in phytoplankton assemblages from contrasting oceanic regimes. *Deep Sea Research Part I: Oceanographic Research Papers*, *57*(4), 553-566. https://doi.org/https://doi.org/10.1016/j.dsr.2009.12.014

Edenborn, H. M., Belzile, N., Mucci, A., Lebel, J., & Silverberg, N. (1986). Observations on the diagenetic behavior of arsenic in a deep coastal sediment. *Biogeochemistry*, *2*(4), 359-376. https://doi.org/10.1007/BF02180326

Edmonds, M., Mason, E., & Hogg, O. (2022). Volcanic Outgassing of Volatile Trace Metals. *Annual Review of Earth and Planetary Sciences*, *50*(Volume 50, 2022), 79-98. https://doi.org/https://doi.org/10.1146/annurev-earth-070921-062047

Eicken, H., Gradinger, R., Gaylord, A., Mahoney, A., Rigor, I., & Melling, H. (2005). Sediment transport by sea ice in the Chukchi and Beaufort Seas: Increasing importance due to changing ice conditions? *Deep Sea Research Part II: Topical Studies in Oceanography*, *52*(24), 3281-3302. https://doi.org/https://doi.org/10.1016/j.dsr2.2005.10.006

Ellwood, M. J., & van den Berg, C. M. G. (2001). Determination of organic complexation of cobalt in seawater by cathodic stripping voltammetry. *Marine Chemistry*, *75*(1), 33-47. https://doi.org/https://doi.org/10.1016/S0304-4203(01)00024-X

Embry, A., & Beauchamp, B. (2019). Chapter 14 - Sverdrup Basin. In *The Sedimentary Basins of the United States and Canada (Second Edition)* (p. 559-592). Elsevier. https://doi.org/https://doi.org/10.1016/B978-0-444-63895-3.00014-0

Faust, J. C., Tessin, A., Fisher, B. J., Zindorf, M., Papadaki, S., Hendry, K. R., Doyle, K. A., & März, C. (2021). Millennial scale persistence of organic carbon bound to iron in Arctic marine sediments. *Nature Communications*, *12*(1), 275. https://doi.org/10.1038/s41467-020-20550-0

Fernex, F., Février, G., Bénaïm, J., & Arnoux, A. (1992). Copper, lead and zinc trapping in Mediterranean deep-sea sediments: probable coprecipitation with Mn and Fe. *Chemical Geology*, *98*(3), 293-306. https://doi.org/https://doi.org/10.1016/0009-2541(92)90190-G

Forsythe, K., Paudel, K., & Marvin, C. (2010). Geospatial analysis of zinc contamination in Lake Ontario sediments. *Journal of Environmental Informatics*, *16*(1), 1-10.

Francesconi, K. A., & Edmonds, J. S. (1996). Arsenic and Marine Organisms. In A. G. Sykes (Ed.), *Advances in Inorganic Chemistry* (Vol. 44, pp. 147-189). Academic Press. https://doi.org/https://doi.org/10.1016/S0898-8838(08)60130-0

Gamboa, A., Montero-Serrano, J.-C., St-Onge, G., Rochon, A., & Desiage, P.-A. (2017). Mineralogical, geochemical, and magnetic signatures of surface sediments from the Canadian Beaufort Shelf and Amundsen Gulf (Canadian Arctic). *Geochemistry, Geophysics, Geosystems*, *18*(2), 488-512. https://doi.org/https://doi.org/10.1002/2016GC006477

Gambrell, R. P. (1994). Trace and Toxic Metals in Wetlands—A Review. *Journal of Environmental Quality*, *23*(5), 883-891. https://doi.org/https://doi.org/10.2134/jeq1994.00472425002300050005x

Garrett, C. L. (1985). *Chemicals in the environment - Pacific and Yukon Region. II, Cadmium*. Vancouver: Department of the Environment, Environmental Protection Service, Pacific and Yukon Region

Gauthier, P. T., Blewett, T. A., Garman, E. R., Schlekat, C. E., Middleton, E. T., Suominen, E., & Crémazy, A. (2021). Environmental risk of nickel in aquatic Arctic ecosystems. *Science of The Total Environment*, *797*, 148921. https://doi.org/https://doi.org/10.1016/j.scitotenv.2021.148921

Glabonjat, R. A., Raber, G., Holm, H. C., Van Mooy, B. A. S., & Francesconi, K. A. (2021). Arsenolipids in Plankton from High- and Low-Nutrient Oceanic Waters Along a Transect in the North Atlantic. *Environmental Science & Technology*, *55*(8), 5515-5524. https://doi.org/10.1021/acs.est.0c06901

Gledhill, M., & Buck, K. N. (2012). The Organic Complexation of Iron in the Marine Environment: A Review [Review]. *Frontiers in Microbiology*, *Volume 3 - 2012*. https://doi.org/10.3389/fmicb.2012.00069

Gobeil, C., Silverberg, N., Sundby, B., & Cossa, D. (1987). Cadmium diagenesis in Laurentian Trough sediments. *Geochimica et Cosmochimica Acta*, *51*(3), 589-596. https://doi.org/https://doi.org/10.1016/0016-7037(87)90071-8

González, V., Vignati, D. A. L., Pons, M.-N., Montarges-Pelletier, E., Bojic, C., & Giamberini, L. (2015). Lanthanide ecotoxicity: First attempt to measure environmental risk for aquatic organisms. *Environmental Pollution*, *199*, 139-147. https://doi.org/https://doi.org/10.1016/j.envpol.2015.01.020

Gorny, J., Billon, G., Noiriel, C., Dumoulin, D., Lesven, L., & Madé, B. (2016). Chromium behavior in aquatic environments: a review. *Environmental Reviews*, *24*(4), 503-516. https://doi.org/10.1139/er-2016-0012

Government of Canada. (2022). *Federal contaminated sites inventory*. https://www.tbs-sct.gc.ca/fcsi-rscf/home-accueil-eng.aspx

Gromet, L. P., Haskin, L. A., Korotev, R. L., & Dymek, R. F. (1984). The "North American shale composite": Its compilation, major and trace element characteristics. *Geochimica et Cosmochimica Acta, 48*(12), 2469-2482. https://doi.org/https://doi.org/10.1016/0016-7037(84)90298-9

Hakanson, L. (1980). An ecological risk index for aquatic pollution control. A sedimentological approach. *Water Research*, *14*(8), 975-1001. https://doi.org/https://doi.org/10.1016/0043-1354(80)90143-8

Hamel, D., Vernal, A. d., Gosselin, M., & Hillaire-Marcel, C. (2002). Organic-walled microfossils and geochemical tracers: sedimentary indicators of productivity changes in the North Water and northern Baffin Bay during the last centuries. *Deep Sea Research Part II: Topical Studies in Oceanography*, *49*(22), 5277-5295. https://doi.org/https://doi.org/10.1016/S0967-0645(02)00190-X

Hannah, C. G., Dupont, F., & Dunphy, M. (2009). Polynyas and Tidal Currents in the Canadian Arctic Archipelago. *Arctic*, *62*(1), 83-95. http://www.jstor.org/stable/40513267

Harrison, J. C., St-Onge, M., Petrov, O., Strelnikov, S., Lopatin, B., Wilson, F., Tella, S., Paul, D., Lynds, T., Shokalsky, S., Hults, C. K., Bergman, S., Jepsen, H., & Solli, A. (2011). *Geological map of the Arctic / Carte géologique de l'Arctique* [ "A" Series Map 2159A, 2011, 2159 sheets, 2151:2155,2000,2000]. Natural Resources Canada.

Heginbottom, J. A. D., M A; Harker, P T. (1995). *Canada, permafrost* [The National Atlas of Canada; Natural Resources Canada, Geomatics Canada, MCR Series no. 4177, 1995, 4171 sheet]. Natural Resources Canada.

Hélie, J. F. (2009). Elemental and stable isotopic approaches for studying the organic and inorganic carbon components in natural samples. *IOP Conference Series: Earth and Environmental Science*, *5*(1), 012005. https://doi.org/10.1088/1755-1307/5/1/012005

Holemann, J. A., Schirmacher, M., Kassens, H., & Prange, A. (1999). Geochemistry of Surficial and Ice-rafted Sediments from the Laptev Sea (Siberia). *Estuarine, Coastal and Shelf Science*, *49*(1), 45-59. https://doi.org/https://doi.org/10.1006/ecss.1999.0485

Huerta-Diaz, M. A., & Morse, J. W. (1992). Pyritization of trace metals in anoxic marine sediments. *Geochimica et Cosmochimica Acta*, *56*(7), 2681-2702. https://doi.org/https://doi.org/10.1016/0016-7037(92)90353-K

Hugelius, G., Strauss, J., Zubrzycki, S., Harden, J. W., Schuur, E. A. G., Ping, C. L., Schirrmeister, L., Grosse, G., Michaelson, G. J., Koven, C. D., O'Donnell, J. A., Elberling, B., Mishra, U., Camill, P., Yu, Z., Palmtag, J., & Kuhry, P. (2014). Estimated stocks of circumpolar permafrost carbon with quantified uncertainty ranges and identified data gaps. *Biogeosciences, 11*(23), 6573-6593. https://doi.org/10.5194/bg-11-6573-2014

Isley, C. F., & Taylor, M. P. (2020). Atmospheric remobilization of natural and anthropogenic contaminants during wildfires. *Environmental Pollution*, *267*, 115400. https://doi.org/https://doi.org/10.1016/j.envpol.2020.115400

Jenkins, R. (2004). Organometallic compounds in the environment: an overview. *Organic metal and metalloid species in the Environment: Analysis, Distribution, Processes and Toxicological Evaluation*, 1-15.

Jensen, J., Adare, K., & Shearer, R. (1997). *Canadian Arctic Contaminants Assessment Report I*. Ottawa, Canada: Department of Indian and Northern Affairs, Government of Canada

Jensen, L., & Colombo, M. (2024). Shelf-basin connectivity drives dissolved Fe and Mn distributions in the western arctic ocean: A synoptic view into polar trace metal cycling. *Oceanography*, *37*(2), 60-71. https://www.jstor.org/stable/27309822

Kalia, K., & Khambholja, D. B. (2023). 28 - Arsenic in the marine environment—Contents, speciation, and its biotransformation. In S. J. S. Flora (Ed.), *Handbook of Arsenic Toxicology (Second Edition)* (pp. 761-789). Academic Press. https://doi.org/https://doi.org/10.1016/B978-0-323-89847-8.00012-2

Krasnodębska-Ostręga, B., Emons, H., & Golimowski, J. (2001). Selective leaching of elements associated with Mn – Fe oxides in forest soil, and comparison of two sequential extraction methods. *Fresenius' Journal of Analytical Chemistry*, *371*(3), 385-390. https://doi.org/10.1007/s002160100982

Kuzyk, Z. Z. A., Gobeil, C., Goñi, M. A., & Macdonald, R. W. (2017). Early diagenesis and trace element accumulation in North American Arctic margin sediments. *Geochimica et Cosmochimica Acta*, *203*, 175-200. https://doi.org/https://doi.org/10.1016/j.gca.2016.12.015

Lavallée, F., & Fedoruk, L. (1989). The elimination of leaded motor gasoline: Effect on Canadian gasoline engines beyond 1990.

Letaïef, S., Montero-Serrano, J. C., & St-Onge, G. (2021). Sedimentary processes within the Canadian Arctic Archipelago: Relationships among sedimentological, geochemical, and magnetic sediment properties. *Geochemistry, Geophysics, Geosystems*, *22*(7), e2021GC009719.

Lewkowicz, A. G., & Young, K. L. (1991). Observations of aeolian transport and niveo-aeolian deposition at three lowland sites, Canadian arctic archipelago. *Permafrost and Periglacial Processes*, *2*(3), 197-210. https://doi.org/https://doi.org/10.1002/ppp.3430020304

Little, M. E., Parsons, M. B., Law, B. A., Milligan, T. G., & Smith, J. N. (2015). Impact of historical gold mining activities on marine sediments in Wine Harbour, Nova Scotia, Canada. *Atlantic Geoscience*, *51*(0), 344 - 363. https://doi.org/10.4138/atlgeol.2015.016

Loring, D. H. (1978). Geochemistry of zinc, copper and lead in the sediments of the estuary and Gulf of St. Lawrence. *Canadian Journal of Earth Sciences*, *15*(5), 757-772. https://doi.org/10.1139/e78-082

Loring, D. H., Dahle, S., Naes, K., Dos Santos, J., Skei, J. M., & Matishov, G. G. (1998). Arsenic and other Trace Metals in Sediments from the Kara Sea and the Ob and Yenisey Estuaries, Russia. *Aquatic Geochemistry*, *4*(2), 233-252. https://doi.org/10.1023/A:1009691314353

Lu, Z. B., Cai, M., Wang, J., Yin, Z., & Yang, H. (2013). Levels and distribution of trace metals in surface sediments from Kongsfjorden, Svalbard, Norwegian Arctic. *Environmental Geochemistry and Health*, *35*(2), 257-269. https://doi.org/10.1007/s10653-012-9481-z

Lu, Z. B., & Kang, M. (2018). Risk assessment of toxic metals in marine sediments from the Arctic Ocean using a modified BCR sequential extraction procedure. *Journal of Environmental Science and Health, Part A*, *53*(3), 278-293. https://doi.org/10.1080/10934529.2017.1397443

Macdonald, R. W., Barrie, L. A., Bidleman, T. F., Diamond, M. L., Gregor, D. J., Semkin, R. G., Strachan, W. M. J., Li, Y. F., Wania, F., Alaee, M., Alexeeva, L. B., Backus, S. M., Bailey, R., Bewers, J. M., Gobeil, C., Halsall, C. J., Harner, T., Hoff, J. T., Jantunen, L. M. M., . . . Yunker, M. B. (2000). Contaminants in the Canadian Arctic: 5 years of progress in understanding sources, occurrence and pathways. *Science of The Total Environment*, *254*(2), 93-234. https://doi.org/https://doi.org/10.1016/S0048-9697(00)00434-4

Macdonald, R. W., & Bewers, J. M. (1996). Contaminants in the arctic marine environment: priorities for protection. *ICES Journal of Marine Science*, *53*(3), 537-563. https://doi.org/10.1006/jmsc.1996.0077

Macdonald, R. W., Harner, T., & Fyfe, J. (2005). Recent climate change in the Arctic and its impact on contaminant pathways and interpretation of temporal trend data. *Science of The Total Environment*, *342*(1), 5-86. https://doi.org/https://doi.org/10.1016/j.scitotenv.2004.12.059

Madison, A. S., Tebo, B. M., Mucci, A., Sundby, B., & Luther, G. W. (2013). Abundant Porewater Mn(III) Is a Major Component of the Sedimentary Redox System. *Science*, *341*(6148), 875-878. https://doi.org/doi:10.1126/science.1241396

Magen, C. (2008). *Origin, sedimentation and diagenesis of organic matter in coastal sediments of the southern Beaufort Sea region, Canadian Arctic* McGill University]. Montreal.

Michel, C., Hamilton, J., Hansen, E., Barber, D., Reigstad, M., Iacozza, J., Seuthe, L., & Niemi, A. (2015). Arctic Ocean outflow shelves in the changing Arctic: A review and perspectives. *Progress in Oceanography*, *139*, 66-88. https://doi.org/https://doi.org/10.1016/j.pocean.2015.08.007

Millot, R., Gaillardet, J. é., Dupré, B., & Allègre, C. J. (2003). Northern latitude chemical weathering rates: clues from the Mackenzie River Basin, Canada. *Geochimica et Cosmochimica Acta*, *67*(7), 1305-1329. https://doi.org/https://doi.org/10.1016/S0016-7037(02)01207-3

Morse, J. W., & Luther, G. W. (1999). Chemical influences on trace metal-sulfide interactions in anoxic sediments. *Geochimica et Cosmochimica Acta*, *63*(19), 3373-3378. https://doi.org/https://doi.org/10.1016/S0016-7037(99)00258-6

Mucci, A. (1988). Manganese uptake during calcite precipitation from seawater: Conditions leading to the formation of a pseudokutnahorite. *Geochimica et Cosmochimica Acta*, *52*(7), 1859-1868. https://doi.org/https://doi.org/10.1016/0016-7037(88)90009-9

Müller, G. (1969). Index of geoaccumulation in sediments of the Rhine River. *Geojournal*, *2*, 108-118.

Naeem, A., Westerhoff, P., & Mustafa, S. (2007). Vanadium removal by metal (hydr)oxide adsorbents. *Water Research*, *41*(7), 1596-1602. https://doi.org/https://doi.org/10.1016/j.watres.2007.01.002

Naidu, A., Kelley, J., Misra, D., & Venkatesan, M. (2005). *Trace metals and hydrocarbons in sediments of the Beaufort Lagoon, Northeast Arctic Alaska, exposed to long-term natural oil seepage, recent anthropogenic acivities and pristine conditions. Final Report to Coastal Marine Institute, Univ. Alaska Fairbanks, Fairbanks, AK*. Press.

Naidu, A. S., Blanchard, A. L., Misra, D., Trefry, J. H., Dasher, D. H., Kelley, J. J., & Venkatesan, M. I. (2012). Historical changes in trace metals and hydrocarbons in nearshore sediments, Alaskan Beaufort Sea, prior and subsequent to petroleum-related industrial development: Part I. Trace metals. *Marine Pollution Bulletin*, *64*(10), 2177-2189. https://doi.org/https://doi.org/10.1016/j.marpolbul.2012.07.037

Nelson, Y. M., Lion, L. W., Shuler, M. L., & Ghiorse, W. C. (1999). Lead binding to metal oxide and organic phases of natural aquatic biofilms. *Limnology and Oceanography*, *44*(7), 1715-1729. https://doi.org/https://doi.org/10.4319/lo.1999.44.7.1715

Niemi, A., Ehrman, A., Ahmed, M., Arey, M., Azetsu-Scott, K., Babin, M., Capelle, D., Christie, L. R., Devred, E., Drake, A. K., Dunmall, K., Elias, J., Falardeau, M., Ferguson, S., Gilbert, M. J. H., Halliday, W. D., Harris, L. N., Hedges, K., Illasiak, J., . . . Yurkowski, D. (2024). *État des mers arctiques du Canada, 2024*. Winnipeg

NRCAN. (2024). *Rare earth elements facts*. Government of Canada. Retrieved 2024-11-27 from https://natural-resources.canada.ca/our-natural-resources/minerals-mining/mining-data-statistics-and-analysis/minerals-metals-facts/rare-earth-elements-facts/20522

Nriagu, J. O., & Kabir, A. (1995). Chromium in the Canadian environment. *Environmental Reviews*, *3*(1), 121-144. https://doi.org/10.1139/a95-005

Nriagu, J. O., & Pacyna, J. M. (1988). Quantitative assessment of worldwide contamination of air, water and soils by trace metals. *Nature, 333*(6169), 134-139. https://doi.org/10.1038/333134a0

O'Donnell, J. A., Carey, M. P., Koch, J. C., Baughman, C., Hill, K., Zimmerman, C. E., Sullivan, P. F., Dial, R., Lyons, T., Cooper, D. J., & Poulin, B. A. (2024). Metal mobilization from thawing permafrost to aquatic ecosystems is driving rusting of Arctic streams. *Communications Earth & Environment*, *5*(1), 268. https://doi.org/10.1038/s43247-024-01446-z

Osterholz, H., Simon, H., Beck, M., Maerz, J., Rackebrandt, S., Brumsack, H.-J., Feudel, U., & Simon, M. (2014). Impact of diatom growth on trace metal dynamics (Mn, Mo, V, U). *Journal of Sea Research*, *87*, 35-45. https://doi.org/https://doi.org/10.1016/j.seares.2013.09.009

Paasivirta, J. (1991). *Chemical ecotoxicology*. CRC Press.

Pacyna, J. M., & Pacyna, E. G. (2001). An assessment of global and regional emissions of trace metals to the atmosphere from anthropogenic sources worldwide. *Environmental Reviews*, *9*(4), 269-298. https://doi.org/10.1139/a01-012

Palaniswamy, S., Nevala, L., Pesonen, P., Rautio, A., Järvelin, M.-R., Abass, K., & Charles, D. (2024). Environmental contaminants in Arctic human populations: Trends over 30 years. *Environment International*, *189*, 108777. https://doi.org/https://doi.org/10.1016/j.envint.2024.108777

Palarea-Albaladejo, J., & Martín-Fernández, J. A. (2013). Values below detection limit in compositional chemical data. *Analytica Chimica Acta*, *764*, 32-43. https://doi.org/https://doi.org/10.1016/j.aca.2012.12.029

Palarea-Albaladejo, J., & Martín-Fernández, J. A. (2015). zCompositions — R package for multivariate imputation of left-censored data under a compositional approach. *Chemometrics and Intelligent Laboratory Systems*, *143*, 85-96. https://doi.org/https://doi.org/10.1016/j.chemolab.2015.02.019

Parsons, M. B., & Cranston, R. E. (2006). Influence of lead smelter emissions on the distribution of metals in marine sediments from Chaleur Bay, eastern Canada. *Geochemistry: Exploration, Environment, Analysis*, *6*(2-3), 259-275. https://doi.org/10.1144/1467-7873/05-082

Pelletier, N. (2021). *Paleolimnological characterization of metal (loid) sources and transport processes in Canadian subarctic lakes* Carleton University]. Ottawa, ON.

Pelletier, N., Chételat, J., Cousens, B., Zhang, S., Stepner, D., Muir, D. C. G., & Vermaire, J. C. (2020). Lead contamination from gold mining in Yellowknife Bay (Northwest Territories), reconstructed using stable lead isotopes. *Environmental Pollution*, *259*, 113888. https://doi.org/https://doi.org/10.1016/j.envpol.2019.113888

Pickhardt, P. C., & Fisher, N. S. (2007). Accumulation of Inorganic and Methylmercury by Freshwater Phytoplankton in Two Contrasting Water Bodies. *Environmental Science & Technology, 41*(1), 125-131. https://doi.org/10.1021/es060966w

Pinto, J. J., García-Vargas, M., & Moreno, C. (2013). A bulk liquid membrane–flow injection (BLM–FI) coupled system for the preconcentration and determination of vanadium in saline waters. *Talanta*, *103*, 161-165. https://doi.org/https://doi.org/10.1016/j.talanta.2012.10.026

Piper, D. Z., & Perkins, R. B. (2004). A modern vs. Permian black shale—the hydrography, primary productivity, and water-column chemistry of deposition. *Chemical Geology*, *206*(3), 177-197. https://doi.org/https://doi.org/10.1016/j.chemgeo.2003.12.006

Poh, S.-C., & Tahir, N. M. (2017). The common pitfall of using enrichment factor in assessing soil heavy metal pollution. *Malays. J. Anal. Sci*, *21*, 52-59.

Poland, J. S., Riddle, M. J., & Zeeb, B. A. (2003). Contaminants in the Arctic and the Antarctic: a comparison of sources, impacts, and remediation options. *Polar Record*, *39*(4), 369-383. https://doi.org/10.1017/S0032247403002985

Pourmand, A., Dauphas, N., & Ireland, T. J. (2012). A novel extraction chromatography and MC-ICP-MS technique for rapid analysis of REE, Sc and Y: Revising CI-chondrite and Post-Archean Australian Shale (PAAS) abundances. *Chemical Geology*, *291*, 38-54. https://doi.org/https://doi.org/10.1016/j.chemgeo.2011.08.011

Quinn, P. K., G., S., E., A., G., D. E., T., R.-A., & and Gong, S. L. (2007). Arctic haze: current trends and knowledge gaps. *Tellus B: Chemical and Physical Meteorology*, *59*(1), 99-114. https://doi.org/10.1111/j.1600-0889.2006.00236.x

R Core Team. (2024). *R: A language and environment for statistical computing*. In R Foundation for Statistical Computing. https://www.R-project.org/

Rainbow, P. S. (2007). Trace metal bioaccumulation: Models, metabolic availability and toxicity. *Environment International*, *33*(4), 576-582. https://doi.org/https://doi.org/10.1016/j.envint.2006.05.007

Reimann, C., & de Caritat, P. (2000). Intrinsic Flaws of Element Enrichment Factors (EFs) in Environmental Geochemistry. *Environmental Science & Technology*, *34*(24), 5084-5091. https://doi.org/10.1021/es001339o

Reimann, C., & de Caritat, P. (2005). Distinguishing between natural and anthropogenic sources for elements in the environment: regional geochemical surveys versus enrichment factors. *Science of The Total Environment*, *337*(1), 91-107. https://doi.org/https://doi.org/10.1016/j.scitotenv.2004.06.011

Ribeiro, S., Limoges, A., Massé, G., Johansen, K. L., Colgan, W., Weckström, K., Jackson, R., Georgiadis, E., Mikkelsen, N., Kuijpers, A., Olsen, J., Olsen, S. M., Nissen, M., Andersen, T. J., Strunk, A., Wetterich, S., Syväranta, J., Henderson, A. C. G., Mackay, H., . . . Davidson, T. A. (2021). Vulnerability of the North Water ecosystem to climate change. *Nature Communications*, *12*(1), 4475. https://doi.org/10.1038/s41467-021-24742-0

Rood, S. B., Kaluthota, S., Philipsen, L. J., Rood, N. J., & Zanewich, K. P. (2017). Increasing discharge from the Mackenzie River system to the Arctic Ocean. *Hydrological Processes*, *31*(1), 150-160. https://doi.org/https://doi.org/10.1002/hyp.10986

Rosenthal, Y., Lam, P., Boyle, E. A., & Thomson, J. (1995). Authigenic cadmium enrichments in suboxic sediments: Precipitation and postdepositional mobility. *Earth and Planetary Science Letters*, *132*(1), 99-111. https://doi.org/https://doi.org/10.1016/0012-821X(95)00056-I

Ruban, A., Dudarev, O., Rudmin, M., & Semiletov, I. (2024). Rare Earth Elements in Sediments from the Laptev Sea Shelf: Insight into Sources and Distribution Factors. *Quaternary, 7*(1), 12. https://www.mdpi.com/2571-550X/7/1/12

Schobert, H. (2013). Formation of fossil fuels. In *Chemistry of Fossil Fuels and Biofuels* (p. 103-131). Cambridge University Press. https://doi.org/https://doi.org/10.1017/CBO9780511844188

Schuster, P. F., Schaefer, K. M., Aiken, G. R., Antweiler, R. C., Dewild, J. F., Gryziec, J. D., Gusmeroli, A., Hugelius, G., Jafarov, E., Krabbenhoft, D. P., Liu, L., Herman-Mercer, N., Mu, C., Roth, D. A., Schaefer, T., Striegl, R. G., Wickland, K. P., & Zhang, T. (2018). Permafrost Stores a Globally Significant Amount of Mercury. *Geophysical Research Letters*, *45*(3), 1463-1471. https://doi.org/https://doi.org/10.1002/2017GL075571

Sen, I. S., & Peucker-Ehrenbrink, B. (2012). Anthropogenic Disturbance of Element Cycles at the Earth's Surface. *Environmental Science & Technology*, *46*(16), 8601-8609. https://doi.org/10.1021/es301261x

Shannon, R. D. (1976). Revised effective ionic radii and systematic studies of interatomic distances in halides and chalcogenides. *Foundations of Crystallography, 32*(5), 751-767.

Sholkovitz, E. R. (1990). Rare-earth elements in marine sediments and geochemical standards. Chemical *Geology, 88*(3), 333-347. https://doi.org/https://doi.org/10.1016/0009-2541(90)90097-Q

Sholkovitz, E. R., Landing, W. M., & Lewis, B. L. (1994). Ocean particle chemistry: The fractionation of rare earth elements between suspended particles and seawater. *Geochimica et Cosmochimica Acta, 58*(6), 1567-1579. https://doi.org/https://doi.org/10.1016/0016-7037(94)90559-2

Shotyk, W., Weiss, D., Heisterkamp, M., Cheburkin, A. K., Appleby, P. G., & Adams, F. C. (2002). New Peat Bog Record of Atmospheric Lead Pollution in Switzerland: Pb Concentrations, Enrichment Factors, Isotopic Composition, and Organolead Species. *Environmental Science & Technology*, *36*(18), 3893-3900. https://doi.org/10.1021/es010196i

Simon, L. (2014). Potentially Harmful Elements in Agricultural Soils. In C. Bini & J. Bech (Eds.), *PHEs, Environment and Human Health: Potentially harmful elements in the environment and the impact on human health* (pp. 85-150). Springer Netherlands. https://doi.org/10.1007/978-94-017-8965-3_3

Simpson, S. L., & Batley, G. E. (2007). Predicting metal toxicity in sediments: A critique of current approaches. *Integrated Environmental Assessment and Management*, *3*(1), 18-31. https://doi.org/10.1002/ieam.5630030103

Skierszkan, E. K., Schoepfer, V. A., Fellwock, M. D., Dockrey, J. W., Hayatifar, A., Bondici, V. F., McBeth, J. M., & Lindsay, M. B. J. (2024). Arsenic Mobilization from Thawing Permafrost. *ACS Earth and Space Chemistry*, *8*(4), 745-759. https://doi.org/10.1021/acsearthspacechem.3c00355

Smrzka, D., Zwicker, J., Bach, W., Feng, D., Himmler, T., Chen, D., & Peckmann, J. (2019). The behavior of trace elements in seawater, sedimentary pore water, and their incorporation into carbonate minerals: a review. *Facies*, *65*(4), 41. https://doi.org/10.1007/s10347-019-0581-4

Statistics Canada. (2023). *Census Profile. 2021 Census of Population*. Ottawa: Statistics Canada Catalogue number 98-316-X2021001. Released November 15, 2023. Retrieved from https://www12.statcan.gc.ca/census-recensement/2021/dp-pd/prof/index.cfm?Lang=E

Stirling, I., & Cleator, H. (1981). *Polynyas in the Canadian Arctic*. (Occasional Paper Number 45). Ottawa: Canadian Wildlife Service

Stockdale, A., Davison, W., Zhang, H., & Hamilton-Taylor, J. (2010). The Association of Cobalt with Iron and Manganese (Oxyhydr)oxides in Marine Sediment. *Aquatic Geochemistry*, *16*(4), 575-585. https://doi.org/10.1007/s10498-010-9092-1

Su, N., Yang, S., Guo, Y., Yue, W., Wang, X., Yin, P., & Huang, X. (2017). Revisit of rare earth element fractionation during chemical weathering and river sediment transport. *Geochemistry, Geophysics, Geosystems, 18*(3), 935-955. https://doi.org/https://doi.org/10.1002/2016GC006659

Sunda, W. (2012). Feedback Interactions between Trace Metal Nutrients and Phytoplankton in the Ocean [Review]. *Frontiers in Microbiology*, *Volume 3 - 2012*. https://doi.org/10.3389/fmicb.2012.00204

Sutherland, R. A. (2000). Bed sediment-associated trace metals in an urban stream, Oahu, Hawaii. *Environmental Geology, 39*(6), 611-627. https://doi.org/10.1007/s002540050473

Sutton, O. F., McCarter, C. P. R., & Waddington, J. M. (2024). Globally-significant arsenic release by wildfires in a mining-impacted boreal landscape. *Environmental Research Letters*, *19*(6), 064024. https://doi.org/10.1088/1748-9326/ad461a

Taylor, S. R., & McLennan, S. M. (1985). *The continental crust: Its composition and evolution*. Blackwell Scientific Publication (312 pp.). https://www.osti.gov/biblio/6582885

Terwisscha van Scheltinga, A. D., Myers, P. G., & Pietrzak, J. D. (2010). A finite element sea ice model of the Canadian Arctic Archipelago. *Ocean Dynamics*, *60*(6), 1539-1558. https://doi.org/10.1007/s10236-010-0356-5

Tessier, A., & Campbell, P. G. C. (1987). Partitioning of trace metals in sediments: Relationships with bioavailability. *Hydrobiologia*, *149*(1), 43-52. https://doi.org/10.1007/BF00048645

Tessier, A., Campbell, P. G. C., & Bisson, M. (1979). Sequential extraction procedure for the speciation of particulate trace metals. *Analytical Chemistry*, *51*(7), 844-851. https://doi.org/10.1021/ac50043a017

Trefry, J. H., Dunton, K. H., Trocine, R. P., Schonberg, S. V., McTigue, N. D., Hersh, E. S., & McDonald, T. J. (2013). Chemical and biological assessment of two offshore drilling sites in the Alaskan Arctic. *Marine Environmental Research*, *86*, 35-45. https://doi.org/https://doi.org/10.1016/j.marenvres.2013.02.008

Trefry, J. H., & Neff, J. M. (2019). Effects of offshore oil exploration and development in the Alaskan Beaufort Sea: A three-decade record for sediment metals. *Integrated Environmental Assessment and Management*, *15*(2), 209-223. https://doi.org/https://doi.org/10.1002/ieam.4069

Trefry, J. H., Rember, R. D., Trocine, R. P., & Brown, J. S. (2003). Trace metals in sediments near offshore oil exploration and production sites in the Alaskan Arctic. *Environmental Geology*, *45*(2), 149-160. https://doi.org/10.1007/s00254-003-0882-2

Tribovillard, N., Algeo, T. J., Lyons, T., & Riboulleau, A. (2006). Trace metals as paleoredox and paleoproductivity proxies: An update. *Chemical Geology*, *232*(1), 12-32. https://doi.org/https://doi.org/10.1016/j.chemgeo.2006.02.012

Turekian, K. K., & Wedepohl, K. H. (1961). Distribution of the Elements in Some Major Units of the Earth's Crust. *GSA Bulletin*, *72*(2), 175-192. https://doi.org/10.1130/0016-7606(1961)72[175:Doteis]2.0.Co;2

US EPA. (1999). *Integrated Risk Information System (IRIS) on Chromium VI*. Washington, DC.: National Center for Environmental Assessment, Office of Research and Development

US EPA. (2007). *Method 3051A (SW-846): Microwave Assisted Acid Digestion of Sediments, Sludges, and Oils*. Washington, DC.

US EPA. (2012). *Rare earth elements: A review of production, processing, recycling, and associated environmental issues*. Cincinnati, OH

Veinott, G., Sylvester, P., Hamoutene, D., Anderson, M. R., Meade, J., & Payne, J. (2003). State of the marine environment at Little Bay Arm, Newfoundland and Labrador, Canada, 10 years after a "do nothing" response to a mine tailings spill. *Journal of Environmental Monitoring*, *5*(4), 626-634.

Vincent, R. F. (2023). An Assessment of the Lancaster Sound Polynya Using Satellite Data 1979 to 2022. *Remote Sensing*, *15*(4), 954. https://www.mdpi.com/2072-4292/15/4/954

Vinogradova, A. A., & Kotova, E. I. (2019). Pollution of Russian Northern Seas with Heavy Metals: Comparison of Atmospheric Flux and River Flow. *Izvestiya, Atmospheric and Oceanic Physics*, *55*(7), 695-704. https://doi.org/10.1134/S0001433819070119

Wagemann, R., Snow, N. B., Rosenberg, D. M., & Lutz, A. (1978). Arsenic in sediments, water and aquatic biota from lakes in the vicinity of Yellowknife, Northwest Territories, Canada. *Archives of Environmental Contamination and Toxicology*, *7*(1), 169-191. https://doi.org/10.1007/BF02332047

Wang, J., Gough, W. A., Yan, J., & Lu, Z. (2022). Ecological Risk Assessment of Trace Metal in Pacific Sector of Arctic Ocean and Bering Strait Surface Sediments. *International Journal of Environmental Research and Public Health*, *19*(8), 4454. https://www.mdpi.com/1660-4601/19/8/4454

Wang, Q., Myers, P. G., Hu, X., & Bush, A. B. G. (2012). Flow Constraints on Pathways through the Canadian Arctic Archipelago. *Atmosphere-Ocean*, *50*(3), 373-385. https://doi.org/10.1080/07055900.2012.704348

Wanty, R. B., & Goldhaber, M. B. (1992). Thermodynamics and kinetics of reactions involving vanadium in natural systems: Accumulation of vanadium in sedimentary rocks. *Geochimica et Cosmochimica Acta*, *56*(4), 1471-1483. https://doi.org/https://doi.org/10.1016/0016-7037(92)90217-7

Wedepohl, K. H. (1971). Environmental influences on the chemical composition of shales and clays. *Physics and Chemistry of the Earth*, *8*, 307-333. https://doi.org/https://doi.org/10.1016/0079-1946(71)90020-6

Whitmore, L. M., Morton, P. L., Twining, B. S., & Shiller, A. M. (2019). Vanadium cycling in the Western Arctic Ocean is influenced by shelf-basin connectivity. *Marine Chemistry*, *216*, 103701. https://doi.org/https://doi.org/10.1016/j.marchem.2019.103701

Xu, G., Hannah, J. L., Bingen, B., Georgiev, S., & Stein, H. J. (2012). Digestion methods for trace element measurements in shales: Paleoredox proxies examined. *Chemical Geology*, *324-325*, 132-147. https://doi.org/https://doi.org/10.1016/j.chemgeo.2012.01.029

Yakovlev, E., Druzhinina, A., Druzhinin, S., Zykov, S., & Ivanchenko, N. (2022). Assessment of physical and chemical properties, health risk of trace metals and quality indices of surface waters of the rivers and lakes of the Kola Peninsula (Murmansk Region, North–West Russia). *Environmental Geochemistry and Health*, *44*(8), 2465-2494. https://doi.org/10.1007/s10653-021-01027-5

Yardley, B. W. D. (2005). 100th Anniversary Special Paper: Metal Concentrations in Crustal Fluids and Their Relationship to Ore Formation. *Economic Geology, 100*(4), 613-632. https://doi.org/10.2113/gsecongeo.100.4.613

Yuan, Z.-F., Gustave, W., Sekar, R., Bridge, J., Wang, J.-Y., Feng, W.-J., Guo, B., & Chen, Z. (2021). Simultaneous measurement of aqueous redox-sensitive elements and their species across the soil-water interface. *Journal of Environmental Sciences*, *102*, 1-10. https://doi.org/https://doi.org/10.1016/j.jes.2020.09.017

Zheng, H., Ren, Q., Zheng, K., Qin, Z., Wang, Y., & Wang, Y. (2022). Spatial distribution and risk assessment of metal(loid)s in marine sediments in the Arctic Ocean and Bering Sea. *Marine Pollution Bulletin*, *179*, 113729. https://doi.org/https://doi.org/10.1016/j.marpolbul.2022.113729

Zhu, C., Tian, H., & Hao, J. (2020). Global anthropogenic atmospheric emission inventory of twelve typical hazardous trace elements, 1995–2012. *Atmospheric Environment*, *220*, 117061. https://doi.org/https://doi.org/10.1016/j.atmosenv.2019.117061